DTRA-TR-99-5

Technical Report

EVENT CHARACTERIZATION DEVELOPMENT AND ANALYSIS AT THE PROTOTYPE IDC

Approved for public release; distribution is unlimited.

October 2000

Prepared for:
Defense Threat Reduction Agency
45045 Aviation Drive
Dulles, VA 20166-7517

F19628-95-C-0101

Mark D. Fisk, et. al.

Prepared by: Mission Research Corporation
P.O. Drawer 719
Santa Barbara, CA 93102-0719

DESTRUCTION NOTICE

FOR CLASSIFIED, documents follow the procedures in DoD 5220.22-M, Industrial Security Manual (NISPOM), Chapter 5, Section 7.

FOR UNCLASSIFIED, limited documents destroy by any method that will prevent disclosure of contents or reconstruction of the document.

Retention of this document by DoD contractors is authorized in accordance with DoD 5220.22-M, Industrial Security Manual.

PLEASE NOTIFY THE DEFENSE THREAT REDUCTION AGENCY, ATTN: ADP, 45045 AVIATION DRIVE, DULLES, VA 20166-7517, IF YOUR ADDRESS IS INCORRECT, IF YOU WISH IT DELETED FROM THE DISTRIBUTION LIST, OR IF THE ADDRESSEE IS NO LONGER EMPLOYED BY YOUR ORGANIZATION.

DISCLAIMER

"The views and conclusions contained in this document are those of the authors and should not be interpreted as representing the official policies, either express or implied, of the Department of Defense or the U.S. Government."

CUT HERE AND RETURN

DISTRIBUTION LIST UPDATE

This mailer is provided to enable DTRA to maintain current distribution lists for reports. (We would appreciate you providing the requested information.)

- ☐ Add the individual listed to your distribution list.
- ☐ Delete the cited organization/individual.
- ☐ Change of address.

Note:
Please return the mailing label from the document so that any additions, changes, corrections or deletions can be made easily. For distribution cancellation or more information call DTRA/ADM (703) 325-1036.

NAME: _____

ORGANIZATION: _____

OLD ADDRESS	NEW ADDRESS
_____	_____
_____	_____
_____	_____

TELEPHONE NUMBER: ( ) _____

DTRA PUBLICATION NUMBER/TITLE	CHANGES/DELETIONS/ADDITIONS, etc.) *(Attach Sheet if more Space is Required)*
_____	_____
_____	_____
_____	_____

DTRA or other GOVERNMENT CONTRACT NUMBER: _____

CERTIFICATION of NEED-TO-KNOW BY GOVERNMENT SPONSOR (if other than DTRA):

SPONSORING ORGANIZATION: _____

CONTRACTING OFFICER or REPRESENTATIVE: _____

SIGNATURE: _____

DEFENSE THREAT REDUCTION AGENCY
ATTN: ADM
45045 AVIATION DRIVE
DULLES, VA 20156-7517

DEFENSE THREAT REDUCTION AGENCY
ATTN: ADM
6801 TELEGRAPH ROAD
ALEXANDRIA, VA 22310-3398

REPORT DOCUMENTATION PAGE

Form Approved
OMB NO. 0704.0188

1. AGENCY USE ONLY *(Leave Blank)*	2. REPORT DATE	3. REPORT TYPE AND DATES COVERED
	15 FEB 1998	Technical 950615 - 981231

4. TITLE AND SUBTITLE
Event Characterization Development and Analysis at the Prototype IDC

5. FUNDING NUMBERS
Contract F19628-95-C-0101

6. AUTHOR(s)
Mark D. Fisk, Steven Bottone, Richard J. Carlson, (MRC)
Henry L. Gray and Gary D. McCartor (SMU)

7. PERFORMING ORGANIZATION NAME(S) AND ADDRESS(ES)
Mission Research Corporation
P. O. Drawer 719
Santa Barbara, CA 93102-0719

8. PERFORMING ORGANIZATION REPORT NUMBER
MRC-R-1548

9. SPONSORING/MONITORING AGENCY NAME(S) AND ADDRESS(ES)
Defense Threat Reduction Agency
45045 Aviation Drive
Dulles, VA 20166-7517
OST/Dainty

10. SPONSORING/MONITORING AGENCY REPORT NUMBER
DTRA-TR-99-5

11. SUPPLEMENTARY NOTES

12a. DISTRIBUTION/AVAILABILITY STATEMENT
Approved for public distribution;
distribution unlimited

12b. DISTRIBUTION CODE

13. ABSTRACT *(Maximum 200 words)*

This report describes our work on implementing seismic event characterization capabilities at the prototype International Data Centre (PIDC) and on quantifying the performance of these capabilities with regard to monitoring the Comprehensive Nuclear Test-Ban Treaty (CTBT). Seismic event-screening procedures and criteria are described, based on standard event characterization parameters computed at the PIDC, with the objective of screening out events that are consistent with natural seismic phenomena. The screening capabilities are based on focal depth, Ms:mb, determination of events with offshore locations, and comparisons of events to regional event populations using high-frequency regional Pn/Lg and Pn/Sn. Uncertainties in the estimates of the event characterization parameters are included in the analyses so that events may be screened out at a specified confidence level. The performance of the screening criteria is assessed for all events above mb 3.5 in the Reviewed Event Bulletin (REB) for 1996 and 1997. During this period there were over 30,000 such events, including two underground nuclear tests at the Lop Nor test site. The screening criteria are also applied to 45 and 48 historical underground nuclear explosions at the Nevada Test Site and Semipalatinsk, respectively. These results are also compared to those obtained using alternative screening criteria. Also described are in-depth analyses of some interesting seismic events, including the two underground nuclear explosions at the Lop Nor test site in China, an event in Southern India, and an event in the Kara Sea on 16 August 1997. Also, preliminary region-specific distance corrections are presented for regional seismic amplitude ratios, Pn/Lg and Pn/Sn in the 2-4, 4-6 and 6-8 Hz bands, for the existing IMS seismic stations. The results utilize regional data from 50 IMS seismic stations, a parameterization of the distance dependence which includes geometrical spreading and attenuation terms, and investigation of subregional effects.

14. SUBJECT TERMS		15. NUMBER OF PAGES
Seismic Event Characterization	Comprehensive Nuclear Test-Ban Treaty	154
Event Screening	International Monitoring System	16. PRICE CODE
Regional Distance Corrections	International Data Centre	

17. Security CLASSIFICATION OF REPORT	18. Security CLASSIFICATION OF THIS PAGE	19. Security CLASSIFICATION OF ABSTRACT	20. LIMITATION OF ABSTRACT
UNCLASSIFIED	UNCLASSIFIED	UNCLASSIFIED	SAR

NSN 7540-01-280-5500

Standard Form 298 (Rev. 2-89)
Prescribed by ANSI Std. 239-18
298-102

CLASSIFIED BY:

DECLASSIFY ON:

7. PERFORMING ORGANIZATION NAME(S) AND ADDRESS(ES) (Continued)

Statistical Data Analysis (Gray)
2703 Valley Creek Trail
McKinney, TX 75070

Southern Methodist University (McCartor)
Department of Physics
Dallas, TX 75275-0175

9. SPONSORING/MONITORING AGENCY NAME(S) AND ADDRESS(ES) (Continued)

Phillips Laboratory
29 Randolph Road
Hanscom AFB, MA 01731-3010

Executive Summary

During the course of this project, our efforts have focused on implementing seismic event characterization capabilities at the prototype International Data Centre (PIDC) and on quantifying the performance of these capabilities with regard to monitoring the Comprehensive Nuclear Test-Ban Treaty (CTBT). We have also been responsible for developing, operating and maintaining the PIDC World Wide Web site. Key accomplishments of these efforts are summarized here and described in more detail in the body of this report.

First, we have developed seismic event-screening procedures and criteria, based on standard event characterization parameters computed at the PIDC, with the objective of screening out events that are consistent with natural phenomena. The screening criteria are based on location, focal depth, and the difference of body (mb) and surface (Ms) wave magnitudes. Uncertainties in the estimates are included in the analyses so that events may be screened out at a specified confidence level. Location error ellipses are being used on an interim basis to categorize offshore events until hydroacoustic screening capabilities are further developed and additional IMS hydroacoustic stations are on-line. A *standard* set of screening criteria are applied on a routine basis to all events above mb 3.5 in the Reviewed Event Bulletin (REB). In Section 1 we describe the event characterization parameters, the screening criteria, and numerical indication of the results.

We have also implemented and tested capabilities at the PIDC to compare events to respective regional event populations using high-frequency (e.g., > 4 Hz) regional amplitude ratios, Pn/Lg and Pn/Sn. Additional work is needed to further quantify region-specific distance dependence and other subregional effects before this analysis can be made operational. We describe the procedure in Section 1 and provide results of applications to some interesting events in Sections 4 and 5.

Second, we have assessed the performance of the screening criteria for all events above mb 3.5 in the REB for 1996 and 1997. During this two-year period there were over 30,000 such events, including two known underground nuclear tests at the Lop Nor test site in China. We have also applied the screening criteria to 45 and 48 historical underground nuclear explosions at the Nevada Test Site and Semipalatinsk, respectively, using data provided to us by Murphy (1998). In addition, we have made comparisons of the results using alternative screening criteria. The results, presented in Section 2, indicate that a significant percentage of events (e.g., about 77% of the events above mb 3.5) can be screened out by the rather conservative criteria considered and none of the 95 known explosions were screened out. Significant improvements in the percentage of events that can be screened out are expected once the screening analyses based on regional seismic data are more fully implemented and as the IMS seismic network is completed.

Third, we have implemented interactive capabilities for custom event-screening that are available on the PIDC World Wide Web site. These on-line capabilities allow remote users to specify and apply their own event selection and screening criteria, as well as view and download the results of the analyses. These capabilities and the data products are described by Fisk et al. (1996a). Carlson and Fisk (1998) provide a user's guide for these capabilities.

Fourth, we have quantified the uncertainties of magnitude (mb and Ms) estimates, including the dependence of the uncertainties on the number and the coverage of stations used in obtaining the magnitude estimates. This work is described by Bottone et al. (1996).

Fifth, we have estimated preliminary region-specific distance corrections for regional seismic amplitude ratios, Pn/Lg and Pn/Sn in the 2-4, 4-6 and 6-8 Hz bands, for the existing IMS seismic stations. Results of our initial work are described by Bottone et al. (1997). More recent results of progressive improvements to the distance corrections, using additional regional seismic data, a parametrization of the distance dependence which includes geometrical spreading and attenuation terms, and treatment of subregional effects, are described in Section 3 of this report.

Last, we have performed in-depth regional analysis of some *interesting* events in the REB. These events include the two underground nuclear explosions on 8 June and 29 July 1996 at the Lop Nor test site in China, an event on 10 November 1996 in Southern India, and an event in the Kara Sea on 16 August 1997. The Lop Nor events are of interest because they provide rare cases with which to test the effectiveness of the seismic event-screening criteria with regard to not screening out simple underground explosions. The 96/07/29 Lop Nor explosion and the other events are of further interest because the depth and Ms:mb screening criteria cannot be applied, based on the available data; thus illustrating the need and utility of the regional analysis. In Section 4 we present results of event characterization analyses for the Lop Nor explosions and the event in Southern India. In Section 5 we present results of the analyses for the 97/08/16 Kara Sea event. (Note: This type of in-depth event analysis is not necessarily considered within the scope of the IDC but, rather, was performed as a contractor to the U.S. Department of Defense.)

Table of Contents

Table of Contents (Continued)

Figures

Figures (Continued)

Figures (Continued)

Figures (Continued)

Figures (Continued)

Figures (Continued)

Figures (Continued)

Figure Page

Tables

Section 1
Event-Screening Approach

In this section we describe the event characterization parameters that are currently being computed on a routine basis at the PIDC for seismic events in the Reviewed Event Bulletin (REB). We also describe the initial version of the *standard* seismic event-screening procedure, including definitions of the event categories, screening criteria, and numerical indication of the results.

1.1 Event-Characterization Parameters.

Here we provide the definitions of seismic event-characterization parameters, in accordance with Annex 2 of the CTBT Protocol, that are currently being computed and tested at the PIDC. (The processing capabilities to compute these parameters were implemented by other contractors.)

1.1.1 Focal Depth and Epicentral Location.

Hypocentral inversion is performed as an iterative non-linear least-squares inversion of travel time, azimuth and/or velocity measurements (see GSE/CRP/243, Vol. 2, Appendix E). The event location and depth, confidence bounds, and residuals are estimated using these measurements from stations at regional and teleseismic distances. If the depth becomes negative for several iterations, the depth estimate is fixed at zero. (The analyst can also constrain the depth estimate to the surface.) The IASPEI91 travel time curves are used as the global standard travel time curves for event location. Where available, regional travel time curves can be incorporated into the analysis.

Error estimation involves determining event error ellipsoid and normalized confidence regions, utilizing the procedure of Jordan and Sverdrup (1981), where the error analysis can be represented as a combination of *a priori* and *a posteriori* distributions, through control of two input parameters, namely, the number of degrees of freedom, *num_dof*, and an *a priori* scale variance factor, *est_std_err* (Bratt and Bache, 1988). Given the covariance matrix of the hypocentral estimate, the error ellipsoid and confidence regions are calculated from the appropriate marginal variances, based on the F-distribution. The default uses *est_std_err* of 1.0 and *num_dof* equal to infinity. In this limit, the F-distribution becomes a chi-squared distribution. The default confidence level is 0.90, which may be modified to other confidence levels between 0.0 and 1.0. The following parameters are estimated:

- The two-dimensional confidence error ellipse of the epicenter, as determined from the 2x2 covariance matrix of the epicenter (marginal with respect to origin time and depth).

- The one-dimensional confidence interval of focal depth, as determined from the scalar variance of the focal depth (marginal with respect to origin time and epicenter).

1.1.2 Body Wave Magnitudes (mb).

Body wave magnitudes, mb, are computed from amplitude and period measurements of associated P phases (GSE/CRP/243, Vol. 2, Appendix F). The network-average magnitude is based on station magnitudes for each station with the first associated arrival either P, Pn, or Pg; and it must have unclipped amplitude and period data. Station magnitudes are calculated with the standard formula:

$$\mathrm{mb} = \log_{10}(A/T) + B(D, z) + S\,, \tag{1}$$

where A is the amplitude, T is the period, S is a station correction term, and the distance corrections, $B(D, z)$ of Veith and Clawson (1972) are used. The network-average magnitude is the weighted mean of the station magnitudes. Weights are inversely proportional to the sum of the variances for the station magnitudes, station noise, and station corrections. Station corrections and noise are stored in the *siteaux* table of the PIDC database. Error in the network-average mb estimate is computed assuming a normal distribution of the station magnitude estimates.

1.1.3 Surface Wave Magnitudes (Ms).

The computation of surface wave magnitudes, Ms, are carried out in a manner similar to that used for the mb calculations. The error is also estimated in a similar way. The formula for Ms station magnitudes is the "Prague formula" of Vanek et al. (1962):

$$\mathrm{Ms} = \log_{10}(A/T) + 1.66 \log_{10}(D) + 0.3\,. \tag{2}$$

where A is the instrument-corrected zero-to-peak amplitude (in nanometers) with period, T, between 18 and 22 seconds, and D is the distance. The arrival is also required to be within a velocity window of ±0.3 km/sec of the predicted arrival time based on a global dispersion model.

1.1.4 Teleseismic P-Wave Complexity.

The measure of complexity implemented at the PIDC follows the energy-ratio technique of Douglas (1980). In this method the coherent beam of the P signal is filtered in the band from 0.8 to 2.0 Hz, squared and smoothed with an exponential window (with a time constant of 1.5 sec). Complexity is then computed as the ratio of the area under the above curve in the *signal_len2* seconds after the P signal to the area in the *signal_len1* seconds of the P signal (S), both corrected for background noise (N). Under the current default, *signal_len1* = 5 and *signal_len2* = 30, and

$$Complexity = \frac{S(5-35\,\text{seconds}) - N}{S(0-5\,\text{seconds}) - N}, \quad (3)$$

with the exception of the following two cases:

- If $S(0–5\ \text{sec}) - N < 0$, complexity is undefined and so is set to -1;
- If $S(5–35\ \text{sec}) - N \leq 0$, all energy is in the first 5 sec, so complexity is set to 0.0.

Complexity is measured only for stations that are associated to an event and are at teleseismic distances (30-90 degrees). If a PcP phase is observed within 35 sec of P, no measurement is made. The complexity measurements are stored in the *complexity* table of the PIDC database.

1.1.5 Regional Phase Time-Domain Amplitudes.

The Detection and Feature Extraction (DFX) code at the PIDC can compute time-domain amplitude measurements on a variety of beams for specified time windows. Amplitude measurement types include absolute maximum amplitude, maximum peak-to-trough, maximum peak-to-peak, RMS amplitude, etc. Beam types include coherent, steered, incoherent, and RMS measured on vertical, radial, or transverse components. Time intervals for the measurements can be based on predicted travel times of seismic phases, or on fixed group velocity windows, or they may be computed from observed arrival times in the database.

Currently, the following time-domain regional phase amplitude measurements are computed for each station that is associated to and within 20 degrees of an event:

a) Absolute maximum amplitude on 2-4, 4-6, 6-8, 8-10 Hz RMS beams for predicted time and/or velocity windows around Pn, Pg, Sn, Lg phases:

Pn:	8s before the theoretical arrival time of Pn to a group velocity of 6.4 km/s
Pg:	6.3 to 5.8 km/s group velocity
Sn:	5s before the theoretical arrival time of Sn and a 20s duration
Lg:	3.7 to 3.0 km/s group velocity

b) Absolute maximum amplitude on 2-4, 4-6, 6-8, 8-10 Hz RMS beams for predicted time and/or velocity windows around pre-Pn, pre-Pg, pre-Sn, and pre-Lg noise:

Pre-Pn:	13s before the theoretical arrival time of Pn and a 5s duration
Pre-Pg:	6.4 to 6.3 km/s group velocity
Pre-Sn:	10s before the theoretical arrival time of Sn and a 5s duration
Pre-Lg:	3.8 to 3.7 km/s group velocity

The instrument response correction at the center frequency is applied to all of the amplitude measurements. Also, amplitudes in the 8-10 Hz band are only calculated for stations with a Nyquist frequency > 10 Hz. These signal and noise amplitude measurements are stored in the *originamp* table of the PIDC database.

1.1.6 Short-Period/Long-Period Energy Ratio (SP/LP).

The SP/LP event-characterization parameter (e.g., Saikia et al., 1996) is the ratio of the integrated energy between the short-period (SP) vertical component P-wave train and the sum of the three long-period (LP) surface wave trains. The calculation of the energy ratio is restricted to 3-component broadband stations within 15 degrees of the event. The P-wave train is the filtered (1-8 Hz) time series between a group velocity of 8.2 km/s and 4.5 km/s, while the LP surface wave trains are the filtered (0.033 - 0.167 Hz) Z, N and E channel time series between a group velocity of 4.5 km/s and 2.5 km/s. SP/LP energy ratio values can be found in database table *splp*.

1.1.7 Spectral and Cepstral Measurements.

Spectral and cepstral analyses are performed on each associated regional phase within 20 degrees (Baumgardt and Zeigler, 1988). The following measurements are made and stored in the database:

(a) The variance of the detrended log spectrum of each associated regional phase is calculated for frequency bands with width 4.0 Hz and with SNR 3.0. The variance and the coefficients of the quadratic trend, removed from the log spectrum, are stored in table *spvar*.

(b) Amplitudes and quefrencies of all cepstral peaks with amplitudes above a default threshold of 0.032, that are not present in the preceding noise window, are calculated. A 5.0 sec window starting 0.3 sec before the time of the associated phase is used for the signal, and the preceding 5.0 sec window is used for the noise. Cepstral peaks are only declared if they are consistent (i.e., the same quefrency) among two or more phases at the same station. The maximum amplitude of the individual phase peaks for that station and the quefrency are stored in database table *ceppks*.

1.2 Screening Methodologies for Seismic Events.

Seismic event-screening criteria that are currently applied on a routine basis to the events in the REB are based on depth, Ms:mb, and location (to determine offshore events). Here we describe the screening methodologies based on these measurements. We also briefly describe the approach to compare events to regional event populations, based on Pn/Lg and Pn/Sn.

1.2.1 Screening Methodology based on Depth.

Given the depth estimate, $\hat{D}$, and its variance, σ_D^2, (*depth* and *szz* in the database schema) from the hypocentral inversion described above, the distribution of the square of the depth estimate (normalized to zero mean and unit variance) is obtained as the marginal distribution of the hypocenter estimate with respect to origin time and epicenter. This is a chi-squared distribution with one degree of freedom, which is equivalent to a normal distribution for the depth estimate. That is, $(\hat{D} - D)/\sigma_D$ has a normal distribution with zero mean and unit variance, where D is the true (unknown) depth. Under this assumption, a one-sided $100(1-\alpha)\%$ confidence interval for the depth, D, is $[\hat{D} - z_\alpha \sigma_D, \infty)$, where z_α is the α-percentile of the normal distribution with zero mean and unit variance. That is, z_α is defined such that $P[z > z_\alpha] = 1 - \Phi(z_\alpha) = \alpha$, where

$$\Phi(z) = \frac{1}{\sqrt{2\pi}} \int_{-\infty}^{z} dx e^{-x^2/2} = 1 - \frac{1}{\sqrt{2\pi}} \int_{z}^{\infty} dx e^{-x^2/2}. \quad (4)$$

An event is screened out at the $100(1-\alpha)\%$ confidence level if the shallowest part of the depth confidence interval is deeper than the depth threshold, i.e., if

$$\hat{D} - z_\alpha \sigma_D > D_0. \quad (5)$$

The *default* depth threshold is set at 10 km. For a confidence level of 97.5%, $z_\alpha = 1.96$.

1.2.2 Screening Methodology based on Ms:mb.

For an event for which there are both mb and Ms magnitude measurements, let N_b be the number of stations (*nsta* in the database schema) with mb measurements. The network average of mb, $\overline{m}_b$, is given by the sample mean of the N_b individual station magnitude measurements, $m_{b,i}$,

$$\overline{m}_b = \frac{1}{N_b} \sum_{i=1}^{N_b} m_{b,i}, \quad (6)$$

The network average of Ms, $\overline{M}_s$, is computed in a slightly more complicated manner. For a given station, j, let n_j be the number of elements at a station which measured Ms and let N_s be the total number of stations measuring Ms. The station average, $M_{s,j}$, is given by the sample mean of the n_j values of Ms at station j, and the network average of Ms is given by

$$\overline{M}_s = \frac{1}{N_s} \sum_{j=1}^{N_s} M_{s,j}. \quad (7)$$

The network-average estimate of *Amb–Ms* is then taken to be $A\overline{m}_b - \overline{M}_s$, where A is a constant slope term to account for possible magnitude dependence of the Ms:mb relation.

The standard deviations for the individual mb and Ms measurements are currently taken to be $\sigma_b = \sigma_s = 0.3$, independent of the value of mb or Ms. This is an upper bound of the standard deviations estimated by Bottone et al. (1996). The variance of the mean of N_b independent measurements of mb is given by σ_b^2/N_b, with a similar expression for Ms. The variance of $A\bar{m}_b - \bar{M}_s$, denoted by σ_M^2, assuming that the mb and Ms measurements are uncorrelated, is

$$\sigma_M^2 = \text{variance}(A\bar{m}_b - \bar{M}_s) = A^2\frac{\sigma_b^2}{N_b} + \frac{\sigma_s^2}{N_s}. \tag{8}$$

Under the assumption that $A\bar{m}_b - \bar{M}_s$ has a normal distribution with variance σ_M^2, a one-sided $100(1-\alpha)\%$ confidence interval for *Amb–Ms* is $(-\infty, A\bar{m}_b - \bar{M}_s + z_\alpha\sigma_M]$. An event is screened out if this confidence interval is entirely less than a threshold, M_0, i.e., if it is entirely outside of the explosion population. Thus, an event is screened out if

$$A\bar{m}_b - \bar{M}_s + z_\alpha\sigma_M < M_0. \tag{9}$$

Marshall and Basham (1972) have suggested a threshold of *mb–Ms* = 1.2, based on historical explosion and earthquake data. After careful calibration of PIDC magnitudes, relative to historical data, Murphy (1997) recommends that a threshold of *1.25mb–Ms* = 2.20 be used at the PIDC. Testing of both of these criteria, using a 97.5% confidence level, is described in Section 2.

1.2.3 Numerical Indication of the Screening Results.

The CTBT Protocol states that, "The standard event bulletin shall indicate numerically for each event the degree to which that event meets or does not meet the event-screening criteria." In light of this requirement, probabilities are computed to indicate the degree to which the depth and Ms:mb estimates are inconsistent with possible values from a shallow explosion source, accounting for the uncertainties in the estimates. An alternative representation of the probabilities in terms of a screening "score" is also presented.

The screening criterion for depth in Equation (5), in terms of the depth confidence interval, is equivalent to performing a test of hypothesis. That is, under the null hypothesis that the true depth, D, is less than or equal to a threshold depth, D_0, the probability of obtaining an estimate, $\hat{D}$, deeper than some fixed depth, $\underline{D}$, given the standard deviation, σ_D, is $P[\hat{D} > \underline{D} | D_0, \sigma_D] = 1-\Phi(\hat{x})$, where $\hat{x} = (\underline{D} - D_0)/\sigma_D$ and $\Phi(\cdot)$ is defined in Equation (4). Thus, if the measured value of the depth is $\hat{D}_1$, the hypothesis that the true depth of the event was less than or equal to D_0 may be rejected at the α significance level if $P[\hat{D} > \hat{D}_1 \,|\, D_0, \sigma_D] \le \alpha$ or, equivalently, if

$$P_{depth} \equiv P[\hat{D} < \hat{D}_1 \,|\, D_0, \sigma_D] = \Phi(\hat{x}) > 1 - \alpha . \tag{10}$$

Note that $P[\hat{D} > \hat{D}_1 \,|\, D_0, \sigma_D]$ is referred to as the "p-value" in the statistics literature and P_{depth} is its complement. An equivalent "score" for the depth screening criterion may also be defined as

$$SCORE_{depth} = (\hat{D}_1 - D_0)/z_\alpha \sigma_D - 1 = \hat{x}/z_\alpha - 1 . \tag{11}$$

Note that a positive *score* corresponds to $P_{depth} > 1 - \alpha$ and a one-sided $100(1-\alpha)\%$ confidence interval for depth entirely deeper than D_0. For a one-sided 97.5% confidence interval, $z_\alpha = 1.96$. Thus, the *score* increments by one for an increment of roughly two-sigma from the decision line.

In this analysis we assume that the errors are distributed according to a Gaussian (normal) distribution for positive depths, with zero probability for values above the ground. (Recall from Section 1.1.1 that negative depth estimates are constrained to the surface.) We also assume that the variance is independent of depth and that the value *szz* used for σ_D^2 sufficiently represents the true uncertainty. In the future we hope to verify or, if necessary, improve on these assumptions.

Similarly, the probability of obtaining an estimate of *Amb-Ms*, $\hat{M}$, less than some fixed value, $\underline{M}$, given that the true value is at the threshold value, M_0, and that the standard deviation is σ_M, is given by $P[\hat{M} < \underline{M} | M_0, \sigma_M] = 1 - \Phi(\hat{y})$, where $\hat{y} = (M_0 - \underline{M})/\sigma_M$. Thus, if a measurement of *Amb-Ms* is $\hat{M}_1$, the null hypothesis that the true value of *Amb-Ms* is greater than or equal to M_0 may be rejected at the α significance level if $P[\hat{M} < \hat{M}_1 \,|\, M_0, \sigma_M] \le \alpha$ or, equivalently, if

$$P_{mbms} \equiv P[\hat{M} > \hat{M}_1 \,|\, M_0, \sigma_M] = \Phi(\hat{y}) > 1 - \alpha . \tag{12}$$

An equivalent "score" for the Ms:mb screening criterion may also be defined as

$$SCORE_{mbms} = (M_0 - \hat{M}_1)/z_\alpha \sigma_M - 1 = \hat{y}/z_\alpha - 1 . \tag{13}$$

Assuming the depth and Ms:mb estimates are approximately independent (which is valid under the null hypothesis that the event is shallow), the combined probability that a shallow ($D \le D_0$) explosion would have given a depth measurement greater than or equal to $\hat{D}_1$ *and* a measurement of *Amb-Ms* less than $\hat{M}_1$ is given by $P = P[\hat{D} > \hat{D}_1 \,|\, D_0, \sigma_D] \cdot P[\hat{M} < \hat{M}_1 \,|\, M_0, \sigma_M]$. (It is straightforward to modify this expression to treat the correlation between the depth and Ms:mb, if the correlation is quantified.) This relation can be used to test the hypothesis that the event could be a shallow explosion, based on depth and Ms:mb. If the hypothesis is rejected, the event would be screened out. The complement of this relation is given by

$$P_{combined} = 1 - (1 - P_{depth})(1 - P_{mbms}) . \tag{14}$$

An equivalent "score" for the combined depth and Ms:mb screening criteria may also be defined as

$$SCORE_{combined} = \hat{z}/z_{\alpha} - 1 . \tag{15}$$

where $\hat{z}$ is determined from the expression $P_{combined} = \Phi(\hat{z})$.

The expressions for P_{depth}, P_{mbms}, and $P_{combined}$ are used to numerically indicate the screening results. Each can have possible values between 0 and 1, with a value of 0 corresponding to the measurements entirely within the possible explosion range and a value of 1 corresponding to the measurements entirely outside of the possible explosion range, accounting for the uncertainties. These expressions can be generalized to an arbitrary set of event-screening criteria.

1.2.4 Screening Methodology based on Location.

Location confidence ellipses are being used on an interim basis to categorize offshore events until additional IMS hydroacoustic stations are on-line and hydroacoustic event-screening capabilities are further developed at the PIDC. An onshore/offshore grid (including islands) with one-degree resolution is currently used. The 90% location confidence ellipse, obtained from the hypocentral inversion, must not touch or contain any "onshore" cells for an event to be categorized as offshore. The percentage of offshore grid cells enclosed or touching the ellipse, *pct_offshore*, is computed. The grid, confidence ellipses, and results of applications are illustrated in Section 2.2.

1.2.5 Screening Methodology for Regional Seismic Events.

The screening methodology for regional seismic events is based on the likelihood-ratio outlier test, as described in detail by Fisk et al. (1996b). The analysis utilizes high-frequency Pn/Lg and Pn/Sn measurements, described above, to compare events to the relevant regional event population. The p-value of the hypothesis test is used to numerically indicate the screening result. The methodology has been implemented and tested on a developmental basis at the PIDC (e.g., Fisk et al., 1996a). Further work is needed to establish regional distance corrections and grids of regional phase blockage before this analysis is ready to be integrated into operations at the PIDC.

1.3 Initial Version of the Seismic Event-Screening Procedure.

We now describe the initial version of the *standard* event-screening procedure that was applied to all REB events on a routine daily basis during 1997, including definitions of the event categories, the explicit screening criteria, the input data and parameters, and the output.

1.3.1 Category Definitions and Event-Screening Criteria.

Table 1 defines the categories and experimental event-screening criteria, based on location, depth and Ms:mb, that were applied on a routine basis to all events in the REB for 1997. Events below mb 3.5 are not considered for the screening analyses because the screening criteria that are currently used are typically applicable to events that are large enough so that depth and mb–Ms measurements can be obtained, and because the existing screening criteria do not include capabilities to screen out chemical mining blasts, which are typically smaller than mb 3.5.

Events with 90% location confidence ellipses that are not entirely offshore, and for which mb–Ms and unconstrained depth estimates are not available, fall in the insufficient data category, a subset of those events that are not screened out. Events with location confidence ellipses that are entirely offshore and with constrained depths and no mb–Ms are placed in a separate category, "Offshore Only". These could be considered as offshore events with insufficient data.

Table 1. Seismic event-screening categories and criteria.

Category	Criteria
Not Considered	• mb < 3.5
Insufficient Data	• 90% location error ellipse not entirely offshore and • depth constrained to the surface and no mb–Ms
Offshore Only	• 90% location error ellipse entirely offshore and • depth constrained to the surface and no mb–Ms
Screened Out	• 97.5% confidence interval for depth > 10 km or • 97.5% confidence interval for mb–Ms < 1.2
Not Screened Out	• 90% location error ellipse is not entirely offshore and • 97.5% confidence interval for depth not > 10 km and • 97.5% confidence interval for mb–Ms not < 1.2

Note that the one-sided 97.5% confidence intervals are equivalent to the two-sided 95% confidence intervals that have been utilized and reported on previously. Also, as of 1 January 1998, the Ms:mb screening criterion is 1.25mb–Ms < 2.20, as recommended by Murphy (1997). Other changes to these provisional event-screening criteria may also be made in the future, based on recommendations by Working Group B of the CTBT Preparatory Commission.

1.3.2 Input Data and Parameters.

Table 2 provides a list of the data used in the existing version of the event-screening code, as well as the database tables in which they are stored and their descriptions. These data are obtained from the *IDCREB* database account, after the seismic analysts have completed their review of the events.

Table 3 lists the input parameters to this version of the code, their default values (used during 1997) and descriptions. The parameter, *ldpflg*, can be set to *true* to require that one or more depth phases be detected for the depth screening analysis to be applied. The parameter, *nsta0*, is the minimum number of stations required to have Ms measurements for the Ms:mb screening criterion to be applied. The user may also specify a custom rectangular region and time interval of interest.

Table 2. Input data to the event-screening procedure.

Attribute Name	Database Table	Attribute Description
lat	*origin*	estimated latitude
lon	*origin*	estimated longitude
depth	*origin*	estimated depth
time	*origin*	epoch origin time
orid	*origin, origerr*	origin identification number
ndp	*origin*	number of depth phases detected
mb	*origin*	body wave magnitude
mbid	*origin, netmag*	mb magnitude identifier (magid)
ms	*origin*	surface wave magnitude
msid	*origin, netmag*	ms magnitude identifier (magid)
smajax	*origerr*	semi-major axis of location error
sminax	*origerr*	semi-minor axis of location error
strike	*origerr*	strike of semi-major axis
szz	*origerr*	variance of depth estimate
nsta	*netmag*	number of stations used in magnitude estimates (corresponding to magid = mbid and magid = msid)

Table 3. Input parameters to the event-screening procedure.

Parameter	Default Value	Description
confloc	0.90	confidence level for the location error ellipse
confdep	0.975	confidence level for the depth criterion
confmbms	0.975	confidence level for the Ms:mb criterion
depth0	10.0	depth threshold in km
ambms0	1.2	threshold for (*A mb – Ms*)
amb_cal	1.0	slope (*A*) of the (*A mb – Ms*) relation
mb0	3.5	magnitude (mb) cut-off for considered events
ldpflg	F	logical flag to require depth phases
nsta0	1	Minimum number of stations required for Ms

1.3.3 Output Data.

The following computed quantities for each event are the output of the event-screening code: P_{depth}, P_{mbms}, $P_{combined}$; as defined in Section 1.2.3; *pct_offshore*, as defined in Section 1.2.4; and the *Category*, as defined in Table 1. The numbers of events in each category are also compiled on a daily basis and provided as output to the Executive Summary (see Fisk et al., 1996a).

Section 2
Results of Experimental Testing at the Prototype IDC

2.1 Introduction.

Here we describe results of experimental testing of the event-screening capabilities at the PIDC. First, we apply a "standard" set of screening criteria to all events in the REB during 1997, and summarize the results. Second, we apply alternative screening criteria for depth and Ms:mb to the events in the REB during 1996 and 1997, and compare the results to those obtained using the *standard* criteria. During this two-year period there were over 30,000 events in the REB above mb 3.5, including two known underground explosions at the Lop Nor test site in China. We also apply the screening criteria to 45 and 48 historical nuclear explosions at the Nevada Test Site and Semipalatinsk, respectively, using data provided to us by Murphy (1998). Third, we compute the screening probabilities and scores (as defined in Section 1.2.3) for these events and describe the results. Last, we provide some conclusions and recommendations.

2.2 Event-Screening Performance Summaries.

Figure 1 shows a map of the existing IMS primary stations (squares) and the screening results for 20094 REB events during 1997. Event markers are color-coded by screening category as defined in the legend. Most of the events below mb 3.5, that were detected by the existing IMS network, occurred in Scandinavia, the U.S., western South America, or Australia, where the network density is relatively high. The majority of events that were not screened out or had insufficient data occurred along the Pacific Rim, in Southern Europe or Central Asia, where a high percentage of the events occur and, in some cases, where the network density is relatively sparse presently.

Figure 2 summarizes the numbers (upper plot) and percentages (lower plot) of events in each screening category per month for all of 1997, based on the screening criteria in Table 1 (above). There were typically between 1400 and 2100 events in the REB per month (black bars), based on the existing IMS seismic network. About 76% to 83% of these events were $mb \geq 3.5$ (cyan bars).

To illustrate how the results depend on event magnitude, Figure 3 shows the percentages of events per month by screening category relative to the number of events above mb 3.5 (upper plot) and above mb 4.5 (lower plot). The upper plot in Figure 3 indicates that, as of 1 May 1997, between 74% to 77% of the events above mb 3.5 were screened out, roughly 18% to 23% have insufficient data with which to perform the screening analyses, and approximately 4% were not screened out based on the experimental screening criteria. The lower plot in Figure 3 indicates that, as of 1 May

1997, between 88% to 98% of the events above mb 4.5 were screened out, roughly 3% to 10% have insufficient data with which to perform the screening analyses, and approximately 3% or less were not screened out based on the current screening criteria.

Note that three events in the "insufficient data" category during 1996 and 1997 were a 96/07/29 Lop Nor explosion, an event in Southern India on 96/11/10, and an event in the Kara Sea on 97/08/16. None of these events were screened out; however, these cases illustrate the need for screening analyses based on regional data, as described further in Sections 4 and 5.

The upper plot in Figure 4 shows more detailed dependence of the screening results on mb for the REB events during JUL-DEC 1997. The solid black line depicts the total number of REB events during this period. The cyan curve indicates the cumulative number of events above the given mb level. The solid blue, red and green curves depict the cumulative numbers of events versus mb with insufficient data, that were not screened out, and that were screened out, respectively. The dashed and dotted curves indicate the cumulative numbers of events that were screened out by the individual depth and mb–Ms criteria, respectively. The intermittent dotted-dashed curve indicates the cumulative numbers of events that were screened out by the depth and/or mb–Ms criteria.

In the lower plot in Figure 4, the cumulative numbers have been converted to percentages, relative to the total number of events above a given magnitude. This plot indicates that about 77% of the events above mb 3.5 and about 91% of the events above mb 4.5 were screened out. It also depicts decreasing percentages of events that are not screened out or have insufficient data as functions of increasing mb. The dashed and dotted curves indicate that about 31% and 24% of the events above mb 3.5 can be screened out by depth and mb–Ms, individually, while about 46% of those events can be screened out by depth and/or mb–Ms, with increasing percentages with increasing mb. The gap between the total percentage of events screened out and the percentage of events screened out by depth and/or mb–Ms corresponds to events that were offshore at the 90% confidence level.

Table 4 lists the numbers and percentages of events screened out by all combinations of individual and combined depth and mb–Ms screening criteria for the REB events during 1997. Of the 20094 events, 15998 (80%) were mb 3.5, of which 8017 (50%) had mb–Ms and/or unconstrained depth estimates for which at least one of the depth and mb–Ms screening criteria could be applied.

Table 4. Numbers and percentages of 1997 REB events (above mb 3.5) screened out by all combinations of individual and combined depth and mb-Ms screening criteria.

Screening Criteria	Number Available	Number Screened	Percentage of Available	Percentage of mb 3.5
depth	5641	4734	84%	30%
mb–Ms	4079	3347	82%	21%
depth AND mb–Ms	1703	1221	72%	7%
depth OR mb–Ms	8017	6860	86%	43%

The results in Table 4 indicate that using the criteria for depth or for mb–Ms, 43% of all events above mb 3.5 can be screened out, while only 7% can be screened out if events must satisfy both the depth and mb–Ms criteria. This result is to be expected since deep seismic events typically do not have large, if any, detectable long-period surface waves. Thus, it would be very ineffective, in terms of screening out events, to require that both the depth and mb–Ms criteria be satisfied.

The *offshore-location* screening algorithm (cf. Section 1.2.4) has also been tested. Figure 5 illustrates the grid and results for events near Australia. The markers and 90% error ellipses in green or red correspond to events that are categorized as offshore or not offshore, respectively. Many of the events with large error ellipses were not screened out because they touch or contain "onshore" grid cells.

For 8152 REB events ($mb \geq 3.5$) that occurred between July and December 1997, 4743 events (58%) were categorized as offshore, and 2238 of these events (27%) had constrained depths and no Ms. These 2238 events are placed in the "Offshore Only" category, i.e., offshore events with insufficient data to apply the seismic depth and Ms:mb screening criteria. In the future, we plan to develop hydroacoustic event-screening criteria for application to such events.

2.3 Comparison of Alternative Screening Criteria.

In addition to the criteria in Table 1 (above), other screening criteria for depth and Ms:mb were tested using the REB events for 1997 with $mb \geq 3.5$. First, alternative depth criteria were tested using 5641 events with unconstrained depth estimates. Requiring that the 99% confidence interval for depth be deeper than a 20 km threshold, 3517 events are screened out, while 4300 events are screened out using a 99% confidence interval and a 10 km threshold. For comparison, 4734 events

are screened out using a 95% depth confidence interval and a 10 km threshold. This illustrates the dependence of the screening results on the thresholds and confidence levels that are used.

Figure 6 shows a comparison of two different Ms:mb criteria for all REB events with $mb \geq 3.5$ and Ms for 1996 (2105 events; upper plots) and 1997 (4079 events; lower plots). The increase in the number of such events for 1997 is due to an improved procedure for detecting long-period surface waves that was implemented early in 1997 (Stevens, 1997). The plots on the left correspond to a screening criterion of requiring that the 95% confidence interval for mb–Ms is entirely less than 1.2, while the plots on the right correspond to a 95% confidence interval for 1.25mb–Ms entirely less than 2.20. The latter Ms:mb criterion is based on a careful calibration study by Murphy (1997), treating systematic differences between PIDC and NEIS magnitudes for historical explosions and earthquakes, as well as the dependence of the Ms:mb screening criterion on mb.

Under the two criteria, 1743 (82.8%) versus 1629 (77.4%) events for 1996, and 3347 (82.1%) versus 3242 (79.5%) events for 1997, were screened out, respectively. Included on both upper plots of Figure 6 are the Ms and mb values for the 96/06/08 Lop Nor explosion, which is not screened out by either criterion. In fact, in both cases the 99% confidence intervals are completely above the respective thresholds. Included on both lower plots of Figure 6 are the Ms and mb values for 45 and 48 historical nuclear explosions at NTS and Semipalatinsk, respectively. The magnitude data have been carefully calibrated by Murphy (1997) to be consistent with PIDC magnitude estimates. Note that none of the explosions were screened out by the latter Ms:mb criterion, while 5 of 93 explosions were screened out by the former criterion, as depicted by the magenta squares. Thus, although slightly fewer events were screened out by the latter Ms:mb criterion, the calibration work by Murphy (1997) and the results presented here indicate that it is more generally valid, in terms of not screening out explosions, over a wider range of PIDC magnitudes. Hence, the latter Ms:mb screening criterion, $1.25mb–Ms < 2.20$, is being used as the experimental *standard* criterion at the PIDC, as of 1 January 1998.

2.4 Screening Probabilities and Scores.

Preliminary testing of the screening probabilities and scores, defined in Section 1.2.3, was also performed. Figure 7 shows scatterplots of depth versus (1.25mb–Ms) estimates for all 1996 (upper plot) and 1997 (lower plot) events above mb 3.5 in the REB. The circles depict events that are screened out at the 95% confidence level, while the triangles depict events that are not screened out. The 95% confidence intervals for two events, including the 96/06/08 Lop Nor explosion, are illustrated in the upper plot. Note that although some of the events have depth and/or Ms:mb

estimates that are in the "screened out" region of the plot, their uncertainties are large enough so that their 95% confidence intervals are not entirely in the "screened out" region.

Figure 8 shows histograms of the screening *probabilities* for REB events above mb 3.5, and with unconstrained depth and/or Ms estimates, for 1996 (upper) and 1997 (lower). The 96/06/08 Lop Nor explosion has the lowest probability, by far, of all the events during these two years. Note that although a significant fraction of events (about 16%) are not screened out by depth and/or Ms:mb, the probabilities indicate which events are the most inconsistent with natural seismic phenomena.

As an alternative numerical representation of the screening results, Figure 9 shows histograms of the screening *scores* for the same events. Included in the upper plot of Figure 9 is the *score* for the 96/06/08 Lop Nor explosion, which is the lowest *score* of all the events in the REB during 1996 and 1997. Included in the lower plot of Figure 9 are the *scores* for the 93 historical underground nuclear explosions at NTS and Semipalatinsk. Note that all of these explosions at Lop Nor, NTS and Semipalatinsk have negative screening *scores* and, hence, none were screened out.

2.5 Conclusions and Recommendations.

The experimental screening results presented here indicate that a significant percentage (about 77%) of the events above mb 3.5 can be screened out by the rather conservative criteria, based on depth, Ms:mb and offshore location, and none of the 95 explosions at Lop Nor, NTS and Semipalatinsk were screened out. About 20% of the events above mb 3.5 had insufficient data with which to apply these screening criteria. Three events in the "insufficient data" category during 1996 and 1997 were a 96/07/29 Lop Nor explosion, an event in Southern India on 96/11/10, and an event in the Kara Sea on 97/08/16. None of these events were screened out; however, these cases illustrate the need for screening analyses based on regional data. Significant improvements in the overall screening performance are expected as the IMS network is completed and once the screening analysis based on regional data is more fully implemented.

Screening analysis based on ratios of regional phase amplitudes (Pn/Lg and Pn/Sn) have also been implemented and tested. Applications to two Lop Nor explosions and other events of interest are described below in Sections 4 and 5. Fisk et al. (1996b) describe other applications to regional earthquakes and explosions. Similar regional analyses have been tested for the other IMS seismic stations; however, additional explosion data are needed before the performance can be more fully assessed. Also, further work is needed to establish regional distance corrections and grids of regional phase blockage before this analysis is ready to be integrated into operations at the PIDC.

Further evaluation of these screening procedures and criteria are needed, utilizing additional explosion data, in particular. To facilitate this evaluation, work is currently being conducted, in coordination with staff at the Australian NDC, to reprocess events in the *Nuclear Explosion Database* at the PIDC. Details of this database are provided on the PIDC Web site (http:// www.pidc.org) under the Data Products section. We plan to report on this work in the near future.

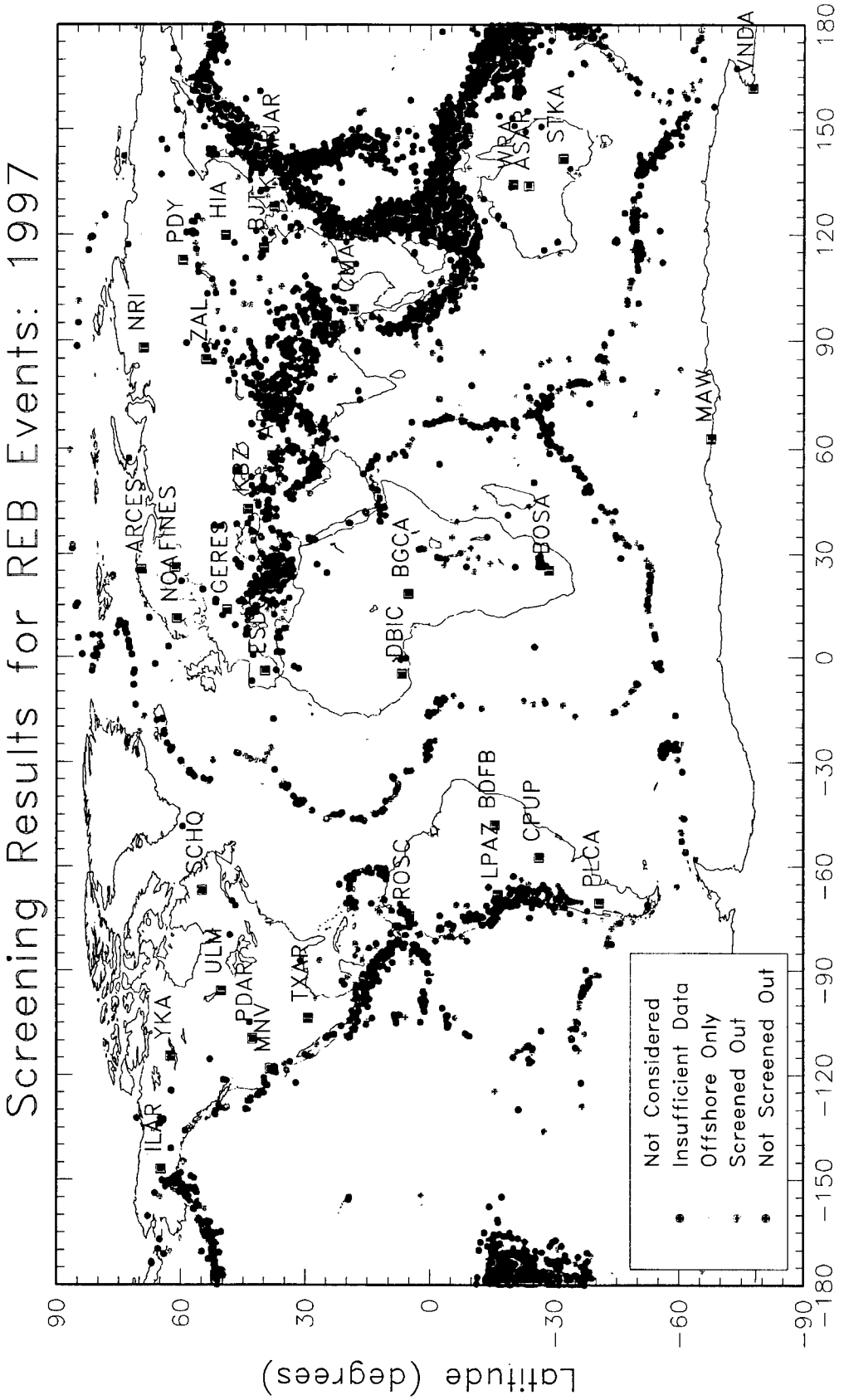

Figure 1. Map of the existing IMS primary seismic stations and the screening results for all 1997 REB events. Event markers are color-coded by screening category as defined in the legend.

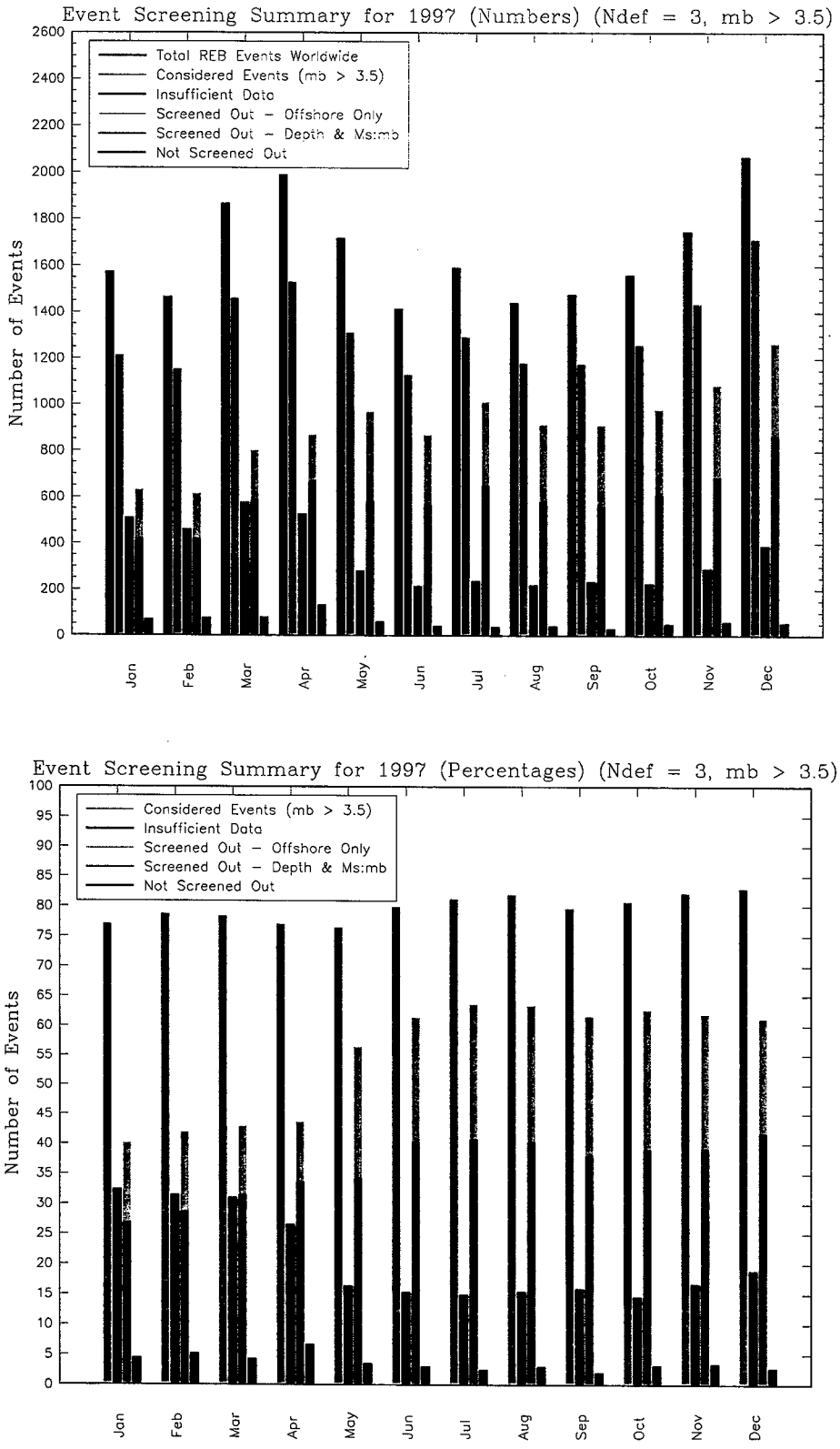

Figure 2. **Numbers (upper plot) and percentages (lower plot) of seismic events in the REB per month by screening category.**

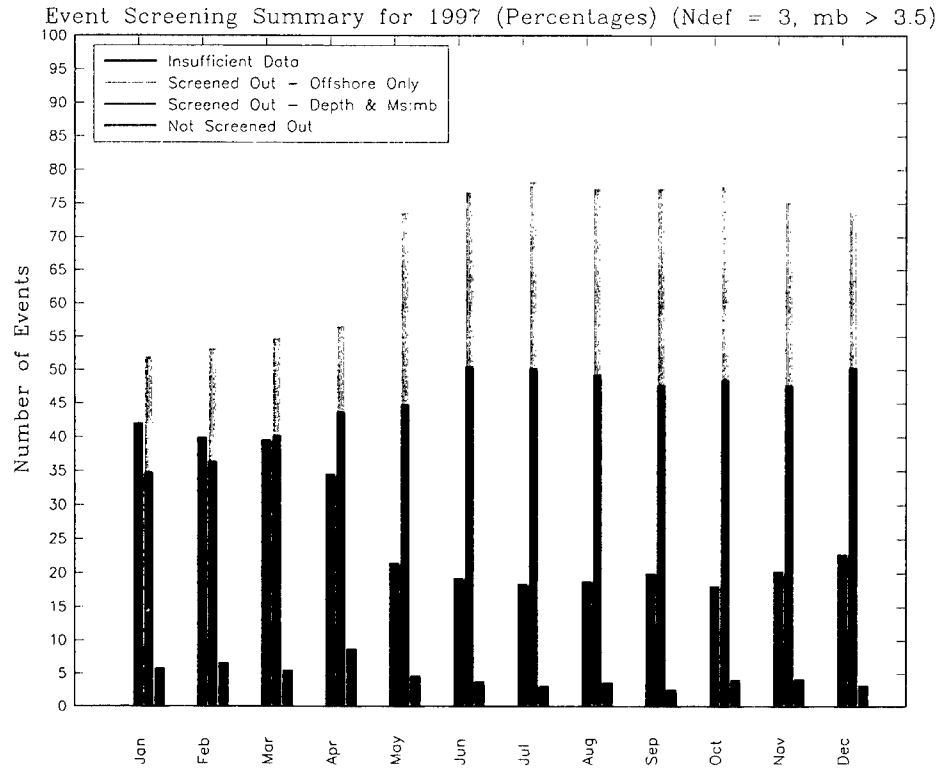

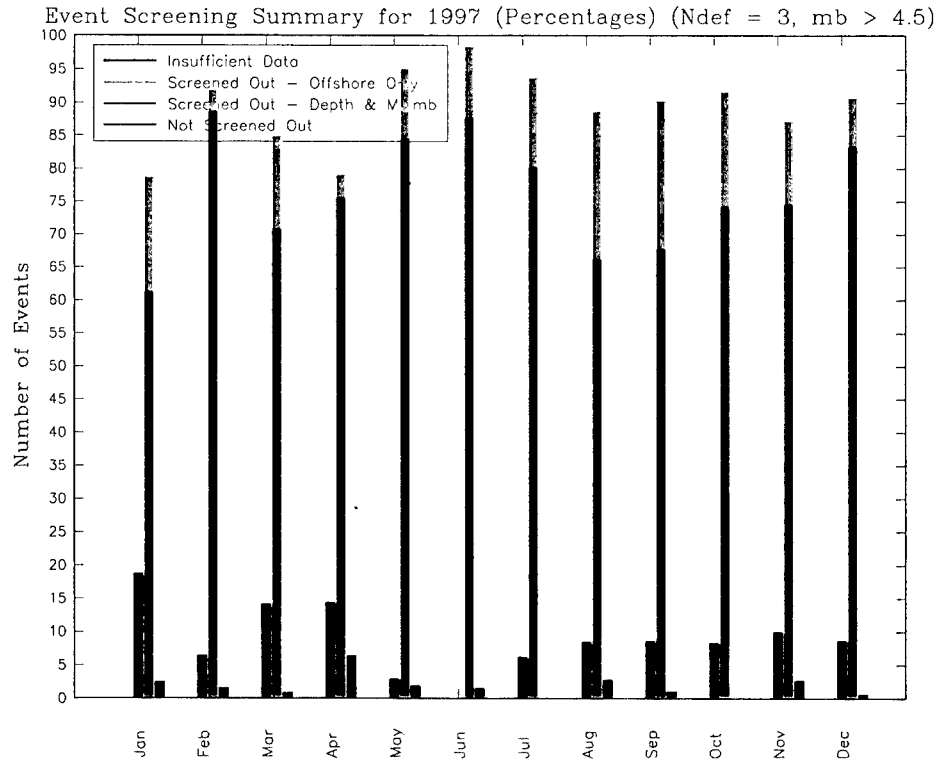

Figure 3. Percentages of seismic events in the REB per month by screening category relative to the number of events above mb 3.5 (upper plot) and above mb 4.5 (lower plot).

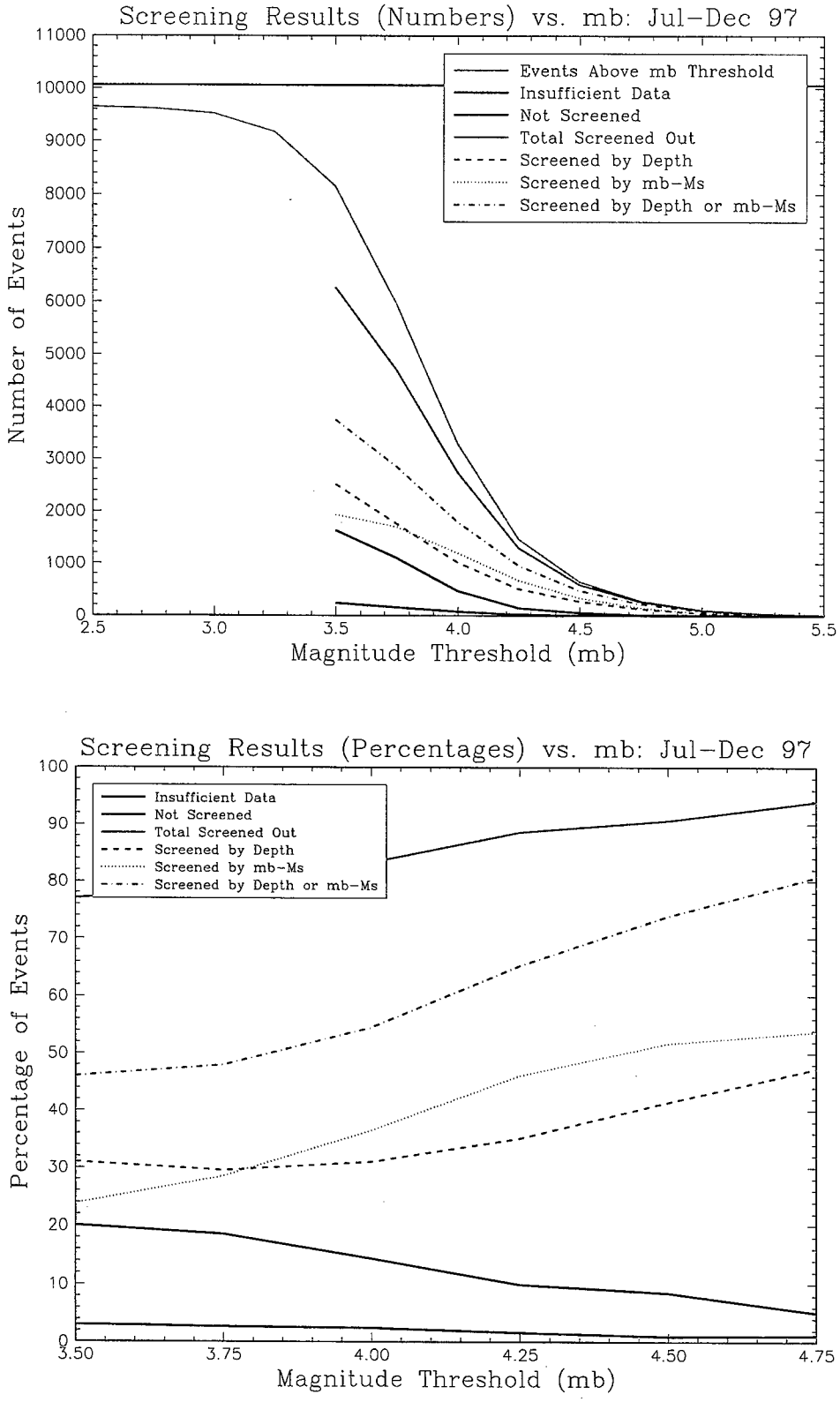

Figure 4. **Cumulative numbers (upper) and percentages (lower) of REB seismic events per screening category as functions of mb for July through December 1997.**

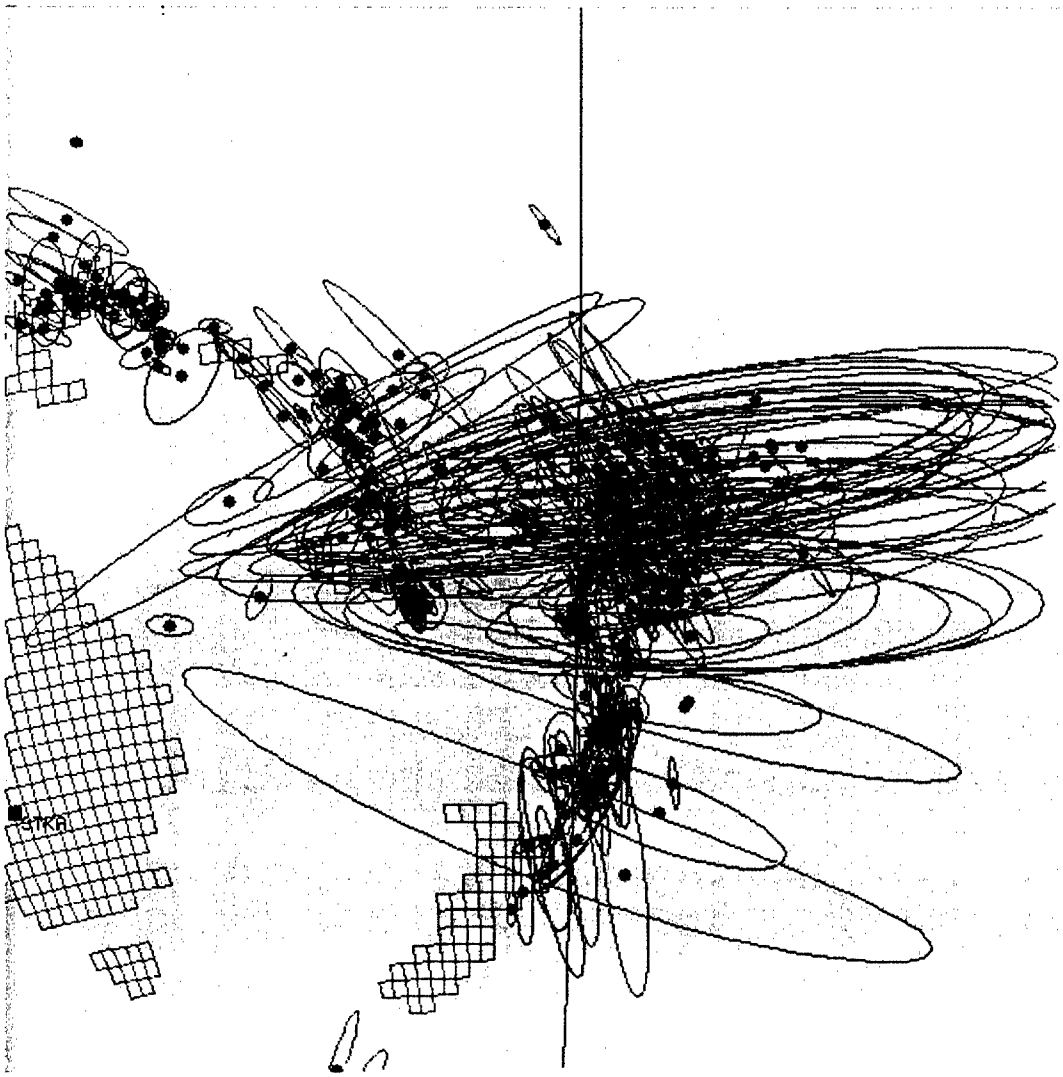

Figure 5. **Example of onshore/offshore location algorithm for REB events near Australia. The markers and 90% location error ellipses shown in green correspond to events that are categorized as offshore, while those shown in red are not.**

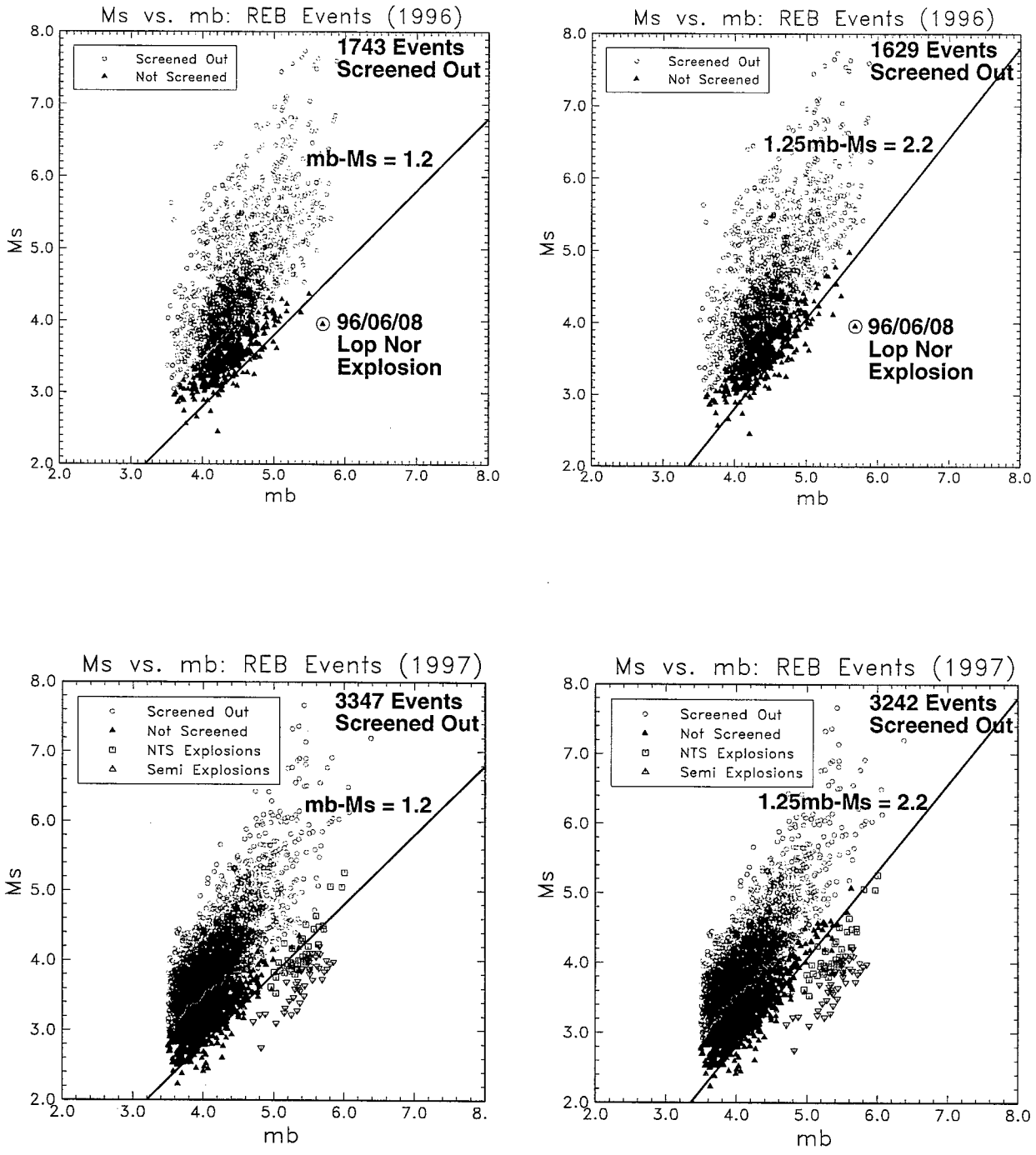

Figure 6. **Comparison of two Ms:mb screening criteria for 1996 (upper plots) and 1997 (lower plots). The plots on the left correspond to a screening criterion requiring that the 95% confidence interval for mb-Ms is less than 1.2, while the plots on the right correspond to a screening criterion requiring that the 95% confidence interval for 1.25mb-Ms is less than 2.2. Events that are screened out are depicted by green circles, while those that are not screened out are depicted by red triangles.**

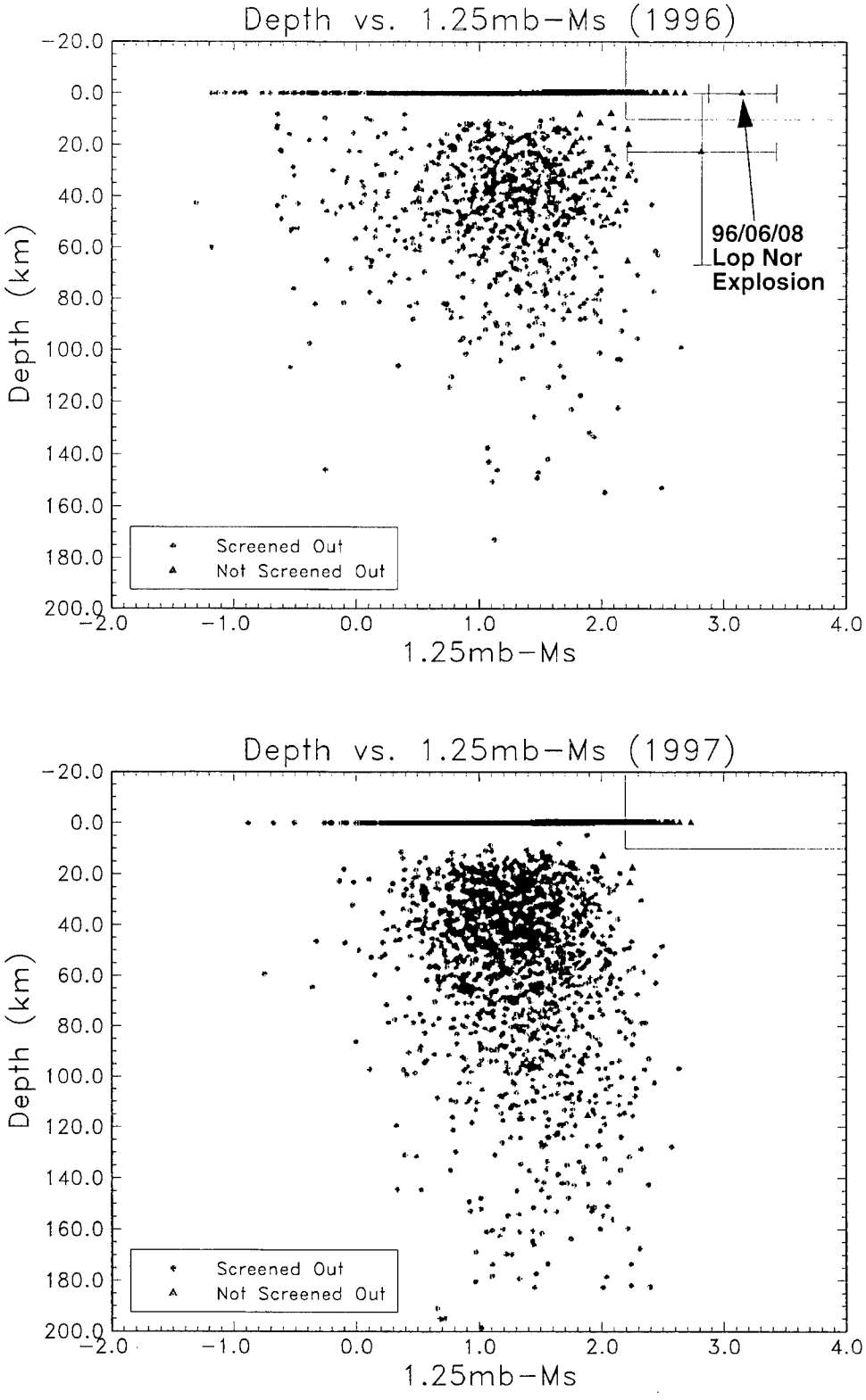

Figure 7. **Plots of depth versus Ms:mb estimates for all 1996 (upper plot) and 1997 (lower plot) events in the REB with mb above 3.5 and an estimate of Ms. The circles represent events that are screened out at the 95% confidence level, while the triangles represent events that are not screened out.**

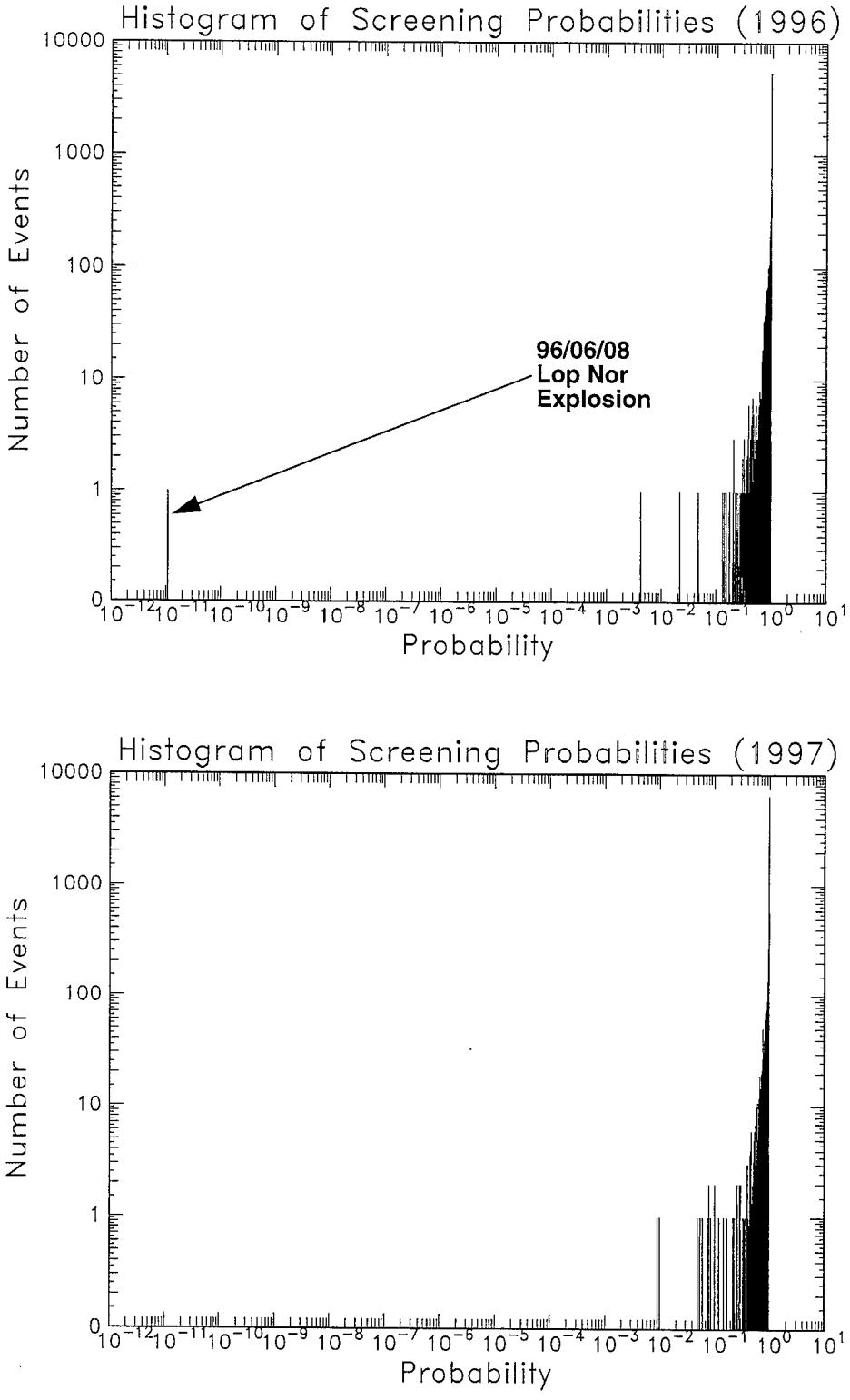

Figure 8. **Histogram plots of the combined probabilities for all REB events with mb above 3.5 and Ms and/or unconstrained depth estimates during 1996 (upper plot) and 1997 (lower plot). The 96/06/08 Lop Nor explosion has the lowest probability of all the events during these two years.**

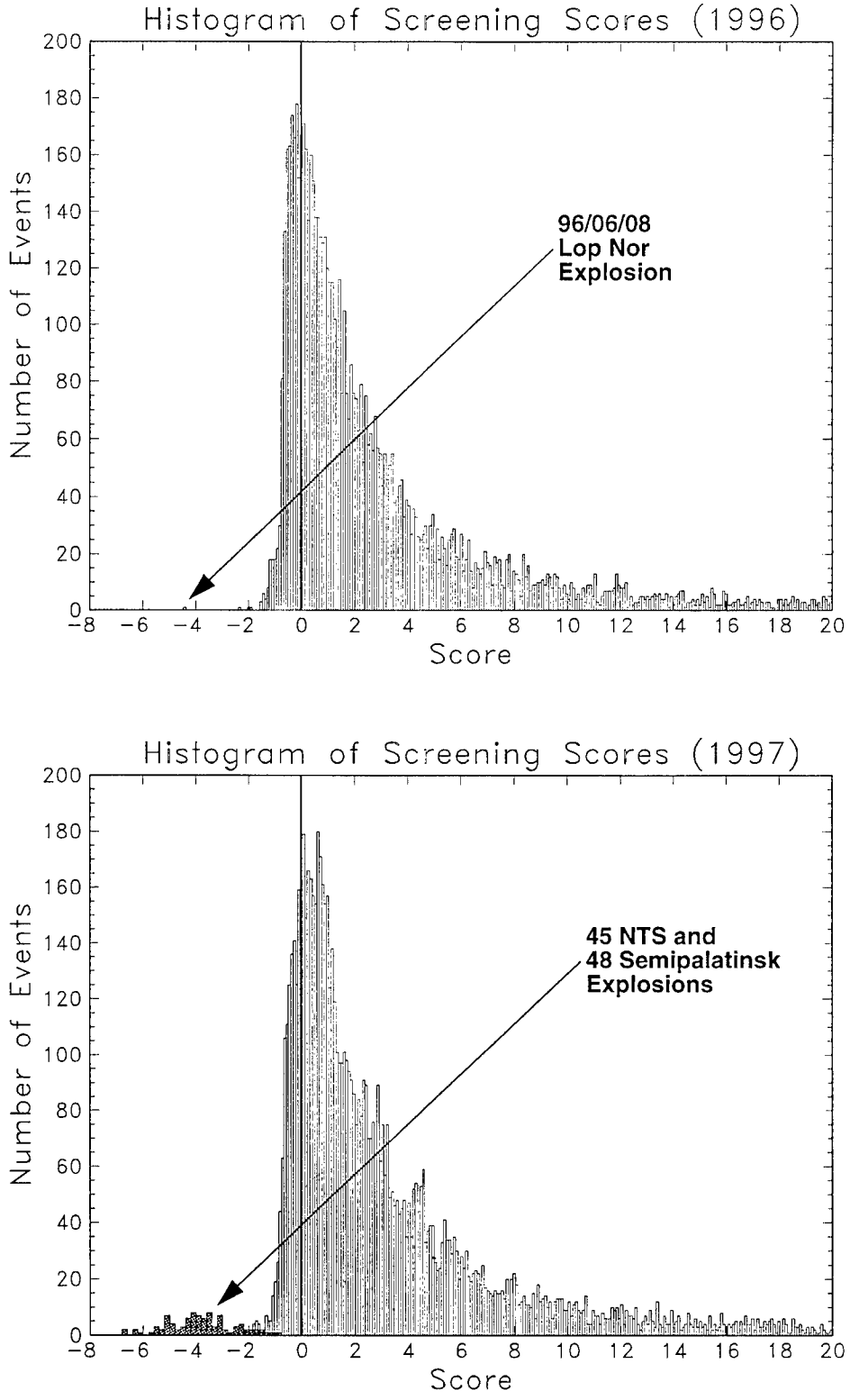

Figure 9. **Histogram plots of the combined scores for all REB events with mb above 3.5 and Ms and/or unconstrained depth estimates during 1996 (upper plot) and 1997 (lower plot). The 96/06/08 Lop Nor explosion has the lowest score of all the events during these two years.**

Section 3
Distance Corrections for Regional Amplitude Ratios

3.1 Introduction.

The importance and necessity of distance corrections for regional seismic amplitude ratios, in order to accurately characterize regional seismic events, are thoroughly discussed in previous reports (e.g., Bottone et al., 1997; Fisk et al., 1994, 1995, 1996b).

Bottone et al. (1997) described initial efforts to compute distance corrections for regional seismic amplitude ratios, Pn/Lg and Pn/Sn in 2-4, 4-6 and 6-8 Hz bands, for regions surrounding individual IMS seismic stations. The term "regional" denotes events within 20 degrees (2220 km) from a given station. In that work, a simple power-law distance relation was used to obtain least-squares fits to the regional data for each IMS station. In that study, the data used included regional events in the Reviewed Event Bulletin (REB) that had occurred between 10 September 1995 and 15 January 1997. The distance corrections for the individual stations were also categorized in terms of the number of available regional events with which to obtain the fits, as well as whether the distance corrections exhibited anomalous (or unexpected) behavior. Distance dependence with either negative slopes or with dramatically steep slopes were considered anomalous.

Here we present results of continuing efforts to quantify and improve the distance corrections for regional seismic amplitude ratios for the existing IMS seismic stations. In this work we utilize an improved parametrization of the distance dependence, including attenuation and geometrical spreading terms. It will be seen that the assumption of a simple power-law distance relation, used in the past, is too simplified to adequately fit the distance dependence over the entire range of regional distances. We also make use of additional regional seismic data, collected at the PIDC between 10 September 1995 and 1 October 1997. In this work, we further utilize more stringent restrictions on the quality of the data, in terms of the signal-to-noise ratio (SNR).

In the remainder of this section, we first provide descriptions of the regional seismic data that are used. We then describe the parameterization of the distance dependence and provide details of the worldwide-average fits for all of the regional data, collectively. In the following subsection, we use the same parameterization to obtain region-specific fits for each individual IMS station, which are compared to the worldwide-average fits. We then summarize the status of the regional distance corrections on a station-by-station basis. We then describe and illustrate two approaches of subregionalization, that have been considered by Rodgers et al. (1997) and Jenkins et al. (1996), to account for variations of path and subregional tectonic effects. Last, we provide conclusions and

recommendations based on this work. An appendix to this report provides further details regarding the distance corrections for the IMS seismic stations with adequate regional data.

3.2 IMS Regional Seismic Data.

For this analysis, we use all regional events above mb 3.5 in the REB between 10 September 1995 and 1 October 1997. The restriction to events above mb 3.5 is intended to avoid potential contamination from mining blasts. During that time period, there were 7,927 regional events recorded by the existing 87 IMS seismic stations (34 primary and 53 auxiliary) which have at least one of the six event characterization parameters, Pn/Lg and Pn/Sn in the 2–4, 4–6, and 6–8 Hz bands, measured with SNR for Pn greater than or equal to 2.0. A more stringent SNR cutoff of 2.0 for both P and S can also be used; here we follow Lay et al. (1997).

It should be noted that for distances less than about 100-300 km the regional Pn phase is not well defined (Richards, 1997). Currently the PIDC computes a quantity labeled as *Pn* by measuring the maximum amplitude in a group velocity window which corresponds to Pn for distances greater than about 300 km. (Section 1.1.5 of this report describes the regional phase amplitude measurements at the PIDC.) Pmax and Smax amplitude measurements, for distances up to 300 km, are planned to be implemented at the PIDC by March 1998 to alleviate the problem (Jepsen, 1998). To avoid potential contamination of Pn and Pg signals, events with distances less than three degrees (a conservative distance cutoff recommended by Kim, Lay and Walter, 1997) are excluded from the analysis. Note that there are only 324 of the 7,927 events with distances less than three degrees. A sample of 7,603 regional events remains.

3.3 Worldwide-Averaged Distance Corrections.

Figure 10 contains semi-log scatterplots of Pn/Lg and Pn/Sn in the three frequency bands versus distance from the recording station for all 7,603 events. The plots indicate that each P/S amplitude ratio increases more rapidly as a function of distance up to about 600 km and then flattens out from about 600 km to 2220 km (20 degrees). (P/S is used here to generically refer to any of the ratios Pn/Lg or Pn/Sn in any frequency band.) To better see the shape of these curves, the data have been separated into 34 bins, each of length 0.5 degrees (55.5 km). The mean of log(P/S) in each bin are depicted by the square markers in Figure 11, with errors bars that are equal to plus or minus the estimated standard deviation of log(P/S) for the data in the bin.

In light of these figures, the distance dependence of each P/S ratio is parametrized as

$$\log(P/S) = \alpha + \beta \log(\Delta/\Delta_0) + \gamma\Delta\,, \qquad (16)$$

where α, β, and γ are parameters depending on the particular amplitude ratio (Pn/Lg or Pn/Sn) and the frequency band, f; Δ is the epicentral distance; and the constant Δ_0 is a reference distance that is set at 1500 km, roughly the mean epicentral distance of the 7,603 regional events considered in this study. Equation (16) is the product of three terms: a constant, a geometrical spreading term, and an attenuation term. This is a linear equation in the unknown parameters, α, β, and γ, which can be estimated using standard multiple linear regression analysis. The regional amplitude ratios are distance-corrected by applying the transformation,

$$\log(\mathrm{P/S})_{\mathrm{corrected}} = \log(\mathrm{P/S})_{\mathrm{uncorrected}} - \hat{\alpha} - \hat{\beta}\log(\Delta/\Delta_0) - \hat{\gamma}\Delta, \tag{17}$$

where $\hat{\alpha}$, $\hat{\beta}$, and $\hat{\gamma}$ are the best least-squares estimates of α, β, and γ. Figure 12 contains plots of Equation (16) for each amplitude ratio using the best least-squares values for α, β, and γ, based on the 7,603 events. Superimposed on each plot are all 7,603 events from Figure 10, in gray, and the binned means from Figure 11. Also included in Figure 12 is a table giving the number of regional amplitude measurements, n, the estimated standard deviations of the data both before and after distance corrections, and the best fit coefficients, $\hat{\alpha}$, $\hat{\beta}$, and $\hat{\gamma}$. If we let $y_i = \log(\mathrm{P/S})_i$, $i = 1, \ldots, n$, then the estimated standard deviation before distance corrections, s, is defined by

$$s^2 = \frac{1}{n-1}\sum_{i=1}^{n}(y_i - \bar{y})^2, \tag{18}$$

where the mean, $\bar{y}$, is given by

$$\bar{y} = \frac{1}{n}\sum_{i=1}^{n} y_i . \tag{19}$$

The estimated standard deviation after distance corrections, s_c, is given by

$$s_c^2 = \frac{1}{n-3}\sum_{i=1}^{n}(y_i - \hat{\alpha} - \hat{\beta}\log(\Delta_i/\Delta_0) - \hat{\gamma}\Delta_i)^2 . \tag{20}$$

As can be seen in the table, the corrected standard deviations are reduced by about 6% compared to the uncorrected values. If a straight-line fit is used, the improvement is only about half as much. This estimate of the reduction in the variance is not pronounced since there are many more events at farther distances (because there is more area at farther distances), where the curve is relatively flat. Another measure of the reduction in variance after distance corrections, which weights each distance equally, is to compute the estimated standard deviations before and after distance corrections for the 34 binned values. In this case, the average estimated standard deviation before distance corrections is about 0.18 and, after distance corrections, about 0.08. This is a reduction of about 58%, as opposed to 33% for the straight-line correction. It is not clear which is the more

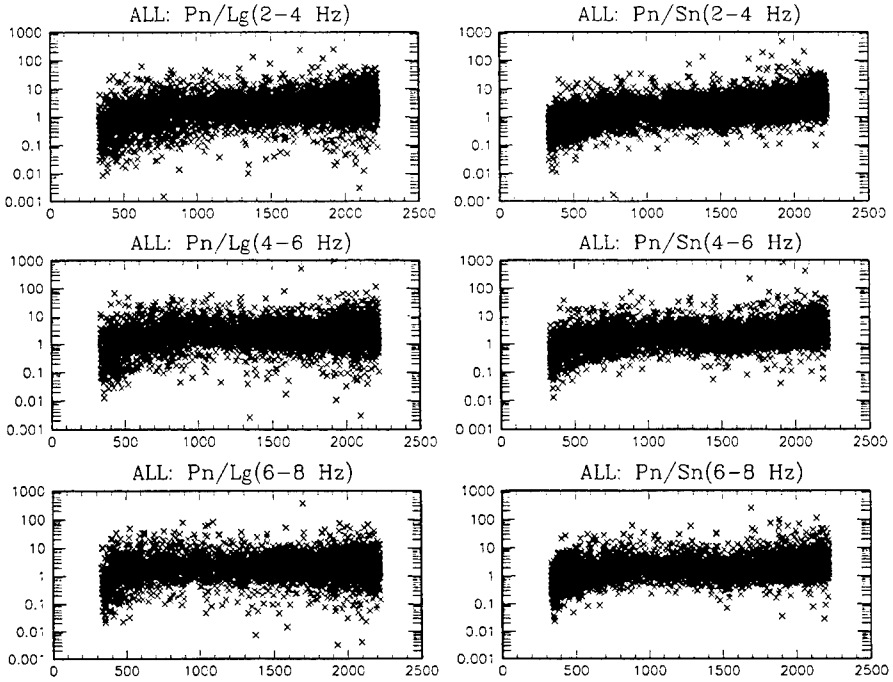

Figure 10. Semi-log scatterplots of regional amplitude ratios versus distance for 7,603 events above mb 3.5 with SNR for Pn greater than or equal to 2.0.

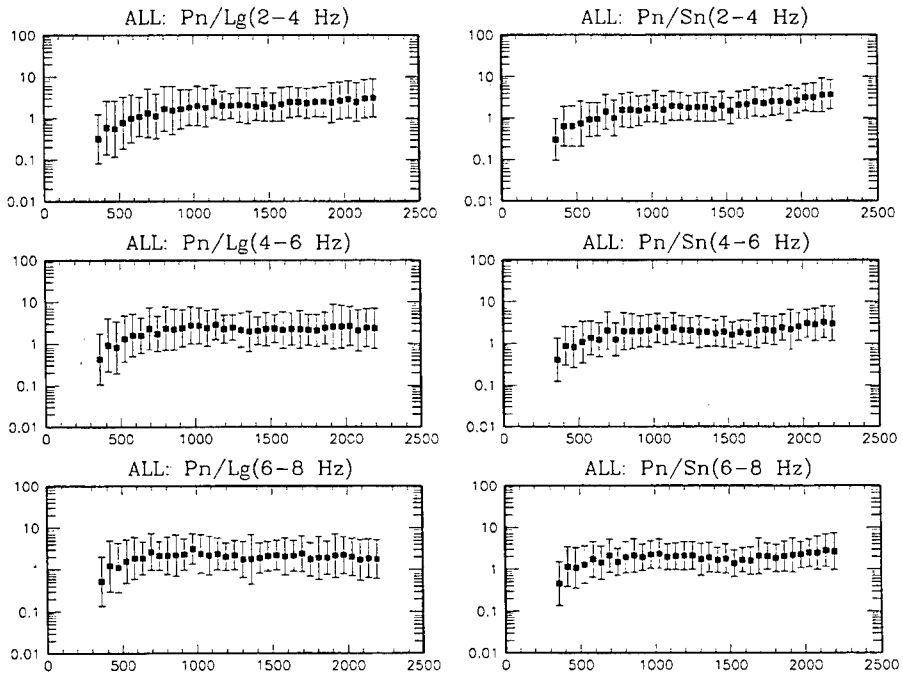

Figure 11. Semi-log plots of mean (log) regional amplitude ratios versus distance for 7,603 events. Data is separated into bins of length 55.5 km (0.5 degrees). Error bars are equal to plus or minus one standard deviation.

appropriate way to estimate the standard deviations, so below the more conservative computation which treats each event with equal weight is used.

Figure 12 indicates that a straight line will not approximate the distance dependence well for all distances, due to the steeper slopes at distances less than about 600 km. Also, the corrections will be most important for distances less than about 600 km. The flatness of the curves beyond about 600 km indicates that distance corrections are not as necessary for events at these distances.

3.4 Region-Specific Distance Corrections.

Equation (16) provides good fits to the combined regional data from all IMS stations, although there is considerable scatter in the data due, in large part, to regional variations. Equation (16) is now used to fit the regional data from individual IMS stations. There are currently 50 IMS stations that have 30 or more regional events (with $SNR \geq 2.0$) with which to estimate the fits.

As an example, plots of the best least-squares fits (solid curves) for 112 regional events recorded by station NIL are shown in Figure 13. Also shown in the plots, for comparison, are the worldwide average fits (dashed) from Figure 12. For reference, the plots also include the P/S values for two underground explosions at the Lop Nor test site during 1996. These two events are enclosed in a circle and are outliers from the rest of the sample population. For a full account of the characterization of the Lop Nor explosions see Fisk et al. (1996a). The table included in Figure 13 gives the estimated standard deviation of the training set both before, s, and after, s_c, distance corrections, in addition to the best-fit parameters for the distance-correction curves. The average reduction in standard deviation is about 10%. It is clear from the plots that the distance-correction curves for NIL are nearly identical to the worldwide average.

Two examples of stations whose distance corrections significantly reduce the variance are PDAR (Figure 14), with 93 regional events, and PDY (Figure 15), with 59 regional events. The average reduction in estimated standard deviation is 24% for PDAR and 53% for PDY. The curves for PDY are quite different than the worldwide-average curves, especially at short distances. This example shows the importance of determining appropriate corrections for each region individually. Before distance corrections, the average standard deviations are greater than 0.5, while after distance corrections, the standard deviations are mostly less than 0.3, a relatively small value, thus improving the event characterization capability in this region.

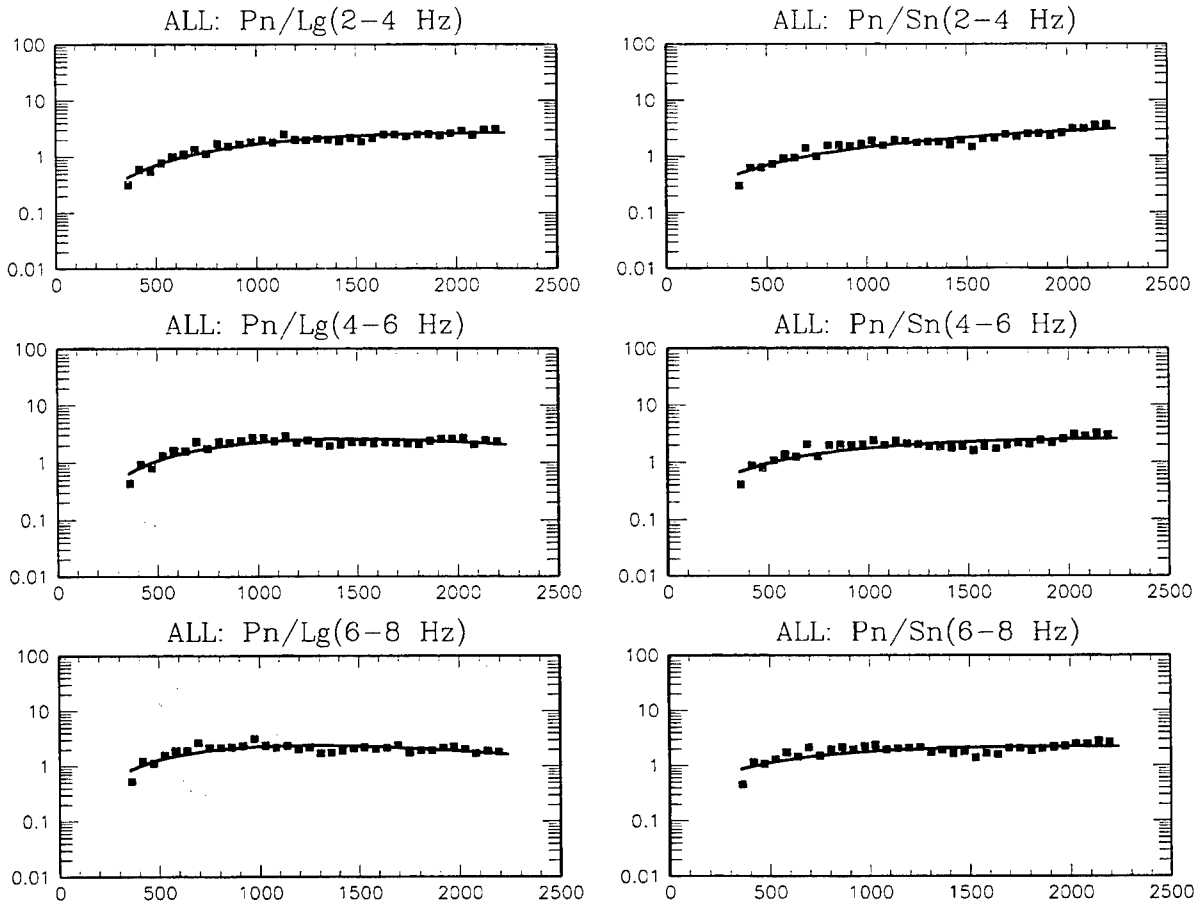

	n	s	s_c	$\hat{\alpha}$	$\hat{\beta}$	$\hat{\gamma}$
Pn/Lg(2-4 Hz)	6654	0.495	0.456	0.921	1.861	-3.666E-04
Pn/Lg(4-6 Hz)	5198	0.481	0.461	1.348	2.105	-6.264E-04
Pn/Lg(6-8 Hz)	4582	0.466	0.456	1.310	1.847	-6.332E-04
Pn/Sn(2-4 Hz)	6825	0.428	0.375	0.413	1.141	-5.023E-05
Pn/Sn(4-6 Hz)	5308	0.418	0.389	0.670	1.228	-2.104E-04
Pn/Sn(6-8 Hz)	4688	0.399	0.384	0.654	1.034	-2.172E-04

Figure 12. Best least-square fit curves for Pn/Lg and Pn/Sn in the 2-4, 4-6 and 6-8 Hz bands, based on 7,603 regional events. Superimposed are the scatterplots as in Figure 10 and the binned means as in Figure 11. The table gives the number of measurements for each amplitude ratio, the estimated standard deviation of the data before and after distance corrections, and the best-fit coefficients.

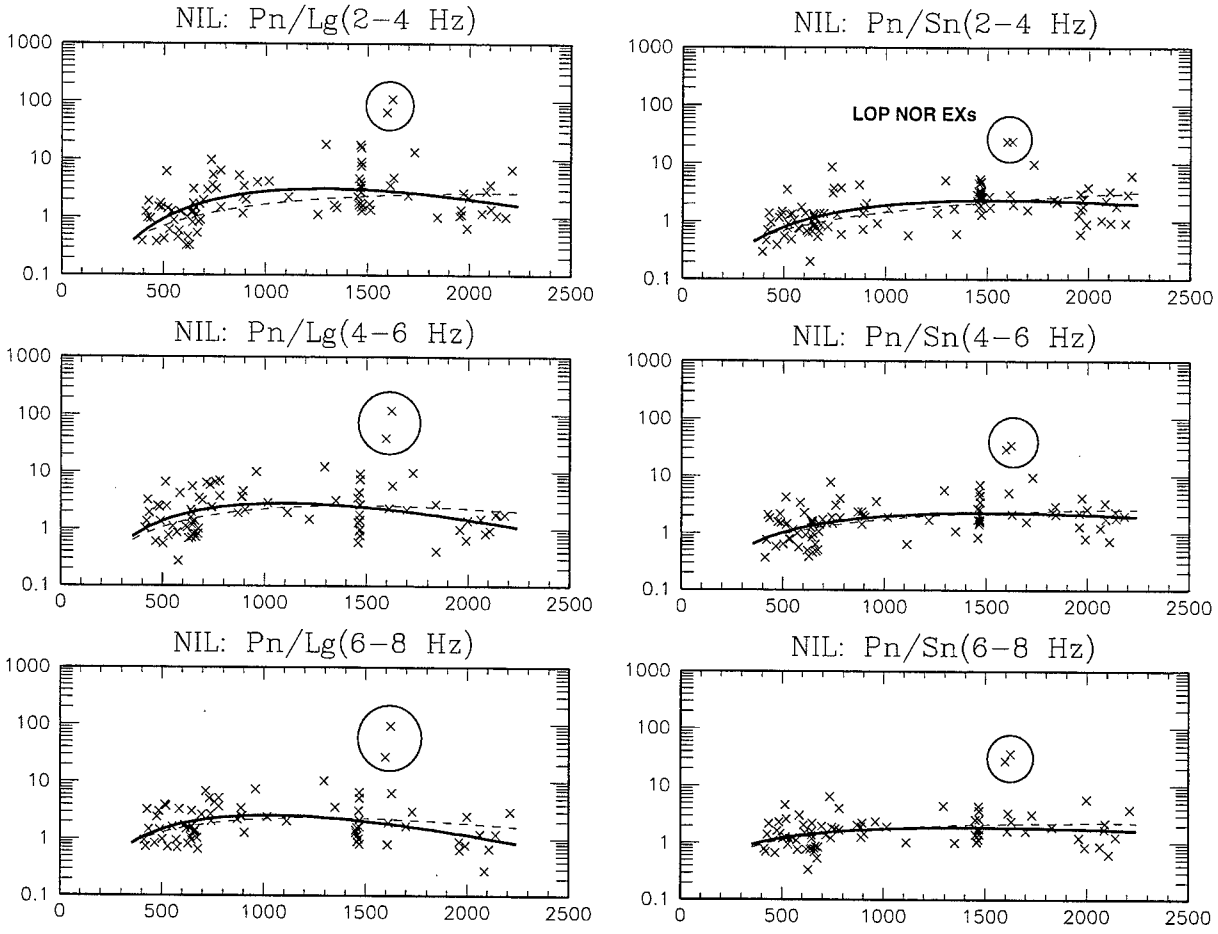

	n	*s*	s_c	$\hat{\alpha}$	$\hat{\beta}$	$\hat{\gamma}$
Pn/Lg(2-4 Hz)	97	0.382	0.330	2.306	3.617	-1.219E-03
Pn/Lg(4-6 Hz)	80	0.356	0.339	2.119	2.935	-1.159E-03
Pn/Lg(6-8 Hz)	74	0.308	0.288	2.070	2.762	-1.172E-03
Pn/Sn(2-4 Hz)	106	0.321	0.263	1.327	2.319	-6.398E-04
Pn/Sn(4-6 Hz)	87	0.303	0.274	1.145	1.834	-5.251E-04
Pn/Sn(6-8 Hz)	79	0.253	0.245	0.783	1.105	-3.381E-04

Figure 13. Best least-square fits (solid curves) for 112 regional events recorded by NIL. The dashed curves are the worldwide averages as in Figure 12. The two Lop Nor explosions are circled.

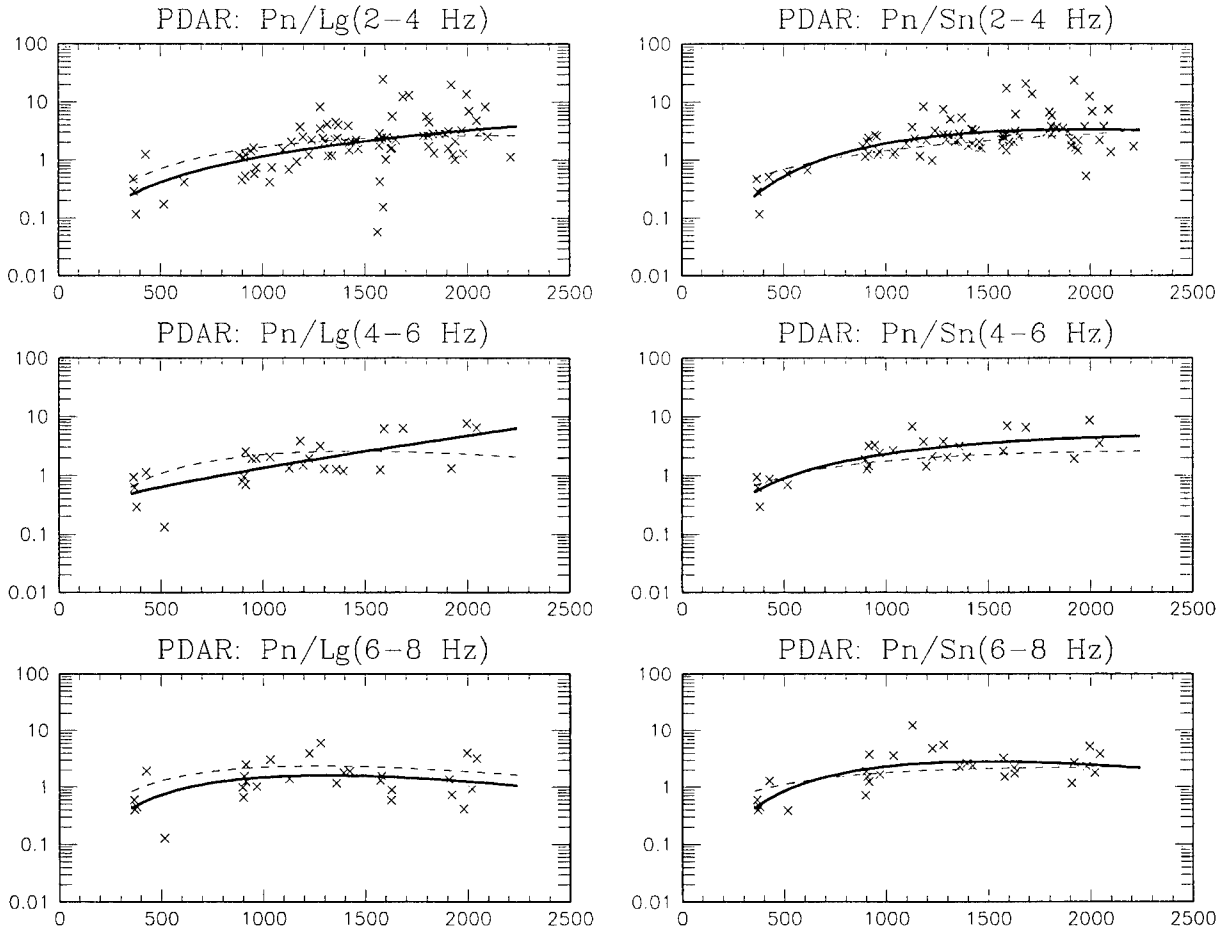

	n	s	s_c	$\hat{\alpha}$	$\hat{\beta}$	$\hat{\gamma}$
Pn/Lg(2-4 Hz)	85	0.460	0.388	0.318	1.474	2.866E-06
Pn/Lg(4-6 Hz)	26	0.406	0.295	-0.282	0.305	4.585E-04
Pn/Lg(6-8 Hz)	28	0.362	0.328	1.355	2.321	-7.741E-04
Pn/Sn(2-4 Hz)	85	0.371	0.281	1.458	2.960	-6.492E-04
Pn/Sn(4-6 Hz)	26	0.352	0.215	0.946	1.812	-2.649E-04
Pn/Sn(6-8 Hz)	28	0.361	0.261	1.667	2.793	-8.118E-04

Figure 14. Best least-square fits (solid curves) for 93 regional events recorded by PDAR. The dashed curves are the worldwide averages as in Figure 12.

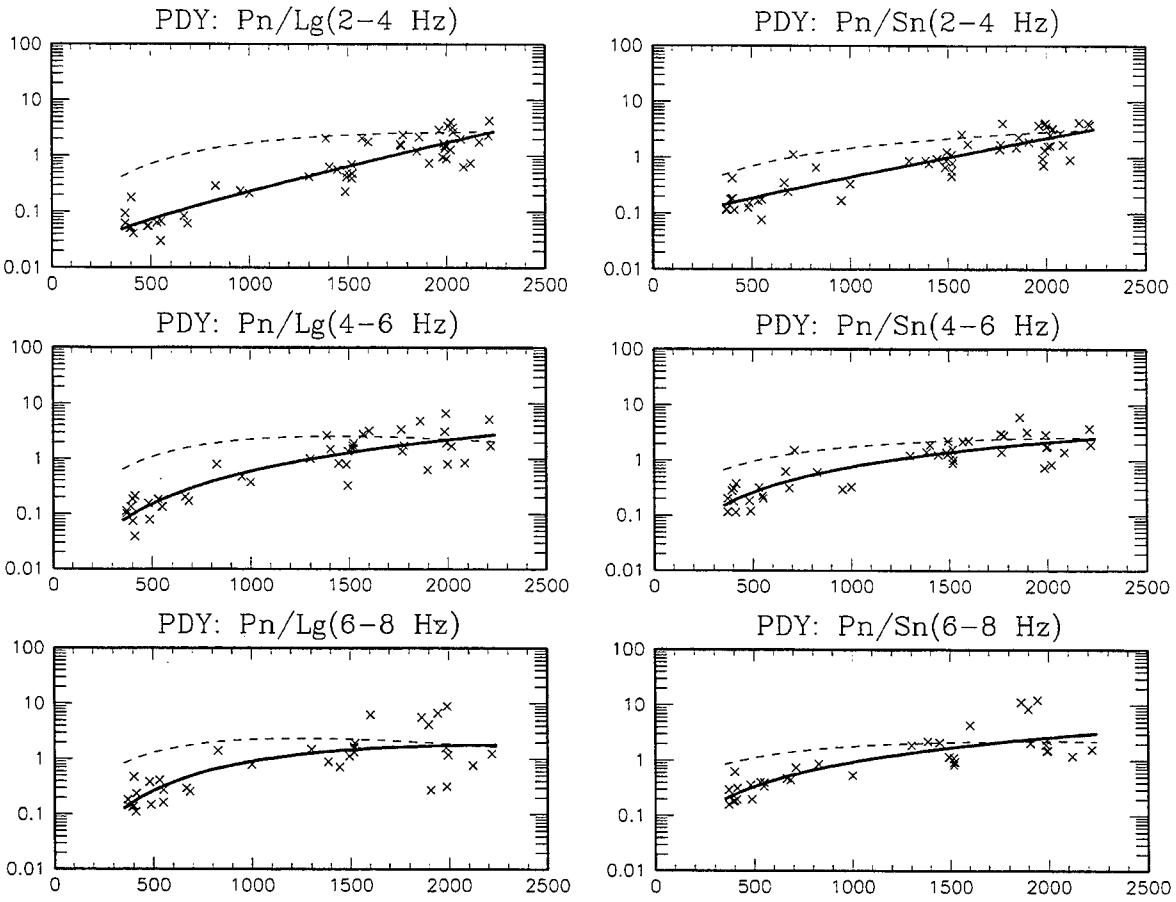

	n	*s*	s_c	$\hat{\alpha}$	$\hat{\beta}$	$\hat{\gamma}$
Pn/Lg(2-4 Hz)	53	0.628	0.249	-1.299	0.442	7.402E-04
Pn/Lg(4-6 Hz)	43	0.588	0.266	0.177	2.050	-4.394E-05
Pn/Lg(6-8 Hz)	35	0.543	0.348	0.905	2.589	-4.920E-04
Pn/Sn(2-4 Hz)	54	0.506	0.232	-0.950	0.202	6.342E-04
Pn/Sn(4-6 Hz)	44	0.466	0.228	0.207	1.616	-4.104E-05
Pn/Sn(6-8 Hz)	36	0.494	0.274	0.228	1.472	1.953E-06

Figure 15. Best least-square fits (solid curves) for 59 regional events recorded by PDY. The dashed curves are the worldwide averages as in Figure 12.

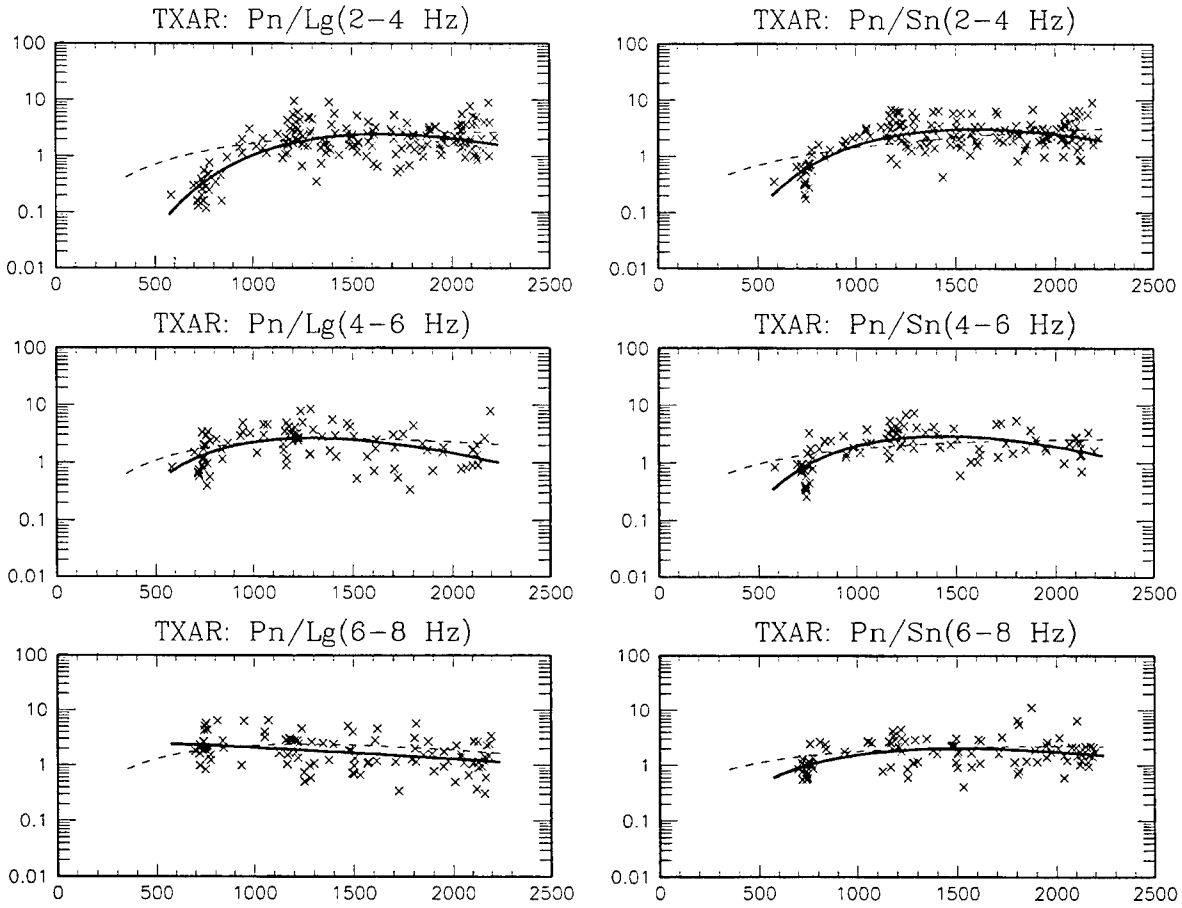

	n	s	s_c	$\hat{\alpha}$	$\hat{\beta}$	$\hat{\gamma}$
Pn/Lg(2-4 Hz)	188	0.387	0.261	3.631	8.216	-2.171E-03
Pn/Lg(4-6 Hz)	94	0.309	0.278	3.086	5.344	-1.796E-03
Pn/Lg(6-8 Hz)	104	0.286	0.270	0.624	0.208	-2.694E-04
Pn/Sn(2-4 Hz)	188	0.327	0.235	3.404	7.132	-1.949E-03
Pn/Sn(4-6 Hz)	94	0.312	0.236	3.529	6.749	-2.046E-03
Pn/Sn(6-8 Hz)	104	0.262	0.239	1.782	3.443	-9.824E-04

Figure 16. Best least-square fits (solid curves) for 211 regional events recorded by TXAR. The dashed curves are the worldwide averages as in Figure 12.

As another example, Figure 16 shows the data and distance-correction curves for TXAR (with 211 regional events). The curves are quite similar to the worldwide-average curves for distances beyond about 800 km, but differ for closer distances. There are, however, no events for TXAR at distances less than about 600 km which satisfy the event selection criteria. Such data are needed in order to improve the fits for distances less than 800 km. The estimated distance corrections do, however, provide good fits to the available data and the scatter in the data is relatively small.

Figure 17 shows the amplitude ratios and distance-correction curves for 1,266 events recorded by WRA, all of which have distances greater than 1000 km. Thus, there are no data, satisfying the data quality restrictions, that can be used to quantify the distance dependence at close distances. Note that for any event at the far regional distances, where there is much training data, the distance dependence is relatively insignificant compared to the scatter in the data. Additional data at closer distances are needed to be able to characterize events in that distance range.

A station with unusual distance dependence is LPAZ, with 282 regional events (Figure 18). Each of the best fit distance-correction curves differ significantly from the respective worldwide averages and there is significant scatter in the data. The complicated subregional effects near LPAZ are described below to shed some light on the underlying reasons for this behavior.

3.5 Status.

The status of the regional distance corrections is now summarized for each existing IMS seismic station. For the purposes of event screening, the important quantities are the standard deviations of the corrected data, relative to the separation of the means for explosions and earthquakes. It is also important to have sufficient high-quality data over a sufficient distance range with which to obtain the fits. As illustrated above, these considerations are often most important for events at distances less than about 600 km where the curves typically exhibit the strongest dependence on distance.

Assessing the utility of the distance corrections would be easier if regional data existed for both earthquakes and explosions at the same station. Unfortunately, explosion data exist for relatively few stations. Thus, our objective is to reduce the variance as much as possible, using distance corrections and other procedures, such as dividing the data into subsets of reduced variance (see Lay et al., 1997, and below). Stations that do have regional explosion data can then be used as a guide in assessing how small the variance should be in order to be useful in event screening.

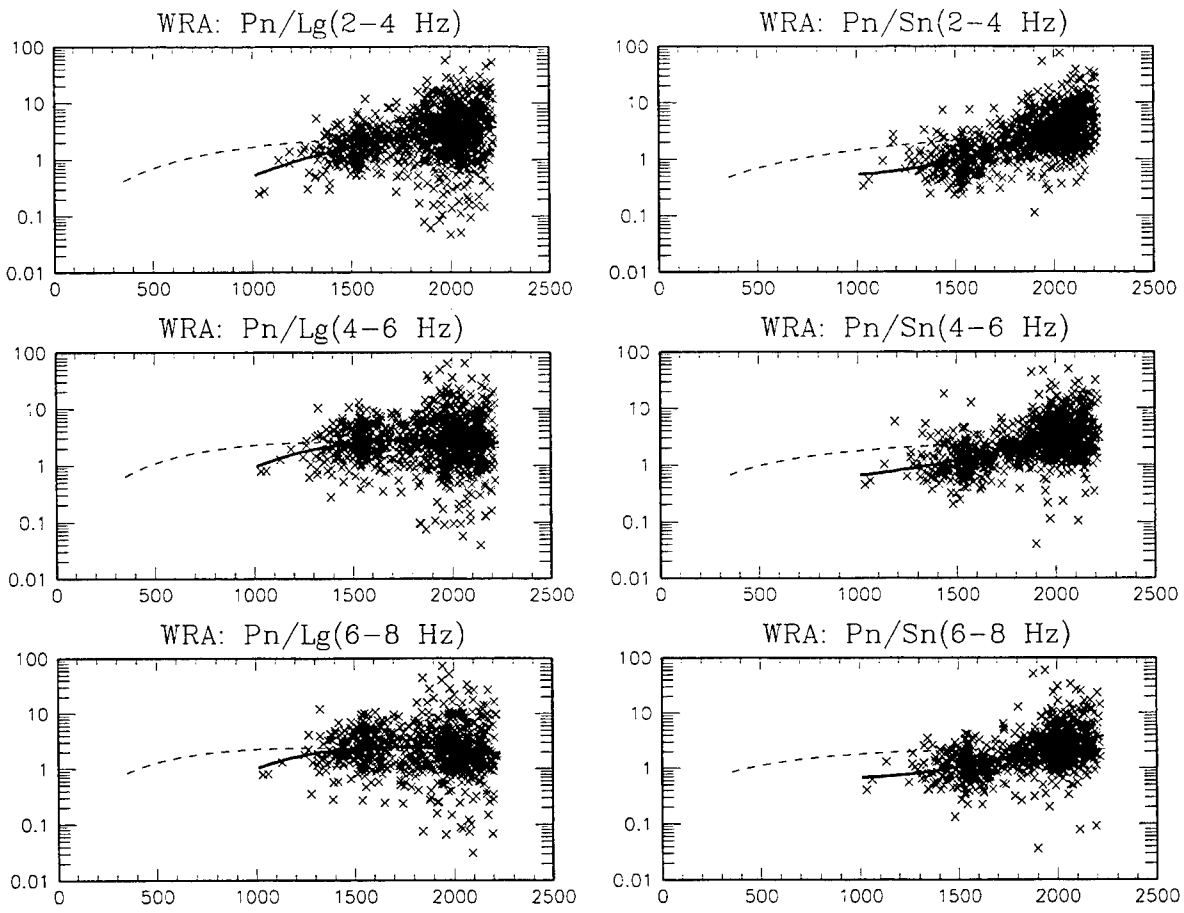

	n	s	s_c	$\hat{\alpha}$	$\hat{\beta}$	$\hat{\gamma}$
Pn/Lg(2-4 Hz)	1187	0.427	0.407	1.137	4.642	-6.104E-04
Pn/Lg(4-6 Hz)	1061	0.415	0.414	2.981	7.328	-1.730E-03
Pn/Lg(6-8 Hz)	894	0.400	0.399	3.217	7.488	-1.901E-03
Pn/Sn(2-4 Hz)	1187	0.397	0.309	-3.427	-5.011	2.278E-03
Pn/Sn(4-6 Hz)	1061	0.379	0.328	-1.928	-2.260	1.338E-03
Pn/Sn(6-8 Hz)	894	0.366	0.317	-2.392	-3.501	1.606E-03

Figure 17. Best least-square fits (solid curves) for 1266 regional events recorded by WRA. The dashed curves are the worldwide averages as in Figure 12.

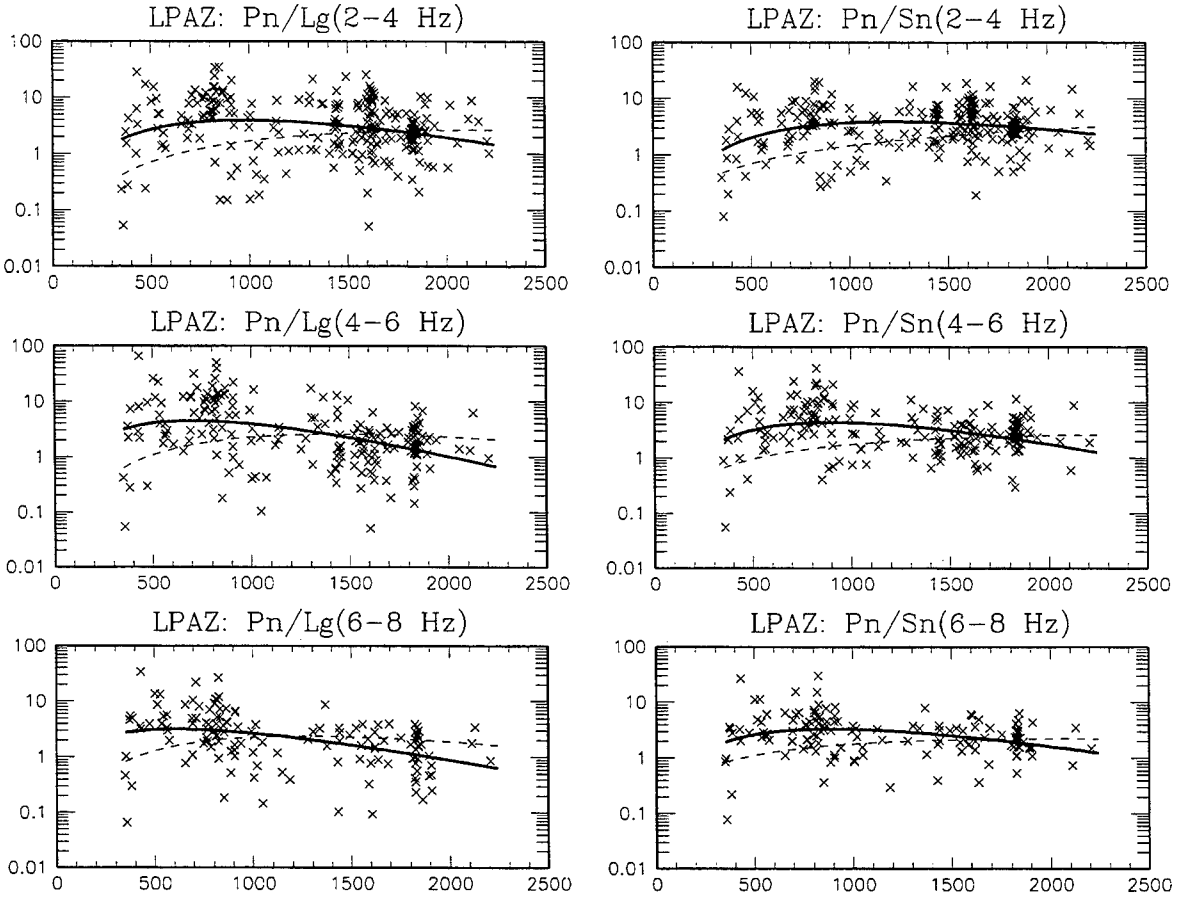

	n	*s*	s_c	$\hat{\alpha}$	$\hat{\beta}$	$\hat{\gamma}$
Pn/Lg(2-4 Hz)	277	0.489	0.481	1.909	2.113	-9.417E-04
Pn/Lg(4-6 Hz)	207	0.542	0.499	2.063	1.853	-1.145E-03
Pn/Lg(6-8 Hz)	139	0.495	0.459	1.441	1.135	-8.181E-04
Pn/Sn(2-4 Hz)	277	0.377	0.368	1.742	2.195	-7.824E-04
Pn/Sn(4-6 Hz)	207	0.407	0.389	2.073	2.190	-1.051E-03
Pn/Sn(6-8 Hz)	139	0.374	0.361	1.616	1.655	-8.073E-04

Figure 18. Best least-square fits (solid curves) for 282 regional events recorded by LPAZ. The dashed curves are the worldwide averages as in Figure 12.

Here, we characterize the training sets in two ways. First, since the distance-correction curves given in Equation (16) generally work quite well, given sufficient data, we categorize stations simply by the number of events with at least one regional amplitude ratio with $SNR \geq 2.0$. Table 5 lists each of the 34 IMS primary stations and their corresponding category. A similar list appears in Table 6 for the 53 IMS auxiliary stations. Stations listed as Category 1 have at least 30 regional seismic events with $SNR \geq 2.0$, while those listed as Category 2 do not. (The station names are those currently used at the PIDC.) Also included in each table are the number of regional events recorded at each station between 10 Sep 1995 and 1 Oct 1997 with $SNR \geq 2.0$. The column labeled *smin* gives the minimum of the six distance-corrected standard deviations. The column labeled *dmin* gives the minimum distance from event to station of all events in the training set.

Summarizing Table 5 and Table 6, there are 50 IMS stations (27 primary and 23 auxiliary) that currently have adequate data with which to estimate region-specific distance corrections and 37 stations (7 primary and 30 auxiliary) that do not. This situation will improve significantly over time, as more regional data are acquired from the IMS seismic stations.

As a second method of categorization, we determine the number of stations for which the standard deviation after distance corrections, s_c, is below a specified level, s_0, for all six regional amplitude ratios. As discussed above, the appropriate value for s_0 can be determined precisely only if the variance and difference in the means of both earthquakes and explosions are known, and is most likely highly station dependent. Without this information, we simply chart the number of stations for various values of s_0, summarized in Table 7. As can be seen in the table, over 80% of the 50 stations with adequate data have standard deviations after distance corrections less than 0.5, for all six regional amplitude ratios, and over 95% less than 0.6.

Figure 19 shows histograms of the number of stations with standard deviations between specified values, both before and after distance corrections. Figure 19 shows, for example, that the number of stations which have standard deviations less than 0.5 for all six regional amplitude ratios before distance corrections is only 27 (54%) as opposed to 41 (82%) after distance corrections. Only 12 stations, as opposed to 25, have all six standard deviations less than 0.4, and only 42 stations, as opposed to 48, have all six standard deviations less than 0.6 before distance corrections.

Table 5. Status of regional distance corrections for IMS primary seismic stations.

Station	Category	# Events (SNR > 2.0)	smin	dmin
ABKT	1	70	0.267	408
ARCES	1	90	0.334	563
ASAR	1	516	0.278	1174
BDFB	2	13	0.031	1038
BGCA	2	25	0.161	1156
BJT	1	48	0.227	488
BOSA	1	32	0.208	336
CMAR	1	227	0.336	341
CPUP	1	128	0.191	705
DBIC	1	70	0.189	453
ESDC	1	129	0.426	361
FINES	1	144	0.265	425
GERES	1	299	0.268	342
HIA	1	30	0.238	719
ILAR	1	216	0.486	347
KBZ	1	43	0.294	335
KSAR	1	284	0.334	377
LPAZ	1	282	0.361	350
MAW	2	0	N/A	N/A
MJAR	1	558	0.283	333
MNV	1	52	0.185	358
NORES	1	130	0.260	435
NRI	2	23	0.153	1134
PDAR	1	93	0.215	365
PDY	1	59	0.228	372
PLCA	1	154	0.284	334
ROSC	2	18	0.206	402
STKA	1	37	0.070	751
TXAR	1	211	0.235	584
ULM	2	23	0.291	913
VNDA	2	26	0.261	452
WRA	1	1266	0.309	1034
YKA	1	88	0.244	491
ZAL	1	139	0.317	403

Table 6. Status of regional distance corrections for IMS primary seismic stations.

Station	Category	# Events (SNR > 2.0)	smin	dmin
AAE	2	1	N/A	356
AFI	1	71	0.385	336
ALQ	1	61	0.162	852
AQU	2	3	N/A	505
ARU	1	30	0.224	1712
BBB	2	27	0.352	333
BORG	2	9	0.213	383
CTA	1	215	0.243	986
DAV	2	20	0.177	404
DAVOS	1	179	0.268	351
DLBC	1	104	0.272	355
EIL	2	27	0.264	573
EKA	1	158	0.252	645
ELK	1	44	0.371	379
FITZ	2	25	0.196	1310
GNI	2	1	N/A	343
HFS	1	111	0.242	569
HNR	1	49	0.332	357
INK	1	118	0.358	355
JCJ	2	0	N/A	N/A
JHJ	2	0	N/A	N/A
JKA	2	0	N/A	N/A
JNU	2	0	N/A	N/A
JOW	2	1	N/A	1418
JTS	2	0	N/A	N/A
KDAK	2	10	0.322	1310
KIEV	1	46	0.336	438
KVAR	1	36	0.198	335
LSZ	2	0	N/A	N/A
MLR	2	0	N/A	N/A
MSEY	2	0	N/A	N/A
NEW	1	50	0.230	362
NIL	1	112	0.245	394
NNA	1	37	0.443	341
NWAO	2	18	0.370	1316
OBN	1	36	0.225	381
PARD	2	9	0.163	370
PFO	1	53	0.280	444
PMG	1	96	0.219	340
PTGA	2	0	N/A	N/A
RAR	2	28	0.207	1367
RPN	2	3	N/A	597
SADO	2	4	0.089	929
SDV	2	0	N/A	N/A
SFJ	2	11	0.373	833
SNZO	1	71	0.266	376
SPITS	1	77	0.346	384
SUR	2	16	0.209	711
TKL	2	7	0.241	1889
TSUM	2	7	0.054	878
ULN	1	33	0.150	465
VRAC	1	58	0.206	414
YAK	2	0	N/A	N/A

Table 7. Number of stations with distance-corrected standard deviations less than s_0

s_0	Primary $n(s_c<s_0)$	Auxiliary $n(s_c<s_0)$	Total $n(s_c<s_0)$
0.1	0	0	0
0.2	0	0	0
0.3	3	0	3
0.4	16	9	25
0.5	23	18	41
0.6	26	22	48
0.7	26	23	49
0.8	27	23	50
0.9	27	23	50
1.0	27	23	50

3.6 Subregional Improvements.

The examples given above for TXAR, WRA and LPAZ show that distance corrections alone do not always appreciably reduce the variance of the training data, due to subregional or path-specific variations. In some cases, subsets of a training set, i.e., data restricted to a particular subregion, can provide better event characterization. Regional amplitude ratios of events in such a subregion could have a standard deviation less than that of the entire regional set. This reduced variance could depend on the properties of the locations of the events or on the path differences from the events to the station, or both. Such variations should be treated in order to provide more effective regional event screening. Tectonic subregion and azimuthal dependence are examined here for TXAR, WRA and LPAZ.

3.6.1 Treatment of Subregional Tectonic Variations.

Figures 20-22 show the locations of the regional events recorded by LPAZ, TXAR and WRA, respectively, on maps of each region. Each map shows the location of the station, as well as a tectonic grid, with two-degree resolution, that was established by Oli Guudmundsson of the Australian National University, and is described further by Jenkins et al. (1996). Each grid is divided into up to eight distinct tectonic subregions, color-coded in the following way:

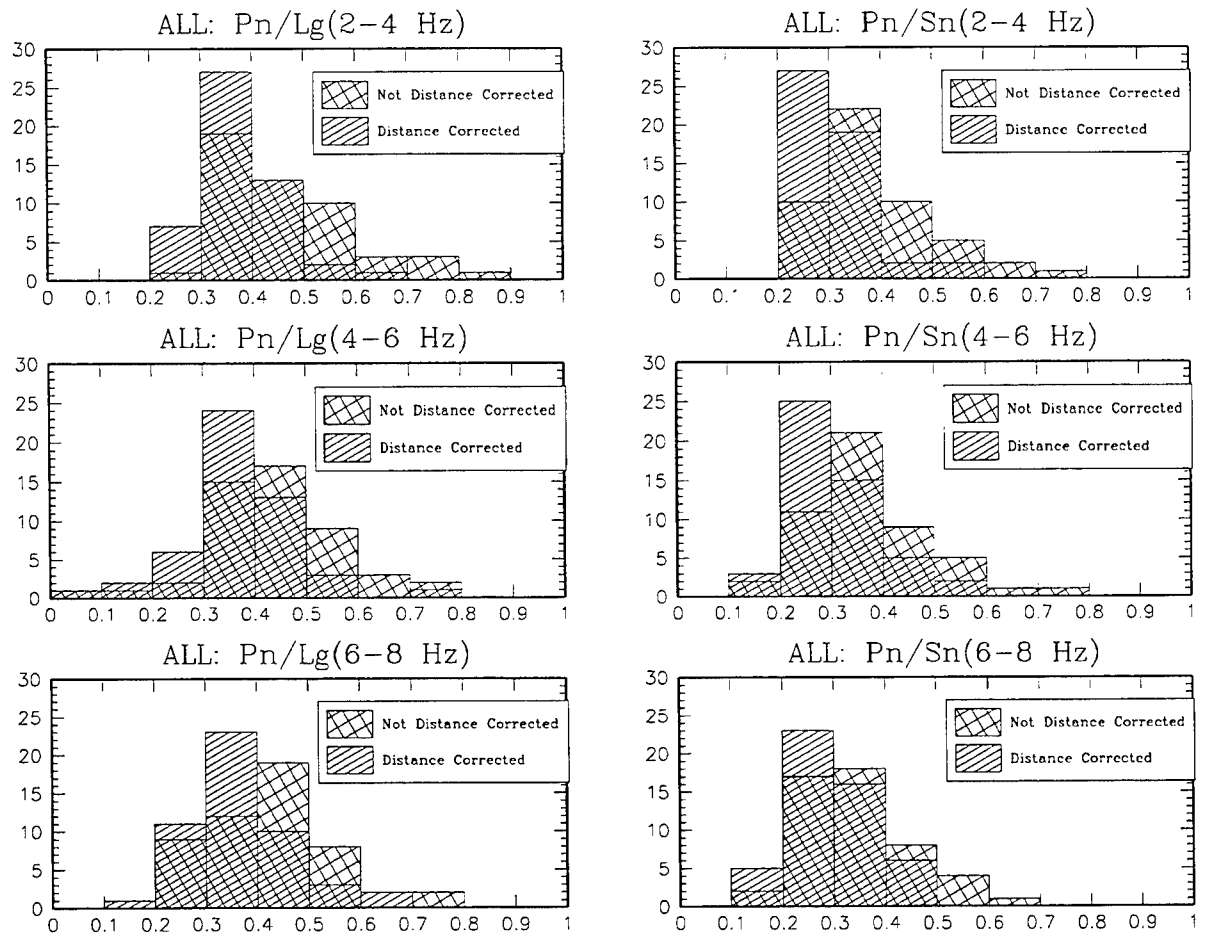

Figure 19. Histograms showing the number of stations with given standard deviation, both before and after distance corrections.

cyan:	Young ocean (<25 Myrs)
blue:	Intermediate ocean (25-100 Myrs)
black:	Old ocean (>100 Myrs)
green:	Cenozoic (alpine)
magenta:	Tectonic
red:	Paleozoic (ca 150-800 Myrs)
yellow:	Proterozoic (800-1700 Myrs)
white:	Archean (>1700 Myrs)

These figures depict the distribution of events relative to tectonic subregion and station location. For example, most regional events recorded by LPAZ occur along the Andes, either to the northwest of the station or to the south, either in the tectonic (magenta), Cenozoic (green), or intermediate ocean (blue) subregions. The regional amplitude ratios for LPAZ are plotted versus distance in Figure 23 for each subregion on the same plot, along with the fits of the distance dependence, color-coded as above. Events from each subregion do have different distance dependence, with only the tectonic (magenta) events consistent with the worldwide averages. The intermediate ocean (blue) events show typical behavior in the 2–4 Hz frequency band, but a decreasing dependence with distance at the higher frequencies. The events in the Cenozoic (green) subregion have a relatively flat distance dependence. The standard deviations of the distance-corrected data for Pn/Sn(6-8 Hz), for example, is 0.30 for the tectonic, 0.30 for the Cenozoic, and 0.27 for the intermediate ocean subregions, as compared to 0.36 for all the data. Thus, in this case, there is something to be gained by making this subregional division. However, additional data and further evaluation are needed for LPAZ to validate/improve these corrections.

Similar plots are shown in Figure 24 for TXAR for four tectonic subregions: tectonic (magenta), Paleozoic (red), young ocean (cyan), and intermediate ocean (blue). The individual distance-correction curves all exhibit similar behavior at far regional distances; the erratic behavior at distances less than 500-1000 km is due to a lack of data in this distance range. Unlike LPAZ, there is hardly any reduction in standard deviation for data confined to any of the tectonic subregions, except for the intermediate ocean events. However, as was pointed out earlier, the variance of all the TXAR regional events is already relatively small. Azimuthal variations in the regional data recorded by TXAR will be studied further below.

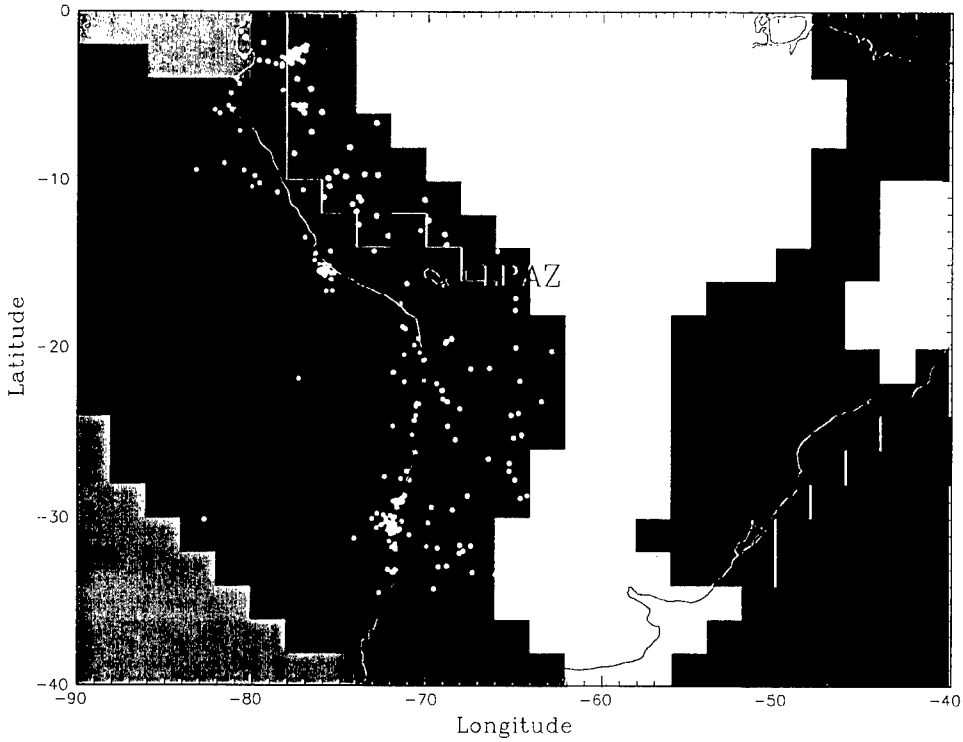

Figure 20. Regional event locations and tectonic grid for LPAZ.

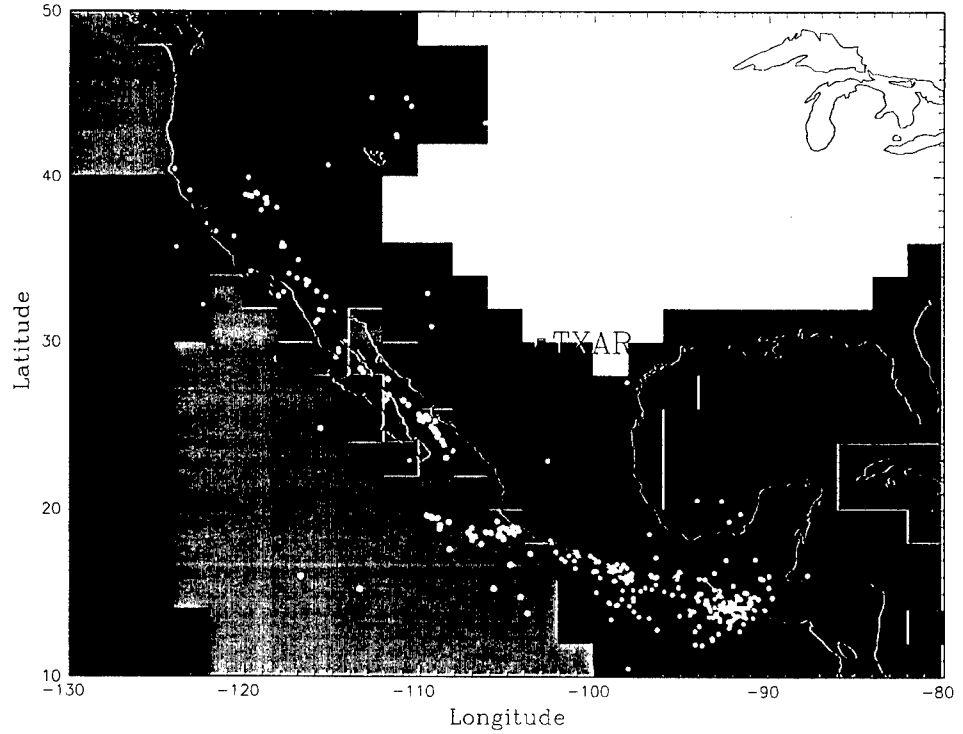

Figure 21. Regional event locations and tectonic grid for TXAR.

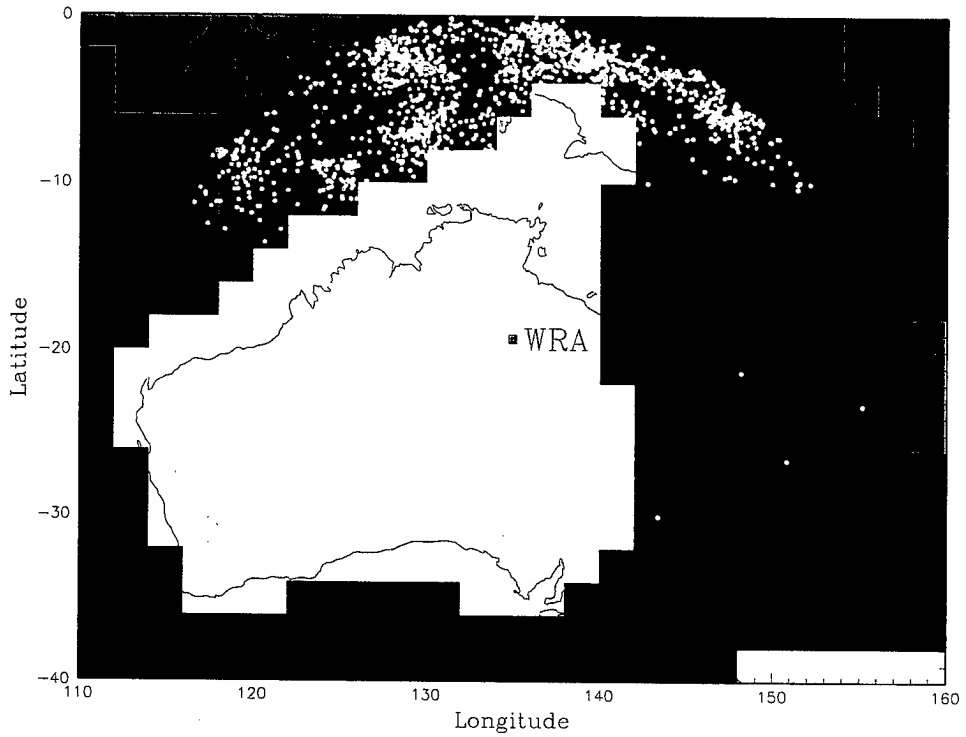

Figure 22. Regional event locations and tectonic grid for WRA.

3.6.2 Treatment of Azimuthal Variations.

Another approach involves dividing regions into azimuthal sectors. Successful application of this approach for ABKT is reported by Rodgers et al. (1997). Events measured at similar distances but different azimuths provide information about path differences. In Figures 25-27, the azimuthal variations for the six P/S ratios are plotted for LPAZ, TXAR and WRA, respectively. Azimuths are measured clockwise from north. The data for LPAZ and TXAR have been divided into azimuthal bins of size 18 degrees and, for WRA, into bins of 5 degrees. The solid line in each plot represents the estimated mean in each bin, and the errors bars are plus and minus one estimated standard deviation of the data in the bin. The two horizontal dashed lines in each plot correspond to plus and minus one standard deviation relative to the mean of the entire data set for that station.

For LPAZ, the large error bars for azimuths between 30 and 120 degrees are most likely due to the lack of data at these angles (see Figure 20). Figure 20 also shows that most events occur to the south (150-210 degrees) and northwest (270-330 degrees) relative to LPAZ. For most of the P/S ratios, the means for northwestern azimuths are somewhat smaller than for southern azimuths, as are the standard deviations. There are two azimuthal bins, at about 135 degrees and 260 degrees, which have significantly smaller standard deviations, as compared to the dashed lines. However, not every azimuthal range has standard deviations less than the overall standard deviation.

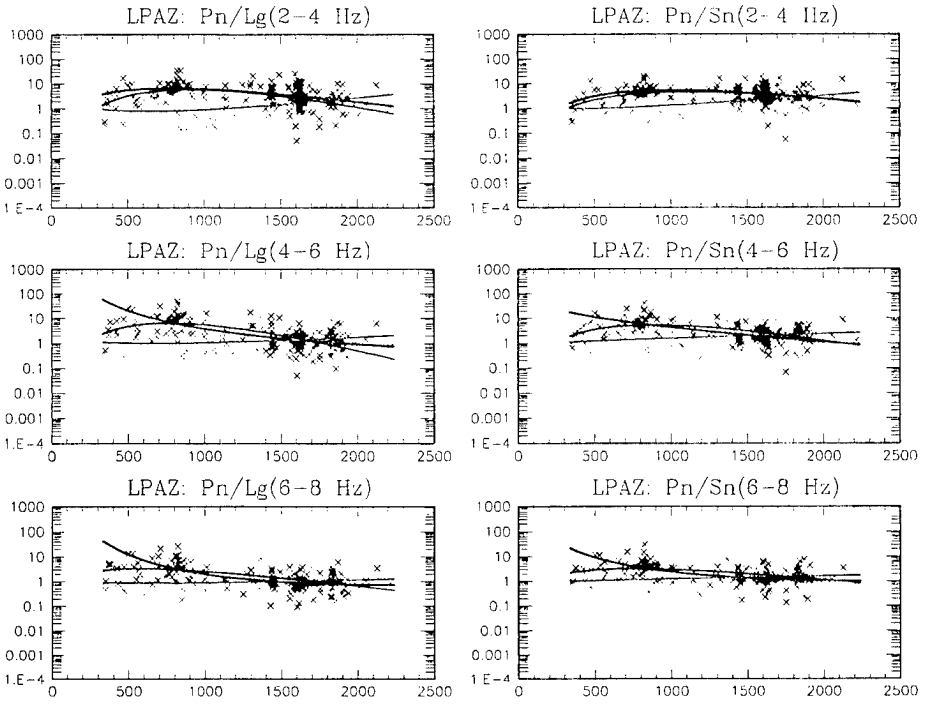

Figure 23. Best least-square fit curves for LPAZ; magenta for events in tectonic subregions, green for Cenozoic, and blue for intermediate ocean.

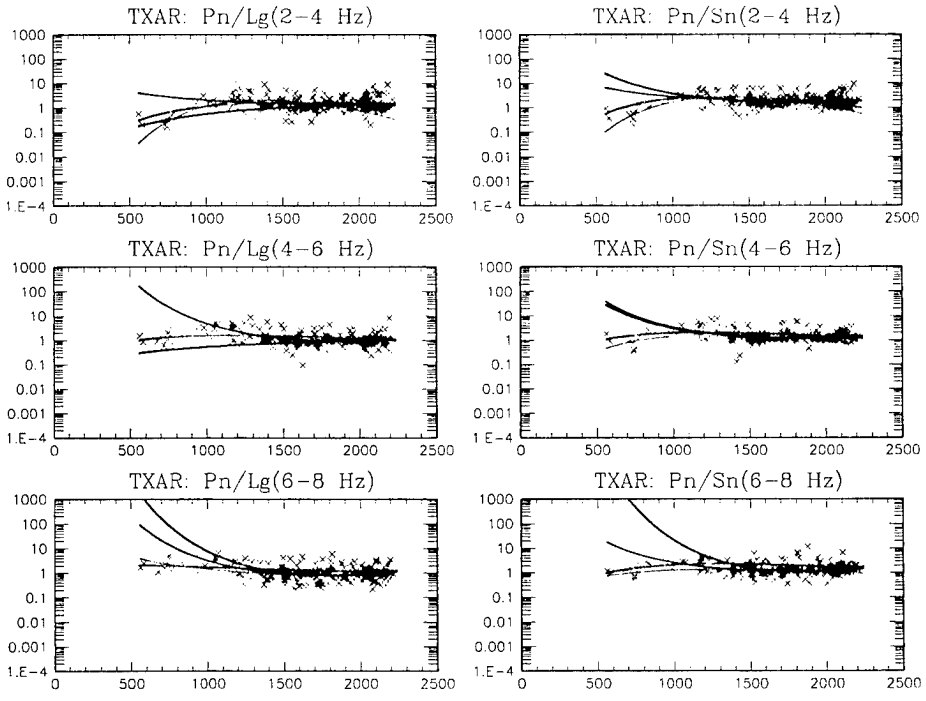

Figure 24. Best least-square fit curves for TXAR; magenta for events in tectonic subregions, red for Paleozoic, cyan for young ocean, and blue for intermediate ocean.

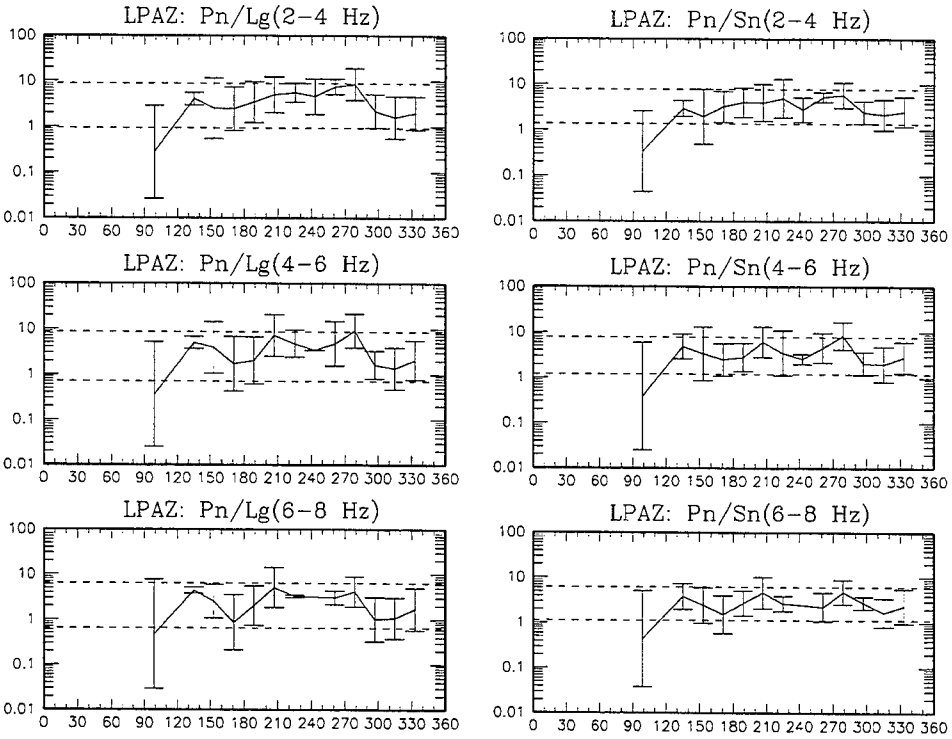

Figure 25. Azimuthal variations at LPAZ. Error bars are plus or minus one standard deviation.

Figure 26 shows that the azimuthal variations of the standard deviations for TXAR do not vary appreciably compared to all of the data. The means of the azimuthal bins, however, do exhibit a significant variation near 240 degrees, for events that are mostly in the Gulf of California, especially at lower frequencies. Treatment of the azimuthal variation can be used to further reduce the variance of the regional amplitude ratios for TXAR.

WRA appears to be a good station to study azimuthal variations because there are numerous events with similar distances from the station, with azimuths ranging from approximately –60 to about 60 degrees, as shown in Figure 22. Figure 27 shows azimuthal variations in 5 degree bins. The means are quite uniform over the entire 120 degree range. There is some variation in standard deviation, the smallest standard deviation having about half the value of the largest standard deviation. It is not the case, as would be most useful, that all standard deviations in the azimuthal bins are less than the values for all the WRA data.

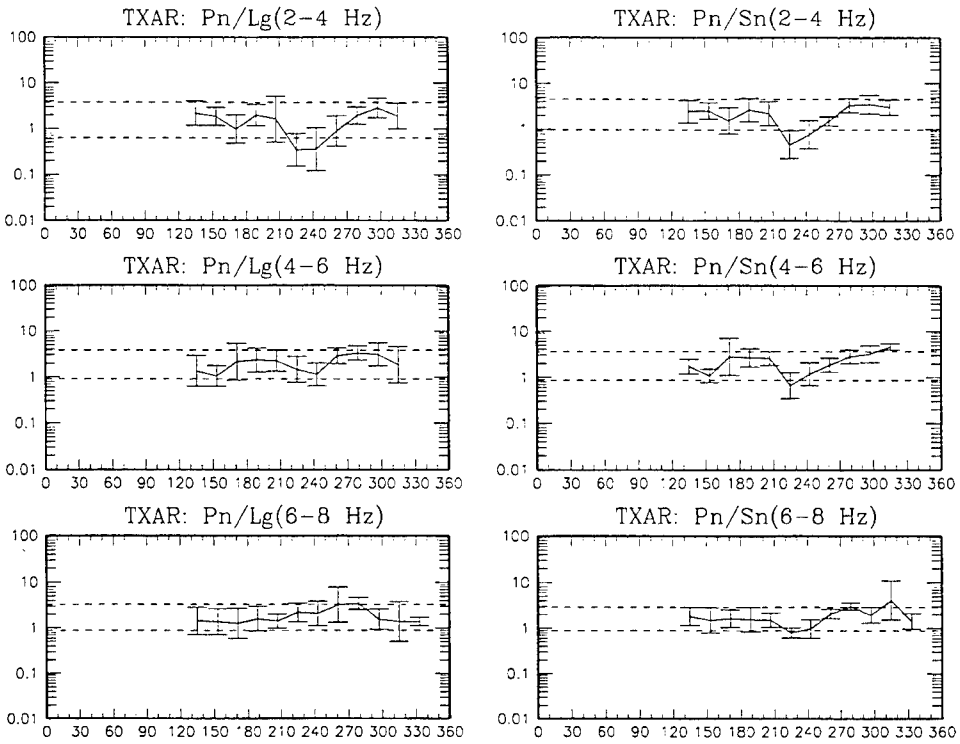

Figure 26. Azimuthal variations at TXAR. Error bars are plus or minus one standard deviation.

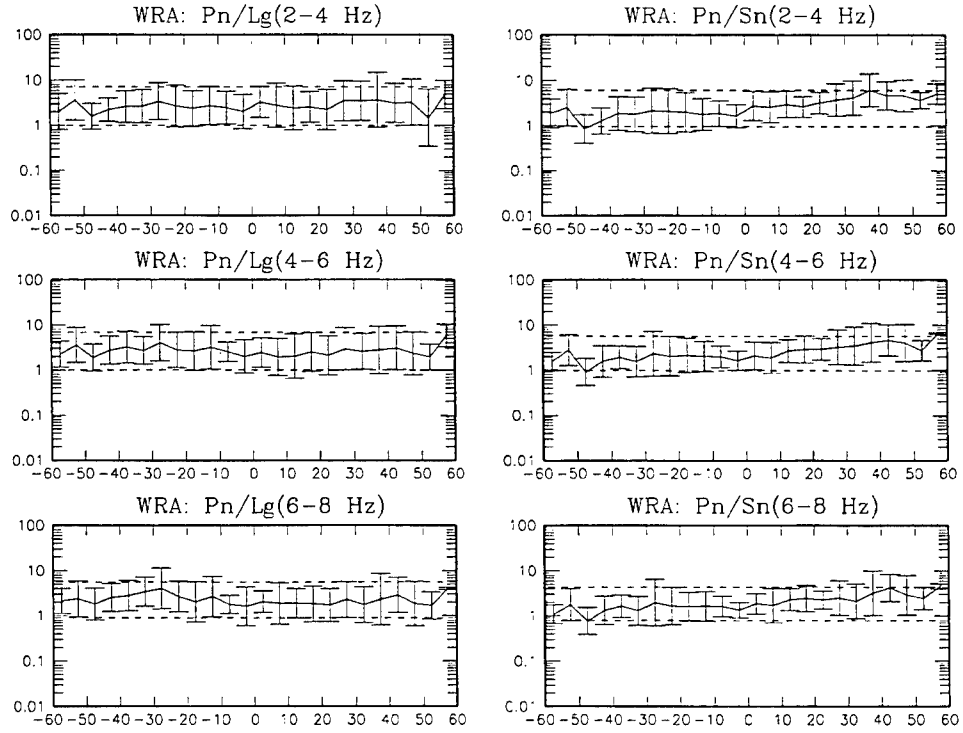

Figure 27. Azimuthal variations at WRA. Error bars are plus or minus one standard deviation.

3.7 Conclusions and Recommendations.

In this section, we described ongoing work to improve distance corrections for regional phase amplitude ratios, utilizing 7,603 regional events recorded by the IMS seismic network. The distance corrections include both geometrical spreading and attenuation terms, and provide a much better approximation of the distance dependence than does a simple power-law parametrization. Roughly 50 of the existing 87 IMS seismic stations have adequate data (i.e., at least 30 events with $SNR \geq 2.0$) with which to compute the distance corrections. Explicit details of the distance corrections for these stations are provided in the appendix to this report.

Anomalous distance dependence at some stations can be attributed, in part, to variations in propagation paths and properties of the near-source media. Treatments of azimuthal variations and tectonic subregions were illustrated for LPAZ, TXAR and WRA, showing possible improvements that can be made by dividing training sets into subregions, each with a smaller variance than the entire set. Another promising approach by Lay et al. (1997), treating other geophysical properties along the path, such as mean topography, crustal thickness, sediment thickness, and roughness, has been applied to station ABKT. These and other approaches need to be examined further.

Another approach that could alleviate the need for distance corrections as IMS regional seismic data accumulate is to compare an event in question to other events that are *close* in distance. The definition of "close" could mean having a similar distance from the station, similar azimuth and/or tectonic subregion. A better definition of "close" would require all training events to be within a certain distance of an event being tested. This would require much more data so as to have enough training events at roughly the same location. In either case, it is a non-trivial problem to quantify the notion of close. Basically, it must be determined if it is better to include a potential training event at a given distance away from the test event than to not include it in the set. This depends on how different the distribution of events are at further locations. If this were known, then a correction could be made; however, in these cases, the dependence on location is not known and it is often difficult to approximate. Thus, the problems of determining the dependence of regional amplitude ratio distributions on location and what is meant by close are intimately related.

As more IMS data become available at the prototype IDC, we plan to progressively improve and validate the regional distance corrections. We are also developing grids of blockage and strong attenuation for regional seismic phases. We plan to further develop, test and evaluate these grids. We recommend that each IMS station be studied individually to determine the best approach of dividing a particular regional training set into subsets of minimized variance. We also recommend that ground-truth data for historical explosions be processed according to standard PIDC techniques and used in the evaluation of the regional distance corrections and screening analysis.

Section 4
Analysis of the 10 November 1996 Southern India Event

4.1 Introduction.

Based on automated and analyst-reviewed processing at the PIDC, an mb 4.17 seismic event occurred on 10 November 1996 (961110) at approximately 09:00:00.4 UTC, 18.087° latitude and 76.506° longitude in Southern India. The event was approximately 35.9° from ZAL, 21.2° from CMAR, and 15.8° from NIL. Signals were also detected by 19 other stations. The focal depth of the event was constrained to the surface in the reviewed location analysis and, hence, it cannot be assumed that it was a deep natural event. Furthermore, there were no long-period surface waves detected. Thus, screening criteria based on depth and mb-Ms could not be applied.

Using seismic waveforms from station NIL in Pakistan, we compare this event to previous events in the region, including presumed earthquakes and two underground nuclear explosions at the Lop Nor test site in China. (Fisk et al., 1996a, provide a more detailed discussion of the Lop Nor events.) Since the 961110 event was not necessarily deep and did not have an estimate of Ms, we use high-frequency regional measurements of Pn/Lg and Pn/Sn to make the comparisons. We apply a statistical outlier test to make a multivariate comparison to previous events, as described in Section 4.3. Last, we provide some conclusions regarding this event.

4.2 Data.

Figure 28 shows the locations of station NIL, the 961110 event, two known underground nuclear explosions at the Lop Nor test site in China, and other regional seismic events (within 20 degrees from NIL) that were considered in the analysis. These other regional events are all mb 3.5 or above, and are presumed to be earthquakes. Their paths to NIL represent a relatively broad range of epicentral distances and azimuths, including another event in India with a similar path to NIL.

Figure 29 shows raw and bandpass-filtered seismograms on the sz channel for the 96/11/10 event at NIL. Preliminary inspection suggests that, although the signal-to-noise ratio was relatively low, the 961110 event generated comparable high-frequency Pn, Lg and Sn phase amplitudes. Pn, Lg and Sn maximum amplitude values were computed at the PIDC. Table 8 summarizes the Pn/Lg and Pn/Sn values in the 2-4, 4-6 and 6-8 Hz bands, before distance corrections were applied.

For comparison, Figure 30 shows the bandpass-filtered (4-8 Hz) seismograms at station NIL for the 961110 event and the 960608 (mb 5.69) and 960729 (mb 4.71) Lop Nor nuclear explosions.

Note that the Lop Nor explosions both occurred approximately 14.4° from station NIL, roughly the same distance (but different azimuth) as the 961110 event in India.

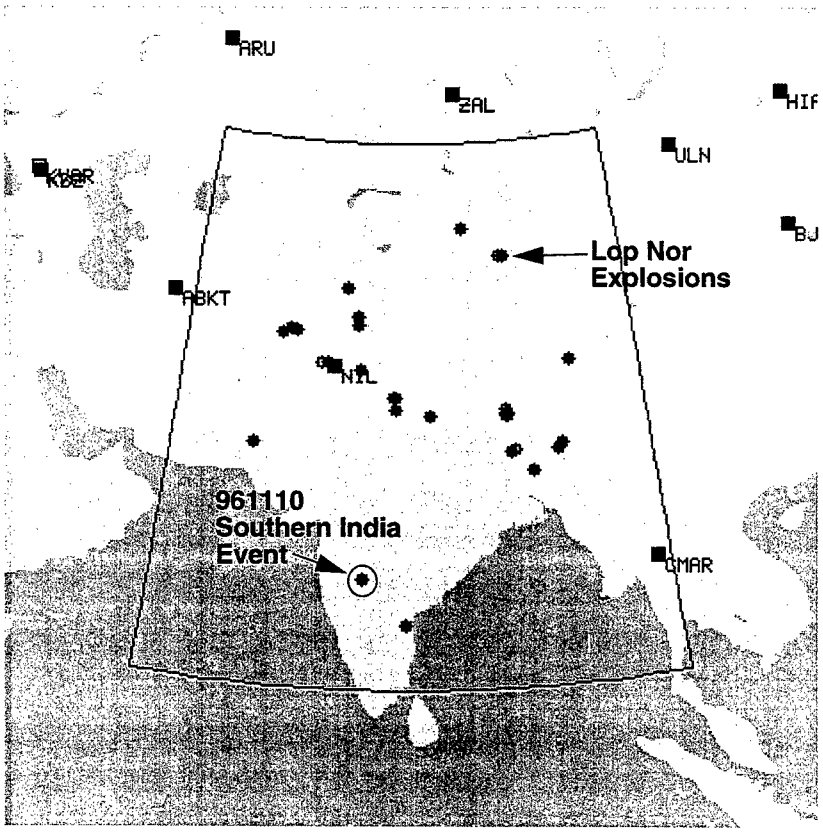

Figure 28. Locations of Auxiliary station NIL and seismic events used in the event characterization analysis of the 961110 Southern India event.

Table 8. Pn/Lg and Pn/Sn values for the *961110* event based on waveforms recorded by NIL.

	2-4 Hz	4-6 Hz	6-8 Hz
Pn/Lg	1.20	0.87	0.65
Pn/Sn	1.30	1.66	1.09

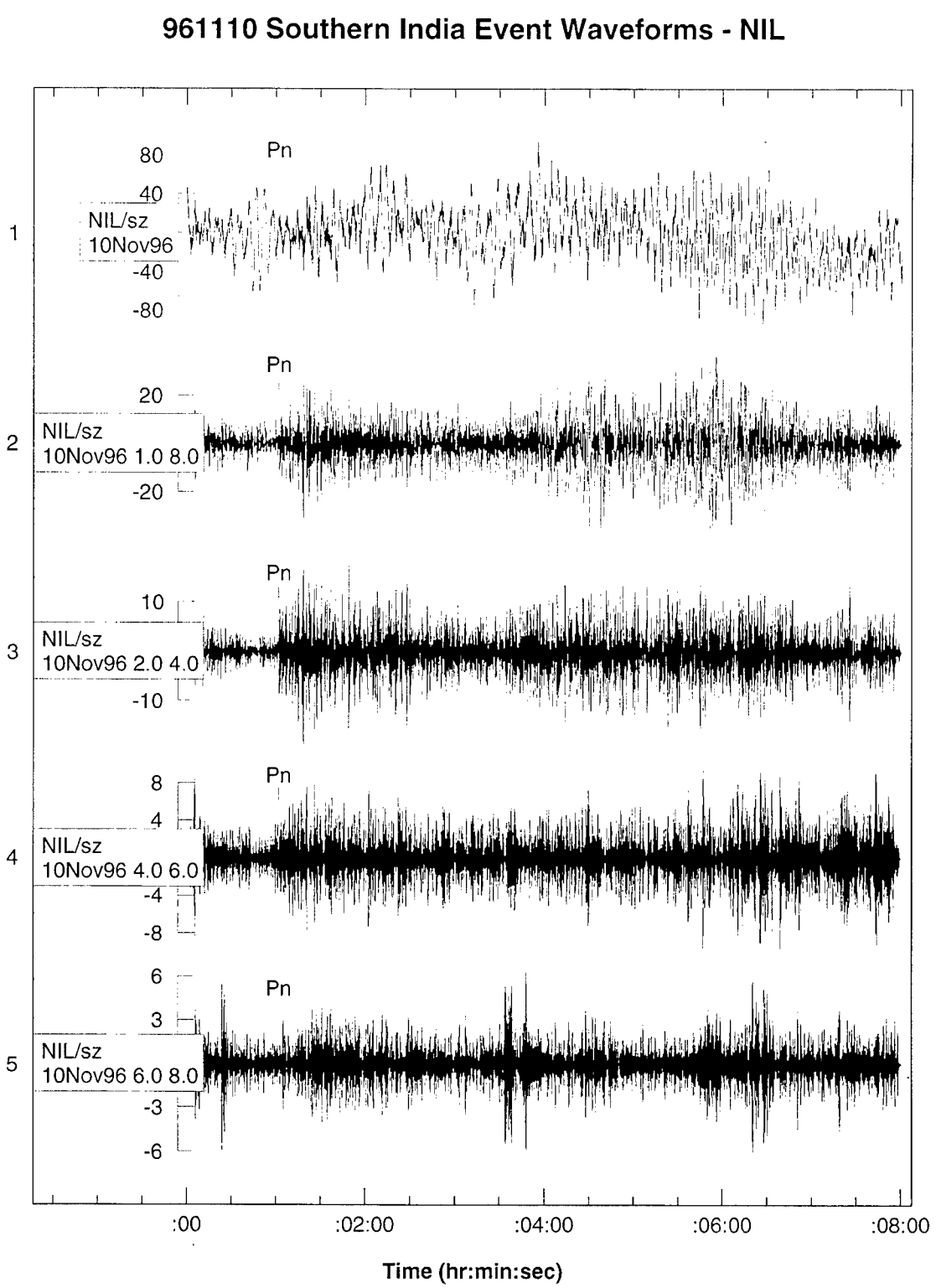

Figure 29. Raw (top) and bandpass filtered (1-8 Hz, 2-4 Hz, 4-6 Hz and 6-8 Hz, in descending order) seismograms recorded by station NIL in Pakistan for the 961110 Southern India Event.

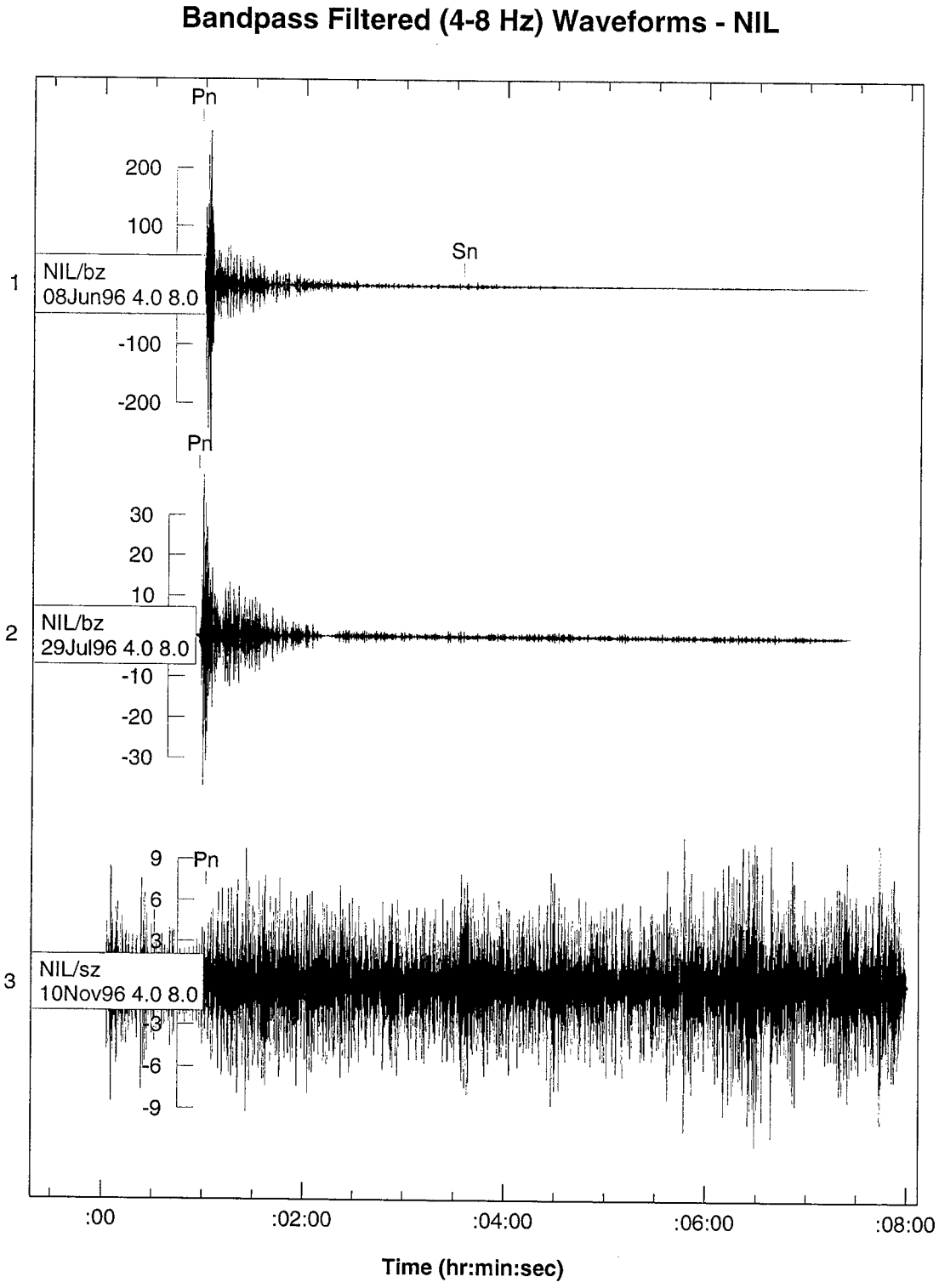

Figure 30. Bandpass filtered (4-8 Hz) seismograms recorded by station NIL for the 960608 and 960729 Lop Nor explosions and the 961110 India event (bottom trace). By comparison, the 961110 India event has considerably lower high-frequency P-to-S energy than the Lop Nor explosions. Its Pn phase is also far less impulsive as compared to the Lop Nor explosions.

Note that both Lop Nor explosions had depth estimates constrained to the surface. The 960608 Lop Nor event has a 99% confidence interval for mb-Ms entirely above a threshold of 1.2, while no Ms measurements were available for the 960729 Lop Nor explosion. Thus, as for the 961110 India event, regional analysis was required in order to characterize the 960729 Lop Nor event.

Figure 31 shows the Pn/Lg (left) and Pn/Sn (right) values versus distance in the various frequency bands for the 961110 Southern India event, the two Lop Nor explosions and the other events in the same region, which are presumed to be earthquakes. Figure 32 shows plots of the distance-corrected Pn/Lg and Pn/Sn values, computed for the NIL recordings in the 2-4, 4-6 and 6-8 Hz bands. The values for the 961110 Southern India event appear to be consistent with other regional seismic activity, and considerably different that the Lop Nor nuclear explosions.

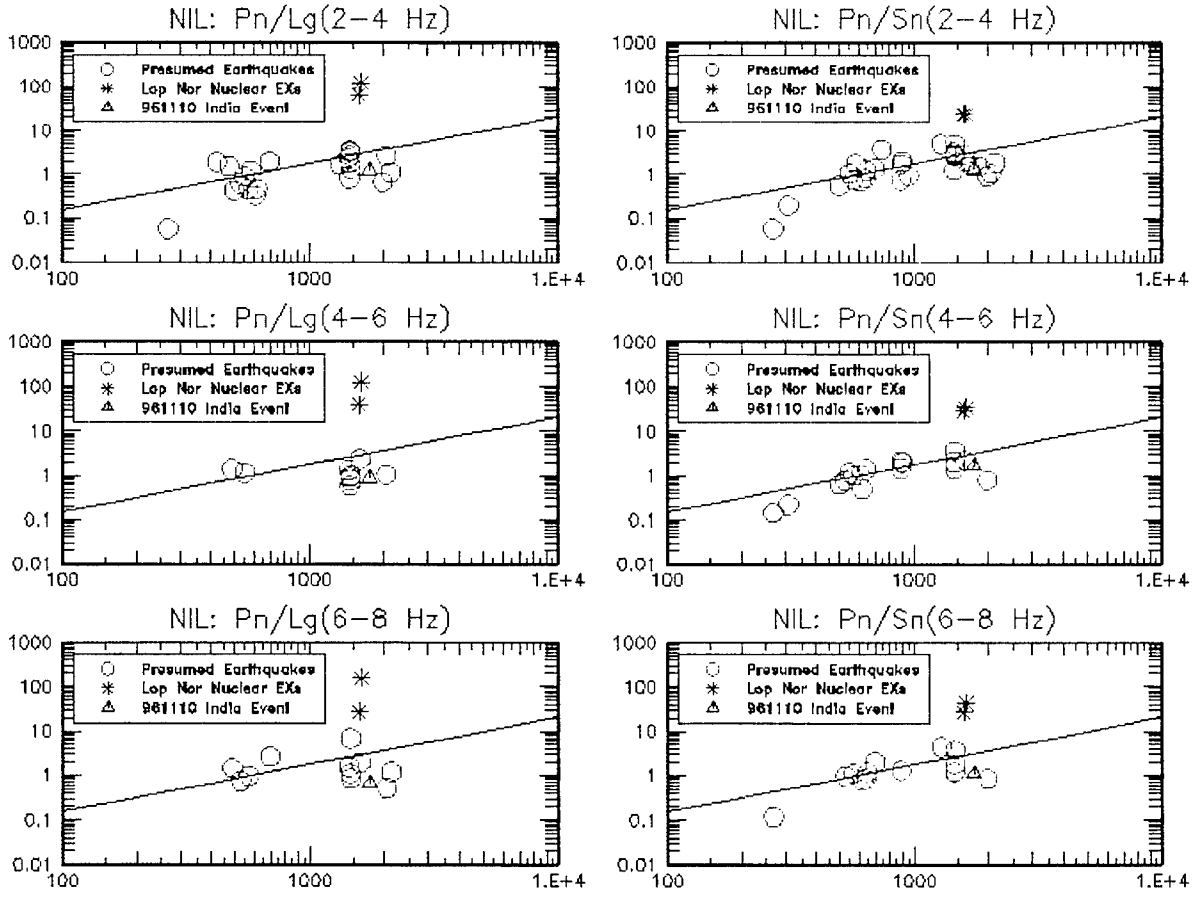

Figure 31. Regional Pn/Lg and Pn/Sn values versus distance, computed for station NIL in the 2-4, 4-6 and 6-8 Hz bands, for presumed earthquakes, two Lop Nor underground nuclear explosions and the 961110 Southern India event. The lines depict the empirical distance dependence that is used to correct for regional attenuation.

4.3 Regional Population Analysis.

To compare the 961110 event to previous seismic activity observed by NIL, we performed a multivariate outlier test, based on the likelihood ratio, in which the 961110 event was tested as an outlier of the regional earthquake group. Pn/Lg and Pn/Sn in the 2-4, 4-6 and 6-8 Hz bands were used as event characterization parameters. For comparison, we also tested each of the two Lop Nor underground nuclear explosions. Using the leave-one-out procedure, we further tested each of the earthquakes as outliers of the remaining earthquake group. (Fisk et al., 1993, 1994, 1995, 1996a, 1996b, describe the outlier procedure and previous applications in greater detail.)

Figure 33 shows the results of this analysis. The distribution shown corresponds to that of the likelihood ratio obtained from the multivariate discriminant values for the training set. Each marker corresponds to the P-values for the individual events being tested. The upper legend associates the various markers with the different types of events. The P-value is the probability that a particular event is called an outlier, given its discriminant values, if it in fact belongs to the training group. That is, it is the area under the distribution of the likelihood ratio to the left of the likelihood ratio value for the particular event. A small P-value indicates that the event is inconsistent with the training set. The vertical line shown corresponds to the threshold of the outlier test for a 0.01 significance level. Events whose P-values fall to the left of this line are considered outliers at the 0.01 significance level.

Note that the P-values for the Lop Nor nuclear explosions are both less than 10^{-10}. This indicates that the regional Pn/Lg and Pn/Sn values for the Lop Nor explosions are extremely inconsistent with those for the regional earthquake group. The P-value for the 961110 event is 0.60. Thus, it is not considered to be an outlier of the regional population.

4.4 Conclusions.

This investigation of the 961110 Southern India event indicates that its regional high-frequency Pn/Lg and Pn/Sn characteristics are consistent with regional earthquakes seen by station NIL. Furthermore, its regional Pn/Lg and Pn/Sn characteristics are considerably different than those of two Lop Nor underground nuclear explosions. The regional population analysis indicates that there is insufficient seismic evidence to reject this event as belonging to the earthquake group in this region, based on the regional amplitude ratios and training events used. By comparison, the regional population analysis clearly indicates that both of the Lop Nor underground nuclear explosions are outliers at the 0.01 (or even a much smaller) significance level. This event and the 960729 Lop Nor event illustrate the necessity and utility of regional event characterization analyses, particularly for cases in which focal depth and Ms:mb do not provide useful evidence.

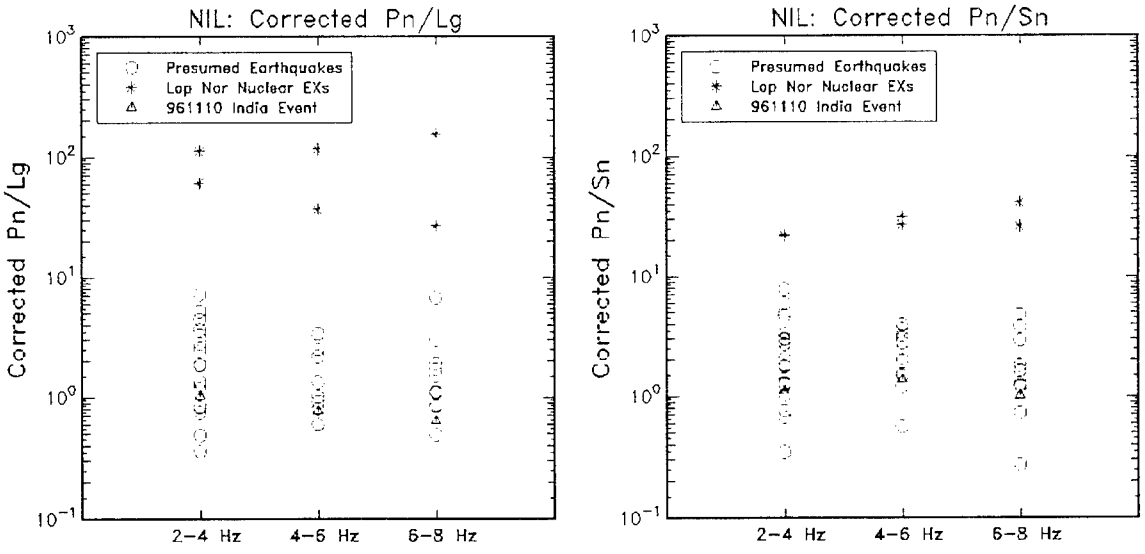

Figure 32. Distance-corrected Pn/Lg and Pn/Sn values, computed for station NIL in the 2-4, 4-6 and 6-8 Hz bands, for presumed earthquakes, two Lop Nor underground nuclear explosions and the 961110 Southern India event. The values for the 961110 Southern India event appear to be consistent with other regional seismic activity, and considerably different than the Lop Nor nuclear explosions.

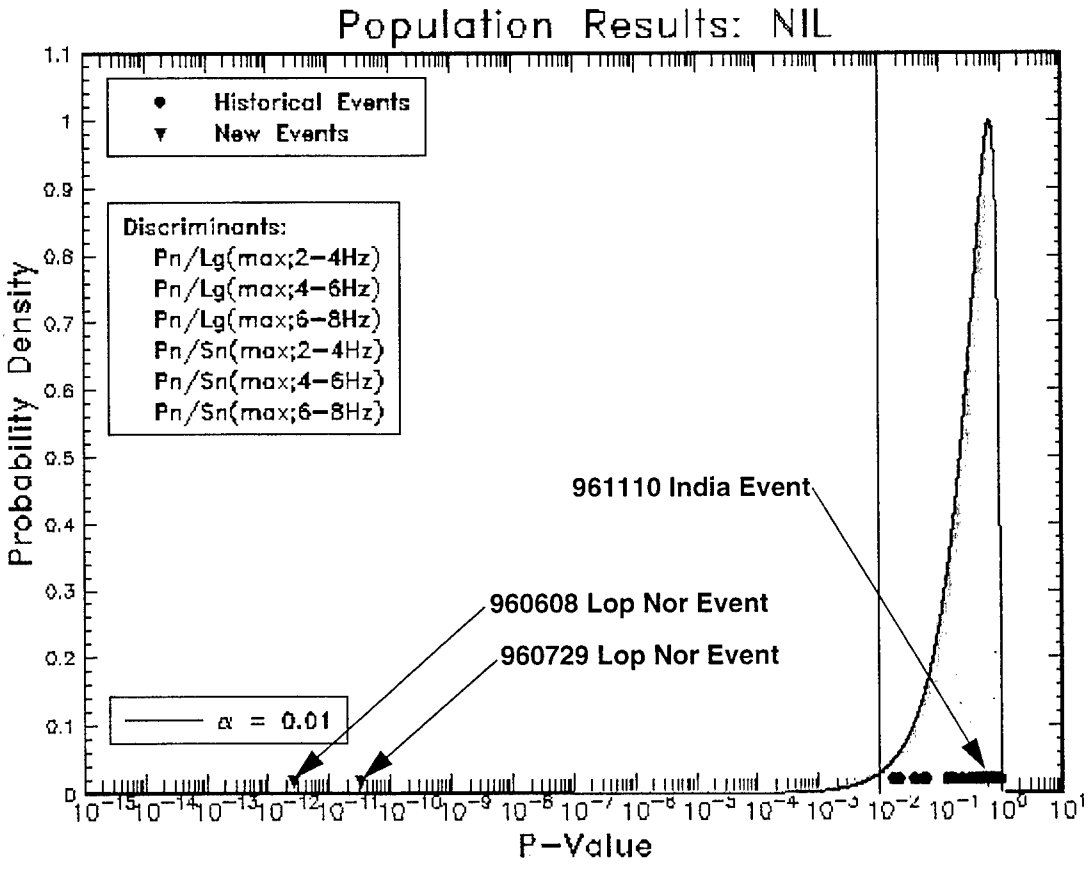

Figure 33. Regional population analysis results for station NIL for the 961110 Southern India event and two Lop Nor nuclear explosions. The event characterization parameters used are listed in the legend. The 961110 event is not an outlier of the regional event population at the 0.01 significance level.

Section 5
Analysis of the 16 August 1997 Event in the Kara Sea

5.1 Introduction.

Based on automatic and analyst-reviewed processing at the PIDC, an mb 3.9 seismic event occurred on 16 August 1997 (970816) at approximately 02:10:59.9 UTC, 72.65° latitude and 57.35° longitude in the Kara Sea near Novaya Zemlya (NZ). Figure 34 shows the Reviewed Event Bulletin (REB) for this event, including the associated arrivals. The event was approximately 10.62° from NRI, 11.44° from SPITS, 16.29° from ARU, 16.30° from FINES, 20.85° from HFS, and 21.00° from NORES. ARCES was not operating at the time.

After extensive review and use of the Joint Hypocenter Determination (JHD) program, using data from additional seismic stations and known event locations at NZ, the refined location estimate remains offshore in the Kara Sea, more than 100 km from the NZ test site, and is consistent with the original estimate in the REB (Israelsson et al., 1997; Bowers et al., 1997). It is also near the location of a presumed earthquake (mb 4.6) on 1 August 1986 (Marshall et al., 1989), as shown in Figure 35. Subsequent analysis, including non-IMS seismic data, revised the magnitude estimate to mb 3.3. A smaller (mb 2.5) event at the same approximate location and with similar seismic characteristics occurred about four hours after the main 970816 event, indicative of a possible aftershock (Ringdal et al., 1997; Richards and Kim, 1997).

The focal depth of the event was constrained to the surface and no long-period surface waves were detected. Hence, screening criteria based on depth and mb-Ms could not be applied and the 970816 event was not screened out, based on insufficient data. This event was not an outlier of the regional earthquake population recorded by NRI. The majority of the regional events available for such comparisons at FINES and SPITS occurred along the Mid Atlantic Ridge. Thus, valid application of the outlier test could not be made for these stations due to significant path differences for the available reference events.

In Section 5.2, all available waveforms for this event are presented and discussed, including those from IMS (NRI, SPITS, ARU, FINES, HFS and NORES) and non-IMS (NORSAR, KEV, and ten additional stations in Finland) stations. Available waveforms from some of these stations for known nuclear explosions at NZ, three events near NZ, and regional earthquakes are compared to the 970816 event. In Section 5.3, a statistical outlier test, using distance-corrected high-frequency Pn/Sn, is used to quantify the comparisons to previous earthquakes and explosions at relevant regional stations, KEV and NRI. In Section 5.4, conclusions regarding this event are provided.

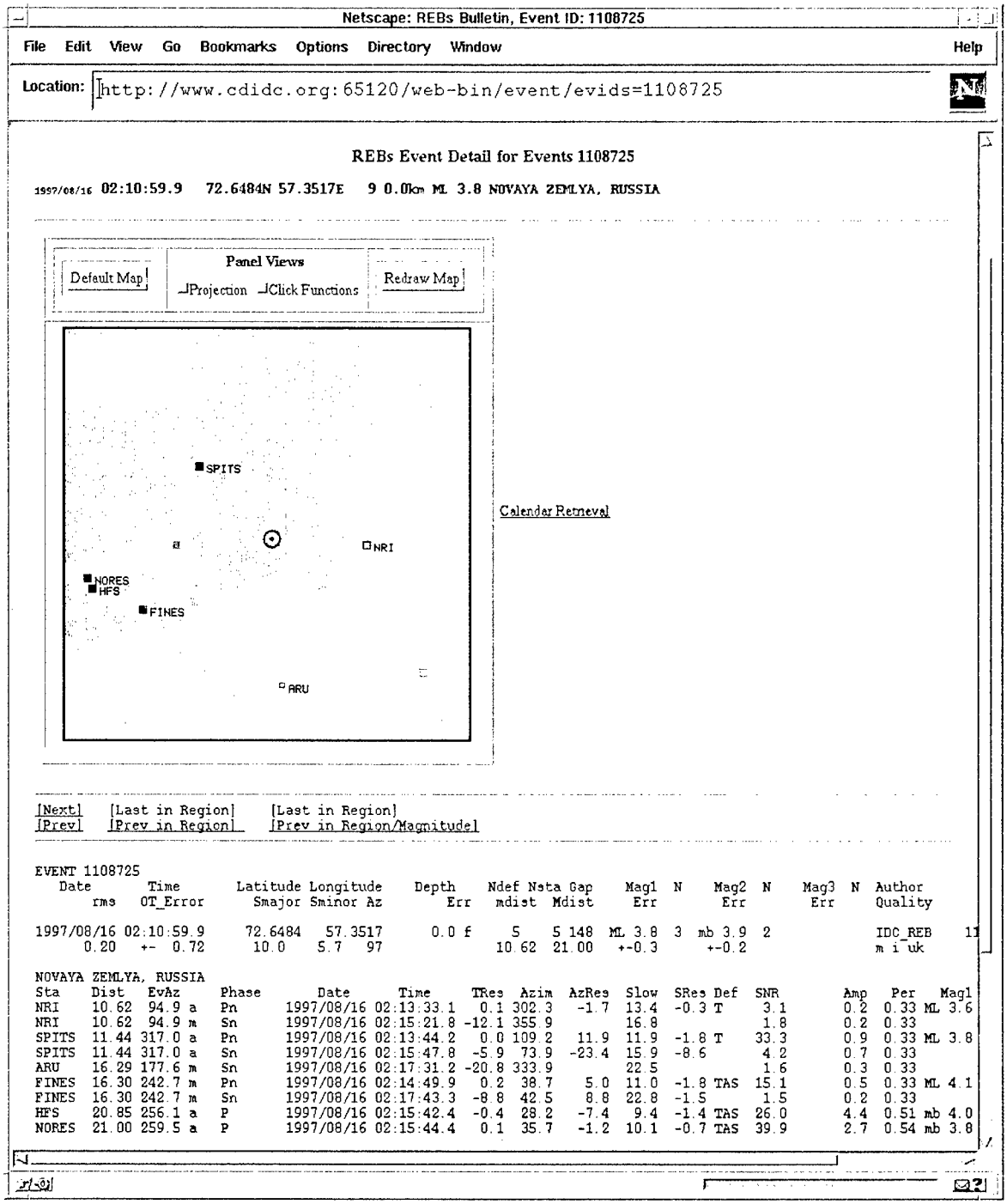

Figure 34. Reviewed Event Bulletin (REB) for the 970816 Kara Sea event. Included is a map showing the locations of the stations with associated phases and the estimated location of the event. Origin and associated arrival information are listed below the map.

5.2 Waveform Data for the 970816 Event.

Table 9 summarizes the available seismic data for the 970816 event and for other relevant nuclear explosions and earthquakes used for comparison. Figure 35 depicts the locations of the events near or on Novaya Zemlya. Columns in Table 9 include: (1) the stations (those with asterisks are IMS stations); (2) the distances of the 970816 event to the stations; (3) the available data for the 970816 event (including waveforms and Pn/Sn measurements at some stations); (4) available data for previous NZ nuclear explosions; (5) available data for other regional events (including the 860801, 950613 and 960113 events near NZ); (6) comments about the data quality at the various stations; and (7) a summary of the regional population analysis results at relevant stations. The stations are ordered by distance from the 970816 event. The entries in Table 9 that are shaded correspond to cases for which no applicable or valid comparison can be made.

Note that at ARU the data for the 970816 event had very poor signal-to-noise ratio (SNR) and Pn was not detected, even after review by an expert analyst. Thus, no comparisons were made at ARU.

At KBS and NUR the data for the NZ nuclear explosions are all long-period (LP). No LP signals were detected for the 970816 event. Thus, no comparisons could be made at these stations.

At NRI the data for the previous NZ nuclear explosions were hand-digitized and are not valid above 4 Hz. Nevertheless, comparisons have been made to the 970816 event for the sake of completeness, but with the caveat that these comparisons should not be regarded as valid above 4 Hz, the frequency range relevant to regional event discrimination.

At KEV, NORES and NORSAR there are digital waveforms for previous NZ underground nuclear explosions that are available for valid comparisons. There are five additional NZ explosions recorded by NORSAR (780810, 801011, 821011, 830925, 841025) that are not listed in Table 9 because the records are clipped. The Sn signals for the 970816 event at NORES and NORSAR have poor SNR, due to its small magnitude and strong Sn attenuation at far regional to teleseismic distances in this region. Waveform comparisons at NORES and NORSAR are made, but the comparisons shown below are inconclusive, due to poor Sn-SNR for the 970816 event.

Based on the available data, comparisons of waveforms for the 970816 event to those for previous nuclear explosions and earthquakes are made for stations KEV, NRI, SPITS, FINES, HFS, NORES, and NORSAR. Of these, the regional outlier analysis, as described in Section 5.3, is performed for stations KEV and NRI.

Table 9. Summary of data for comparison to the 970816 Kara Sea event

Station	Distance (Degrees)	970816 Event	NZ Explosions	Regional Earthquakes	Comment	Population Analysis
KEV	9.42	Waveforms Pn/Sn	821011, 841025 870802, 880507 881204, 901024	0	Good SNR for both Pn and Sn	Inconsistent with NZ EXs at 0.01 significance level
NRI*	10.62	Waveforms Pn/Sn	771009, 801011 (hdsz only)	21 EQs	hdsz records for EXs invalid above 4 Hz	Consistent with regional EQs
SPITS*	11.44	Waveforms Pn/Sn	0	950613 960113	Good SNR for both Pn and Sn	N/A
SDF	11.68	Waveforms	0	0	No records for comparison	N/A
KBS	12.41	Waveforms	4 (l* only)	0	No SP records for comparison	N/A
JOF	13.70	Waveforms	0	0	No records for comparison	N/A
KJN	13.71	Waveforms	0	0	No records for comparison	N/A
SUF	15.23	Waveforms	0	0	No records for comparison	N/A
KAF	15.68	Waveforms	0	0	No records for comparison	N/A
VAF	15.94	Waveforms	0	0	No records for comparison	N/A
KEF	16.03	Waveforms	0	0	No records for comparison	N/A
FINES*	16.30	Waveforms	0	950613	1800 km from FINES Strong Sn attenuation	N/A
PVF	17.11	Waveforms	0	0	No records for comparison	N/A
ARU*	17.15	Waveforms Poor SNR	16 (hdsz only)	0	hdsz records for EXs invalid above 4 Hz	N/A
NUR	17.46	Waveforms	8 (l* only)	0	No SP records for comparison	N/A
PKK	17.93	Waveforms	0	0	No records for comparison	N/A
HFS*	20.85	Waveforms	0	950613 (Poor SNR)	Beyond 20 degrees No regional phases Strong S attenuation	N/A
NORES*	21.00	Waveforms	841025, 870802 880507, 881204 901024	860801 950613 (Poor SNR)	Beyond 20 degrees No regional phases Strong S attenuation	N/A
NORSAR	21.77	Waveforms	761020 (sz) 771009 (sz) 840826 (sz)	860801	Beyond 20 degrees No regional phases Strong S attenuation	N/A

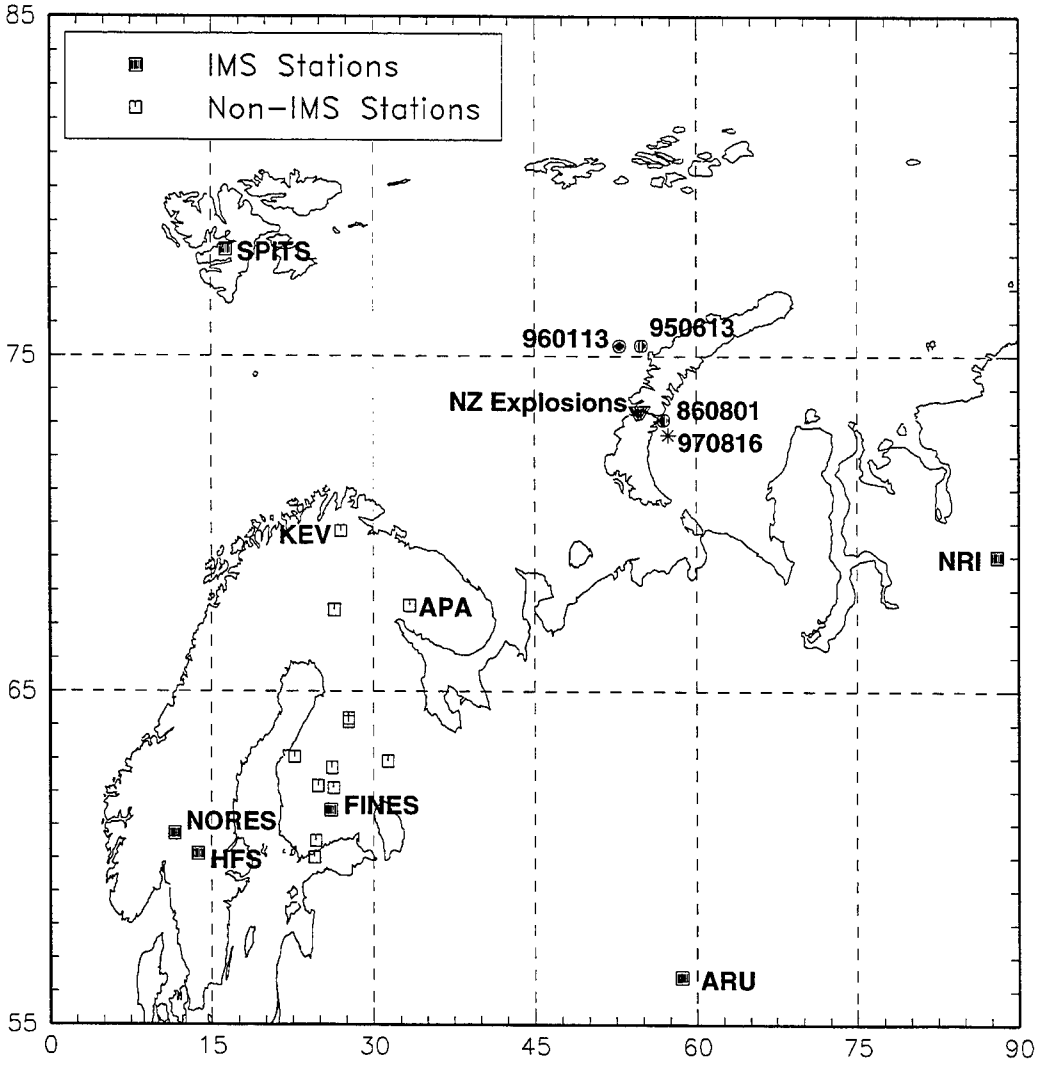

Figure 35. **Map showing the locations of the 970816 event, nuclear explosions at the Novaya Zemlya test site, and the 860801, 950613, 960113 events near Novaya Zemlya. Also shown are the IMS (solid squares) and non-IMS (open squares) seismic stations which recorded the 970816 event.**

Figures 36-43 show the available waveform data for the 970816 event at IMS seismic stations (NRI, ARU, SPITS, FINES, HFS and NORES), as well as non-IMS seismic stations (NORSAR and 11 stations in Finland). All of the waveforms shown in these figures have been bandpass filtered in the 4-8 Hz band.

Figure 36 shows that the 4-8 Hz Pn and Sn signals for the 970816 event are comparable in amplitude on all three components at NRI. Figure 37 shows that the signals recorded by ARU have very poor SNR, particularly for Pn.

Figure 38 shows that the 4-8 Hz Sn signals are smaller than the corresponding Pn signals on the sz and bz channels at SPITS, while the 4-8 Hz bandpass filtered Sn signals are significantly larger than the corresponding Pn signals on the bn and be channels at SPITS.

Figure 39 shows the 4-8 Hz bandpass filtered waveforms from FINES. The maximum Sn signals, while prominent, are smaller than the maximum Pn signals on all of the vertical channels.

Figures 40-42 show 4-8 Hz bandpass filtered waveform segments from HFS, NORES and NORSAR, respectively, all of which are approximately 21 degrees from the location of the 970816 event. Note that only teleseismic P arrivals were associated to this event at these stations. The P waves appear impulsive and there are no prominent S waves above the noise. These characteristics are typically thought to be consistent with signals from underground explosions, but it will be shown that regional earthquakes at similar distances and locations also exhibit this behavior.

Figure 43 shows the 4-8 Hz bandpass filtered waveforms from eleven Finnish stations, including KEV. At the present, we have available data for previous NZ explosions only from KEV and we do not have any earthquake data from these stations for comparison. However, these records show that for many of these stations the Sn signals for the 970816 event are comparable to or larger than the Pn signals (e.g., JOF, KEF, KEV, KJN, SDF, SUF). These waveforms further illustrate that there are distance and station-dependent variations in the signals.

Figures 44-56 show comparisons of the waveforms for the 970816 event to NZ nuclear explosions and regional earthquakes recorded by KEV, NRI, SPITS, FINES, HFS, NORES, NORSAR. All of the waveforms in these figures are filtered in the 4-8 Hz passband.

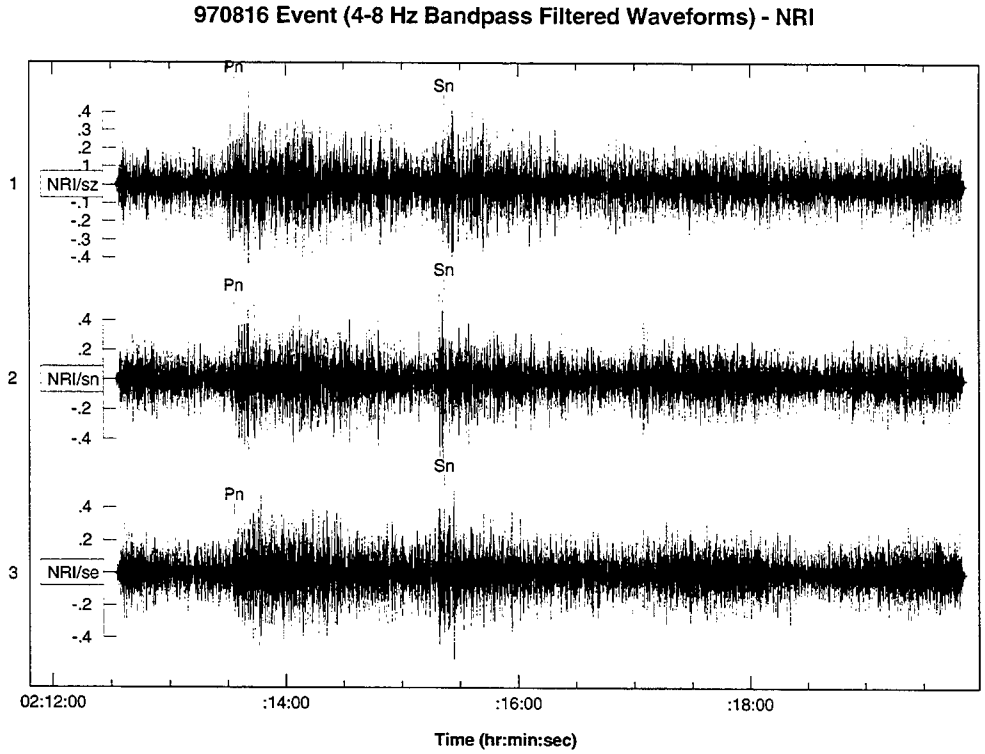

Figure 36. Bandpass-filtered (4-8 Hz) seismograms recorded by NRI for the 970816 event.

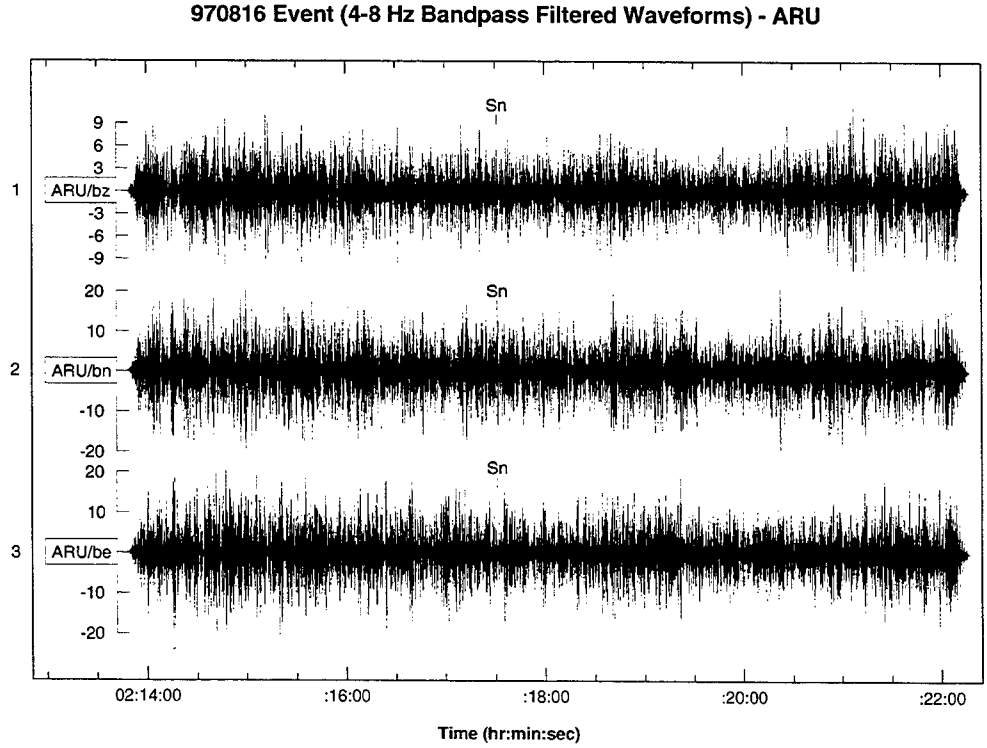

Figure 37. Bandpass-filtered (4-8 Hz) seismograms recorded by ARU for the 970816 event.

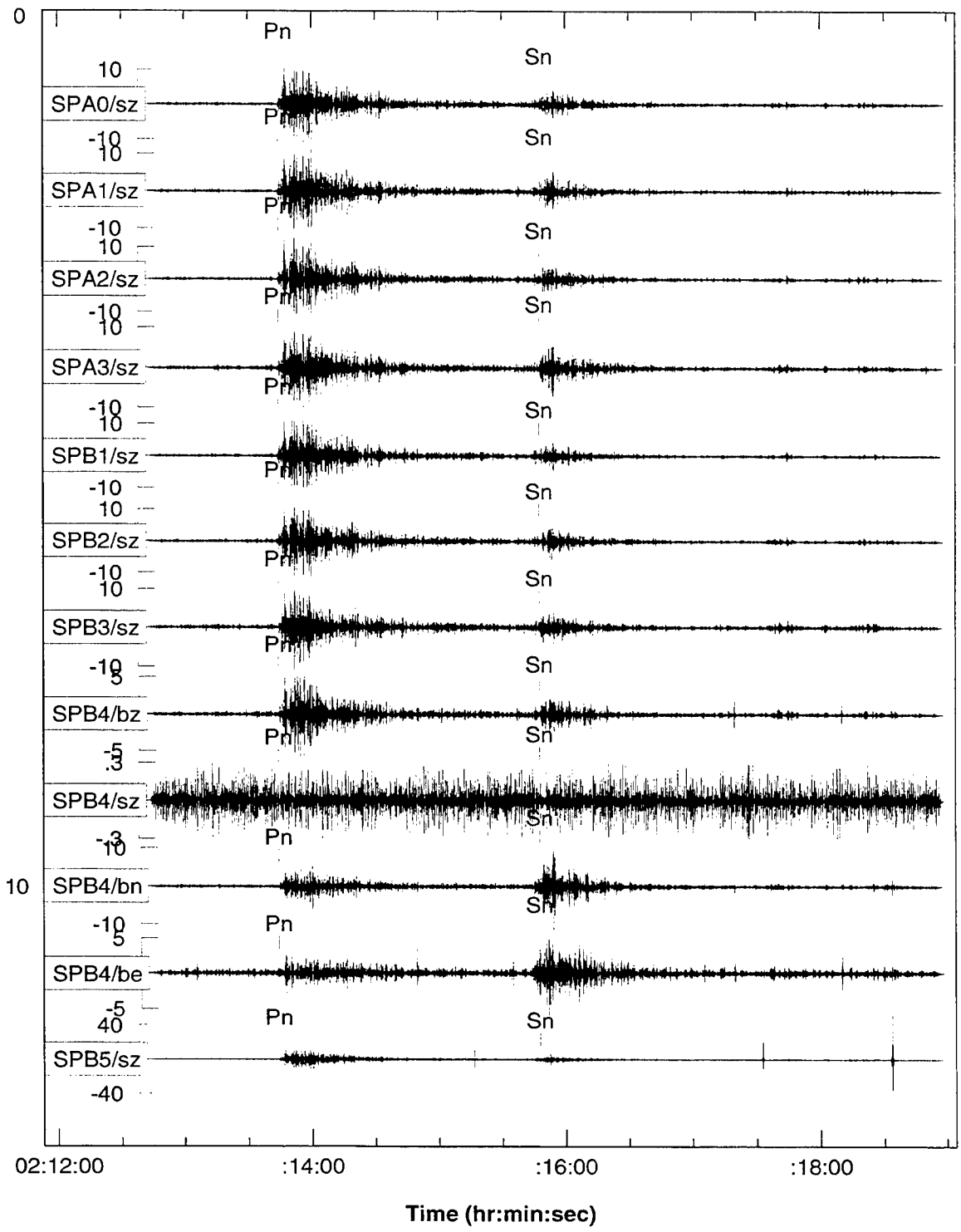

Figure 38. Bandpass-filtered (4-8 Hz) seismograms recorded by SPITS for the 970816 event.

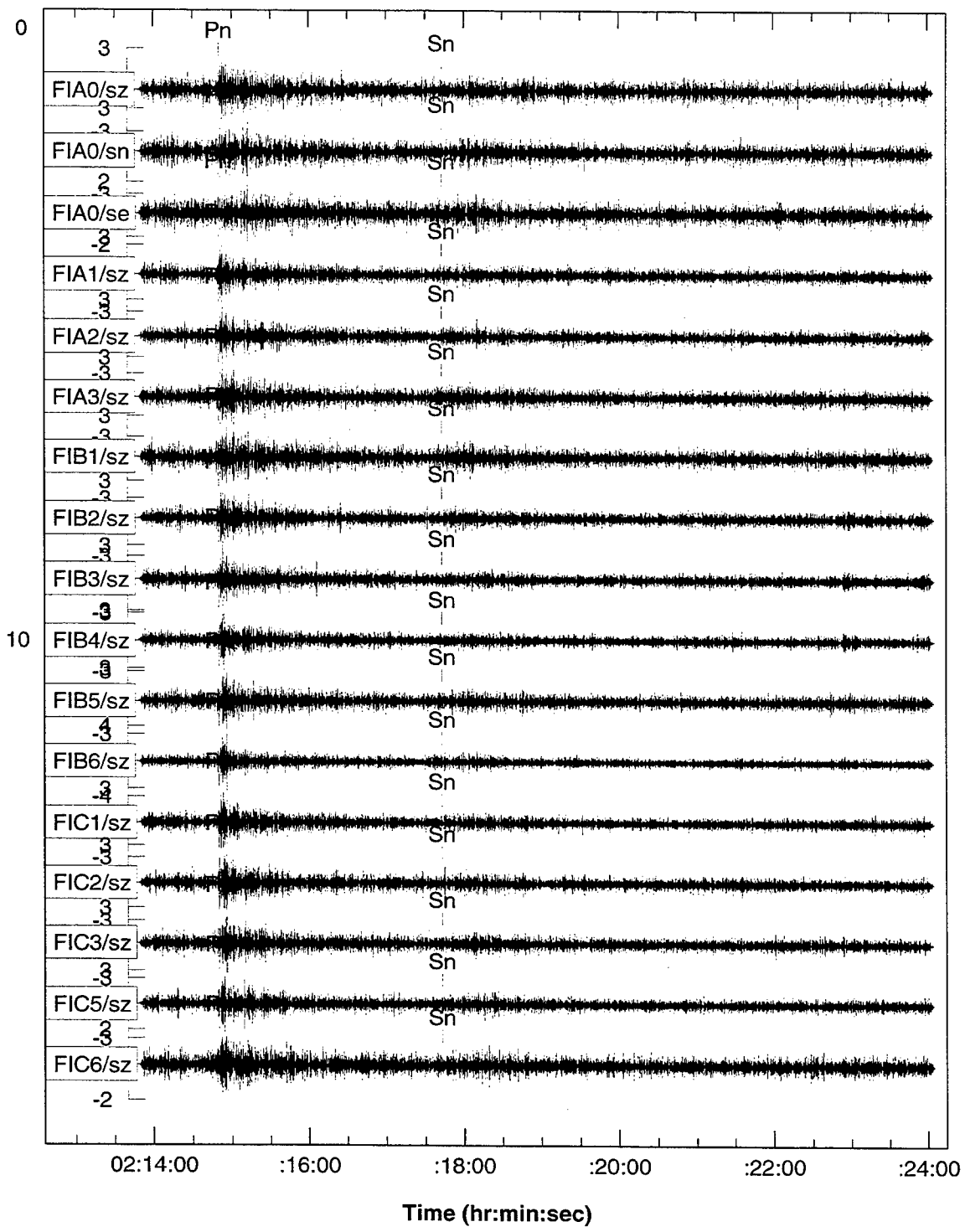

Figure 39. Bandpass-filtered (4-8 Hz) seismograms recorded by FINES for the 970816 event.

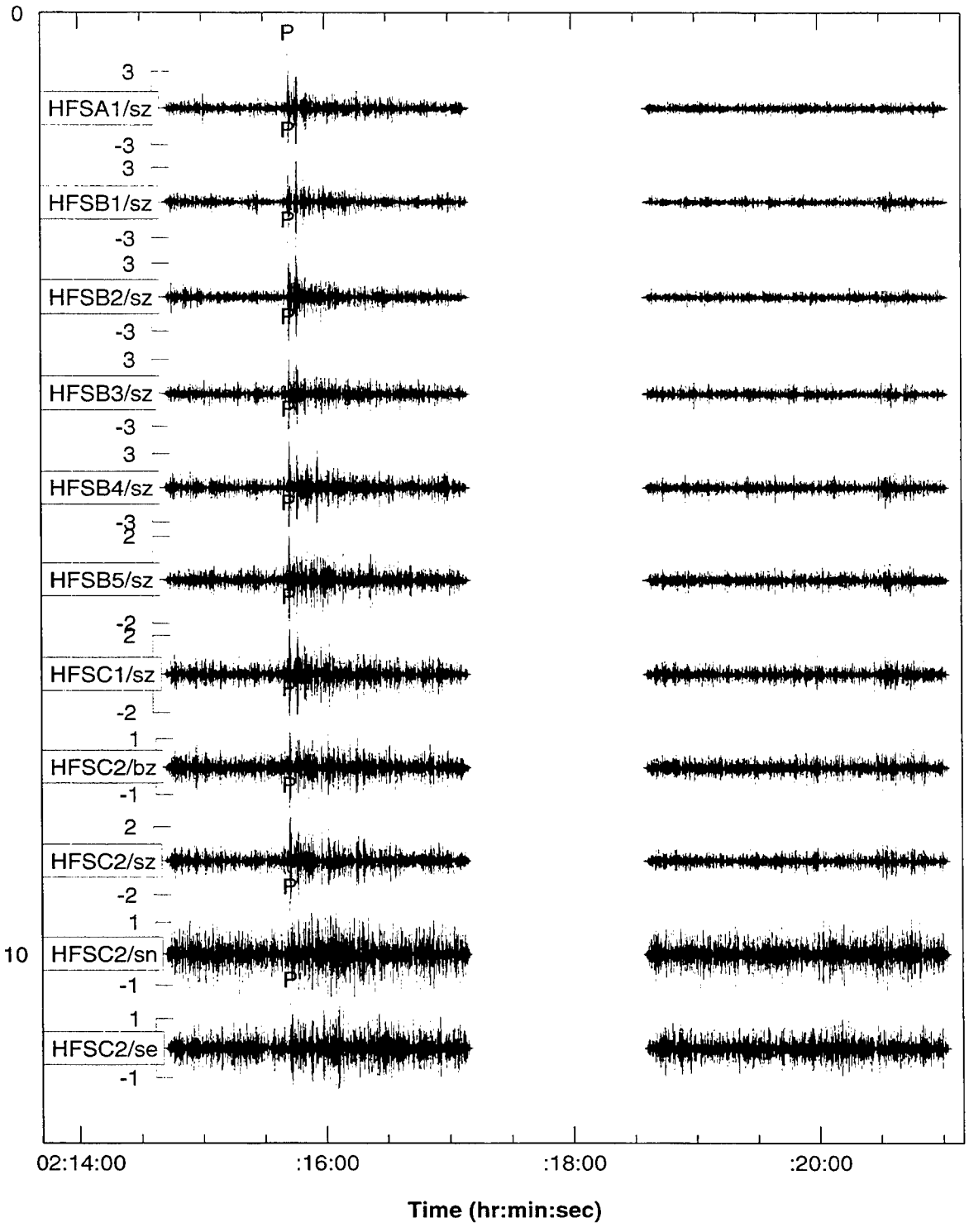

Figure 40. Bandpass-filtered (4-8 Hz) waveform segments from HFS for the 970816 event.

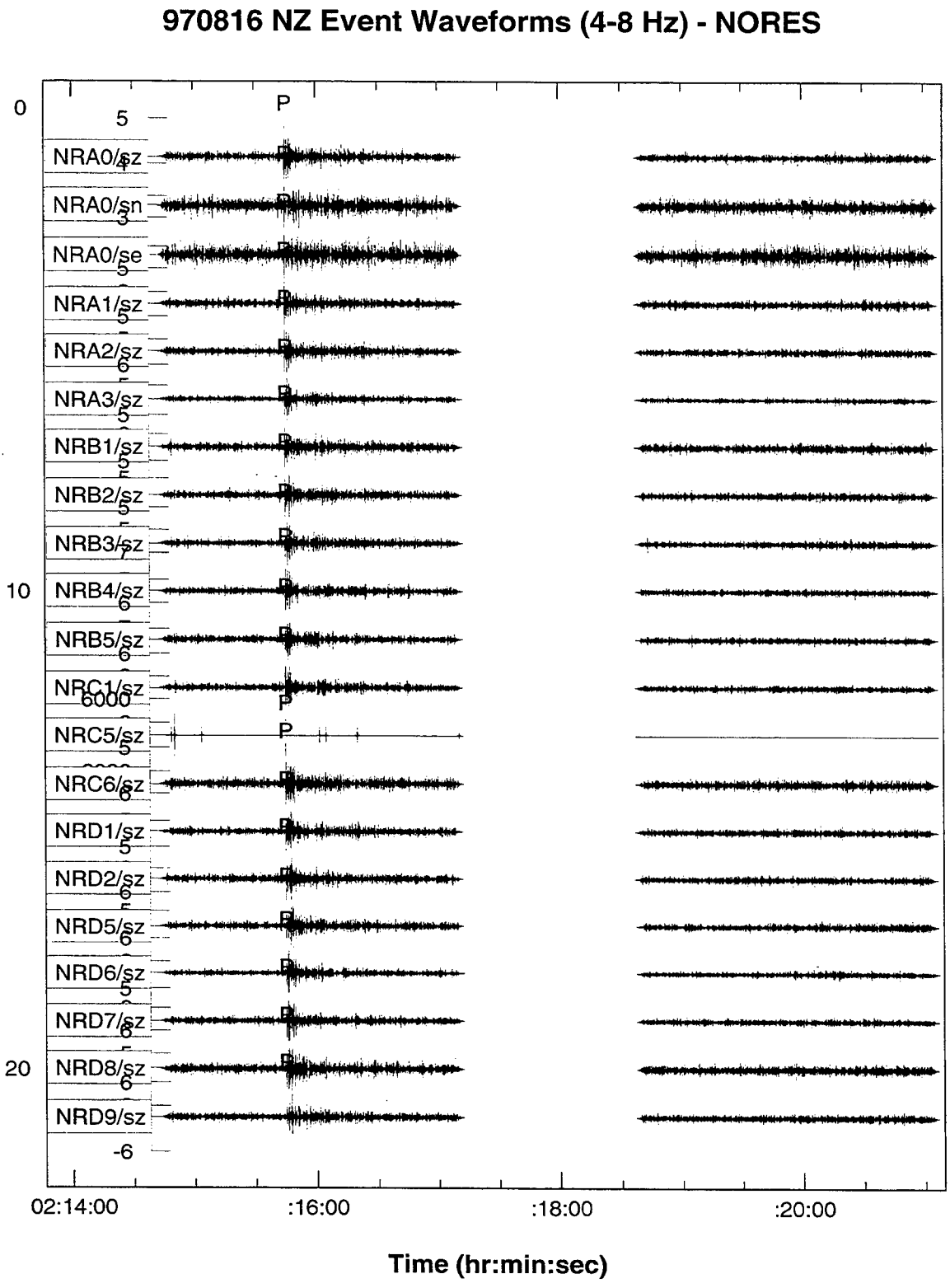

Figure 41. Bandpass-filtered (4-8 Hz) waveform segments from NORES for the 970816 event.

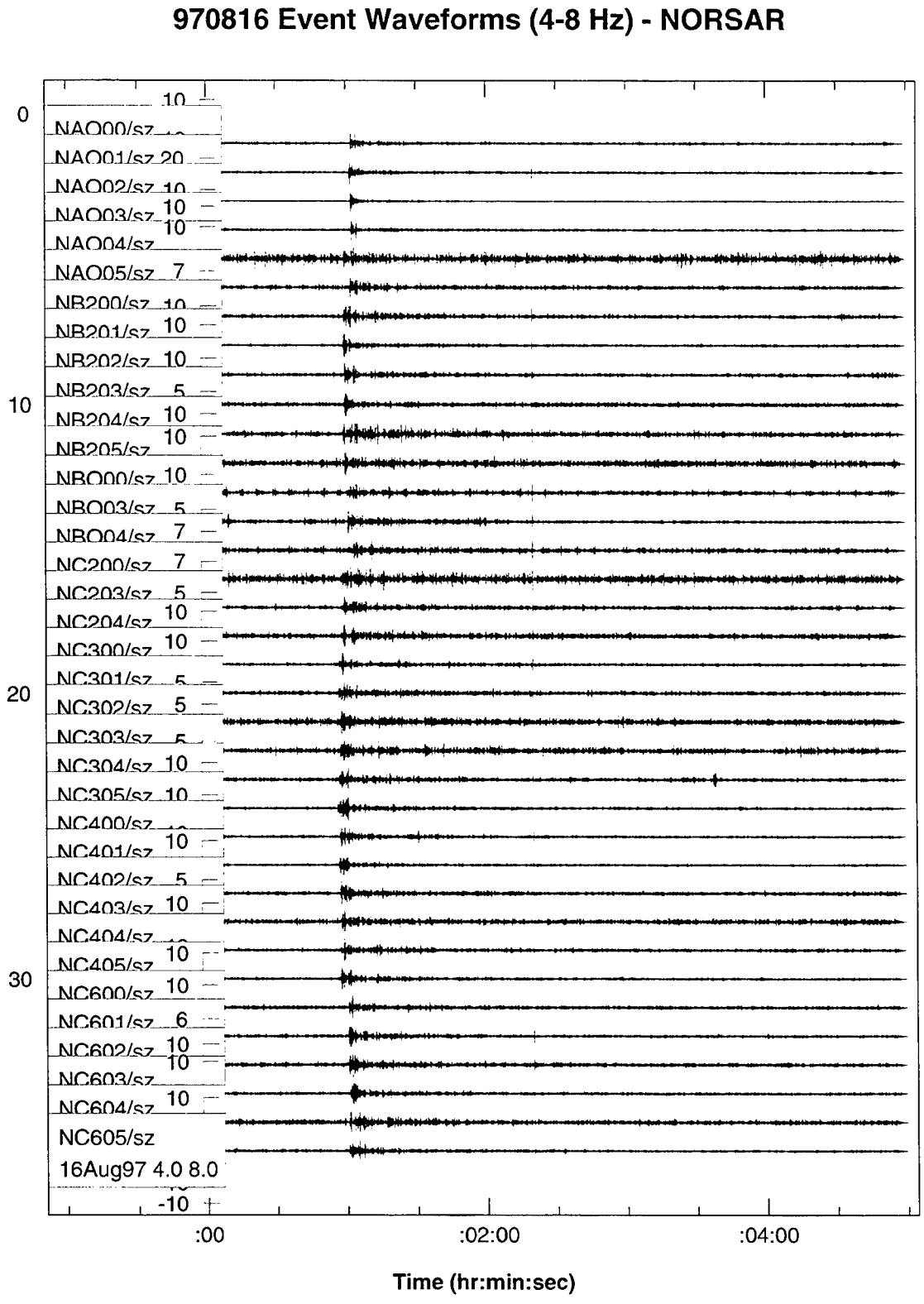

Figure 42. Bandpass-filtered (4-8 Hz) seismograms recorded by NORSAR for the 970816 event.

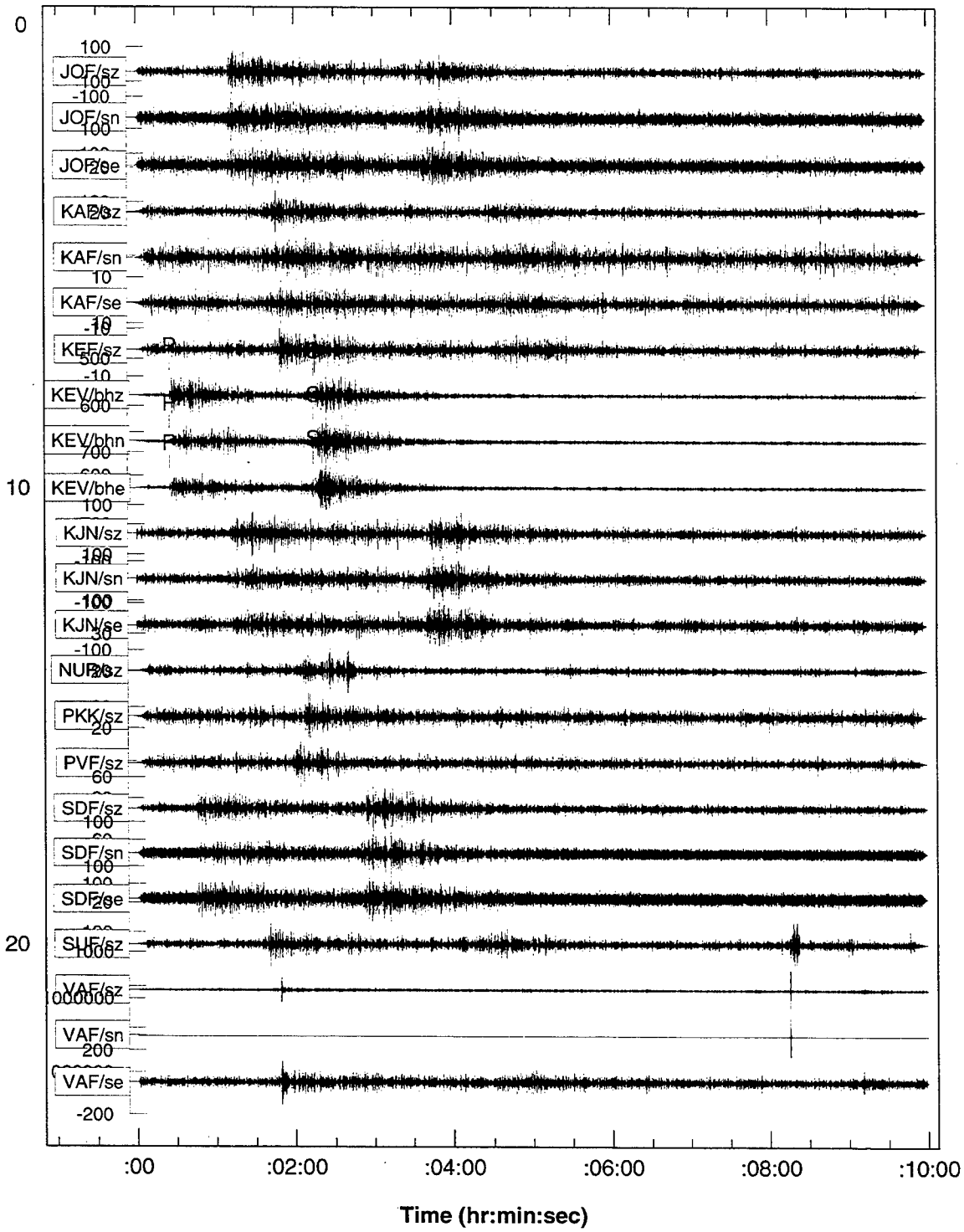

Figure 43. Bandpass-filtered (4-8 Hz) seismograms recorded by eleven Finnish stations for the 970816 event.

5.2.1 Waveform Comparisons at KEV.

Figure 44 shows vertical-component (4-8 Hz) waveforms at KEV for six NZ explosions (821011, 841025, 870802, 880507, 881204, 901024) and the 970816 event. The maximum Pn amplitudes are scaled the same for comparison. Sn for the 970816 event is considerably larger than Sn for the explosions. Pn/Sn(4-6 Hz) for the 970816 event is 0.90, less than half the smallest value for the explosions, which are between 1.95 and 3.39. Figure 45 shows horizontal-component (4-8 Hz) waveforms at KEV for three NZ explosions and the 970816 event. As for the vertical components, the 970816 event has much smaller Pn/Sn values than the NZ nuclear explosions.

Figure 46 shows unfiltered and 4-8 Hz bandpass filtered waveforms for the six nuclear explosions on all available bz and sz channels at KEV. There were no bz recordings for the 821011, 841025 and 870802 explosions and there were no sz recordings available for the 970816 event. To validate the comparisons of bz and sz channels, note that the 880507 and 901024 explosions were recorded on both channels and their Pn/Sn(4-8 Hz) values are equivalent on both for each event. (The sz waveform for the 881204 event contains spurious high-frequency content in the 4-8 Hz passband.)

A second significant point to make regarding Figure 46 is that although the unfiltered waveforms for the NZ explosions have larger Sn than Pn amplitudes, the Sn signals are significantly smaller than the Pn signals in the 4-8 Hz band. Thus, as many other previous authors have noted, regional Pn/Sn ratios typically provide valid discrimination above 3-4 Hz. Unfiltered seismograms or passbands at lower frequencies can lead to misleading comparisons.

5.2.2 Waveform Comparisons at NRI.

Figure 47 shows the 4-8 Hz bandpass filtered waveforms at NRI for two NZ explosion signals (771009 and 801011), a 970314 earthquake and the 970816 event. The 970314 earthquake had a different azimuth to NRI than the 970816 event, but they both occurred roughly 10 to 11 degrees from NRI and have similar magnitudes. The 970314 and 970816 events have similar Pn/Sn in the 4-8 Hz band. The signals for the two NZ explosions were hand-digitized; hence, the passband filtered signals exhibit spurious spikes and should not be considered valid in this frequency range.

5.2.3 Waveform Comparisons at SPITS.

Figure 48 shows a comparison of 4-8 Hz filtered waveforms for the 970816 event at SPITS to those for the 950613 and 960113 events. Figure 49 shows the SPA0/sz channels for the three events in the 4-6 and 6-8 Hz bands. All three events have similar waveforms, although Sn for the 970816 event is smaller than those for the other two events. Note that the 970816 event was farther away from SPITS than the other events; hence, relative attenuation of Pn and Sn must be considered.

Table 10 lists the distances and Pn/Sn values in the 4-6 and 6-8 Hz bands for these three events before and after applying distance corrections. The slopes of the corrections for the 4-6 and 6-8 Hz bands are 1.0 and 0.9, respectively. Although the 970816 event has the largest Pn/Sn values before applying corrections, its corrected values are not inconsistent with the 950613 and 960113 events near NZ, given the variation in the Pn/Sn values. Even using conservatively low slopes of 0.6 and 0.5, there is insufficient evidence to reject the 970816 event as being consistent with the 950613 and 960113 events.

Table 10. Pn/Sn values at SPITS before and after applying distance corrections.

Date	Lat	Lon	Distance (km)	4-6 Hz Before	6-8 Hz Before	4-6 Hz After	6-8 Hz After
950613	75.32	54.85	1009.32	1.27	1.40	1.88	2.00
960113	75.31	52.86	964.30	0.85	1.97	1.31	2.93
970816	72.65	57.35	1264.19	2.31	2.52	2.74	2.93

5.2.4 Waveform Comparisons at FINES.

Figure 50 shows a comparison of bandpass filtered waveforms for the 970816 event at FINES to those for the 950613 event (FIA0 only). Both events exhibit similar waveform characteristics; however, due to poor SNR for both events, the comparison is inconclusive.

5.2.5 Waveform Comparisons at HFS.

Figure 51 shows a comparison of bandpass filtered waveforms for the 970816 event at HFS to those for the 950613 event (HFSC2/sz channel only). As for FINES, both events exhibit similar characteristics but, due to the relatively poor SNR for both events, the comparison is inconclusive.

5.2.6 Waveform Comparisons at NORES.

Figure 52 shows a comparison of filtered waveforms (4-8 Hz) from NORES for the 970816 event, the 860801 earthquake, and six NZ nuclear explosions (NRB1/sz channel). All of the waveforms exhibit very impulsive P waves, even those for the 860801 earthquake. The explosions exhibit negligible S waves. Although the S waves for the 860801 earthquake are much smaller than the P waves, they are more prominent than the S waves for the explosions. The S waves for the 970816 event are obscured by noise.

To improve the SNR, beams were formed from the NORES array data for the same events (Figure 53). As for the NRB1/sz channel, the beams indicate that all of the events have very impulsive P waves and very small S waves, although the 860801 earthquake has noticeably larger S waves than the explosions. The S waves for the 970816 event appear to be slightly greater than the noise. This may indicate that the 970801 event is more consistent with the 860801 earthquake than the NZ nuclear explosions, although the evidence, due to relatively poor SNR, is inconclusive.

A very important point, however, is that an earthquake at this distance from NORES (21 degrees or 2331 km) can have very impulsive P waves and very small S waves, due to strong attenuation of S relative to P at far regional to teleseismic distances in this region.

5.2.7 Waveform Comparisons at NORSAR.

Figure 54 shows a comparison of the 4-8 Hz bandpass filtered beam for the 970816 event at NORSAR to those for the 860801 earthquake and the 761020, 771009, 840826 NZ nuclear explosions. As in Figure 53, all of these beams exhibit very impulsive P waves and very small S waves, although the S waves for the 860801 earthquake are much more prominent than those for the NZ explosions. The S waves for the 970816 event are obscured by noise. Hence, as for NORES, this comparison is inconclusive.

5.2.8 Summary of Waveform Comparisons.

Figures 55 and 56 illustrate a final comparison of waveforms for the 970816 event and a 961225 mb 4.1 event in the Jan Mayen Island region. The 961225 event was offshore, deeper than 10 km at the 95% confidence level and with mb-Ms < 1.2 at the 95% confidence level. Hence, there is strong evidence that the 961225 event in the Jan Mayen Island region was an earthquake. Figure 55 shows that Sn attenuates rapidly with distance and may also depend on azimuth. Figure 56 further illustrates that it is possible for an earthquake in this region to have very impulsive P waves and very large high-frequency Pn/Sn at some stations, possibly due to combined effects of strong Sn attenuation along certain paths and the shear-wave radiation pattern of the focal mechanism. Both events have at least one station for which Pn/Sn in the 4-8 Hz band is close to one.

To summarize, there is evidence at KEV that the 970816 event is inconsistent with six previous NZ nuclear explosions. There is no other evidence supported by these seismic data at any of the stations that indicates that the 970816 event is inconsistent with a natural event.

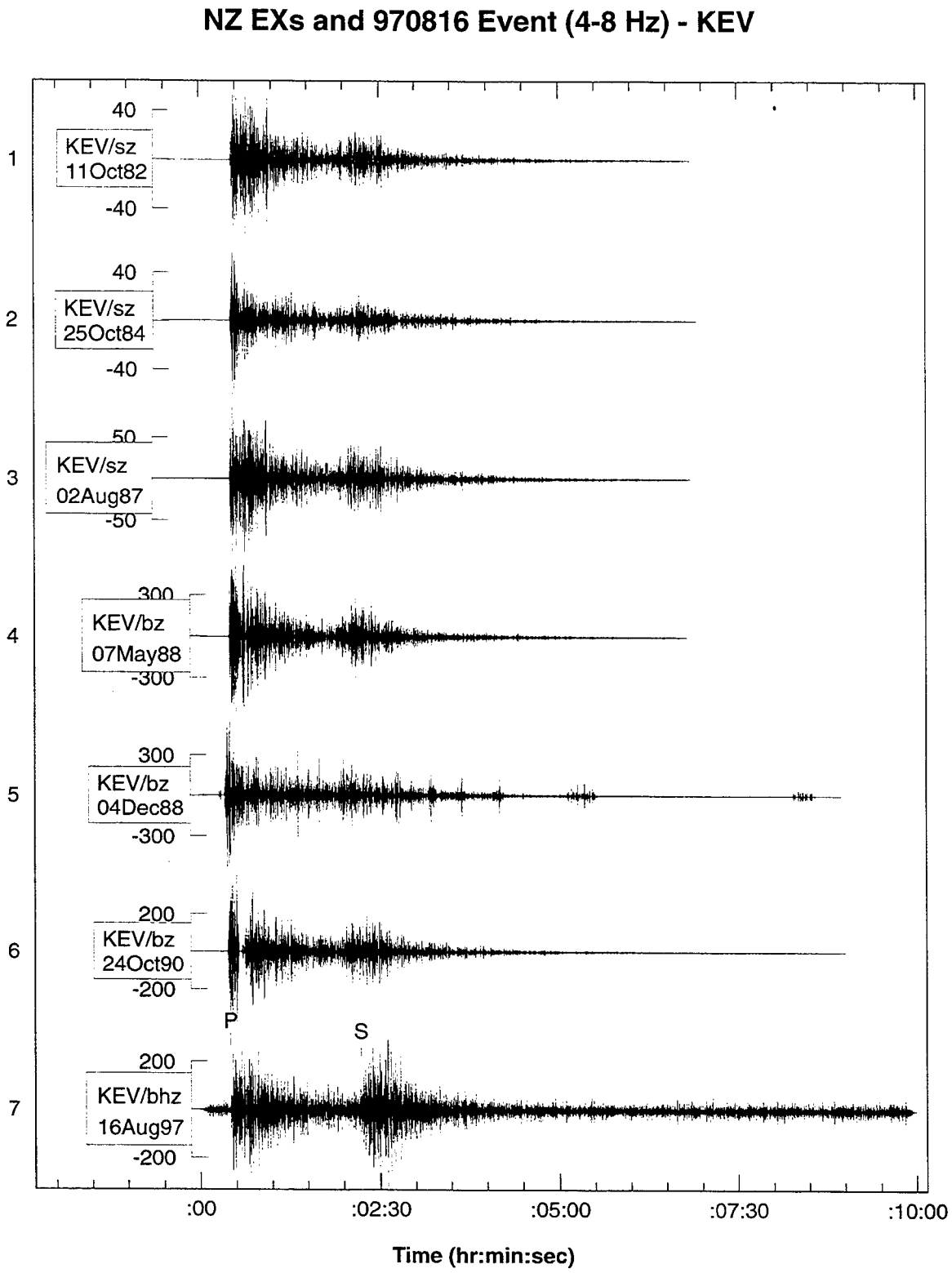

Figure 44. **Comparison of bandpass-filtered (4-8 Hz) vertical-component seismograms recorded by KEV for the 970816 event and six Novaya Zemlya nuclear explosions.**

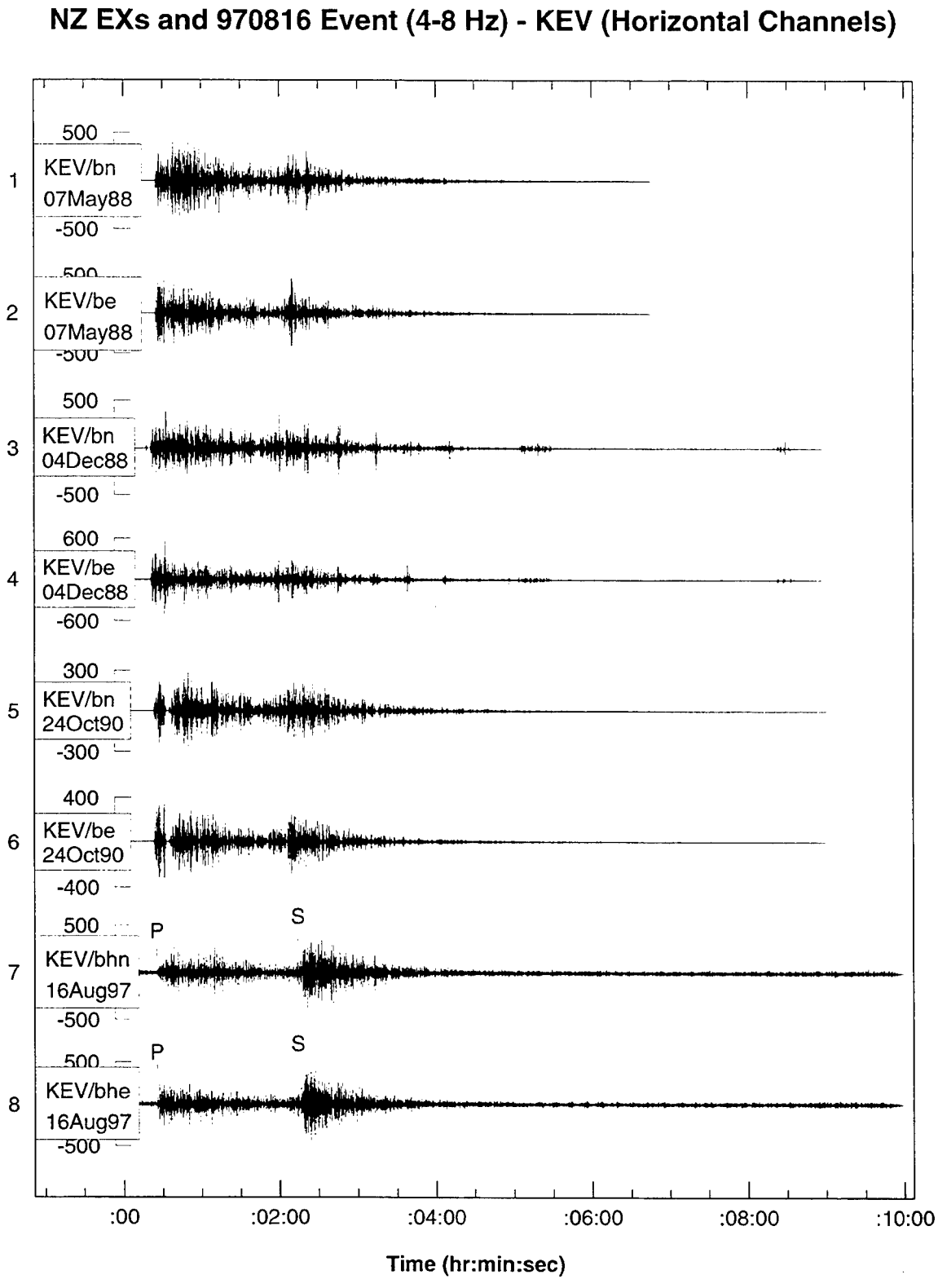

Figure 45. Comparison of bandpass-filtered (4-8 Hz) horizontal-component seismograms recorded by KEV for the 970816 event and three Novaya Zemlya nuclear explosions.

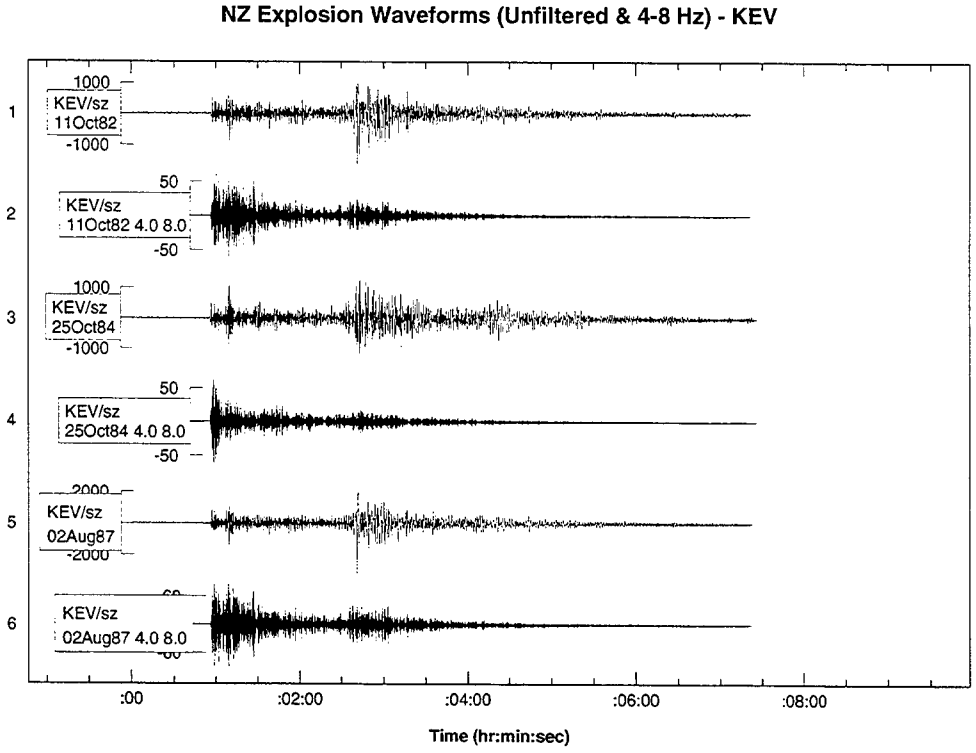

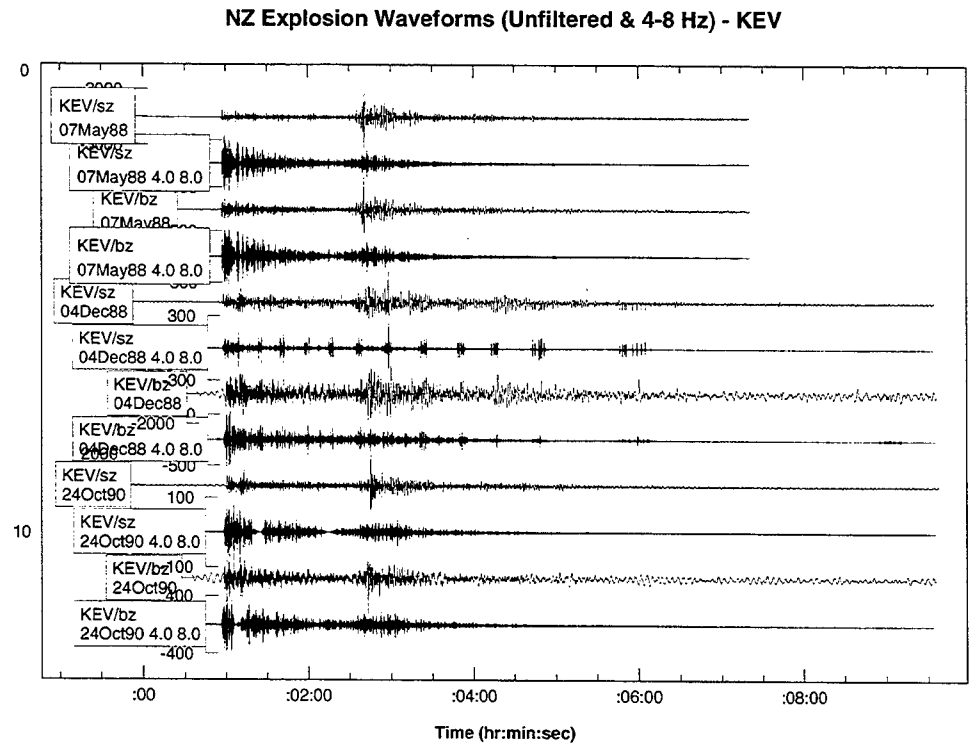

Figure 46. Unfiltered and bandpass-filtered (4-8 Hz) seismograms (sz and bz channels) recorded by KEV for six Novaya Zemlya explosions.

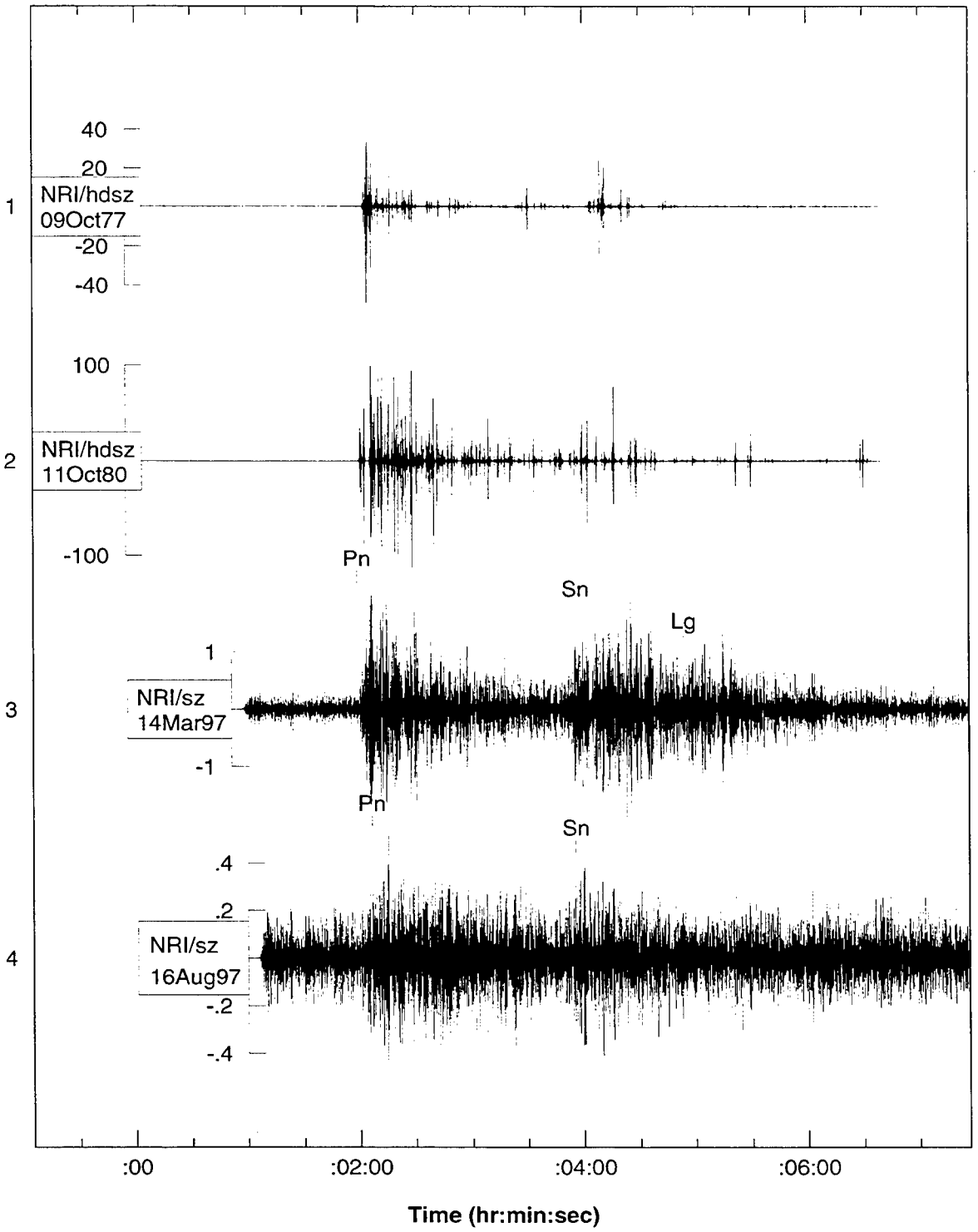

Figure 47. Comparison of bandpass-filtered (4-8 Hz) seismograms recorded by NRI for the 970816 event, a 970314 earthquake, and two Novaya Zemlya nuclear explosions (hand-digitized).

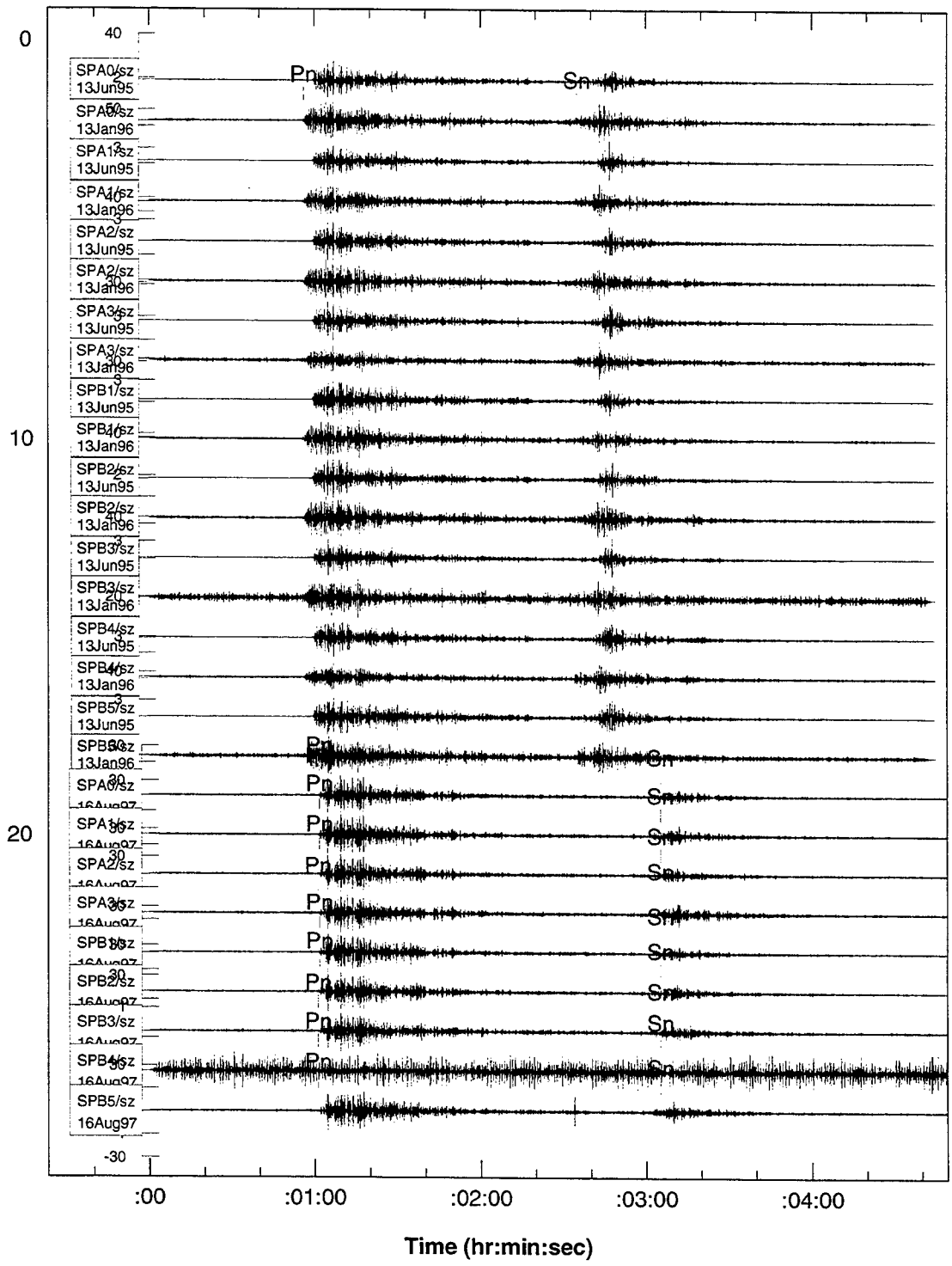

Figure 48. **Comparison of bandpass-filtered (4-8 Hz) seismograms recorded by SPITS for the 950613, 960113 and 970816 events near Novaya Zemlya. The waveform tags indicate the channel and event.**

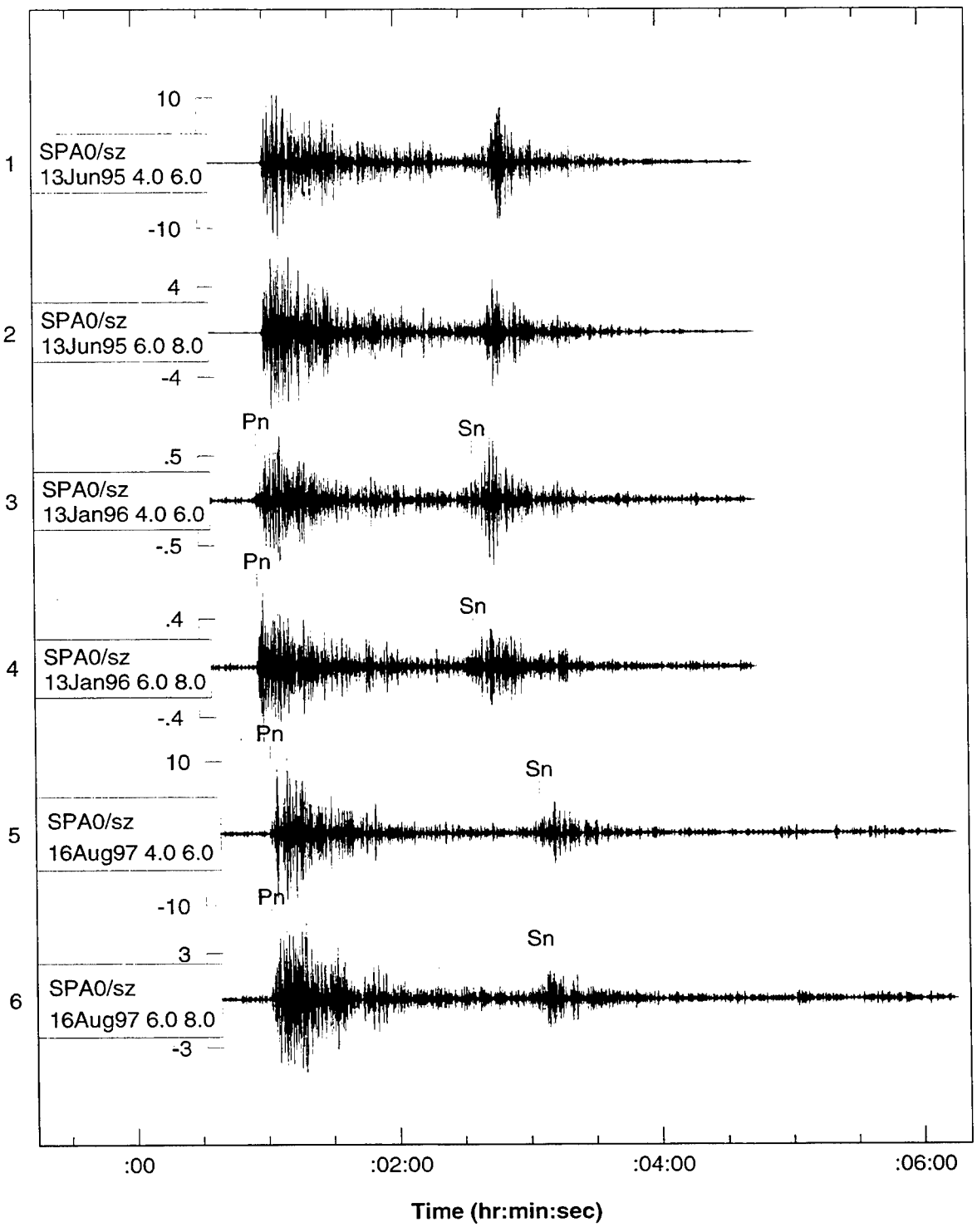

Figure 49. Comparison of bandpass-filtered (4-6 and 6-8 Hz) seismograms recorded by SPA0 for the 950613, 960113 and 970816 events near Novaya Zemlya.

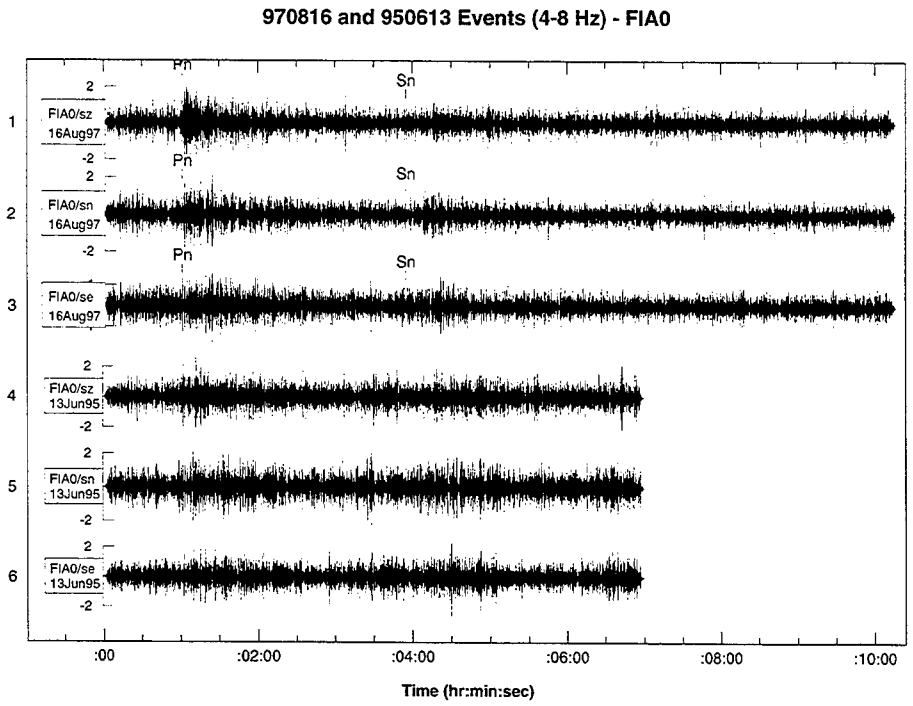

Figure 50. Comparison of bandpass-filtered (4-8 Hz) seismograms recorded by FIA0 for the 970816 and 950613 events near Novaya Zemlya.

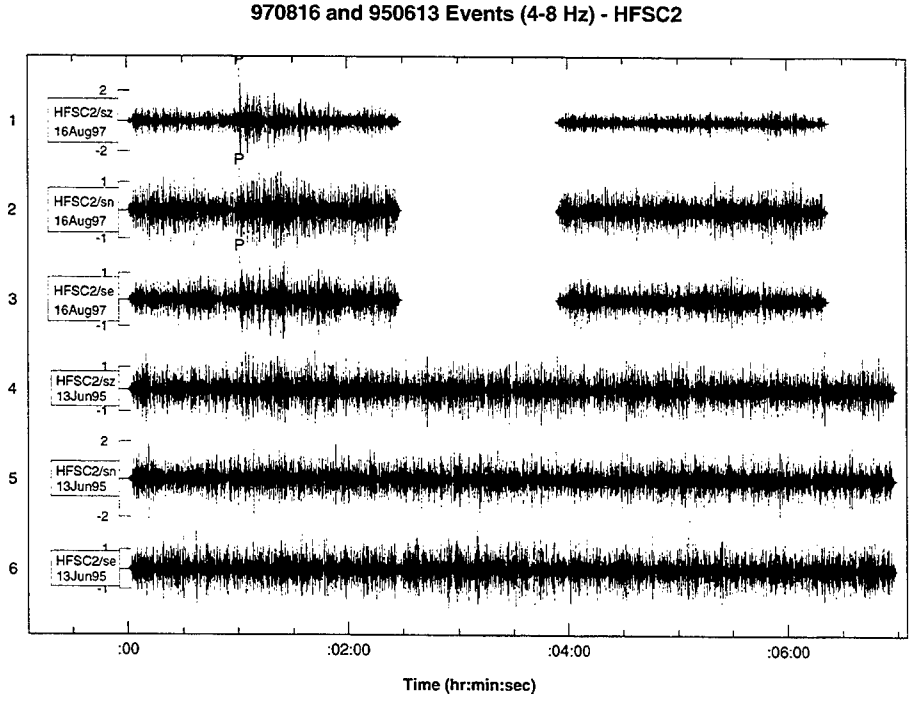

Figure 51. Comparison of bandpass-filtered (4-8 Hz) seismograms recorded by HFSC2 for the 970816 and 950613 events near Novaya Zemlya.

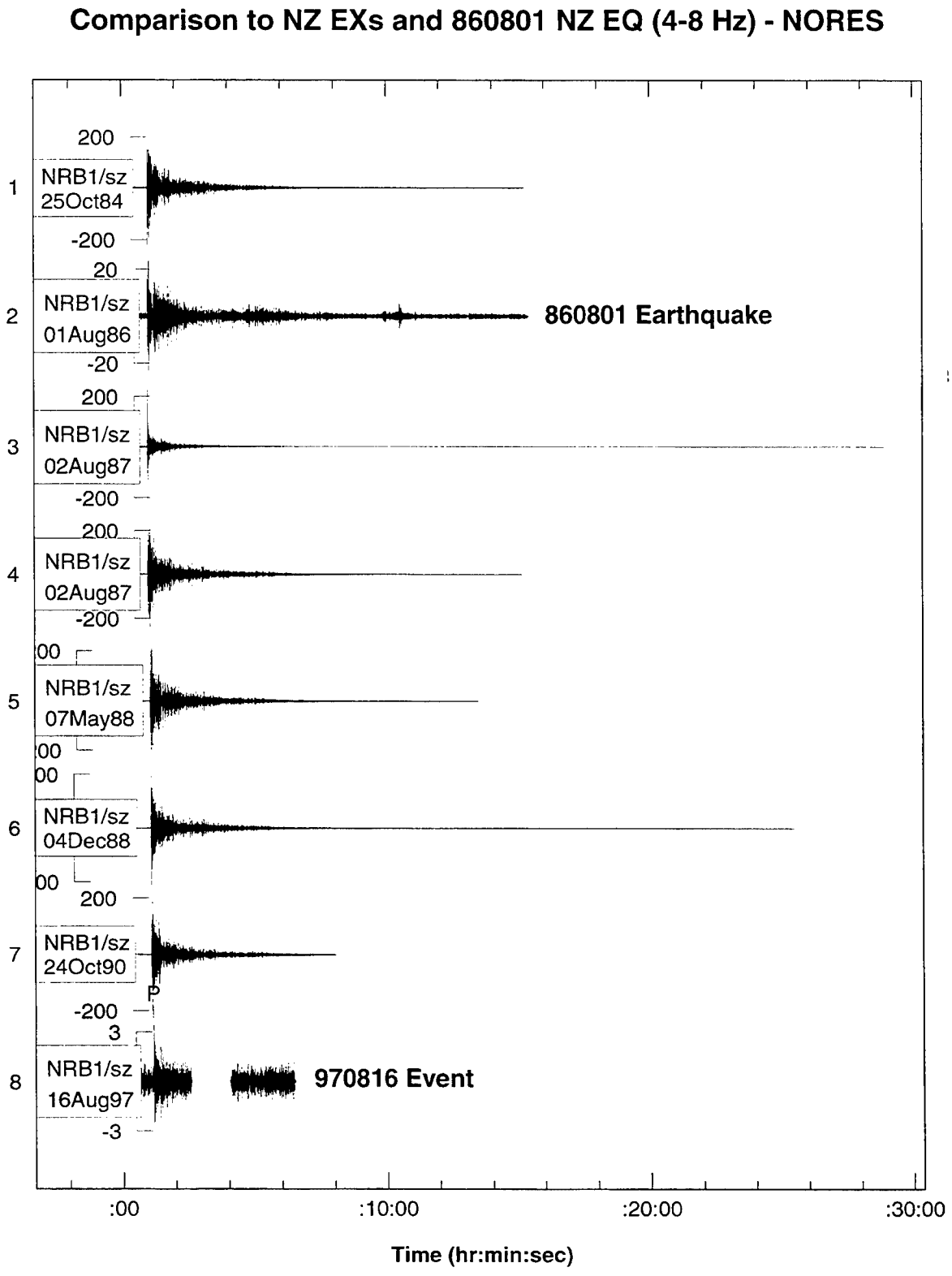

Figure 52. Comparison of filtered (4-8 Hz) seismograms recorded by NRB1 for the 970816 event, the 860801 NZ earthquake and the 841025, 870802, 880507, 881204 and 901024 NZ nuclear explosions.

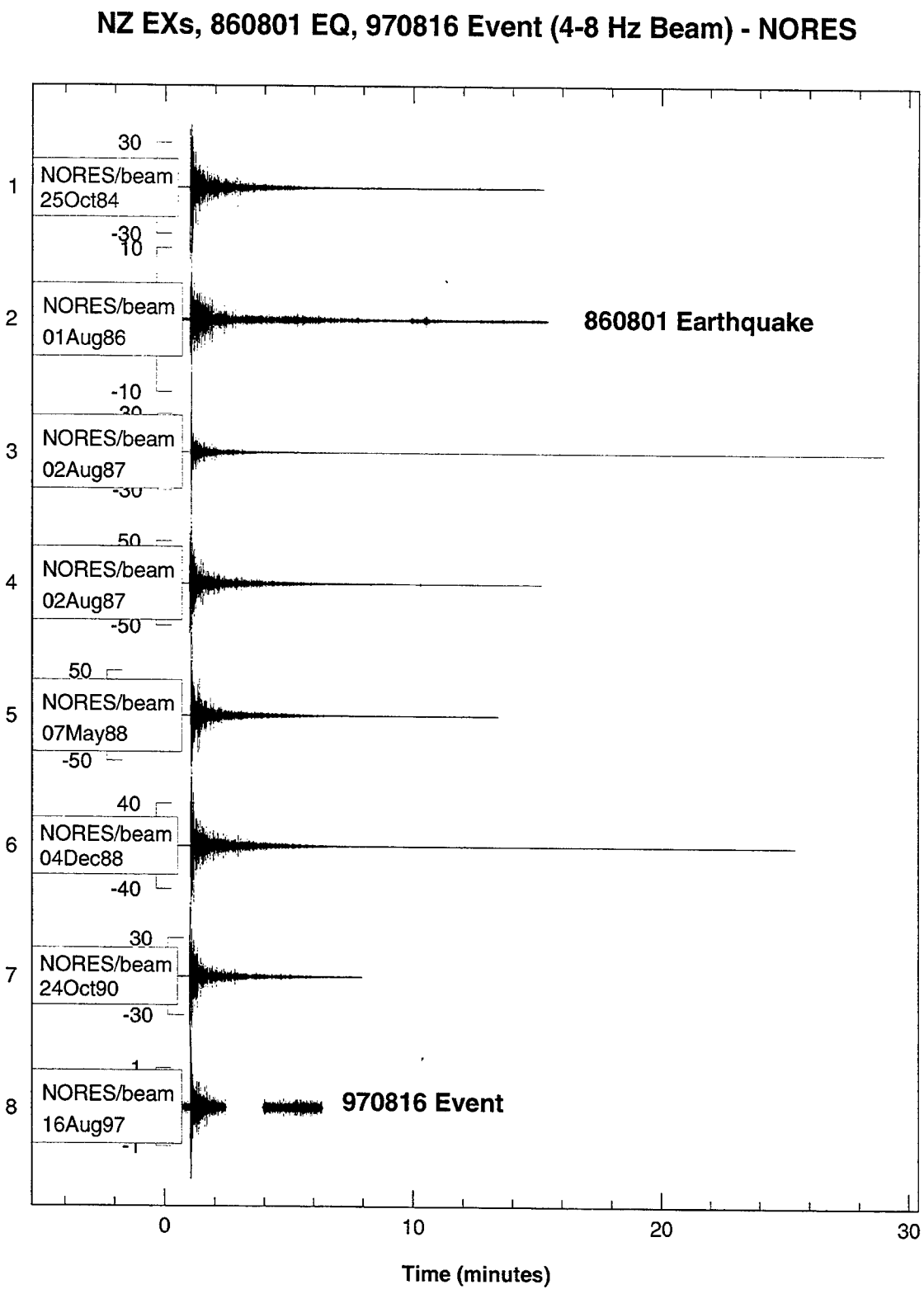

Figure 53. Comparison of bandpass-filtered (4-8 Hz) beams recorded by NORES for the 970816 event, the 860801 NZ earthquake and the 841025 and 870802 NZ nuclear explosions.

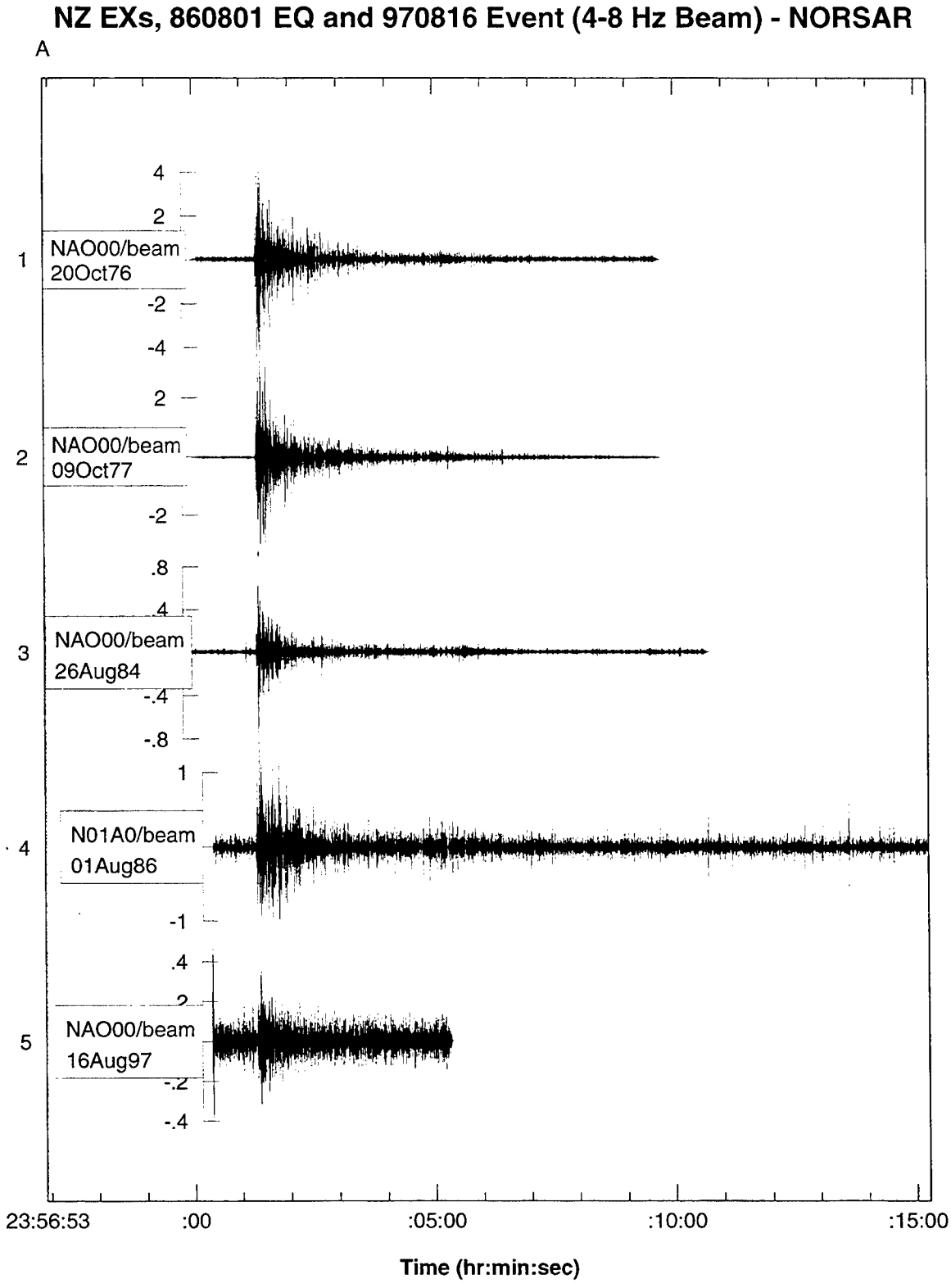

Figure 54. **Comparison of bandpass-filtered (4-8 Hz) beams recorded by NORSAR for the 970816 event, the 860801 NZ earthquake and the 761020, 771009 and 840826 Novaya Zemlya nuclear explosions.**

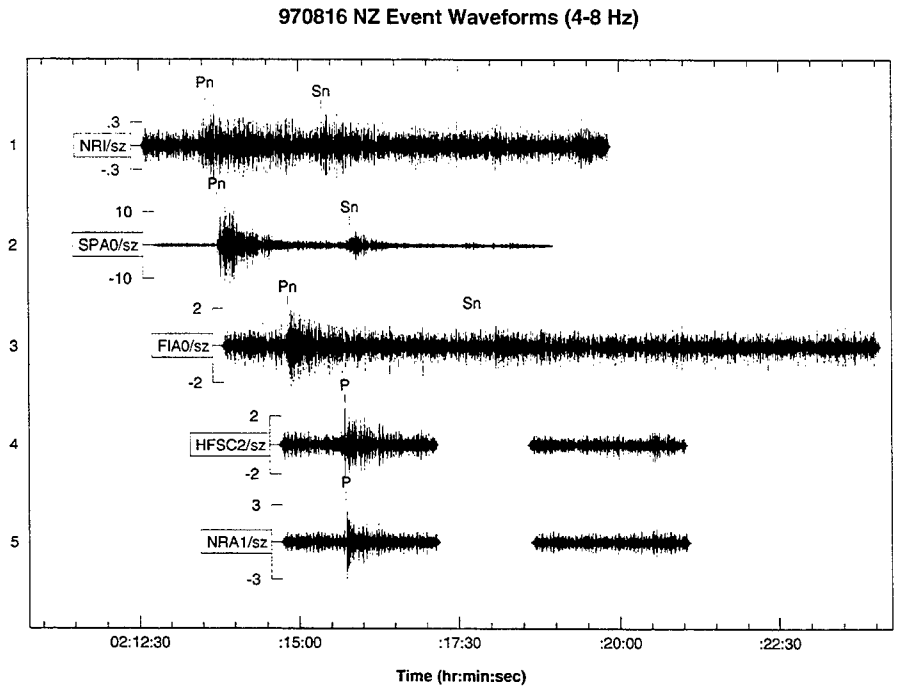

Figure 55. Bandpass-filtered (4-8 Hz) waveforms recorded by NRI (10.62°), SPA0 (11.44°), FIA0 (16.30°), HFSC2 (20.85°), NRA1 (21.00°) for the 970816 event.

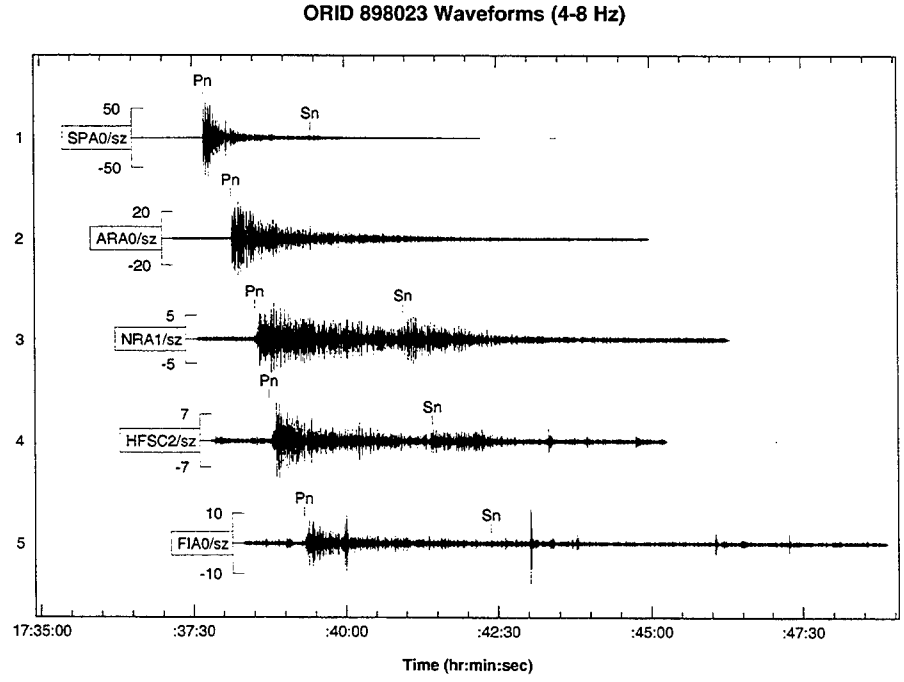

Figure 56. Bandpass-filtered (4-8 Hz) waveforms recorded by SPA0, ARA0, HFSC2, NRA1, FIA0 for an mb 4.1 earthquake in the Jan Mayen Island region.

5.3 Regional Population Analysis.

An outlier test, using distance-corrected Pn/Sn, is applied here to quantify comparisons of the 970816 event to the NZ nuclear explosions recorded by KEV, and to regional earthquakes recorded by NRI. The reference events used at NRI are all above mb 3.5, to eliminate potential contamination from mining blasts, and do not include events near the NZ test site. Using the leave-one-out procedure, each reference event is also tested as an outlier of the remaining group. (Fisk et al., 1993, 1994, 1995, 1996a, 1996b, describe the outlier procedure and previous applications.)

5.3.1 KEV.

Figure 57 shows the results for KEV, comparing the 970816 event to six previous NZ nuclear explosions. On the left is a plot of log Pn/Sn values in the 4-6 Hz band for the six NZ explosions and the 970816 event. (Note that two of the NZ explosions have nearly identical Pn/Sn values.) The plot on the right shows the results of the outlier test using log Pn/Sn(4-6 Hz). Only one discriminant was used since there were only six events in the reference set. The distribution shown corresponds to that of the likelihood ratio obtained from the Pn/Sn values for the explosions. The vertical line corresponds to the threshold of the test at 0.01 significance level. Figure 57 (right) shows that the 970816 event is an outlier of the NZ nuclear explosions recorded by KEV. This indicates that the 970816 event is inconsistent with these previous NZ nuclear explosions.

5.3.2 NRI.

Figure 58 (left) shows plots of log Pn/Sn in the 2-4, 4-6 and 6-8 Hz bands versus log distance for 21 regional events and the 970816 event. Figure 58 (right) shows the results of the outlier test using log Pn/Sn in the 4-6 and 6-8 Hz band, indicating that the 970816 event is clearly not an outlier of the regional earthquakes recorded by NRI. Figure 59 shows the locations of the events that were recorded by NRI. The 970816 event and the 970314 earthquake included in the waveform comparison of Figure 47 are indicated. Since the 21 regional events recorded by NRI have a significant range of distances and azimuths, it is important to understand what effect this may have on the distribution of the Pn/Sn values, particularly for events along the Mid Atlantic Ridge versus those at other distances and azimuths.

Figure 60 shows plots of Pn/Sn in the 4-6, 6-8 and 8-10 Hz bands versus distance (left) and azimuth (right) for the events recorded by NRI. Markers shown in gray correspond to outliers that were removed from the reference set before the 970816 event was tested. The data exhibit relatively little variation in their Pn/Sn values over a relatively wide range of distances and azimuths. This suggests that these events can be treated as a single earthquake population at NRI.

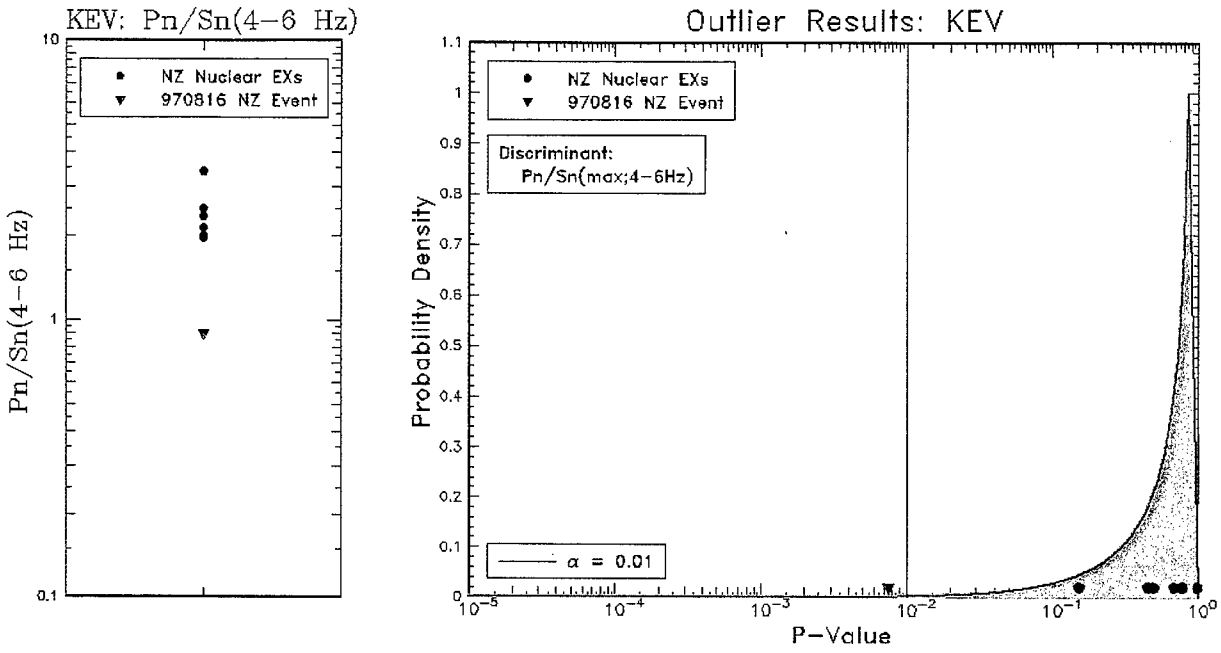

Figure 57. **On the left is a plot of log Pn/Sn values in the 4-6 Hz band at KEV for six NZ nuclear explosions and the 970816 event. The results of the outlier test using log Pn/Sn(4-6 Hz) is shown on the right. The 970816 event is an outlier of the NZ explosion population at the 0.01 significance level.**

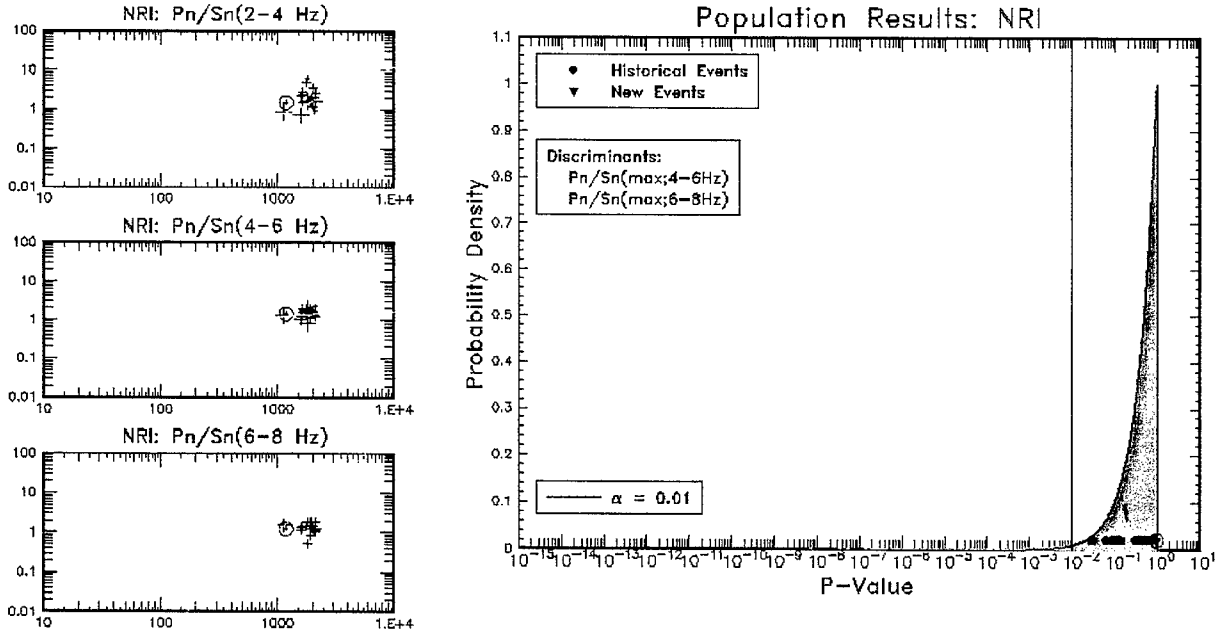

Figure 58. **Plots of log Pn/Sn values in the 2-4, 4-6 and 6-8 Hz bands versus log distance at NRI for 21 earthquakes and the 970816 event are shown on the left. The results of the regional outlier analysis at NRI using log Pn/Sn in the 4-6 and 6-8 Hz bands are shown on the right. The 970816 event is <u>not</u> an outlier of the regional earthquake population recorded by NRI.**

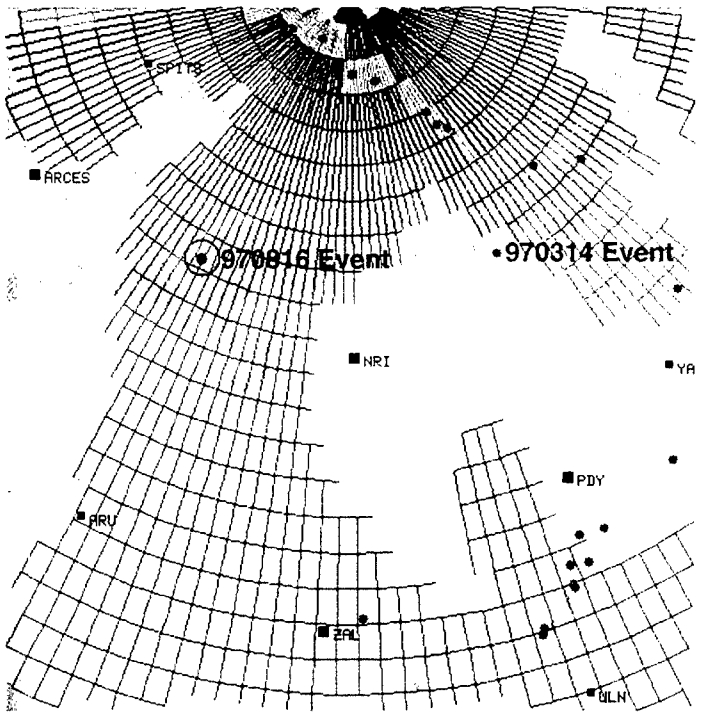

Figure 59. Map showing the locations of the 970816 event and the 21 reference events used in the regional population analysis at NRI. The overlay is a tectonic grid established by Oli Guudmundsson.

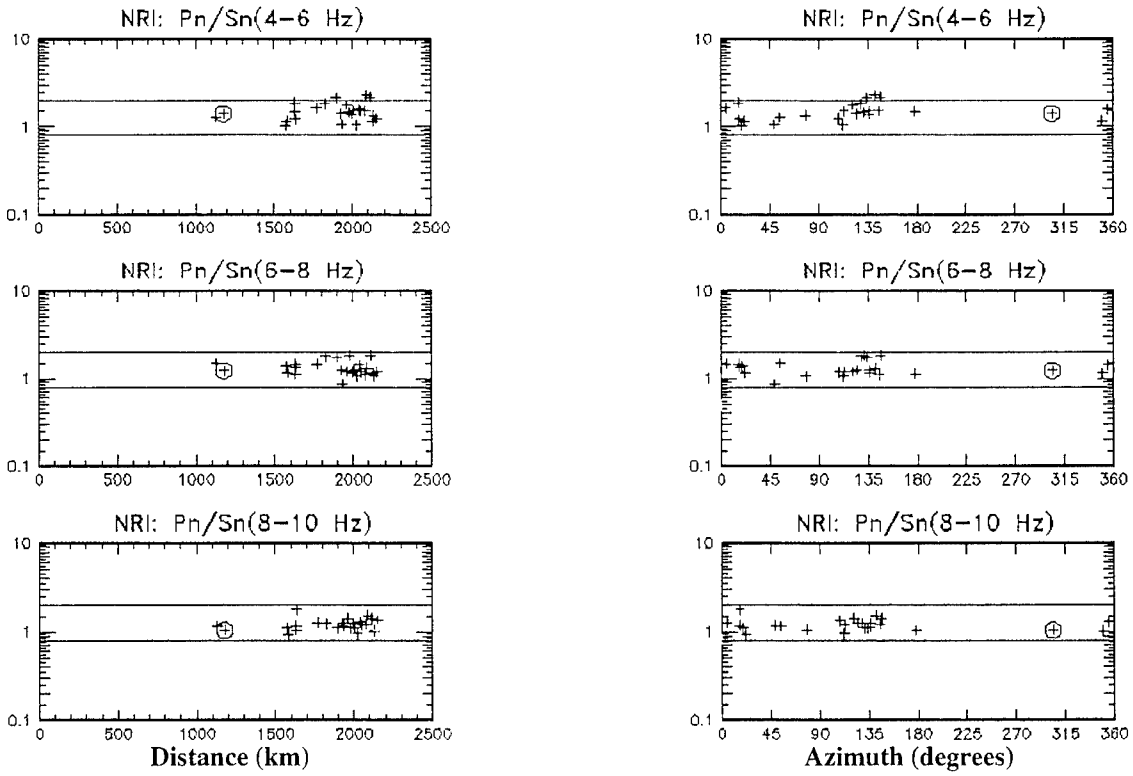

Figure 60. Plots of log Pn/Sn versus distance (left) and azimuth (right) for the events recorded by NRI.

5.4 Conclusions.

Table 11 summarizes the comparisons that were made of the 970816 event to regional earthquakes and explosions. This investigation of the 970816 event indicates that its high-frequency Pn/Sn values are inconsistent with six previous NZ nuclear explosions recorded by KEV and that they are consistent with 21 regional earthquakes recorded by NRI. Comparisons at NRI further indicate that the 970816 event has nearly identical high-frequency Pn/Sn values as a 970314 event at a similar distance. The comparison at NRI to hand-digitized data for previous NZ nuclear explosions is not valid above 4 Hz, the frequency range relevant to regional event discrimination.

Table 11. Summary of conclusions for the 970816 Kara Sea event.

Station	Distance (Degrees)	Comparison	Comment	Conclusion
KEV	9.42	Waveforms and Pn/Sn compared to six NZ EXs	Good SNR for both Pn and Sn	• Inconsistent with six NZ EXs at the 0.01 significance level using log Pn/Sn in the 4-6 Hz band
NRI[a]	10.62	Waveforms and Pn/Sn compared to regional EQs	hdsz records for EXs are invalid above 4 Hz	• Consistent with 21 regional EQs using log Pn/Sn in the 4-6 and 6-8 Hz bands
SPITS*	11.44	Waveforms and Pn/Sn compared to two NZ EQs	Good SNR for both Pn and Sn	• Insufficient evidence to conclude that the 970816 event is different than the NZ EQs
FINES*	16.30	Waveforms compared to 950613 NZ event	1800 km from FINES Strong Sn attenuation	• Inconclusive evidence based on poor SNR for the 970816 event
HFS*	20.85	Waveforms compared to 950613 NZ event	Beyond 20 degrees Strong S attenuation	• Inconclusive evidence based on poor SNR for the 970816 event
NORES*	21.00	Waveforms compared to 2 NZ EXs and the 860801 EQ	Beyond 20 degrees Strong S attenuation	• Inconclusive evidence based on poor SNR for the 970816 event
NORSAR	21.77	Waveforms compared to 3 NZ EXs and the 860801 EQ	Beyond 20 degrees Strong S attenuation	• Inconclusive evidence based on poor SNR for the 970816 event

a. Seismic stations of the International Monitoring System (IMS).

Comparisons at SPITS to the 950613 and 960113 events near NZ indicate similar waveforms in the 4-6 and 6-8 Hz bands. Although Pn/Sn in these bands are higher for the 970816 event than for the other two events prior to correcting for distance, all three events have more comparable values after applying distance corrections. There is insufficient evidence to conclude that the 970816 event is significantly different than the 950613 and 960113 events.

Comparisons at FINES, HFS, NORES and NORSAR to specific NZ explosions and other nearby events are inconclusive due to poor SNR, although there may be some evidence using beams at NORES that the 970816 event is more consistent with the 860801 presumed earthquake near NZ than with the 841025 and 870802 NZ explosions.

Examination of 4-8 Hz bandpass filtered waveforms at eleven Finnish stations showed that for many of these stations the Sn signals are comparable to or larger than the Pn signals (e.g., JOF, KEF, KEV, KJN, SDF, SUF). These waveforms further illustrate that there are distance and station-dependent variations in the signals. At the present, however, there are no available explosion or earthquake data from these stations for comparison.

Based on the available data, the seismic evidence supports the following conclusions:

- The 970816 event is inconsistent with previous known explosions at the NZ test site recorded by KEV, the closest station;
- The 970816 event is consistent with earthquakes recorded by NRI, the next closest station;
- There is insufficient evidence to conclude that the 970816 event is significantly different than the 950613 and 960113 events near NZ recorded by SPITS, the third closest station;
- Evidence at the other stations, which are at far regional to teleseismic distances (e.g., 1800-2300 km) is inconclusive due to poor signals and strong Sn attenuation.

These conclusions are consistent with those obtained independently by Bennett et al. (1997); Bowers et al. (1997); Richards and Kim (1997); and Hartse (1998).

Since this study was originally conducted, it was discovered that a smaller (mb 2.5) event at approximately the same location and with similar seismic characteristics occurred about four hours after the main 970816 Kara Sea event, indicative of a possible earthquake aftershock (Ringdal et al., 1997; Richards and Kim, 1997).

Further analysis of the waveform data indicates that this event does not exhibit any of the expected spectral behavior expected for an explosion in the water column (Baumgardt, 1998; Herrin, 1998).

Section 6
References

Baumgardt, D. R. (1998). Special Event Discrimination Analysis: The TEXAR Blind Test and Identification of the August 16, 1997 Kara Sea Event, AFRL-VS-HA-TR-98-0049, Air Force Research Laboratory, Hanscom AFB, MA.

Baumgardt, D. R. and K. A. Ziegler (1988). Spectral evidence for source multiplicity in explosions: applications to regional discrimination of earthquakes and explosions, *Bull. Seis. Soc. Am.*, **78**, 1773-1775.

Bennett, T. J., R. W. Cook and J. R. Murphy (1997). A Discrimination Analysis of the August 16, 1997 Event Near Novaya Zemlya, S-Cubed Technical Report, Private Distribution.

Bottone, S., M. D. Fisk, H. L. Gray and G. D. McCartor (1996). The Dependence of Magnitude Uncertainty on Station Coverage, PL-TR-96-2250, Phillips Laboratory, Hanscom AFB, MA.

Bottone, S., M. D. Fisk, G. D. McCartor and R. J. Carlson (1997). Initial Regionalization Efforts for the IMS Seismic Network, PL-TR-97-2090, Phillips Laboratory, Hanscom AFB, MA.

Bowers, D., H. Trodd and A. Douglas (1997). The Novaya Zemlya Seismic Disturbance of 16 August 1997, AWE/97/DFS Draft Technical Report, AWE, Blacknest, UK.

Bratt, S. R. and T. C. Bache (1988). Locating events with a sparse network of regional arrays, *Bull. Seis. Soc. Am.*, **78**, 780-798.

Carlson, R. J. and M. D. Fisk (1998). Initial User's Guide for Event Screening Products and Services at the Prototype IDC, MRC-R-1555, Mission Research Corporation, Santa Barbara, CA, to appear as a Phillips Laboratory Technical Report, Hanscom AFB, MA.

Douglas, A. (1980). Seismic Source Identification: A Review of Past and Present Research Efforts, *Identification of Seismic Sources - Earthquakes or Underground Explosions*, E.S. Husebye and S. Mykkeltveit (eds.), 1-48.

Fisk, M. D., R. J. Carlson, V. Burlacu and G. D. McCartor (1996a). Interactive World Wide Web Pages for Custom Event Screening at the Prototype International Data Center, PL-TR-96-2269, Phillips Laboratory, Hanscom AFB, MA, ADA322284.

Fisk, M. D., H. L. Gray and G. D. McCartor (1996b). Regional event discrimination without transporting thresholds, *Bull. Seis. Soc. Am.*, **86**, 1545-1558.

Fisk, M. D., H. L. Gray and G. D. McCartor (1995). Statistical Methodology and Assessment of Seismic Event Characterization Capability, PL-TR-95-2156, Phillips Laboratory, Hanscom AFB, MA, ADA305487.

Fisk, M. D., H. L. Gray and G. D. McCartor (1994). Preliminary Assessment of Seismic CTBT/ NPT monitoring Capability, PL-TR-94-2300, Phillips Laboratory, Hanscom AFB, MA, ADA293188.

Fisk, M. D., H. L. Gray and G. D. McCartor (1993). Applications of Generalized Likelihood Ratio Tests to Seismic Event Identification, PL-TR-93-2221, Phillips Laboratory, Hanscom AFB, MA, ADA279479.

GSE/CRP/243. Group of Scientific Experts, Conference Room Paper, 243, Operations, Volume 2.

Hartse H. E. (1998). The 16 August 1997 Novaya Zemlya seismic event as viewed from GSN stations KEV and KBS, *Seism. Research Letters*, **69**, 3, 206-215.

Herrin E. (1998). Explosions in shallow seas, Technical Memorandum, Southern Methodist University, Private Distribution.

Israelsson, H., M. D. Fisk, X. Yang and R. G. North (1997). The August 16, 1997 Event in the Kara Sea, CMR-97/38, Center for Monitoring Research, Arlington, VA.

Jenkins, R. D., A. A. Velasco, D. J. Williams and T. J. Sereno (1996). Regional Attenuation at GSETT-3 Stations and the Transportability of the Lg/P Discriminant, PL-TR-96-2159, Phillips Laboratory, Hanscom AFB, MA.

Jepsen D. (1998). Private communication.

Jordan, T. H. and K. A. Sverdup (1981). Teleseismic location techniques and their application to earthquake clusters in the south-central Pacific, *Bull. Seis. Soc. Am.*, **71**, 1105-1130.

Kim, W.-Y., T. Lay, W. Walter (1997). Private communication.

Lay, T., G. Fan and A. Rodgers (1997). Crustal Waveguide Effects on Regional Phases in China and Southeast Asia, PL-TR-97-2028, Phillips Laboratory, Hanscom AFB, MA.

Marshall, P. D. and P. W. Basham (1972). Discriminating between earthquakes and underground explosions employing an improved Ms scale, *Geophys. J. Roy. Astron. Soc.*, **28**, 431-458.

Marshall, P. D., R. C. Stewart and R. C. Lilwall (1989). The seismic disturbance on 1986 August 1 near Novaya Zemlya: a source of concern?, *Geophysical Journal*, **98**, 565-573.

Murphy, J. R. (1998). Private communication.

Murphy, J. R. (1997). Calibration of IMS Magnitudes for Event Screening Using the Ms/mb Criterion, in the Proceedings of the Event Screening Workshop: Beijing, China, 4-7 November 1997.

Richards, P. G. (1997). Private communication.

Richards, P. G. and W. Y. Kim (1997). Testing the nuclear test-ban treaty, *Nature*, **389**, 781-782.

Ringdal F. (1997). The seismic event near Novaya Zemlya on 16 August 1997, Semiannual Technical Summary, 1 April 1997 - 30 September 1997, NORSAR Sci. Rep. No. 1 97/98, 110-119, Kjeller, Norway.

Rodgers, A., W. Walter and T. Lay (1997). Calibration of Distance and Path Effects on Regional P/S Discriminants at Station ABKT (Alibek, Turkmenistan): Azimuthal Sector Regionalization,

Lawrence Livermore National Laboratory UCRL-JC-128318, submitted to *Bull. Seis. Soc. Am.*

Saikia, C. K., H. K. Thio, B. B. Woods, X. Song, L. Zhu and D. V. Helmberger (1996). Path Calibration, Source Estimation and Regional Discrimination for the Middle East and Western Mediterranean, PL-TR-96-2307, Phillips Laboratory, Hanscom AFB, MA.

Stevens, J. L. (1997). Private communication.

Vanek, J., A. Zatopek, V. Karnik, N. V. Kondorskaya, Y. V. Riznichenko, Y. F. Savarensky, S. L. Solov'ev and N. V. Shebalin (1962). Standardization of magnitude scales, *Bull. (Izvestiya) Acad. Sci. USSR, Geophys. Ser.*, **2**, 108.

Veith, K. F. and G. E. Clawson (1972). Magnitude of short-period P-wave data, *Bull. Seis. Soc. Am.*, **62**, 435-453.

Appendix A
Preliminary Regional Distance Corrections for IMS Seismic Stations

Compiled in this appendix are scatterplots of the regional amplitude ratios, Pn/Lg and Pn/Sn in the 2-4, 4-6 and 6-8 Hz frequency bands, versus distance, for regional events recorded by 43 IMS seismic stations (26 Primary, 17 Auxiliary) between 10 September 1997 and 1 October 1997. These stations recorded 30 or more regional events with SNR for Pn greater than or equal to 2.0. There were an additional 7 IMS seismic stations (1 Primary, 6 Auxiliary) with 30 or more events that are not represented here because the estimated distance corrections exhibit anomalous behavior. The convention for the station names is that used currently at the PIDC. The solid curves in each plot represent the best least-square fits of the regional distance dependence. The dashed curves correspond to the worldwide-average distance dependence.

Included with each figure is a table providing the number of regional amplitude measurements, n, the estimated standard deviations of the data before, s, and after, s_c, distance corrections, and the best-fit coefficients, $\hat{\alpha}$, $\hat{\beta}$, and $\hat{\gamma}$.

The figures are ordered by Primary and then Auxiliary seismic stations. Within the two sets of stations, they are ordered alphabetically.

Note that these distance corrections are in the very preliminary stages of development and have not been validated. As such, they are not recommended for operational use at this time. In addition, the distance corrections for many of the stations require additional data and treatment of subregional effects in order to adequately improve and/or validate these results.

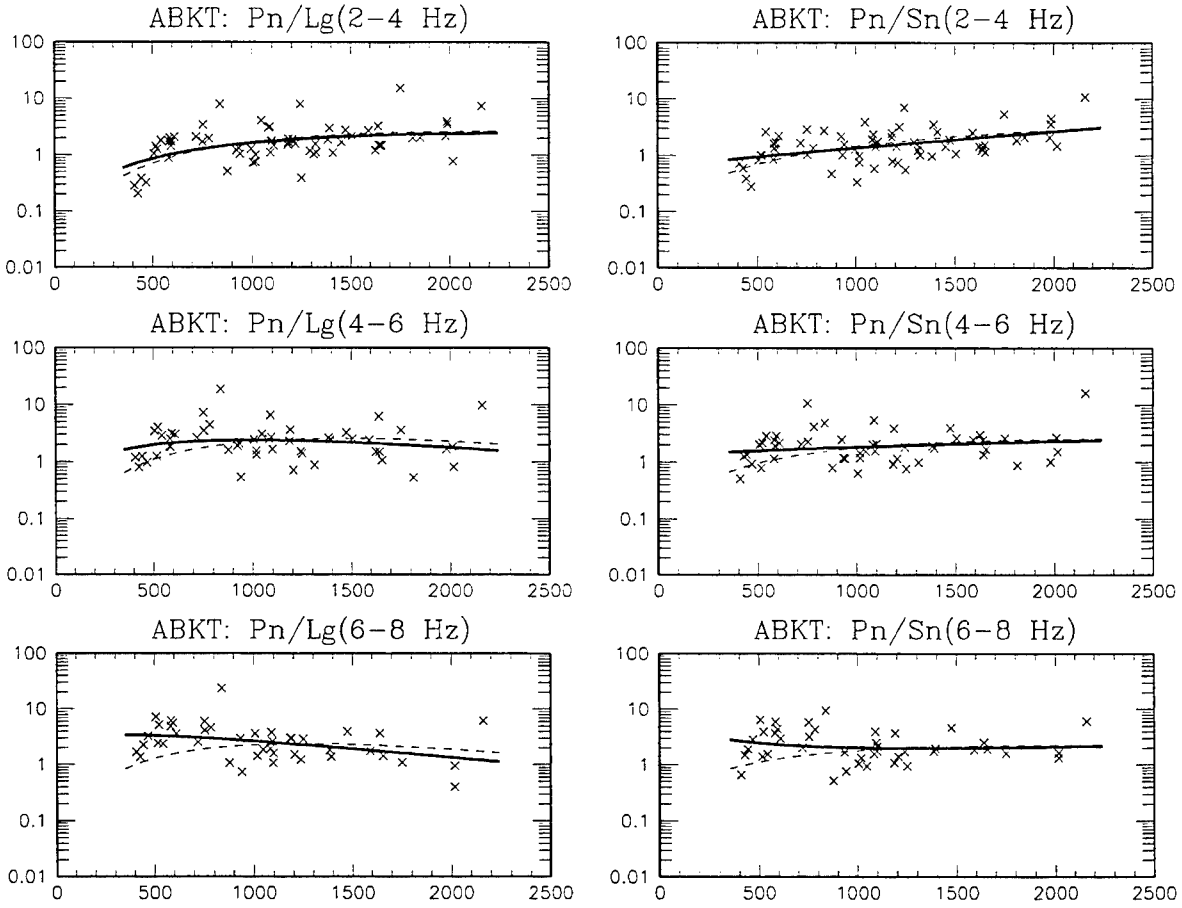

	n	*s*	s_c	$\hat{\alpha}$	$\hat{\beta}$	$\hat{\gamma}$
Pn/Lg(2-4 Hz)	66	0.328	0.295	0.680	1.322	-2.327E-04
Pn/Lg(4-6 Hz)	51	0.306	0.309	0.978	0.989	-4.264E-04
Pn/Lg(6-8 Hz)	43	0.317	0.301	0.859	0.306	-3.841E-04
Pn/Sn(2-4 Hz)	66	0.297	0.267	-0.126	0.074	2.713E-04
Pn/Sn(4-6 Hz)	51	0.289	0.290	0.211	0.101	6.914E-05
Pn/Sn(6-8 Hz)	43	0.286	0.290	0.008	-0.599	1.943E-04

Figure A-1. Regional data and best least-square fits (solid curves) of the distance dependence for 70 regional events recorded by ABKT.

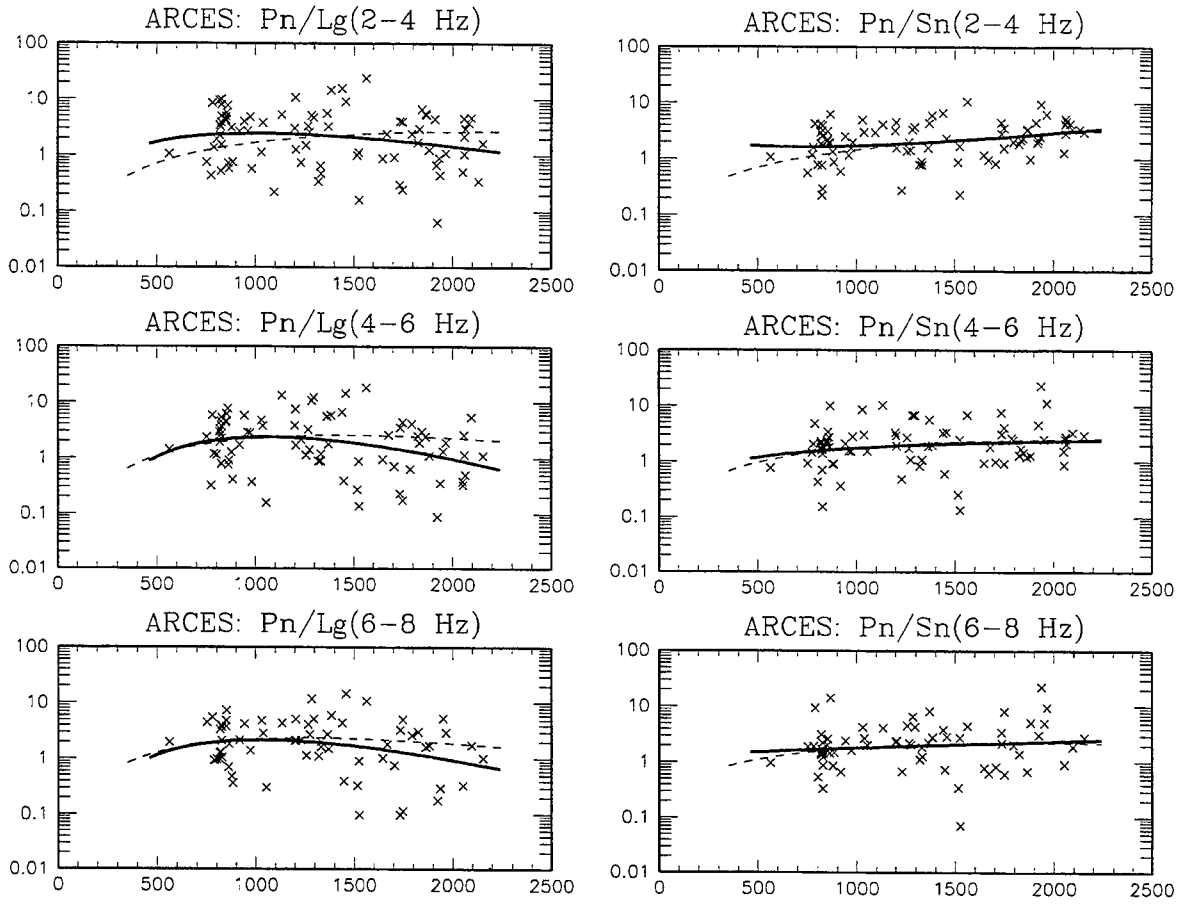

	n	*s*	s_c	$\hat{\alpha}$	$\hat{\beta}$	$\hat{\gamma}$
Pn/Lg(2-4 Hz)	84	0.501	0.499	1.470	1.791	-7.668E-04
Pn/Lg(4-6 Hz)	81	0.506	0.492	2.527	3.701	-1.504E-03
Pn/Lg(6-8 Hz)	68	0.484	0.477	2.106	2.967	-1.249E-03
Pn/Sn(2-4 Hz)	84	0.344	0.334	-0.356	-0.744	4.572E-04
Pn/Sn(4-6 Hz)	81	0.391	0.389	0.461	0.729	-8.990E-05
Pn/Sn(6-8 Hz)	68	0.406	0.409	0.202	0.125	7.940E-05

Figure A-2. Regional data and best least-square fits (solid curves) of the distance dependence for 90 regional events recorded by ARCES.

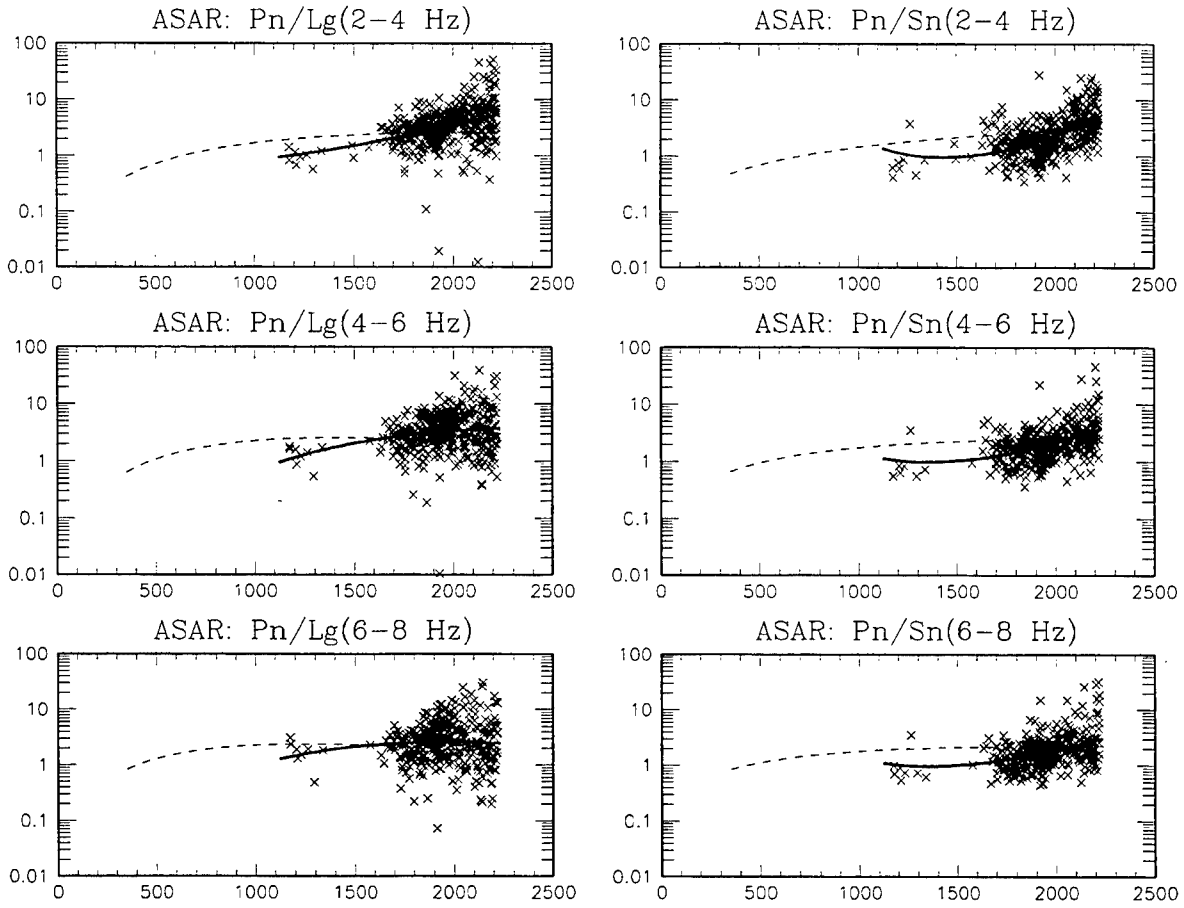

	n	s	s_c	$\hat{\alpha}$	$\hat{\beta}$	$\hat{\gamma}$
Pn/Lg(2-4 Hz)	505	0.365	0.339	-1.740	-2.210	1.281E-03
Pn/Lg(4-6 Hz)	457	0.365	0.359	1.703	5.453	-9.288E-04
Pn/Lg(6-8 Hz)	410	0.409	0.409	2.069	5.286	-1.161E-03
Pn/Sn(2-4 Hz)	505	0.343	0.293	-6.343	-13.872	4.222E-03
Pn/Sn(4-6 Hz)	457	0.308	0.278	-4.243	-8.846	2.840E-03
Pn/Sn(6-8 Hz)	410	0.312	0.290	-3.732	-7.753	2.493E-03

Figure A-3. Regional data and best least-square fits (solid curves) of the distance dependence for 516 regional events recorded by ASAR.

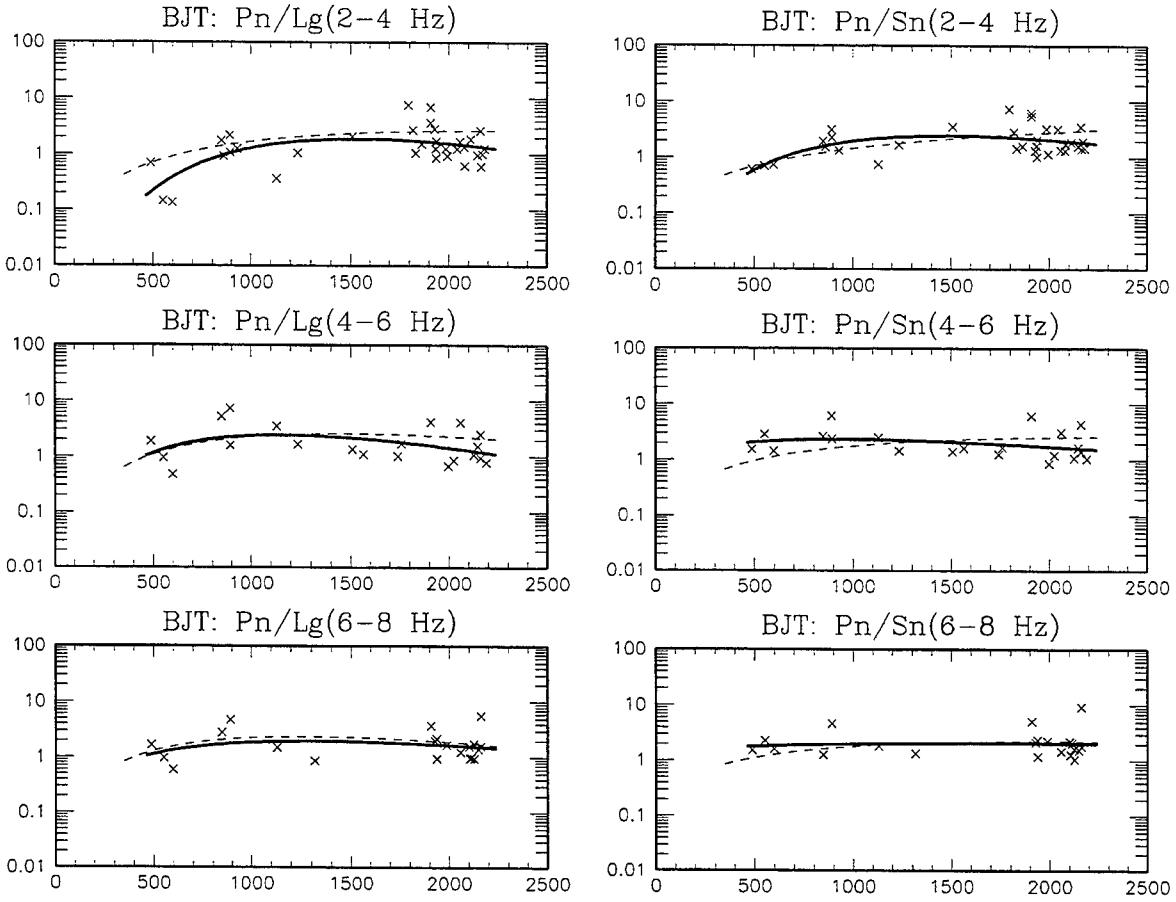

	n	*s*	s_c	$\hat{\alpha}$	$\hat{\beta}$	$\hat{\gamma}$
Pn/Lg(2-4 Hz)	33	0.370	0.305	2.318	4.804	-1.362E-03
Pn/Lg(4-6 Hz)	21	0.314	0.308	1.903	2.765	-1.046E-03
Pn/Lg(6-8 Hz)	21	0.249	0.256	1.078	1.585	-5.291E-04
Pn/Sn(2-4 Hz)	33	0.262	0.227	1.860	3.343	-9.780E-04
Pn/Sn(4-6 Hz)	21	0.241	0.246	0.868	0.788	-3.646E-04
Pn/Sn(6-8 Hz)	21	0.231	0.242	0.406	0.250	-6.256E-05

Figure A-4. Regional data and best least-square fits (solid curves) of the distance dependence for 48 regional events recorded by BJT.

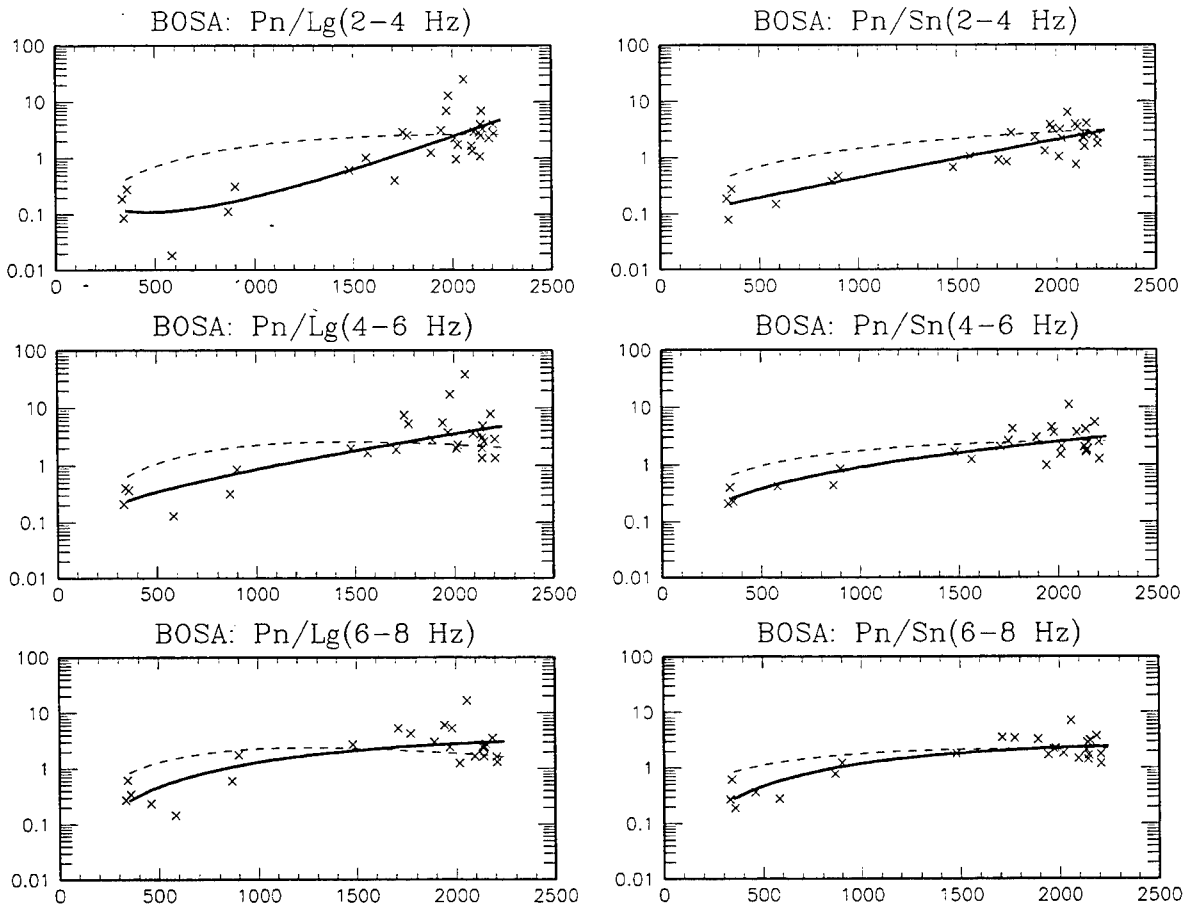

	n	s	s_c	$\hat{\alpha}$	$\hat{\beta}$	$\hat{\gamma}$
Pn/Lg(2-4 Hz)	31	0.662	0.381	-2.571	-1.719	1.585E-03
Pn/Lg(4-6 Hz)	28	0.553	0.361	-0.411	0.580	4.421E-04
Pn/Lg(6-8 Hz)	25	0.487	0.312	0.661	1.847	-2.232E-04
Pn/Sn(2-4 Hz)	31	0.467	0.217	-0.972	0.110	6.372E-04
Pn/Sn(4-6 Hz)	28	0.417	0.233	-0.015	0.997	1.447E-04
Pn/Sn(6-8 Hz)	25	0.397	0.208	0.630	1.756	-2.450E-04

Figure A-5. Regional data and best least-square fits (solid curves) of the distance dependence for 32 regional events recorded by BOSA.

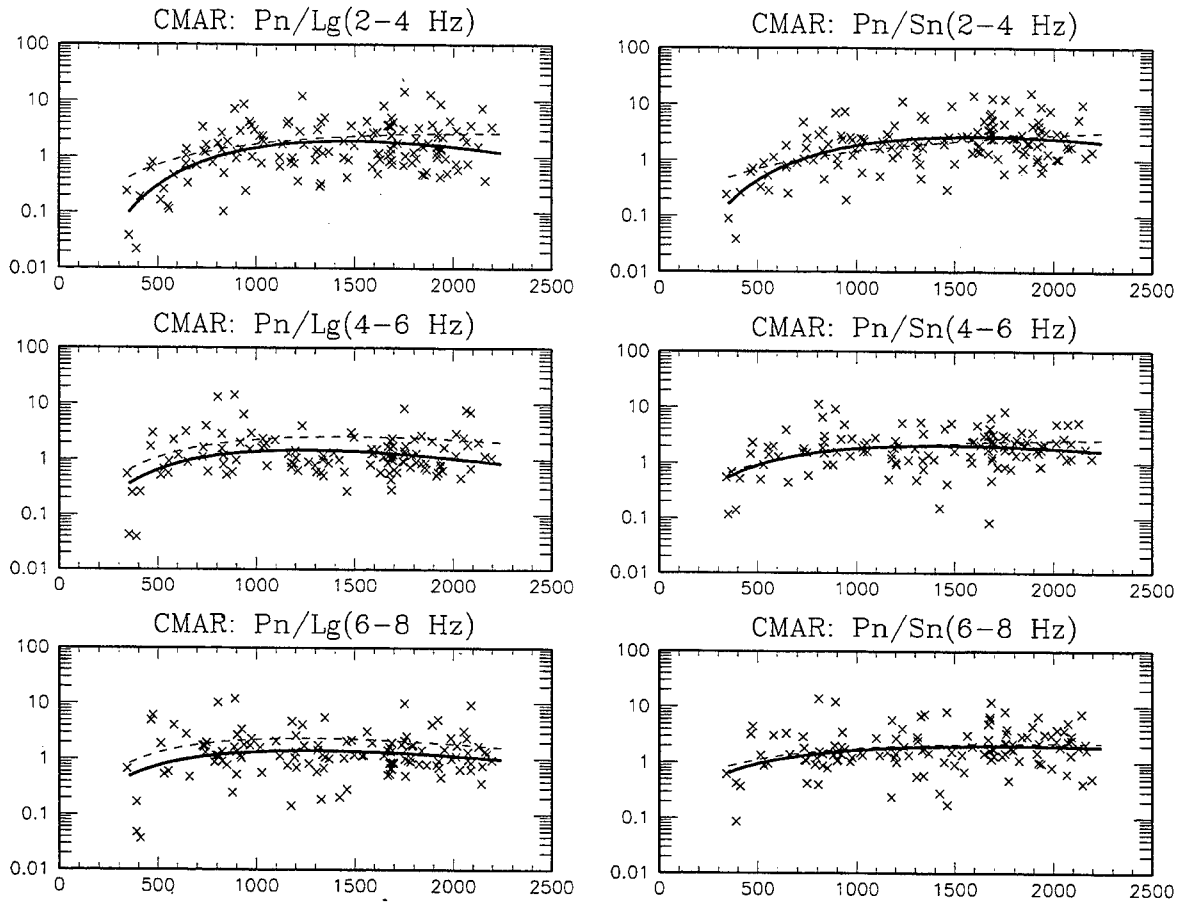

	n	s	s_c	$\hat{\alpha}$	$\hat{\beta}$	$\hat{\gamma}$
Pn/Lg(2-4 Hz)	141	0.461	0.386	2.273	4.464	-1.325E-03
Pn/Lg(4-6 Hz)	121	0.370	0.350	1.492	2.584	-8.981E-04
Pn/Lg(6-8 Hz)	124	0.393	0.387	1.100	1.888	-6.386E-04
Pn/Sn(2-4 Hz)	141	0.424	0.341	1.963	3.801	-1.027E-03
Pn/Sn(4-6 Hz)	121	0.357	0.336	1.242	2.052	-6.219E-04
Pn/Sn(6-8 Hz)	124	0.371	0.359	0.821	1.407	-3.508E-04

Figure A-6. Regional data and best least-square fits (solid curves) of the distance dependence for 227 regional events recorded by CMAR.

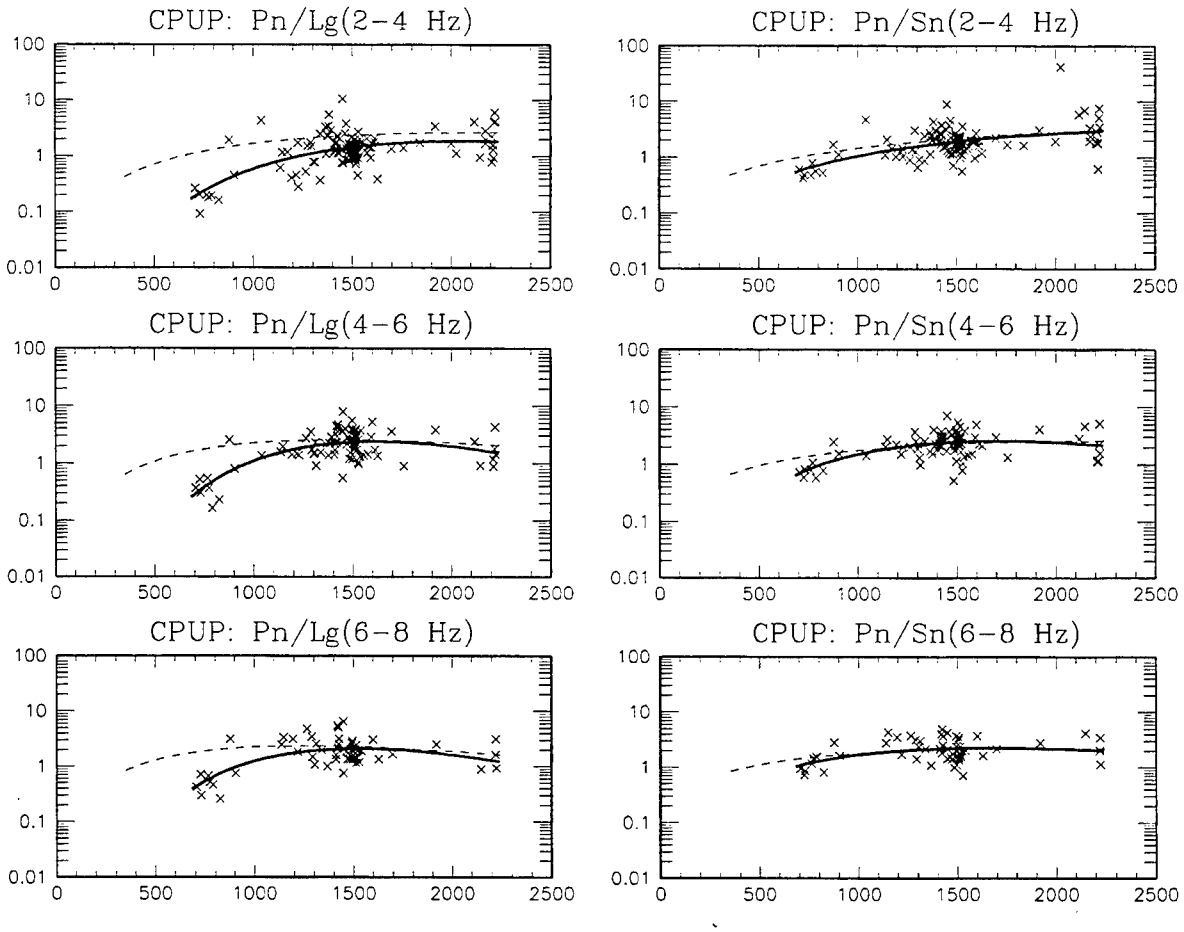

	n	s	s_c	$\hat{\alpha}$	$\hat{\beta}$	$\hat{\gamma}$
Pn/Lg(2-4 Hz)	125	0.322	0.252	1.882	5.468	-1.147E-03
Pn/Lg(4-6 Hz)	92	0.304	0.219	3.516	7.828	-2.099E-03
Pn/Lg(6-8 Hz)	59	0.293	0.225	3.145	6.631	-1.882E-03
Pn/Sn(2-4 Hz)	125	0.270	0.231	0.721	2.307	-2.905E-04
Pn/Sn(4-6 Hz)	92	0.229	0.191	2.023	4.300	-1.088E-03
Pn/Sn(6-8 Hz)	59	0.212	0.196	1.344	2.558	-6.635E-04

Figure A-7. Regional data and best least-square fits (solid curves) of the distance dependence for 128 regional events recorded by CPUP.

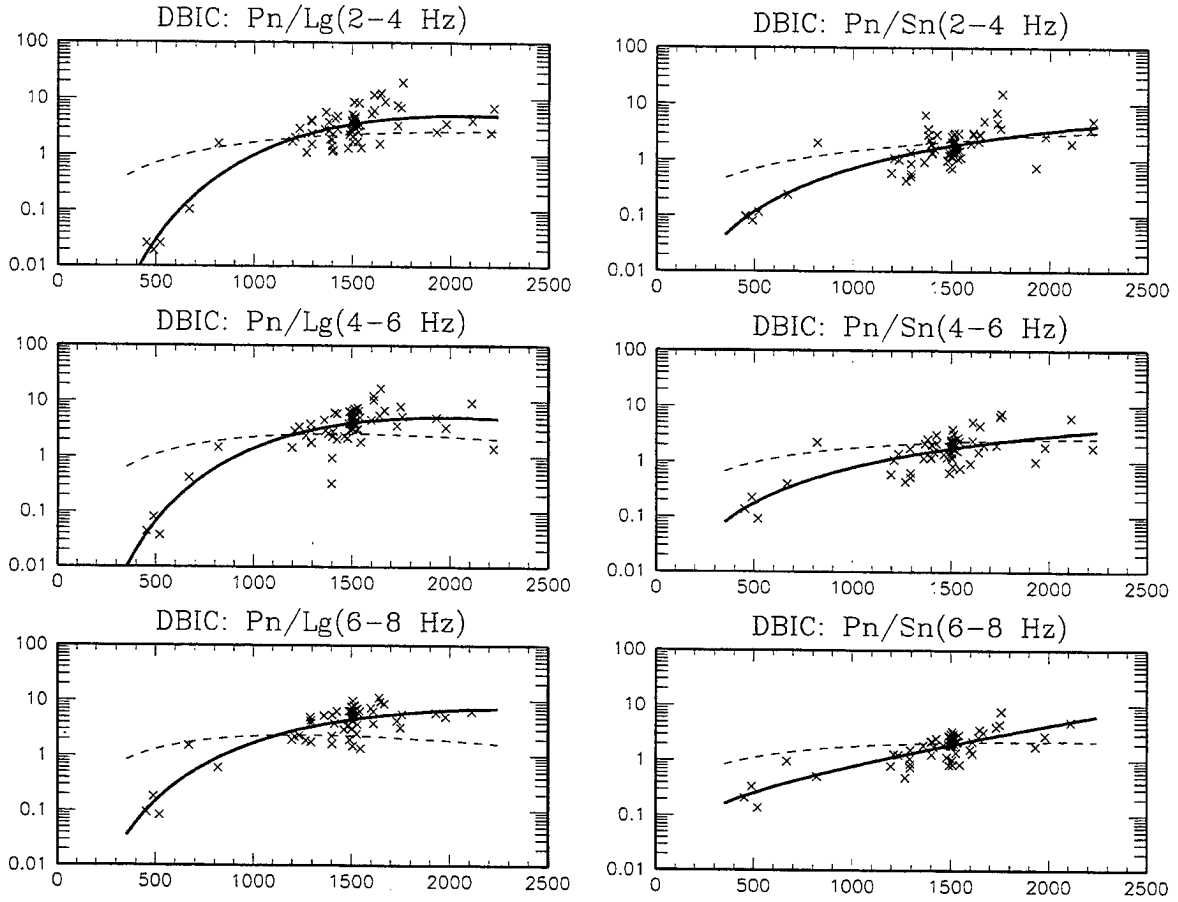

	n	*s*	s_c	$\hat{\alpha}$	$\hat{\beta}$	$\hat{\gamma}$
Pn/Lg(2-4 Hz)	69	0.543	0.251	2.997	7.760	-1.631E-03
Pn/Lg(4-6 Hz)	64	0.496	0.256	2.889	6.932	-1.523E-03
Pn/Lg(6-8 Hz)	59	0.431	0.215	2.021	5.012	-9.100E-04
Pn/Sn(2-4 Hz)	69	0.394	0.257	0.616	2.995	-2.328E-04
Pn/Sn(4-6 Hz)	64	0.354	0.246	0.484	2.433	-1.623E-04
Pn/Sn(6-8 Hz)	59	0.317	0.189	-0.487	0.760	5.167E-04

Figure A-8. Regional data and best least-square fits (solid curves) of the distance dependence for 70 regional events recorded by DBIC.

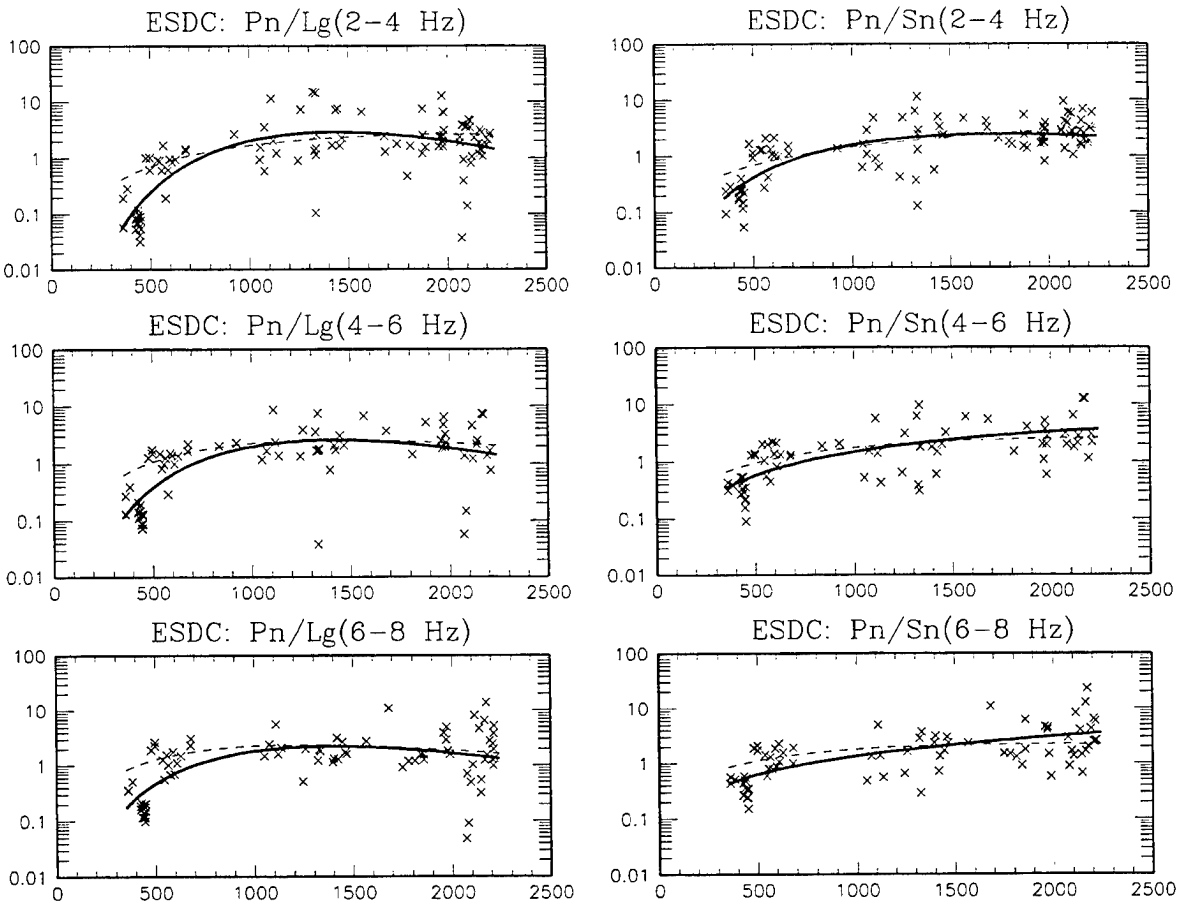

	n	s	s_c	$\hat{\alpha}$	$\hat{\beta}$	$\hat{\gamma}$
Pn/Lg(2-4 Hz)	104	0.645	0.426	3.210	6.081	-1.835E-03
Pn/Lg(4-6 Hz)	74	0.610	0.450	2.640	4.851	-1.489E-03
Pn/Lg(6-8 Hz)	82	0.533	0.427	2.208	4.015	-1.244E-03
Pn/Sn(2-4 Hz)	105	0.624	0.512	1.558	3.226	-7.907E-04
Pn/Sn(4-6 Hz)	75	0.548	0.427	0.569	1.566	-1.254E-04
Pn/Sn(6-8 Hz)	83	0.539	0.435	0.264	1.026	4.755E-05

Figure A-9. Regional data and best least-square fits (solid curves) of the distance dependence for 129 regional events recorded by ESDC.

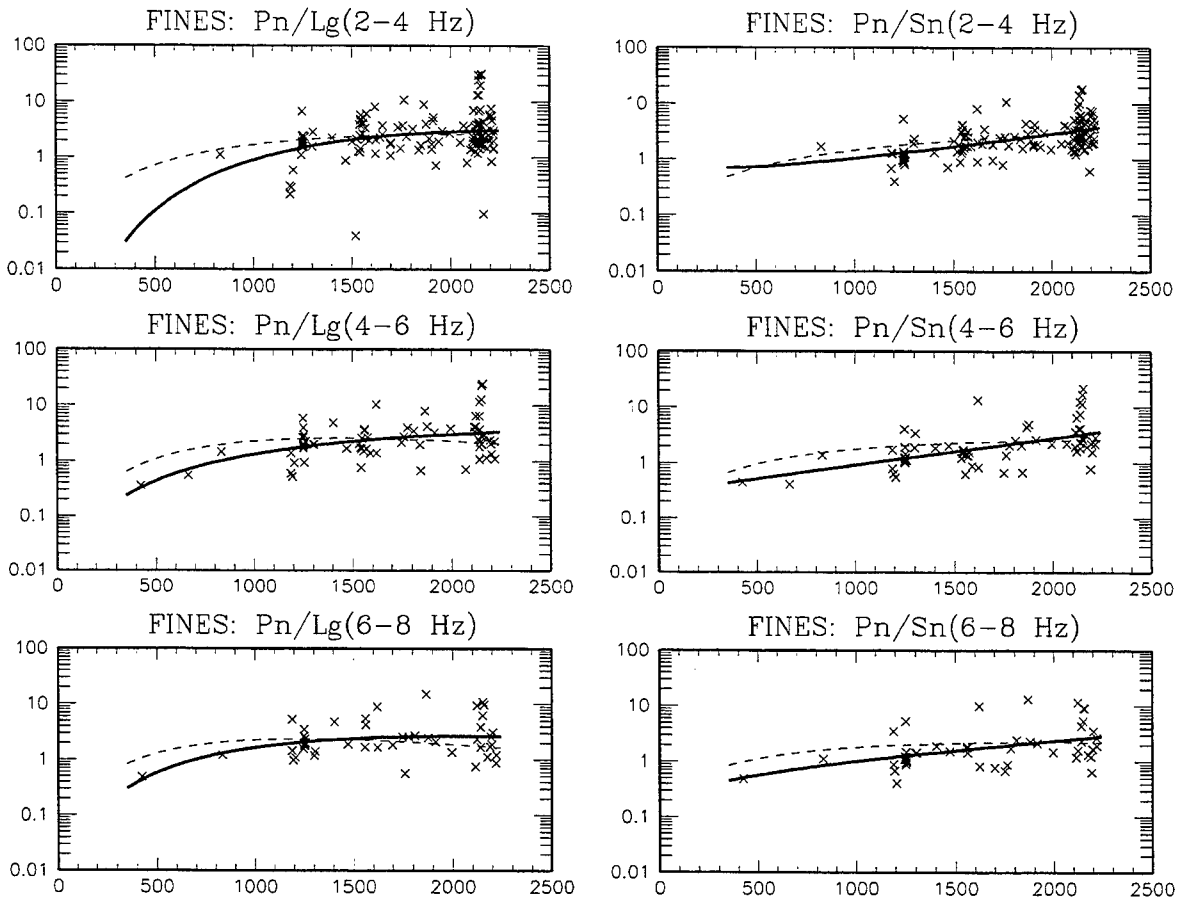

	n	*s*	s_c	$\hat{\alpha}$	$\hat{\beta}$	$\hat{\gamma}$
Pn/Lg(2-4 Hz)	137	0.400	0.383	1.527	4.382	-8.069E-04
Pn/Lg(4-6 Hz)	69	0.357	0.319	0.704	1.989	-2.354E-04
Pn/Lg(6-8 Hz)	48	0.329	0.312	1.125	2.336	-4.969E-04
Pn/Sn(2-4 Hz)	137	0.310	0.265	-0.636	-0.439	5.778E-04
Pn/Sn(4-6 Hz)	69	0.359	0.298	-0.495	0.056	4.656E-04
Pn/Sn(6-8 Hz)	48	0.361	0.328	-0.164	0.428	2.422E-04

Figure A-10. Regional data and best least-square fits (solid curves) of the distance dependence for 144 regional events recorded by FINES.

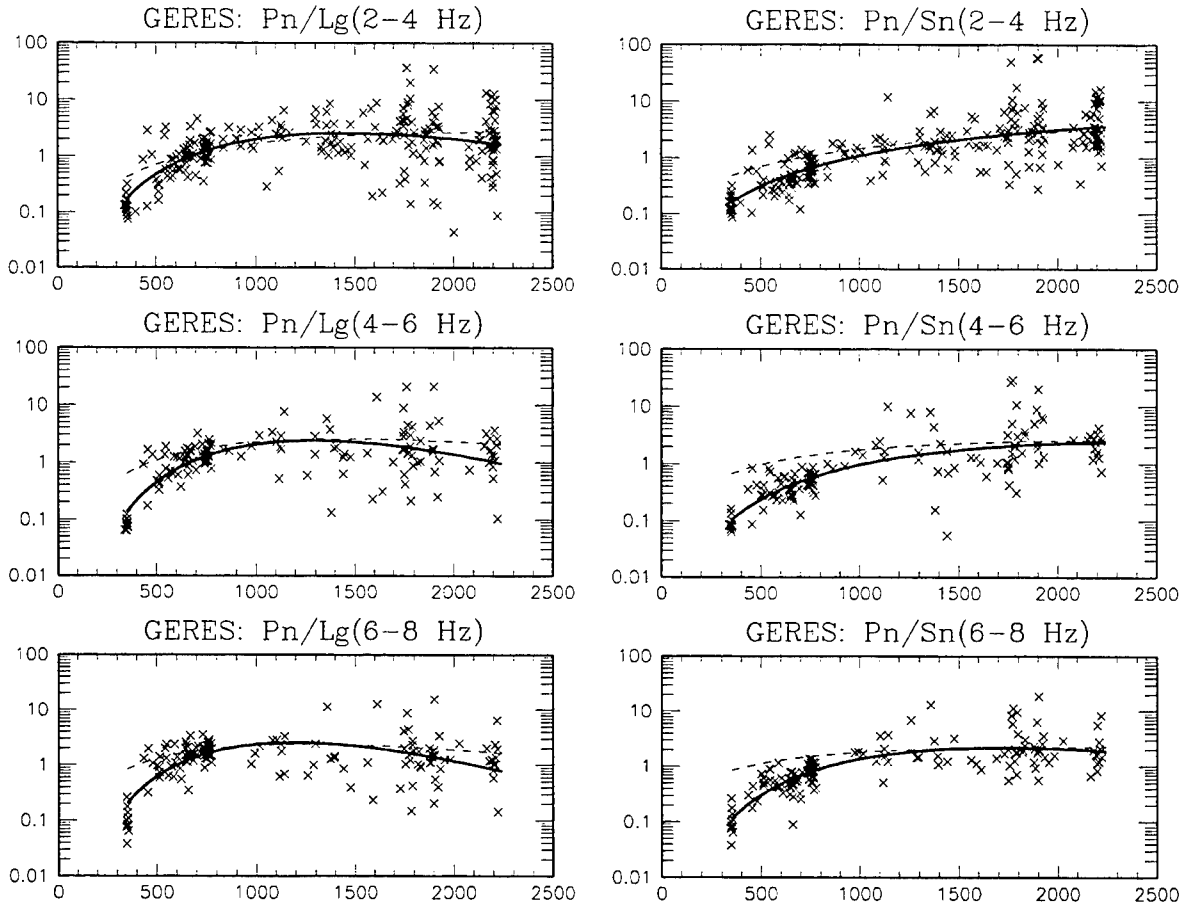

	n	s	s_c	$\hat{\alpha}$	$\hat{\beta}$	$\hat{\gamma}$
Pn/Lg(2-4 Hz)	261	0.495	0.396	2.237	4.083	-1.221E-03
Pn/Lg(4-6 Hz)	151	0.478	0.348	2.876	5.011	-1.682E-03
Pn/Lg(6-8 Hz)	152	0.422	0.334	2.978	4.845	-1.755E-03
Pn/Sn(2-4 Hz)	261	0.527	0.330	0.555	2.065	-1.583E-04
Pn/Sn(4-6 Hz)	151	0.540	0.341	0.942	2.803	-4.686E-04
Pn/Sn(6-8 Hz)	153	0.456	0.268	1.726	3.721	-9.363E-04

Figure A-11. Regional data and best least-square fits (solid curves) of the distance dependence for 299 regional events recorded by GERES.

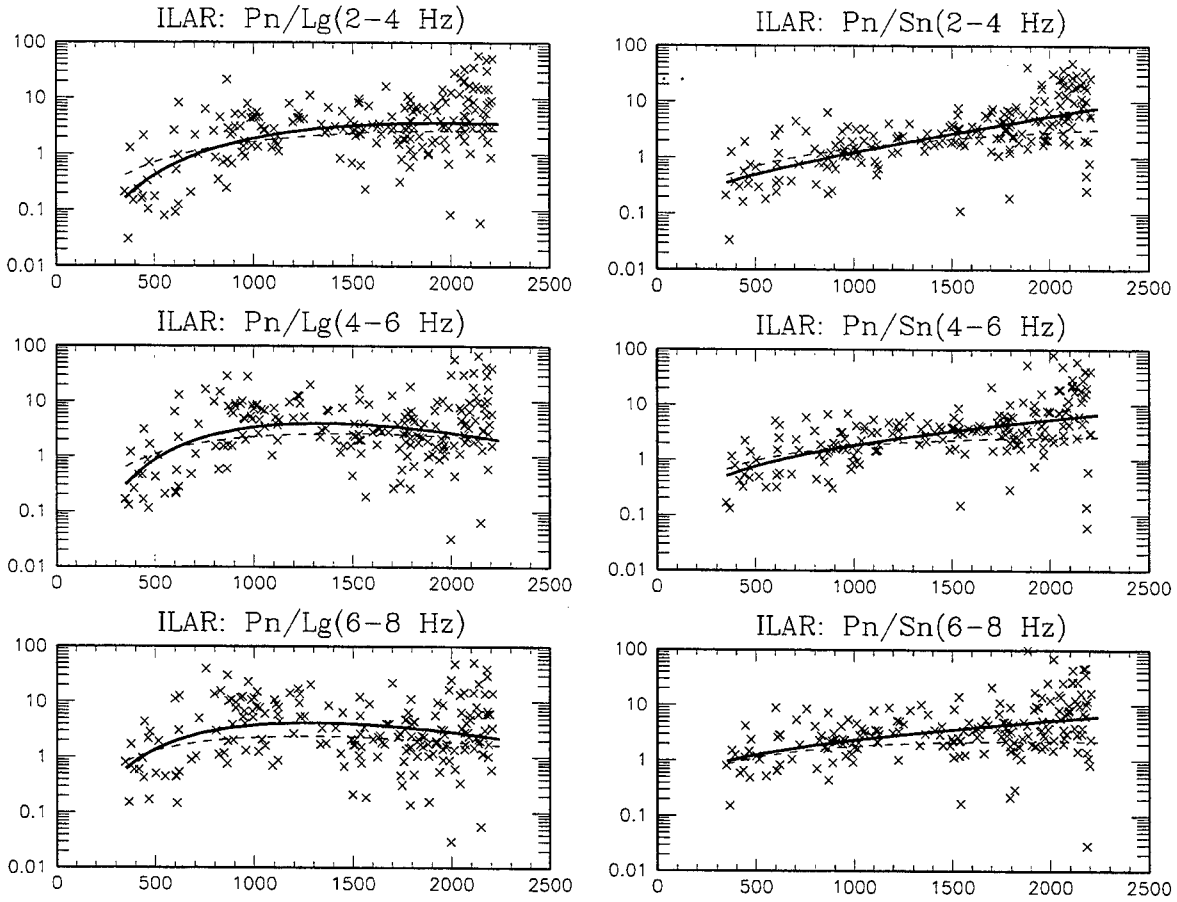

	n	*s*	s_c	$\hat{\alpha}$	$\hat{\beta}$	$\hat{\gamma}$
Pn/Lg(2-4 Hz)	203	0.736	0.672	1.629	3.419	-7.466E-04
Pn/Lg(4-6 Hz)	198	0.776	0.750	2.672	4.291	-1.392E-03
Pn/Lg(6-8 Hz)	195	0.711	0.697	2.289	3.339	-1.127E-03
Pn/Sn(2-4 Hz)	203	0.630	0.511	-0.346	0.453	5.143E-04
Pn/Sn(4-6 Hz)	198	0.634	0.564	0.240	0.957	1.864E-04
Pn/Sn(6-8 Hz)	195	0.531	0.486	0.303	0.610	1.711E-04

Figure A-12. Regional data and best least-square fits (solid curves) of the distance dependence for 216 regional events recorded by ILAR.

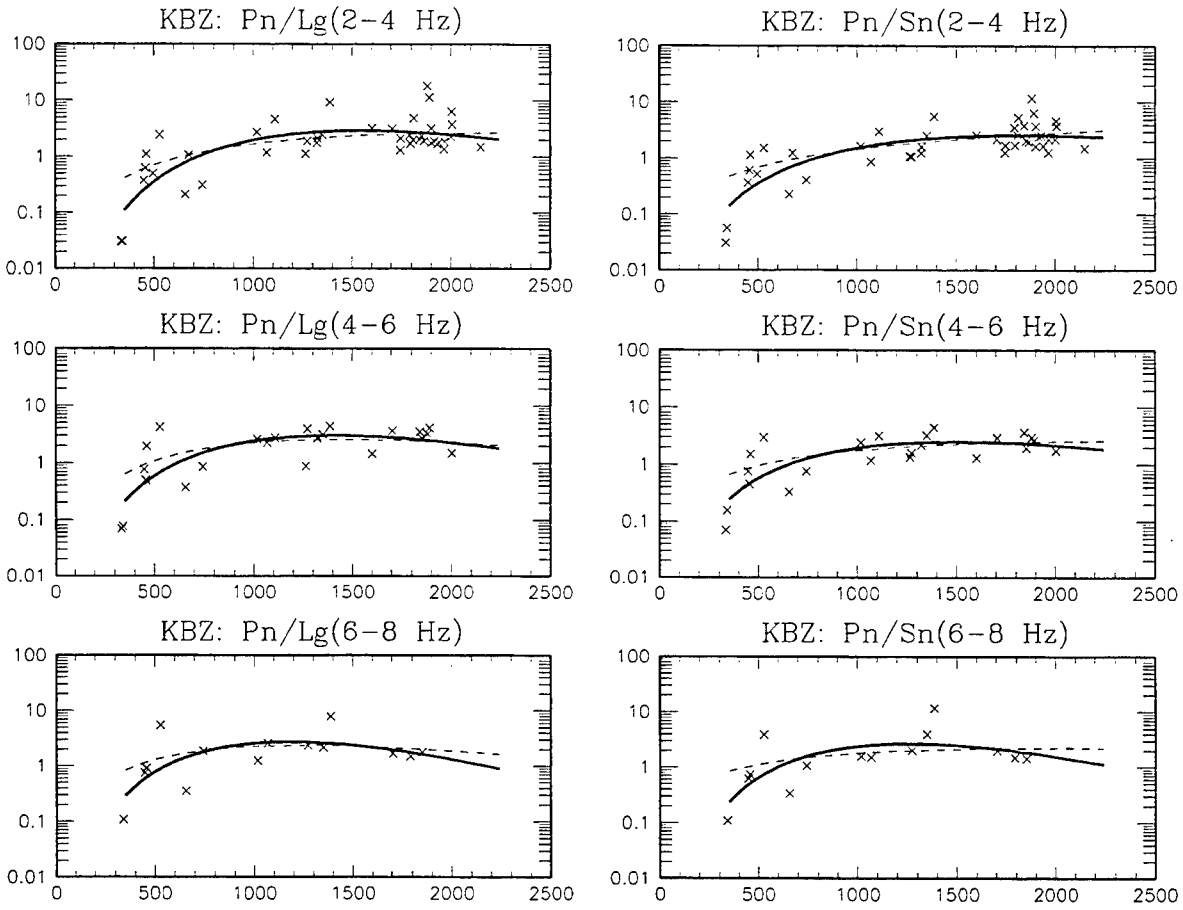

	n	*s*	s_c	$\hat{\alpha}$	$\hat{\beta}$	$\hat{\gamma}$
Pn/Lg(2-4 Hz)	43	0.534	0.343	2.375	4.574	-1.277E-03
Pn/Lg(4-6 Hz)	23	0.514	0.335	2.380	4.140	-1.270E-03
Pn/Lg(6-8 Hz)	14	0.464	0.375	2.789	4.388	-1.607E-03
Pn/Sn(2-4 Hz)	43	0.484	0.296	1.602	3.442	-8.132E-04
Pn/Sn(4-6 Hz)	23	0.456	0.294	1.857	3.387	-9.736E-04
Pn/Sn(6-8 Hz)	14	0.491	0.378	2.633	4.344	-1.490E-03

Figure A-13. Regional data and best least-square fits (solid curves) of the distance dependence for 43 regional events recorded by KBZ.

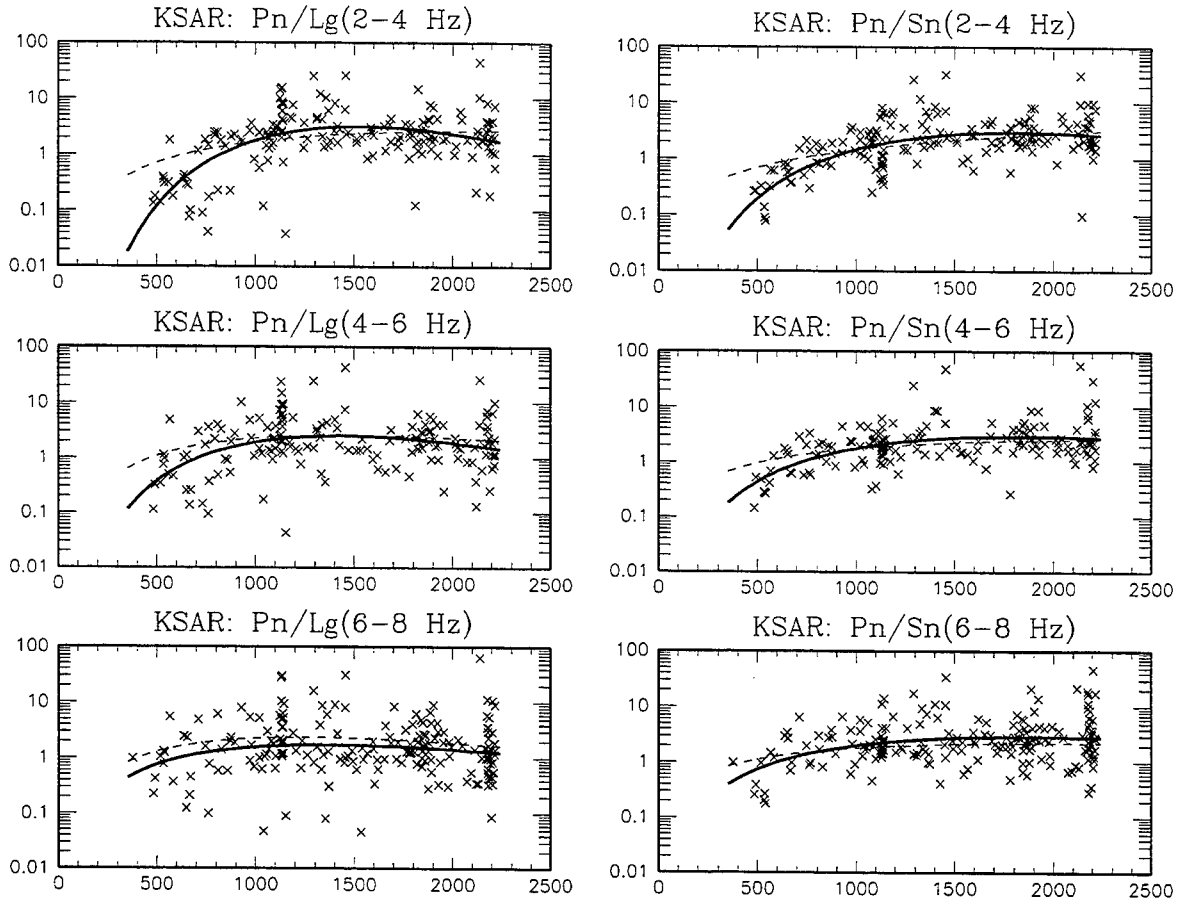

	n	s	s_c	$\hat{\alpha}$	$\hat{\beta}$	$\hat{\gamma}$
Pn/Lg(2-4 Hz)	187	0.562	0.470	3.653	7.391	-2.103E-03
Pn/Lg(4-6 Hz)	158	0.484	0.451	2.543	4.731	-1.432E-03
Pn/Lg(6-8 Hz)	196	0.520	0.516	1.303	2.239	-7.136E-04
Pn/Sn(2-4 Hz)	187	0.482	0.391	2.170	4.825	-1.154E-03
Pn/Sn(4-6 Hz)	158	0.391	0.334	1.612	3.316	-7.815E-04
Pn/Sn(6-8 Hz)	196	0.416	0.393	1.251	2.325	-5.402E-04

Figure A-14. Regional data and best least-square fits (solid curves) of the distance dependence for 284 regional events recorded by KSAR.

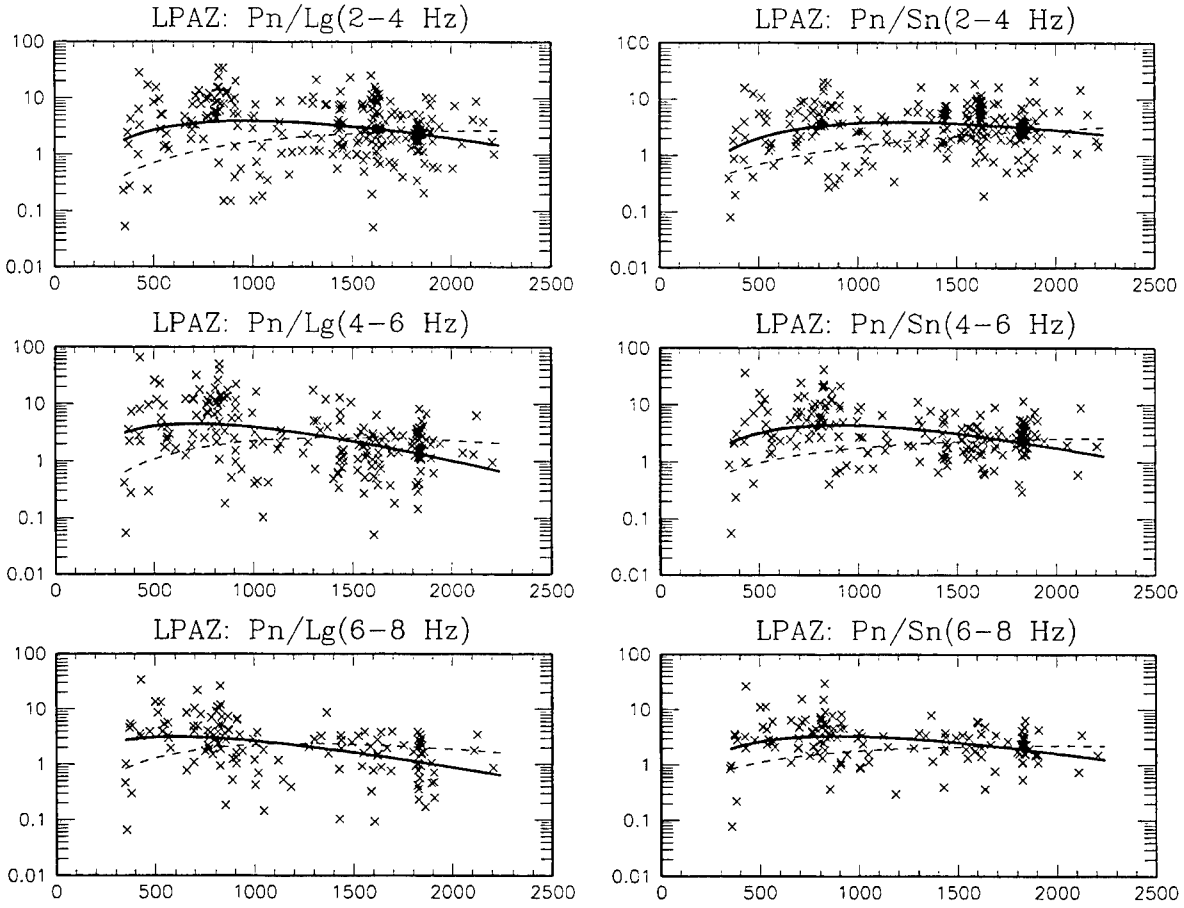

	n	s	s_c	$\hat{\alpha}$	$\hat{\beta}$	$\hat{\gamma}$
Pn/Lg(2-4 Hz)	277	0.489	0.481	1.909	2.113	-9.417E-04
Pn/Lg(4-6 Hz)	207	0.542	0.499	2.063	1.853	-1.145E-03
Pn/Lg(6-8 Hz)	139	0.495	0.459	1.441	1.135	-8.181E-04
Pn/Sn(2-4 Hz)	277	0.377	0.368	1.742	2.195	-7.824E-04
Pn/Sn(4-6 Hz)	207	0.407	0.389	2.073	2.190	-1.051E-03
Pn/Sn(6-8 Hz)	139	0.374	0.361	1.616	1.655	-8.073E-04

Figure A-15. Regional data and best least-square fits (solid curves) of the distance dependence for 282 regional events recorded by LPAZ.

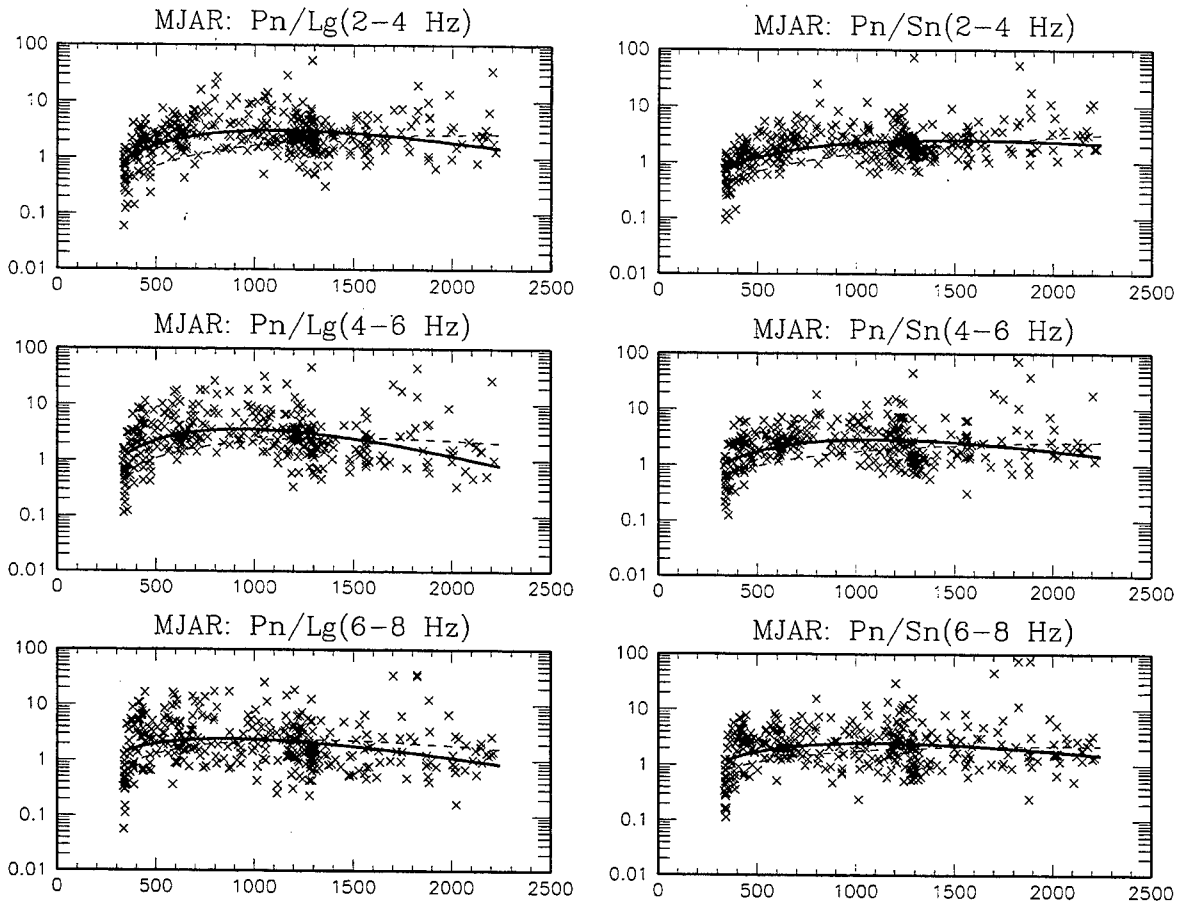

	n	*s*	s_c	$\hat{\alpha}$	$\hat{\beta}$	$\hat{\gamma}$
Pn/Lg(2-4 Hz)	456	0.361	0.324	1.845	2.423	-9.336E-04
Pn/Lg(4-6 Hz)	380	0.409	0.378	2.388	2.876	-1.331E-03
Pn/Lg(6-8 Hz)	380	0.426	0.415	1.477	1.619	-8.126E-04
Pn/Sn(2-4 Hz)	456	0.328	0.283	1.105	1.636	-4.679E-04
Pn/Sn(4-6 Hz)	380	0.364	0.339	1.638	2.073	-8.197E-04
Pn/Sn(6-8 Hz)	381	0.387	0.375	1.279	1.546	-6.122E-04

Figure A-16. Regional data and best least-square fits (solid curves) of the distance dependence for 558 regional events recorded by MJAR.

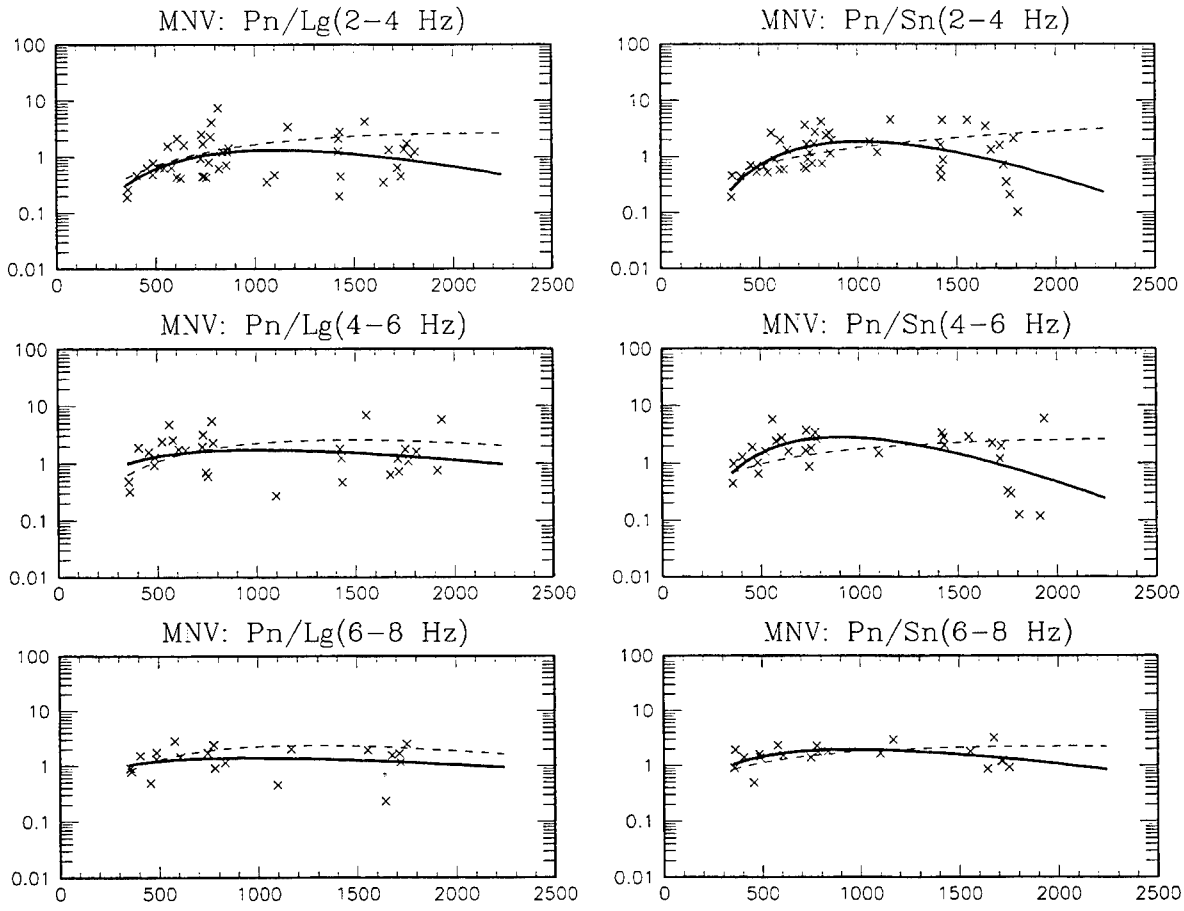

	n	s	s_c	$\hat{\alpha}$	$\hat{\beta}$	$\hat{\gamma}$
Pn/Lg(2-4 Hz)	46	0.364	0.340	1.896	3.130	-1.228E-03
Pn/Lg(4-6 Hz)	30	0.361	0.368	1.067	1.368	-5.897E-04
Pn/Lg(6-8 Hz)	20	0.275	0.288	0.647	0.797	-3.625E-04
Pn/Sn(2-4 Hz)	46	0.382	0.327	3.271	4.962	-2.129E-03
Pn/Sn(4-6 Hz)	30	0.429	0.381	3.260	4.310	-2.065E-03
Pn/Sn(6-8 Hz)	20	0.193	0.185	1.364	1.706	-7.752E-04

Figure A-17. Regional data and best least-square fits (solid curves) of the distance dependence for 52 regional events recorded by MNV.

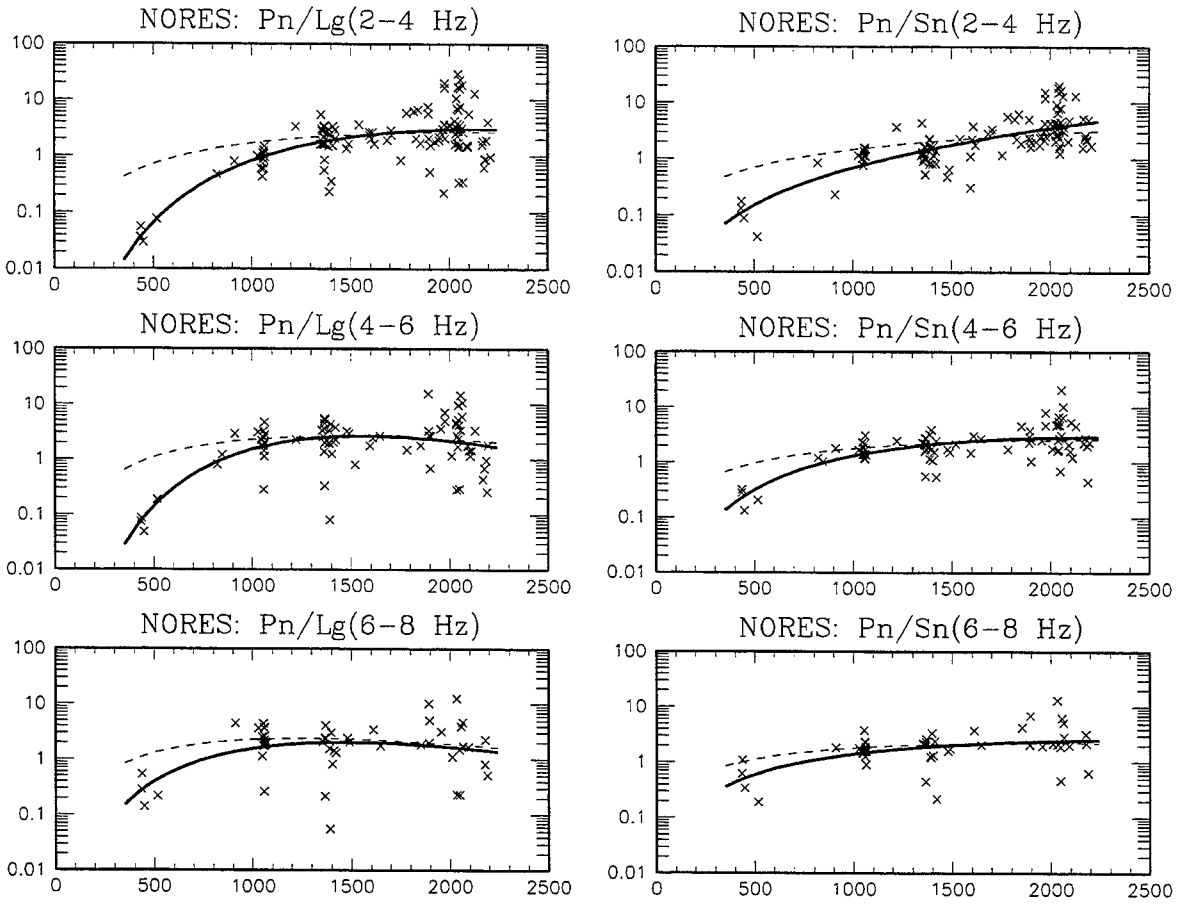

	n	s	s_c	$\hat{\alpha}$	$\hat{\beta}$	$\hat{\gamma}$
Pn/Lg(2-4 Hz)	119	0.514	0.375	1.954	5.447	-1.082E-03
Pn/Lg(4-6 Hz)	81	0.498	0.396	3.040	6.334	-1.748E-03
Pn/Lg(6-8 Hz)	51	0.480	0.442	1.999	3.851	-1.129E-03
Pn/Sn(2-4 Hz)	119	0.448	0.296	0.124	2.079	8.328E-05
Pn/Sn(4-6 Hz)	81	0.351	0.260	1.202	2.983	-5.641E-04
Pn/Sn(6-8 Hz)	51	0.344	0.301	0.719	1.693	-2.752E-04

Figure A-18. Regional data and best least-square fits (solid curves) of the distance dependence for 130 regional events recorded by NORES.

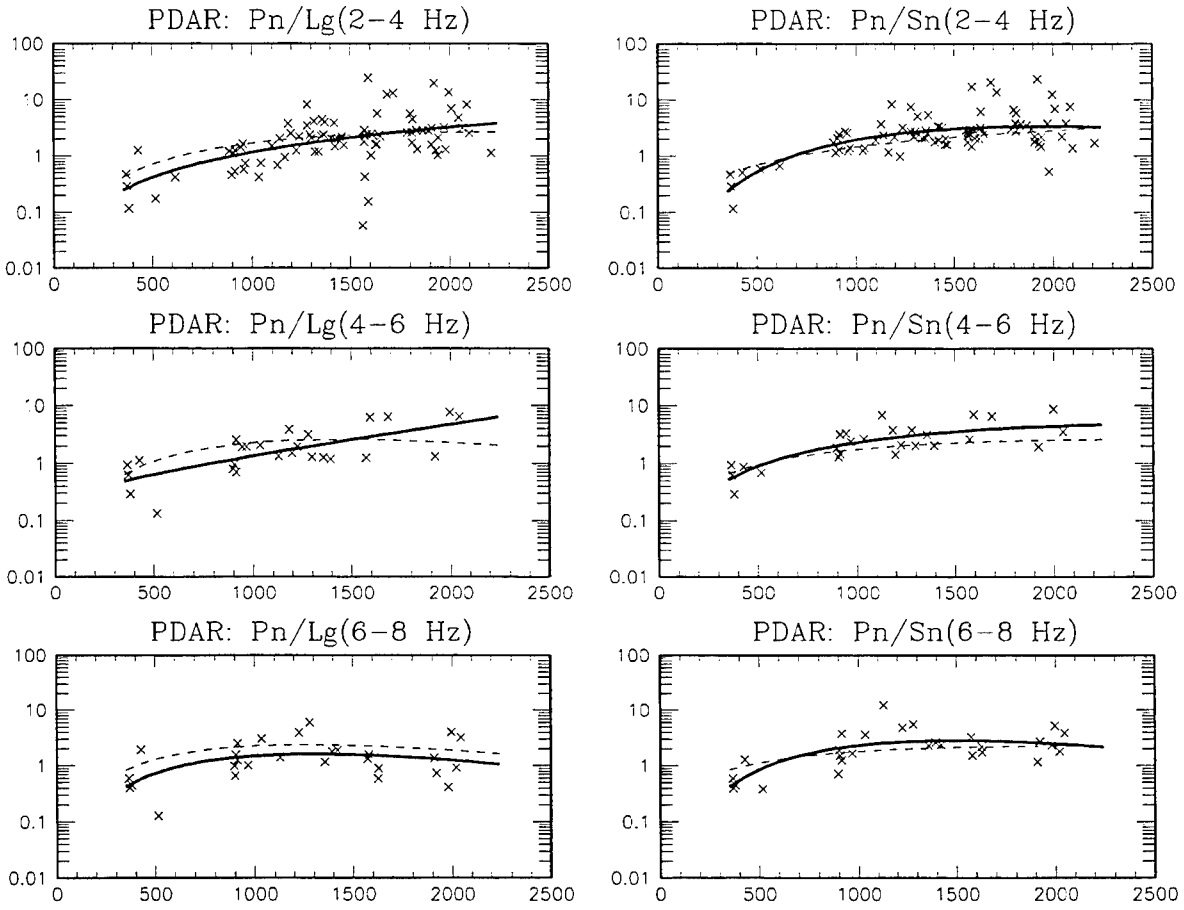

	n	s	s_c	$\hat{\alpha}$	$\hat{\beta}$	$\hat{\gamma}$
Pn/Lg(2-4 Hz)	85	0.460	0.388	0.318	1.474	2.866E-06
Pn/Lg(4-6 Hz)	26	0.406	0.295	-0.282	0.305	4.585E-04
Pn/Lg(6-8 Hz)	28	0.362	0.328	1.355	2.321	-7.741E-04
Pn/Sn(2-4 Hz)	85	0.371	0.281	1.458	2.960	-6.492E-04
Pn/Sn(4-6 Hz)	26	0.352	0.215	0.946	1.812	-2.649E-04
Pn/Sn(6-8 Hz)	28	0.361	0.261	1.667	2.793	-8.118E-04

Figure A-19. Regional data and best least-square fits (solid curves) of the distance dependence for 93 regional events recorded by PDAR.

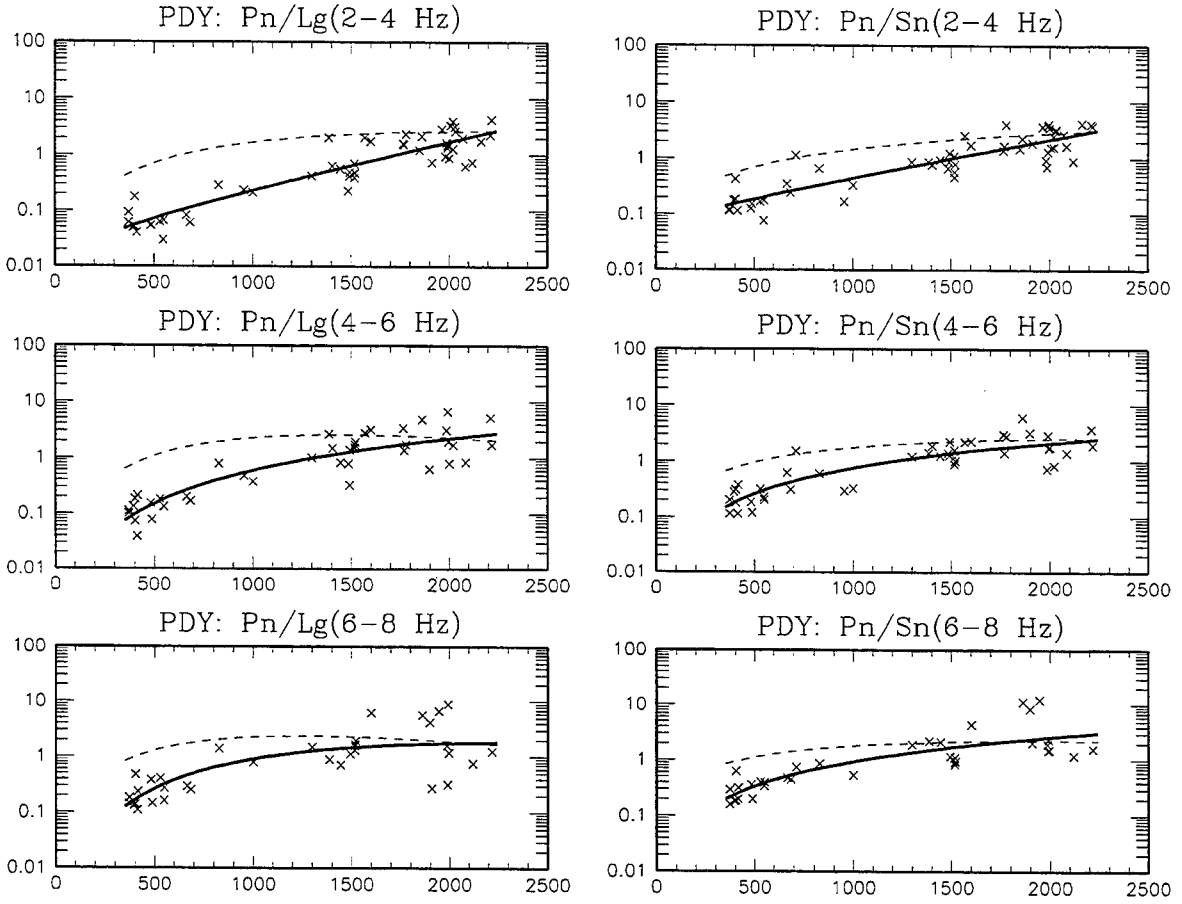

	n	*s*	s_c	$\hat{\alpha}$	$\hat{\beta}$	$\hat{\gamma}$
Pn/Lg(2-4 Hz)	53	0.628	0.249	-1.299	0.442	7.402E-04
Pn/Lg(4-6 Hz)	43	0.588	0.266	0.177	2.050	-4.394E-05
Pn/Lg(6-8 Hz)	35	0.543	0.348	0.905	2.589	-4.920E-04
Pn/Sn(2-4 Hz)	54	0.506	0.232	-0.950	0.202	6.342E-04
Pn/Sn(4-6 Hz)	44	0.466	0.228	0.207	1.616	-4.104E-05
Pn/Sn(6-8 Hz)	36	0.494	0.274	0.228	1.472	1.953E-06

Figure A-20. Regional data and best least-square fits (solid curves) of the distance dependence for 59 regional events recorded by PDY.

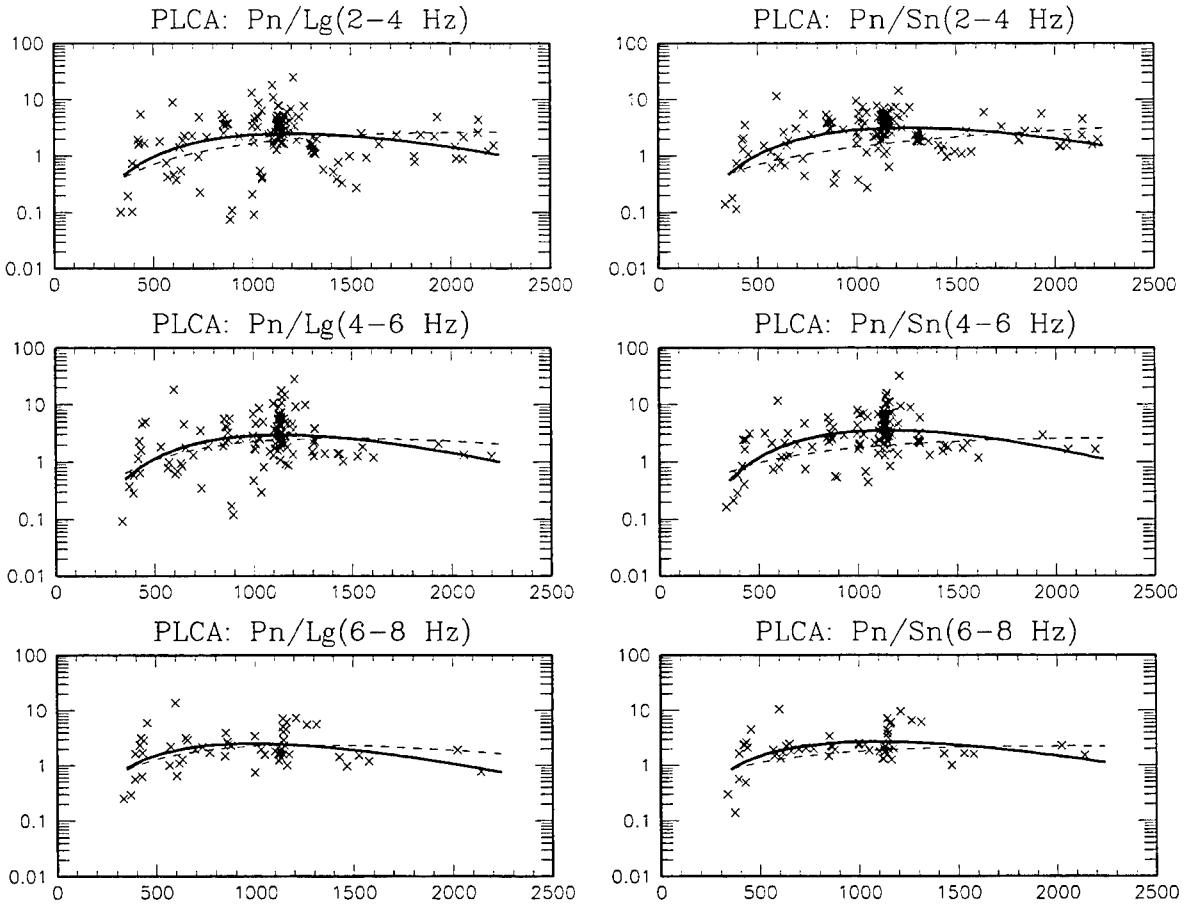

	n	s	s_c	$\hat{\alpha}$	$\hat{\beta}$	$\hat{\gamma}$
Pn/Lg(2-4 Hz)	149	0.451	0.422	2.198	3.350	-1.230E-03
Pn/Lg(4-6 Hz)	123	0.427	0.389	2.526	3.702	-1.418E-03
Pn/Lg(6-8 Hz)	58	0.330	0.305	2.041	2.662	-1.174E-03
Pn/Sn(2-4 Hz)	149	0.358	0.309	2.273	3.469	-1.201E-03
Pn/Sn(4-6 Hz)	123	0.381	0.323	2.798	4.103	-1.547E-03
Pn/Sn(6-8 Hz)	58	0.318	0.284	1.913	2.583	-1.032E-03

Figure A-21. Regional data and best least-square fits (solid curves) of the distance dependence for 154 regional events recorded by PLCA.

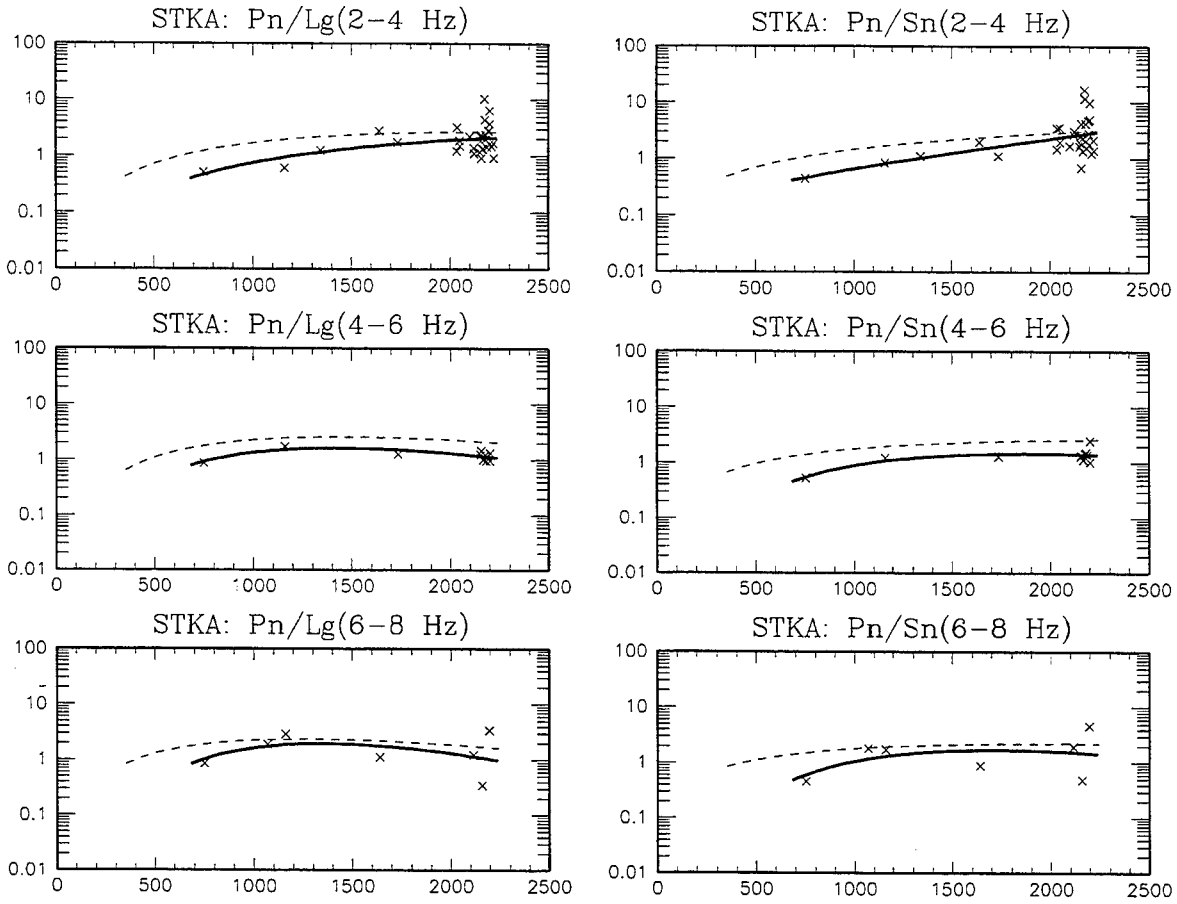

	n	*s*	s_c	$\hat{\alpha}$	$\hat{\beta}$	$\hat{\gamma}$
Pn/Lg(2-4 Hz)	32	0.269	0.242	0.509	2.179	-2.514E-04
Pn/Lg(4-6 Hz)	11	0.088	0.070	1.750	3.389	-1.029E-03
Pn/Lg(6-8 Hz)	7	0.338	0.386	2.480	4.554	-1.465E-03
Pn/Sn(2-4 Hz)	32	0.339	0.296	-0.484	0.493	3.881E-04
Pn/Sn(4-6 Hz)	11	0.158	0.109	1.220	3.121	-7.251E-04
Pn/Sn(6-8 Hz)	7	0.360	0.399	1.743	3.997	-1.015E-03

Figure A-22. Regional data and best least-square fits (solid curves) of the distance dependence for 37 regional events recorded by STKA.

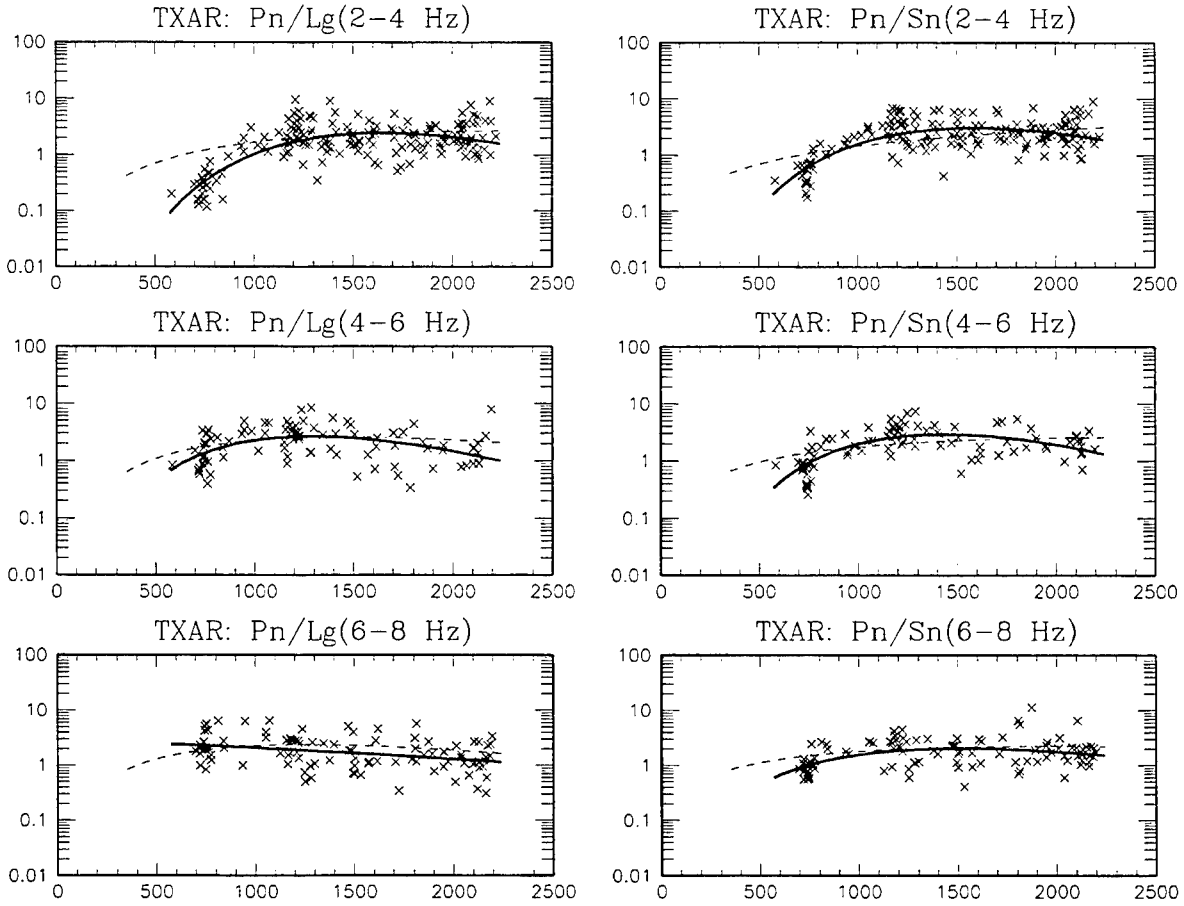

	n	s	s_c	$\hat{\alpha}$	$\hat{\beta}$	$\hat{\gamma}$
Pn/Lg(2-4 Hz)	188	0.387	0.261	3.631	8.216	-2.171E-03
Pn/Lg(4-6 Hz)	94	0.309	0.278	3.086	5.344	-1.796E-03
Pn/Lg(6-8 Hz)	104	0.286	0.270	0.624	0.208	-2.694E-04
Pn/Sn(2-4 Hz)	188	0.327	0.235	3.404	7.132	-1.949E-03
Pn/Sn(4-6 Hz)	94	0.312	0.236	3.529	6.749	-2.046E-03
Pn/Sn(6-8 Hz)	104	0.262	0.239	1.782	3.443	-9.824E-04

Figure A-23. Regional data and best least-square fits (solid curves) of the distance dependence for 211 regional events recorded by TXAR.

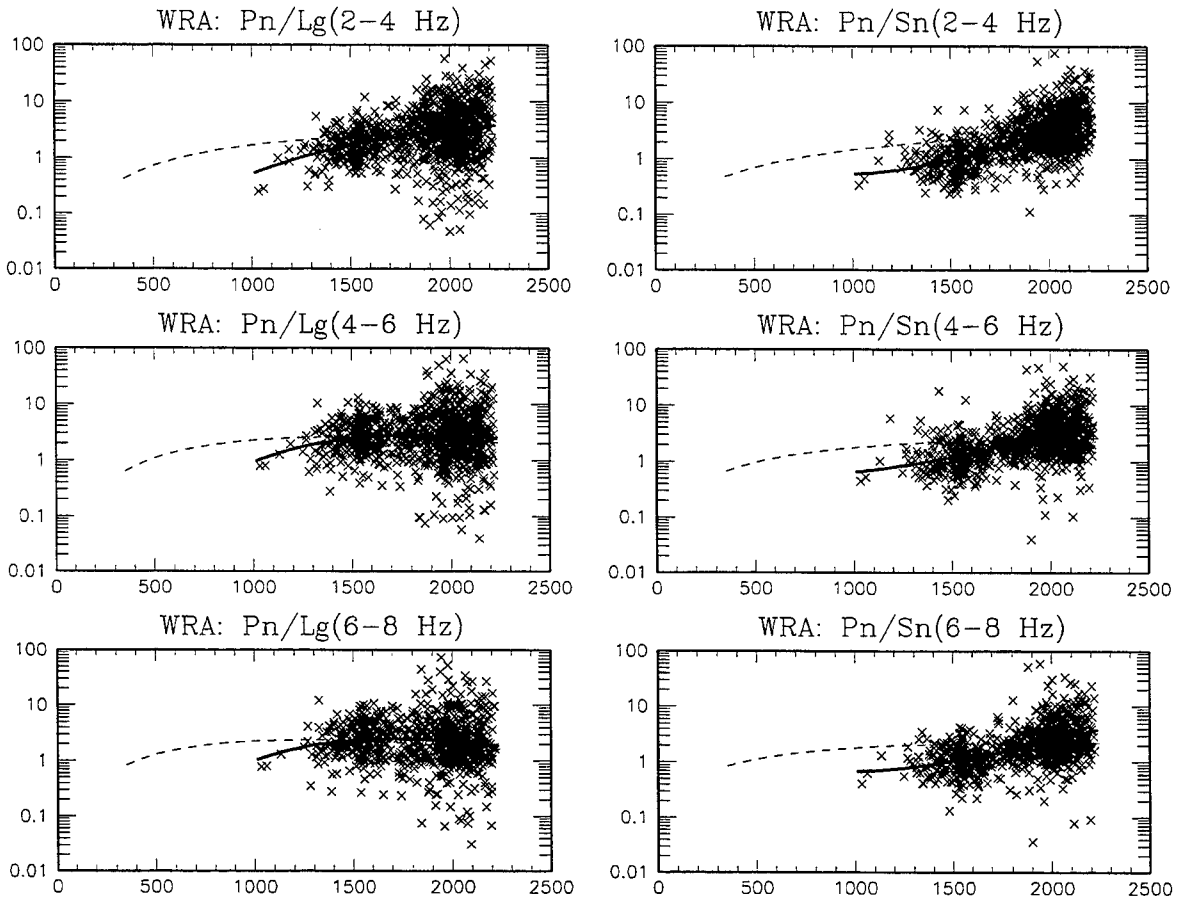

	n	*s*	s_c	$\hat{\alpha}$	$\hat{\beta}$	$\hat{\gamma}$
Pn/Lg(2-4 Hz)	1187	0.427	0.407	1.137	4.642	-6.104E-04
Pn/Lg(4-6 Hz)	1061	0.415	0.414	2.981	7.328	-1.730E-03
Pn/Lg(6-8 Hz)	894	0.400	0.399	3.217	7.488	-1.901E-03
Pn/Sn(2-4 Hz)	1187	0.397	0.309	-3.427	-5.011	2.278E-03
Pn/Sn(4-6 Hz)	1061	0.379	0.328	-1.928	-2.260	1.338E-03
Pn/Sn(6-8 Hz)	894	0.366	0.317	-2.392	-3.501	1.606E-03

Figure A-24. Regional data and best least-square fits (solid curves) of the distance dependence for 1266 regional events recorded by WRA.

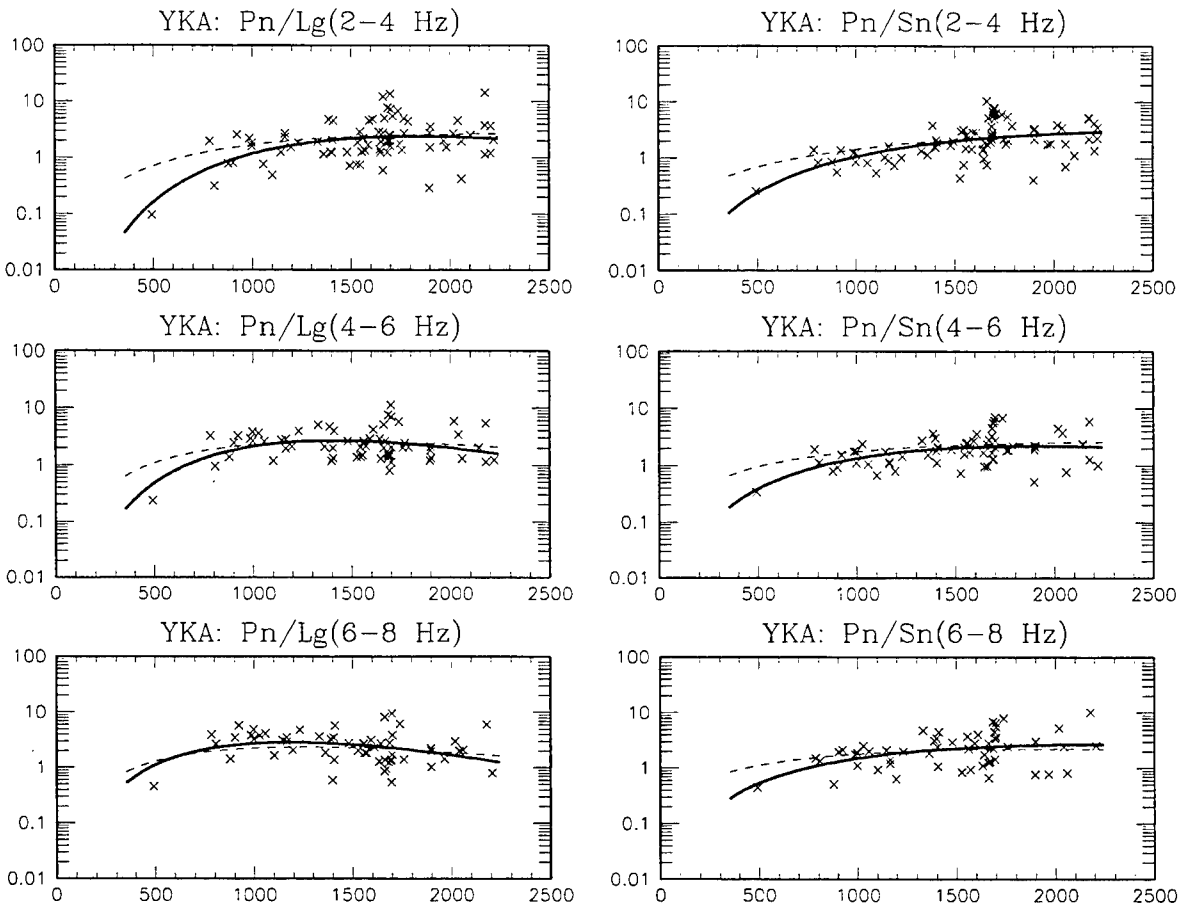

	n	s	s_c	$\hat{\alpha}$	$\hat{\beta}$	$\hat{\gamma}$
Pn/Lg(2-4 Hz)	82	0.361	0.318	2.012	4.706	-1.114E-03
Pn/Lg(4-6 Hz)	63	0.273	0.252	2.417	4.344	-1.330E-03
Pn/Lg(6-8 Hz)	56	0.288	0.278	2.217	3.293	-1.201E-03
Pn/Sn(2-4 Hz)	82	0.325	0.273	1.019	2.923	-4.731E-04
Pn/Sn(4-6 Hz)	63	0.273	0.244	1.277	2.859	-6.461E-04
Pn/Sn(6-8 Hz)	56	0.310	0.286	0.993	2.216	-4.243E-04

Figure A-25. Regional data and best least-square fits (solid curves) of the distance dependence for 88 regional events recorded by YKA.

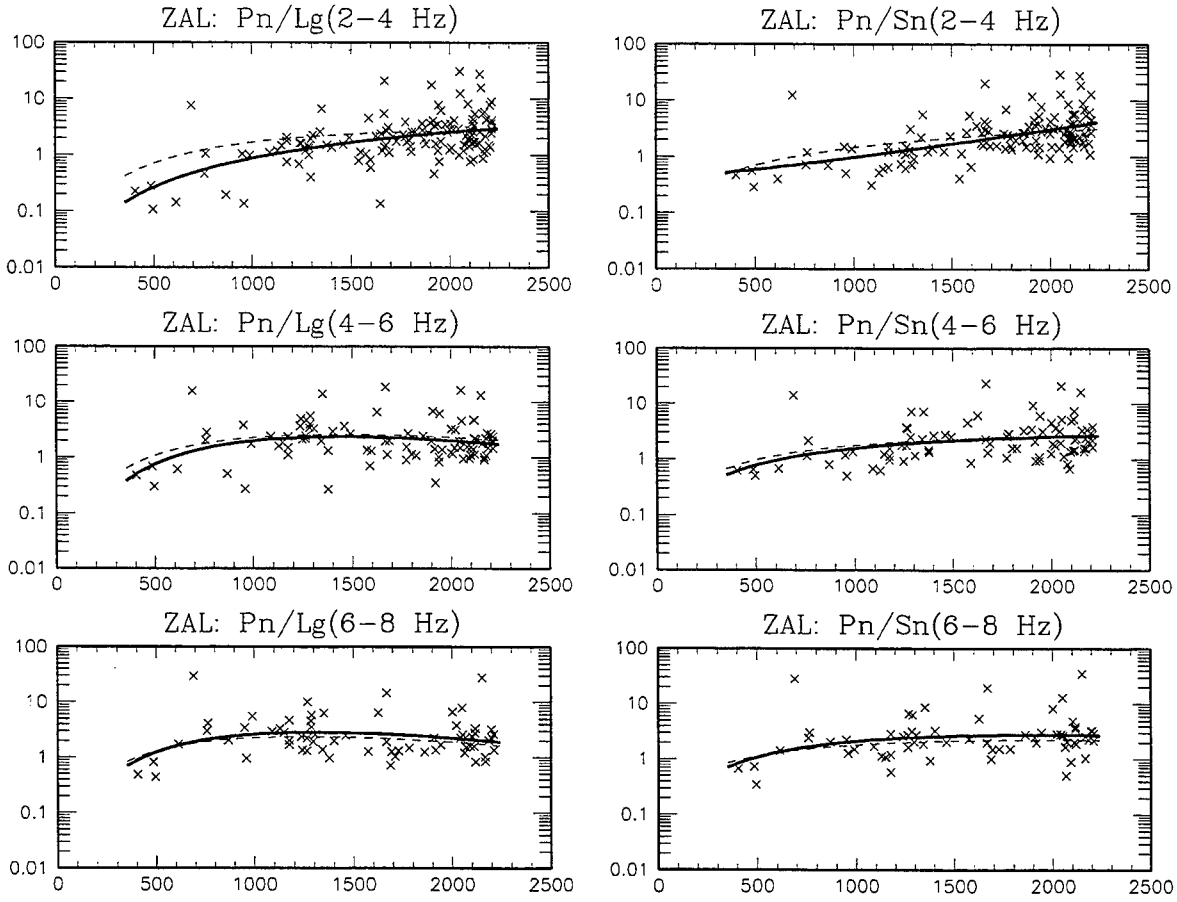

	n	*s*	s_c	$\hat{\alpha}$	$\hat{\beta}$	$\hat{\gamma}$
Pn/Lg(2-4 Hz)	134	0.421	0.356	0.391	1.911	-1.121E-04
Pn/Lg(4-6 Hz)	89	0.370	0.357	1.607	2.767	-8.264E-04
Pn/Lg(6-8 Hz)	67	0.353	0.345	1.615	2.370	-7.824E-04
Pn/Sn(2-4 Hz)	130	0.384	0.317	-0.608	-0.203	5.600E-04
Pn/Sn(4-6 Hz)	86	0.357	0.335	0.618	1.331	-1.905E-04
Pn/Sn(6-8 Hz)	64	0.372	0.361	0.928	1.525	-3.390E-04

Figure A-26. Regional data and best least-square fits (solid curves) of the distance dependence for 139 regional events recorded by ZAL.

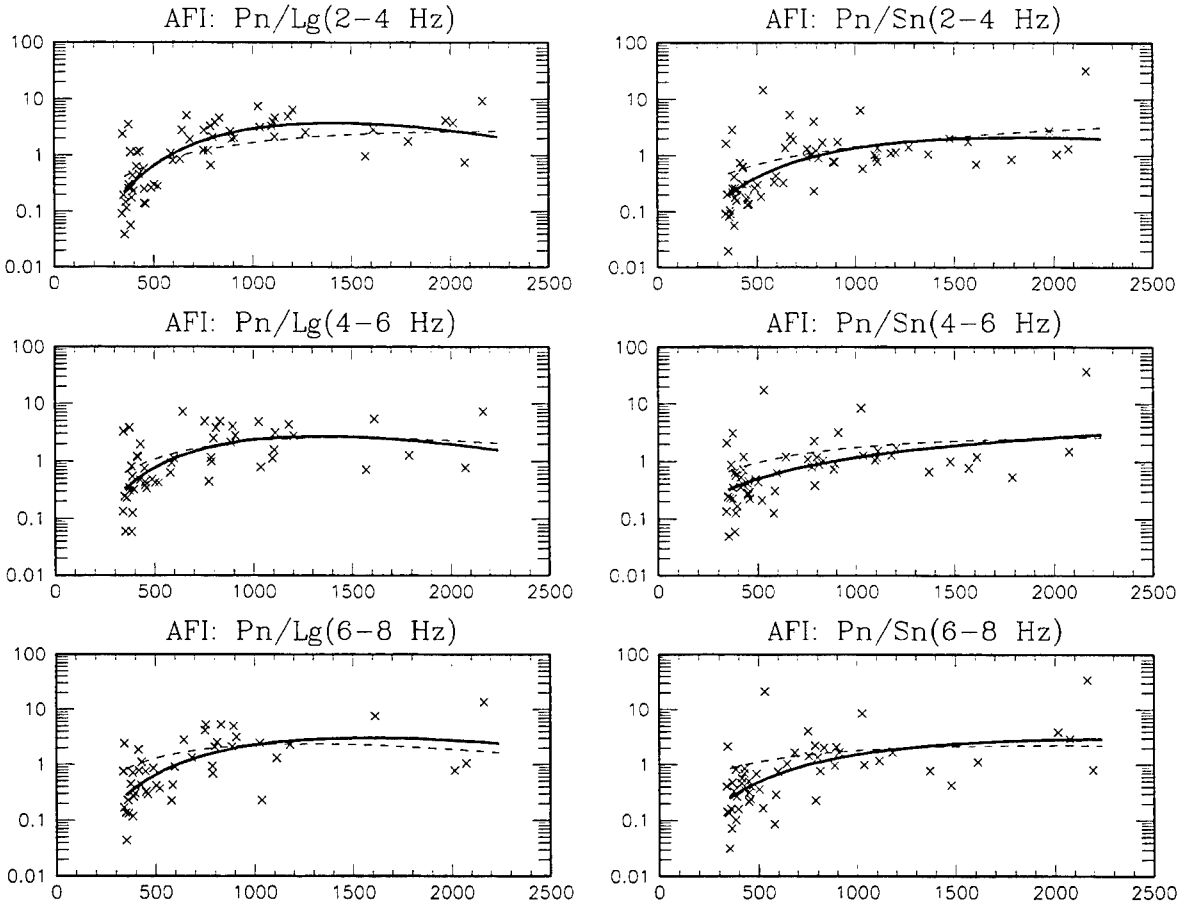

	n	s	s_c	$\hat{\alpha}$	$\hat{\beta}$	$\hat{\gamma}$
Pn/Lg(2-4 Hz)	59	0.588	0.385	2.636	4.470	-1.377E-03
Pn/Lg(4-6 Hz)	50	0.527	0.416	2.124	3.508	-1.134E-03
Pn/Lg(6-8 Hz)	46	0.544	0.417	1.839	3.291	-9.058E-04
Pn/Sn(2-4 Hz)	66	0.573	0.447	1.292	2.814	-6.602E-04
Pn/Sn(4-6 Hz)	57	0.520	0.446	0.345	1.312	-4.664E-05
Pn/Sn(6-8 Hz)	53	0.583	0.473	1.043	2.370	-4.442E-04

Figure A-27. Regional data and best least-square fits (solid curves) of the distance dependence for 71 regional events recorded by AFI.

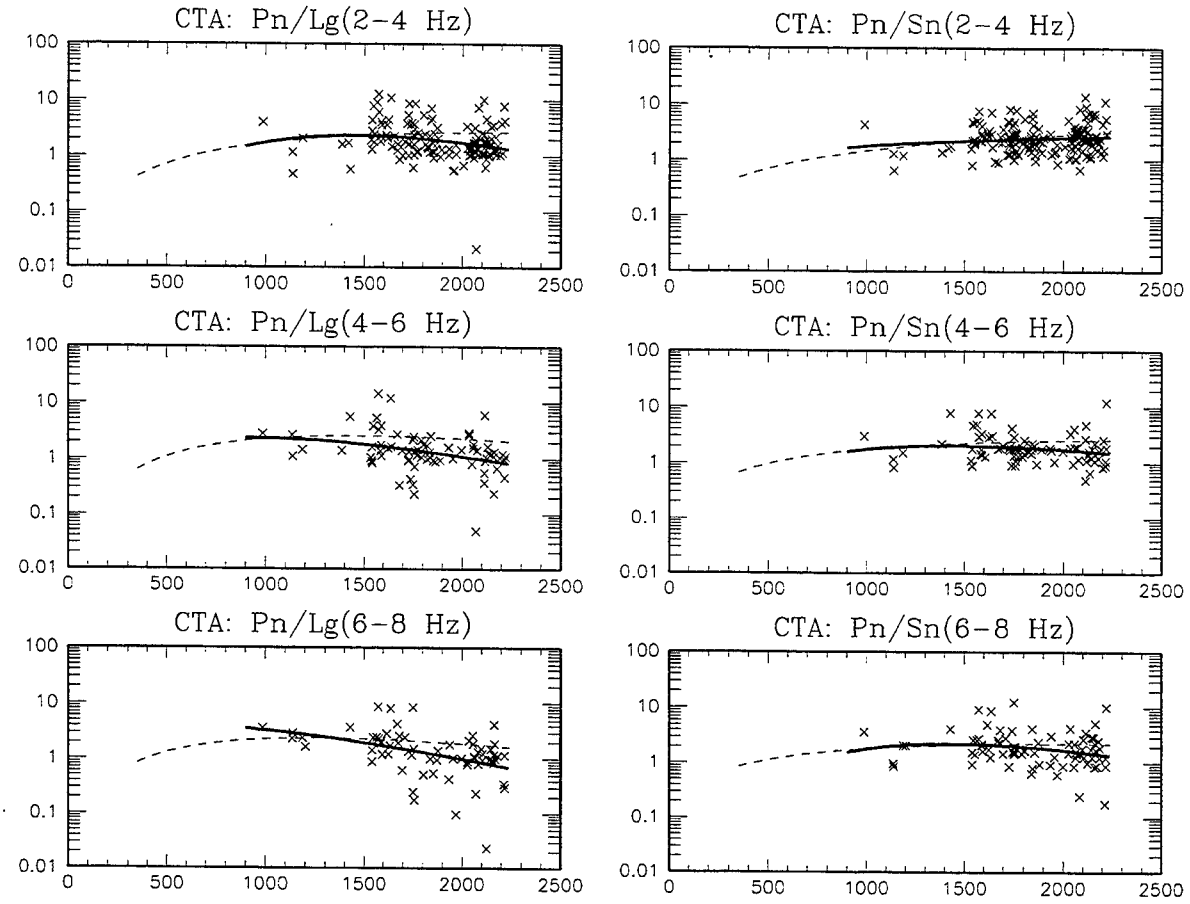

	n	*s*	s_c	$\hat{\alpha}$	$\hat{\beta}$	$\hat{\gamma}$
Pn/Lg(2-4 Hz)	145	0.329	0.324	2.622	5.009	-1.504E-03
Pn/Lg(4-6 Hz)	75	0.366	0.350	1.705	2.127	-9.648E-04
Pn/Lg(6-8 Hz)	67	0.424	0.393	1.679	1.349	-9.254E-04
Pn/Sn(2-4 Hz)	175	0.243	0.243	0.411	0.663	-4.621E-05
Pn/Sn(4-6 Hz)	83	0.249	0.248	1.509	2.649	-8.002E-04
Pn/Sn(6-8 Hz)	78	0.312	0.309	2.203	4.054	-1.238E-03

Figure A-28. Regional data and best least-square fits (solid curves) of the distance dependence for 215 regional events recorded by CTA.

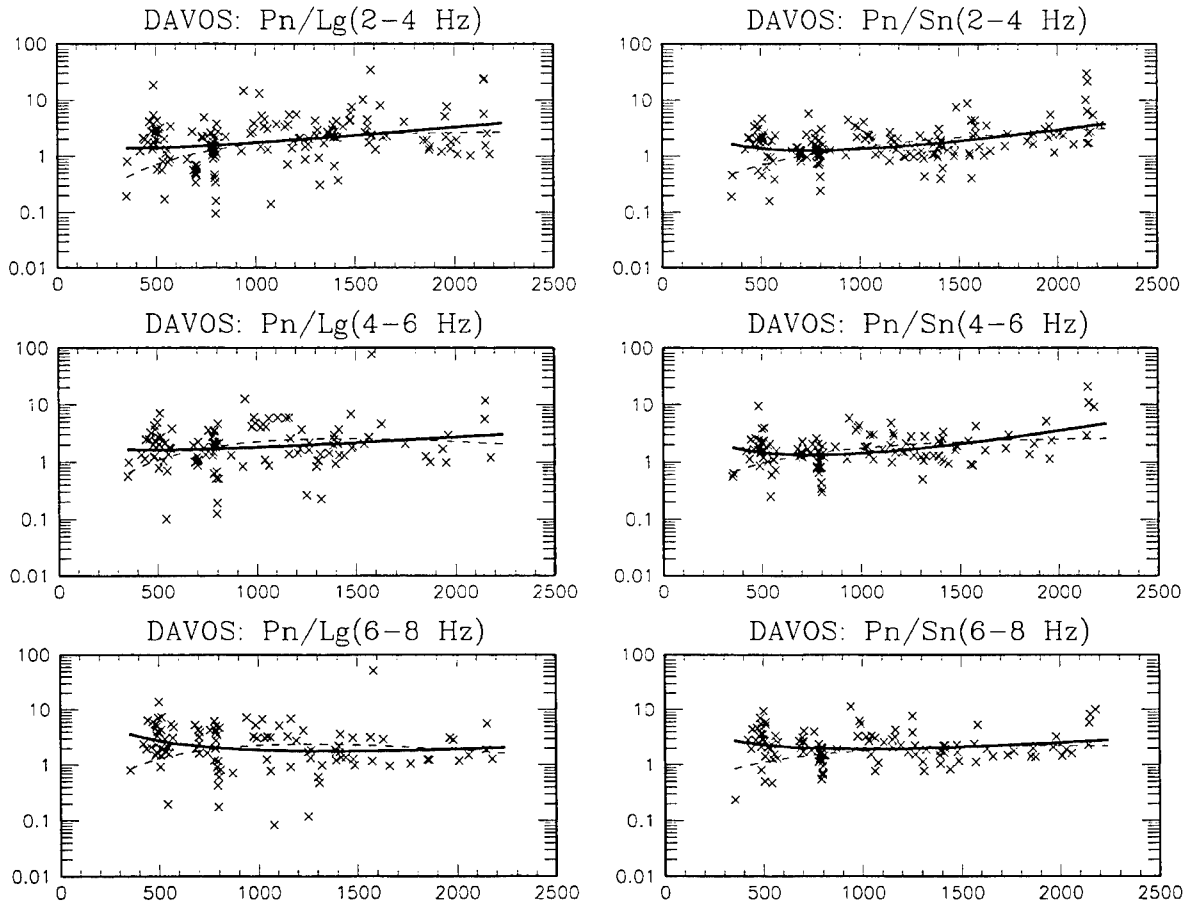

	n	s	s_c	$\hat{\alpha}$	$\hat{\beta}$	$\hat{\gamma}$
Pn/Lg(2-4 Hz)	163	0.409	0.393	-0.186	-0.316	3.713E-04
Pn/Lg(4-6 Hz)	118	0.387	0.385	-0.054	-0.281	2.617E-04
Pn/Lg(6-8 Hz)	109	0.402	0.398	-0.300	-1.160	3.657E-04
Pn/Sn(2-4 Hz)	172	0.311	0.285	-0.783	-1.202	7.029E-04
Pn/Sn(4-6 Hz)	123	0.291	0.268	-0.892	-1.371	8.052E-04
Pn/Sn(6-8 Hz)	114	0.288	0.288	-0.230	-0.853	3.696E-04

Figure A-29. Regional data and best least-square fits (solid curves) of the distance dependence for 179 regional events recorded by DAVOS.

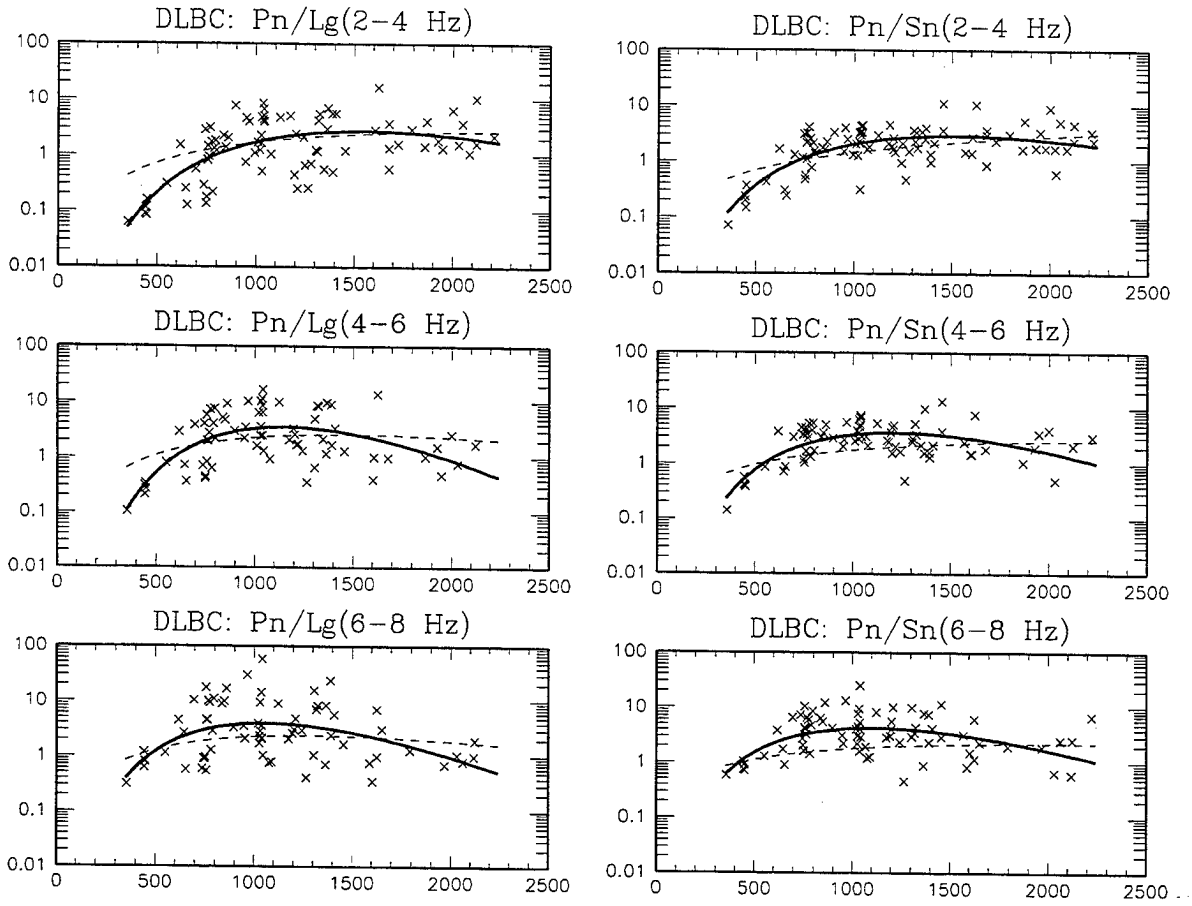

	n	s	s_c	$\hat{\alpha}$	$\hat{\beta}$	$\hat{\gamma}$
Pn/Lg(2-4 Hz)	84	0.542	0.417	2.808	5.645	-1.585E-03
Pn/Lg(4-6 Hz)	72	0.502	0.401	4.508	7.193	-2.726E-03
Pn/Lg(6-8 Hz)	71	0.513	0.463	3.766	5.391	-2.224E-03
Pn/Sn(2-4 Hz)	93	0.392	0.285	2.468	4.662	-1.335E-03
Pn/Sn(4-6 Hz)	78	0.357	0.272	3.334	5.248	-1.889E-03
Pn/Sn(6-8 Hz)	76	0.375	0.332	3.013	4.201	-1.656E-03

Figure A-30. Regional data and best least-square fits (solid curves) of the distance dependence for 104 regional events recorded by DLBC.

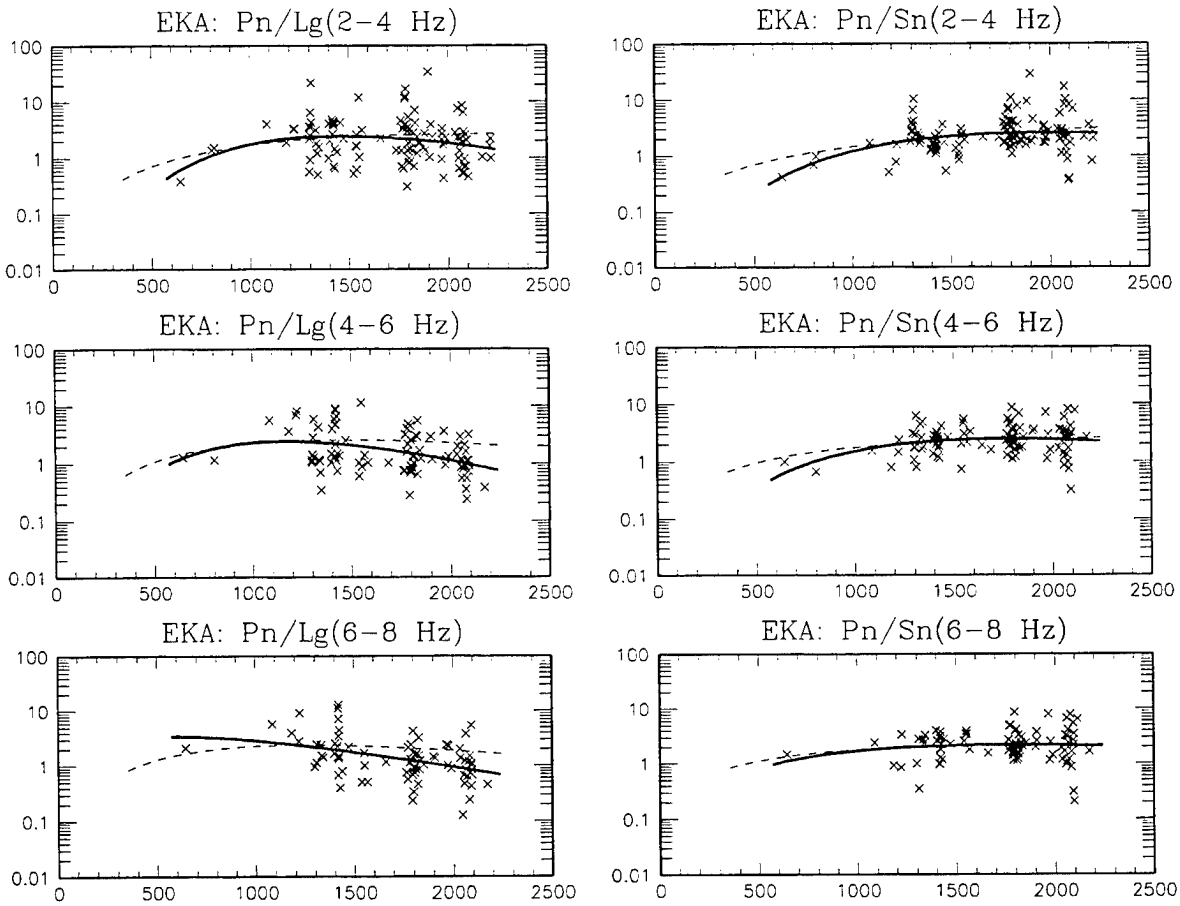

	n	*s*	s_c	$\hat{\alpha}$	$\hat{\beta}$	$\hat{\gamma}$
Pn/Lg(2-4 Hz)	120	0.374	0.367	2.739	5.278	-1.570E-03
Pn/Lg(4-6 Hz)	92	0.369	0.345	2.764	4.392	-1.630E-03
Pn/Lg(6-8 Hz)	80	0.373	0.343	1.445	1.081	-8.022E-04
Pn/Sn(2-4 Hz)	131	0.304	0.288	1.645	3.973	-8.640E-04
Pn/Sn(4-6 Hz)	101	0.259	0.252	1.695	3.609	-8.818E-04
Pn/Sn(6-8 Hz)	88	0.282	0.284	0.964	1.751	-4.242E-04

Figure A-31. Regional data and best least-square fits (solid curves) of the distance dependence for 158 regional events recorded by EKA.

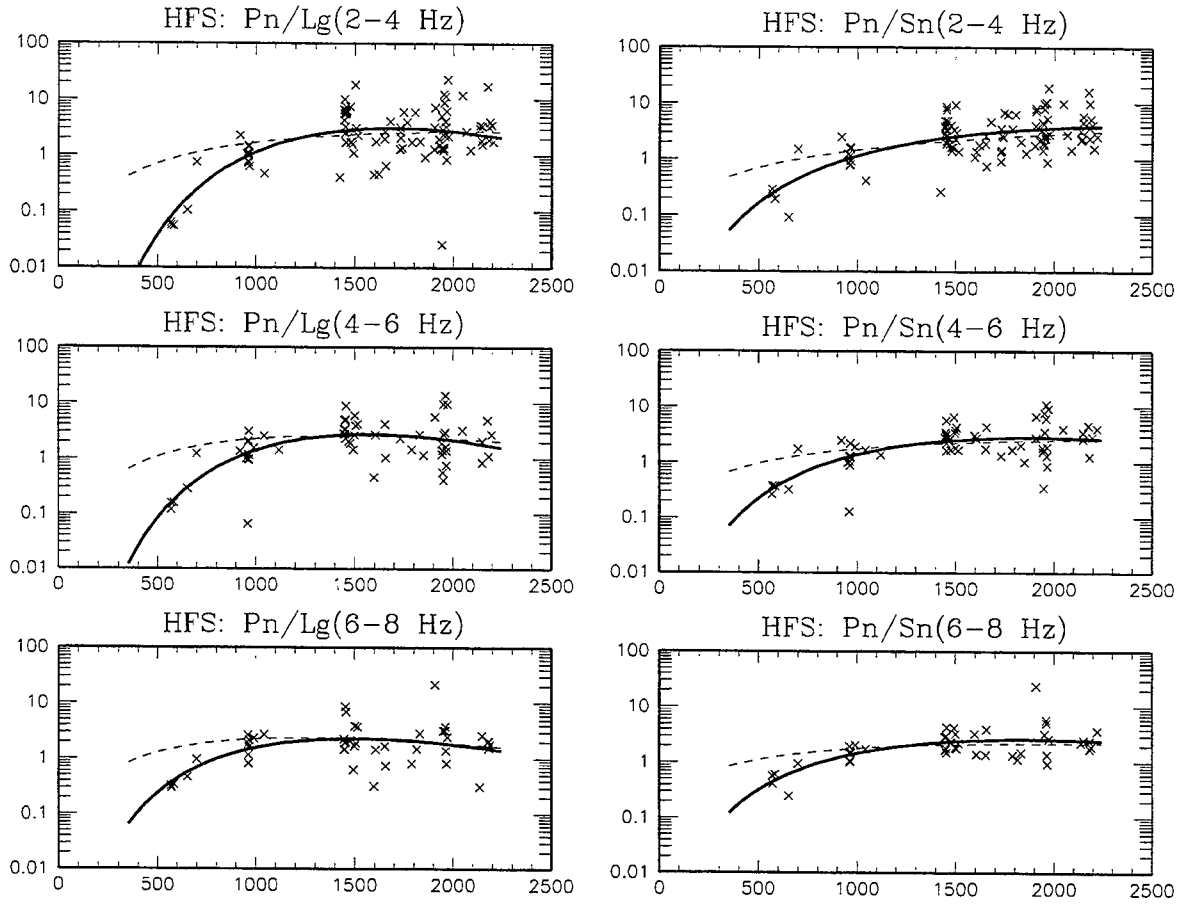

	n	*s*	s_c	$\hat{\alpha}$	$\hat{\beta}$	$\hat{\gamma}$
Pn/Lg(2-4 Hz)	97	0.525	0.414	3.752	8.542	-2.195E-03
Pn/Lg(4-6 Hz)	62	0.457	0.353	3.547	7.526	-2.077E-03
Pn/Lg(6-8 Hz)	44	0.389	0.333	2.617	5.205	-1.504E-03
Pn/Sn(2-4 Hz)	102	0.405	0.309	1.418	3.906	-6.715E-04
Pn/Sn(4-6 Hz)	65	0.372	0.290	1.866	4.260	-9.751E-04
Pn/Sn(6-8 Hz)	45	0.324	0.242	1.626	3.575	-8.288E-04

Figure A-32. Regional data and best least-square fits (solid curves) of the distance dependence for 111 regional events recorded by HFS.

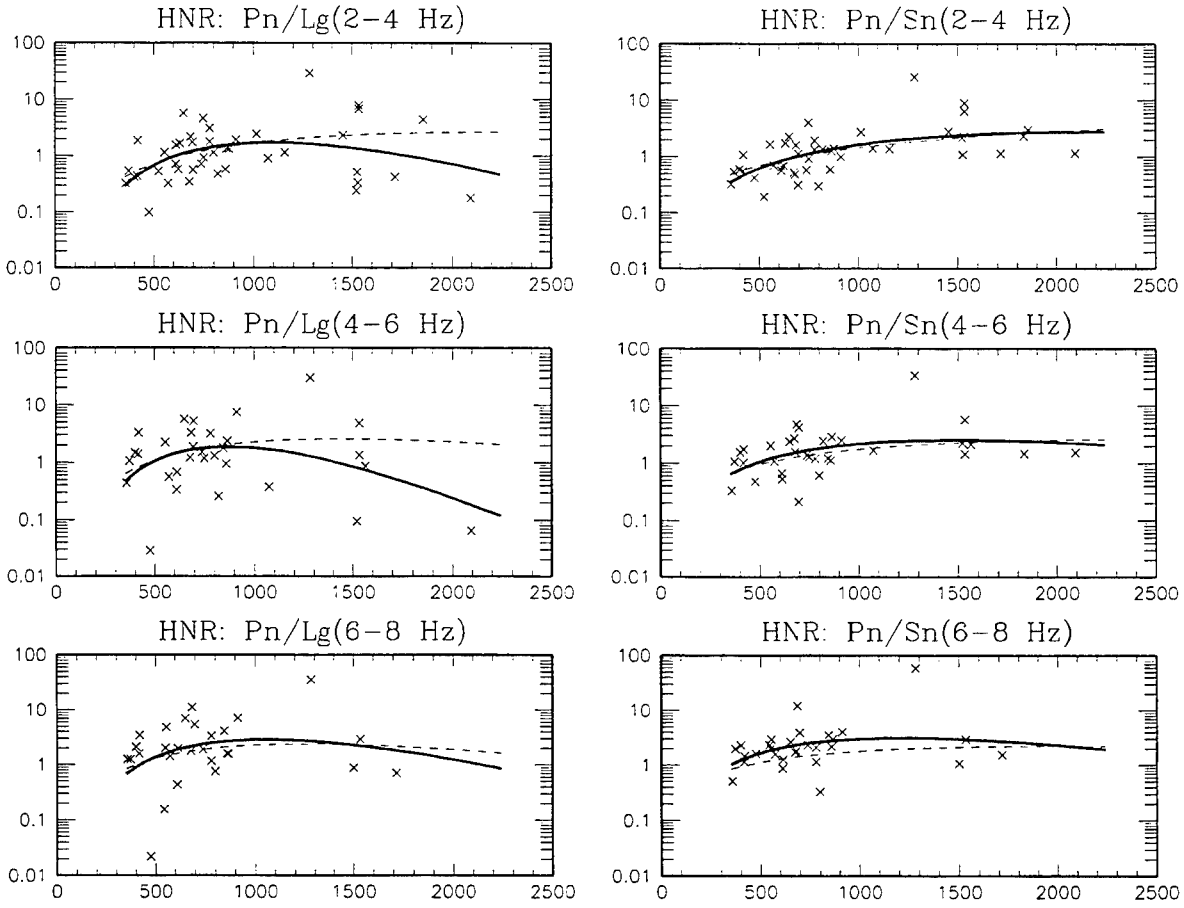

	n	*s*	s_c	$\hat{\alpha}$	$\hat{\beta}$	$\hat{\gamma}$
Pn/Lg(2-4 Hz)	42	0.491	0.460	2.478	3.922	-1.556E-03
Pn/Lg(4-6 Hz)	31	0.619	0.591	3.240	4.435	-2.207E-03
Pn/Lg(6-8 Hz)	28	0.590	0.586	2.385	3.296	-1.353E-03
Pn/Sn(2-4 Hz)	44	0.408	0.332	0.966	2.044	-3.915E-04
Pn/Sn(4-6 Hz)	33	0.394	0.367	1.264	1.995	-5.771E-04
Pn/Sn(6-8 Hz)	29	0.399	0.390	1.594	2.096	-7.467E-04

Figure A-33. Regional data and best least-square fits (solid curves) of the distance dependence for 49 regional events recorded by HNR.

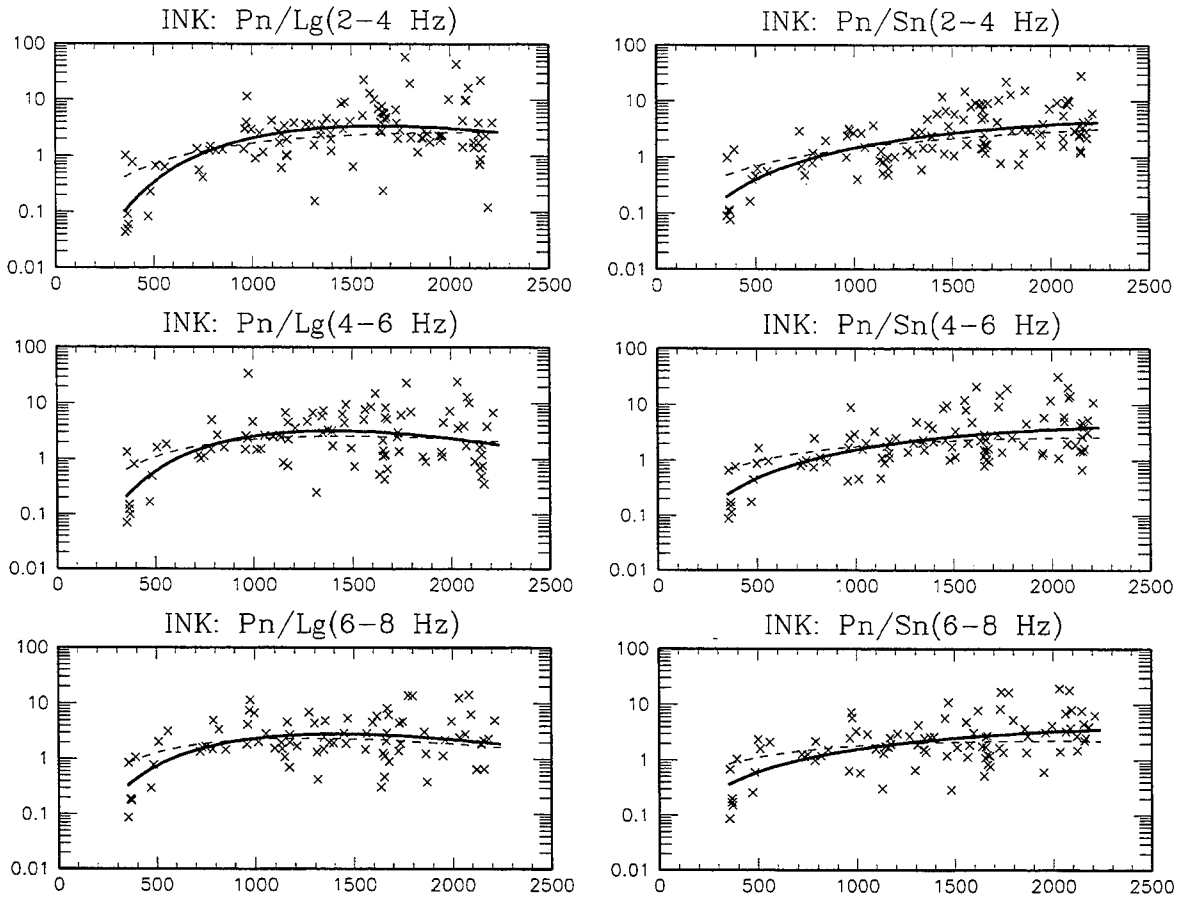

	n	*s*	s_c	$\hat{\alpha}$	$\hat{\beta}$	$\hat{\gamma}$
Pn/Lg(2-4 Hz)	107	0.573	0.439	2.369	4.666	-1.231E-03
Pn/Lg(4-6 Hz)	91	0.523	0.437	2.515	4.339	-1.345E-03
Pn/Lg(6-8 Hz)	82	0.456	0.390	1.990	3.364	-1.029E-03
Pn/Sn(2-4 Hz)	116	0.489	0.358	0.872	2.355	-2.934E-04
Pn/Sn(4-6 Hz)	100	0.491	0.376	0.877	2.219	-3.000E-04
Pn/Sn(6-8 Hz)	90	0.457	0.373	0.679	1.683	-1.868E-04

Figure A-34. Regional data and best least-square fits (solid curves) of the distance dependence for 118 regional events recorded by INK.

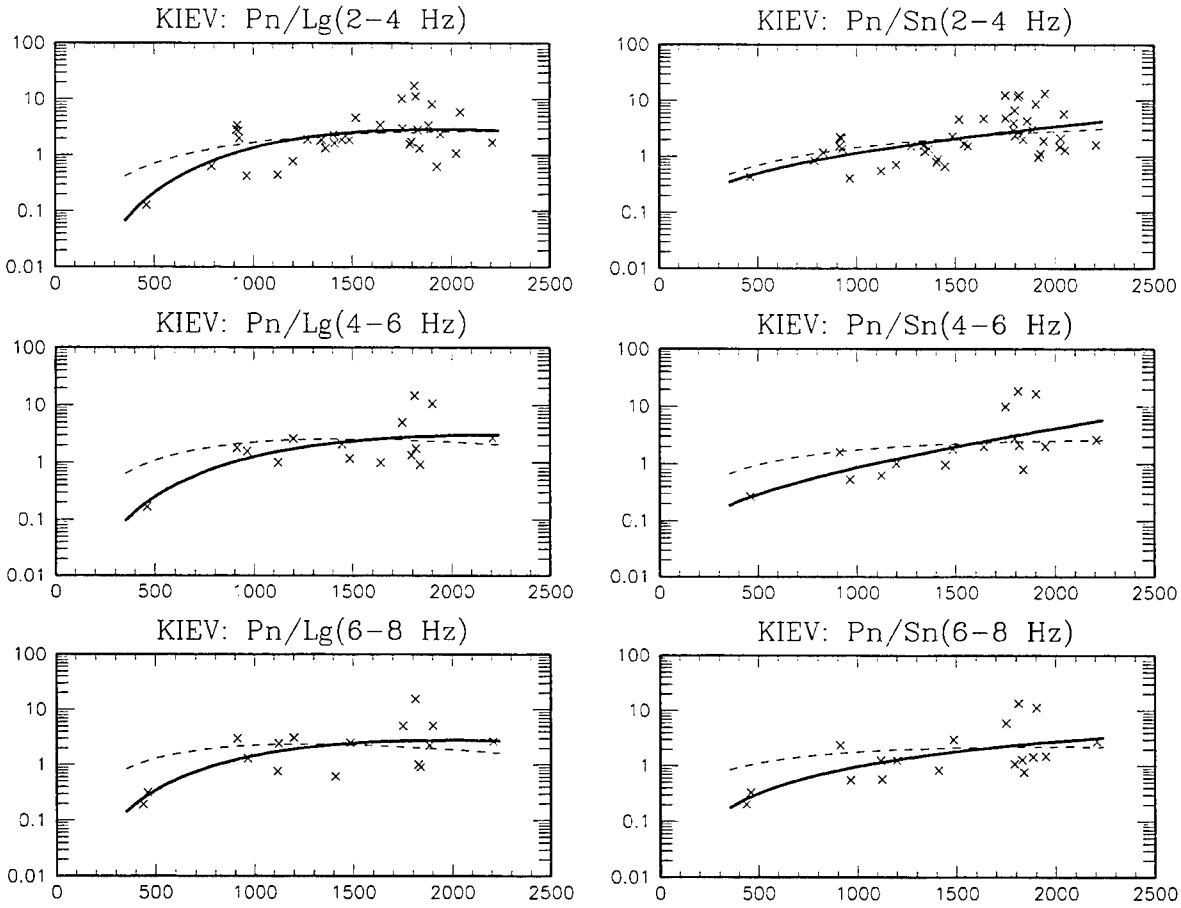

	n	*s*	s_c	$\hat{\alpha}$	$\hat{\beta}$	$\hat{\gamma}$
Pn/Lg(2-4 Hz)	34	0.429	0.360	1.832	4.251	-9.518E-04
Pn/Lg(4-6 Hz)	15	0.463	0.375	1.348	3.407	-6.508E-04
Pn/Lg(6-8 Hz)	16	0.482	0.373	1.442	3.258	-7.025E-04
Pn/Sn(2-4 Hz)	44	0.392	0.336	-0.024	0.816	2.299E-04
Pn/Sn(4-6 Hz)	16	0.515	0.411	-0.345	0.852	4.285E-04
Pn/Sn(6-8 Hz)	18	0.484	0.385	0.378	1.760	-7.822E-05

Figure A-35. Regional data and best least-square fits (solid curves) of the distance dependence for 46 regional events recorded by KIEV.

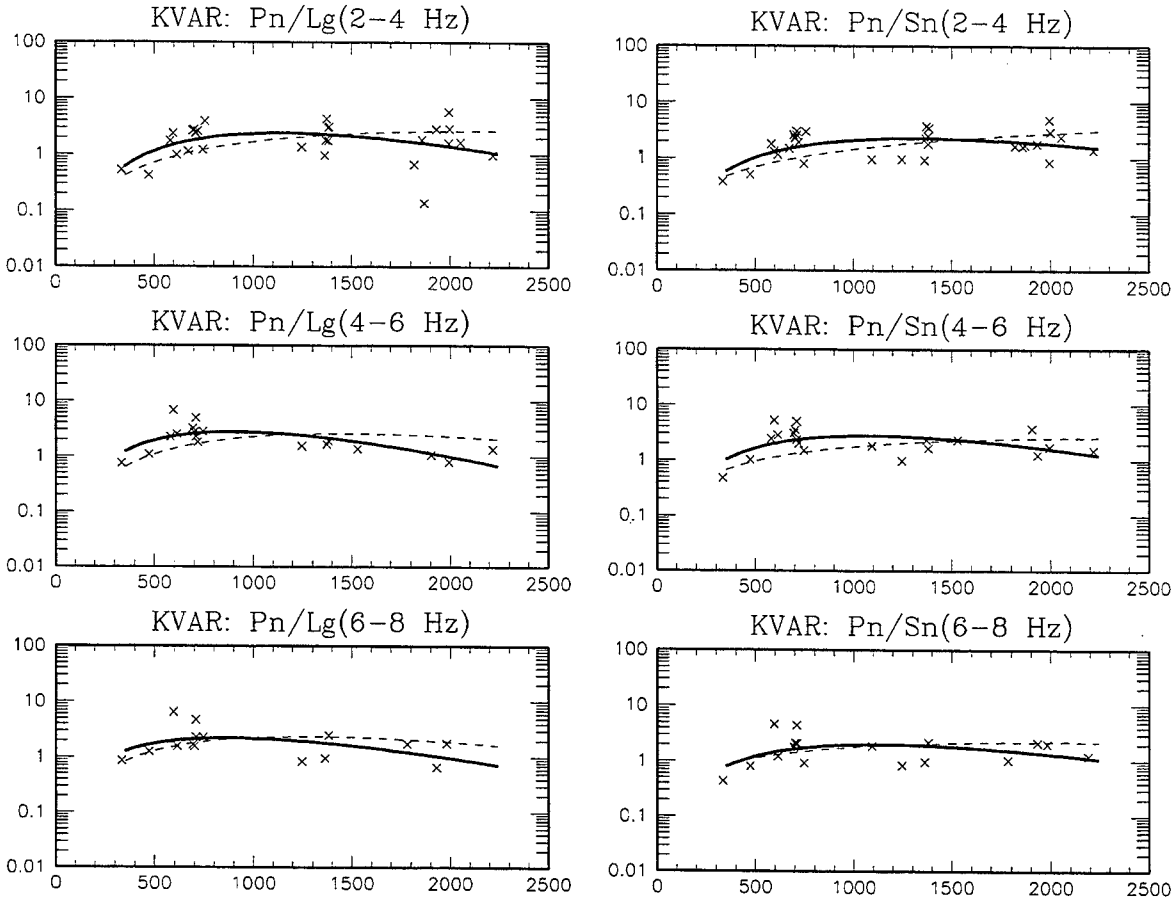

	n	*s*	s_c	$\hat{\alpha}$	$\hat{\beta}$	$\hat{\gamma}$
Pn/Lg(2-4 Hz)	29	0.338	0.322	1.945	2.828	-1.076E-03
Pn/Lg(4-6 Hz)	18	0.253	0.198	2.055	2.477	-1.184E-03
Pn/Lg(6-8 Hz)	15	0.271	0.262	1.544	1.786	-8.910E-04
Pn/Sn(2-4 Hz)	30	0.256	0.226	1.489	2.308	-7.561E-04
Pn/Sn(4-6 Hz)	20	0.252	0.234	1.771	2.291	-9.264E-04
Pn/Sn(6-8 Hz)	17	0.267	0.260	1.406	1.972	-7.632E-04

Figure A-36. Regional data and best least-square fits (solid curves) of the distance dependence for 36 regional events recorded by KVAR.

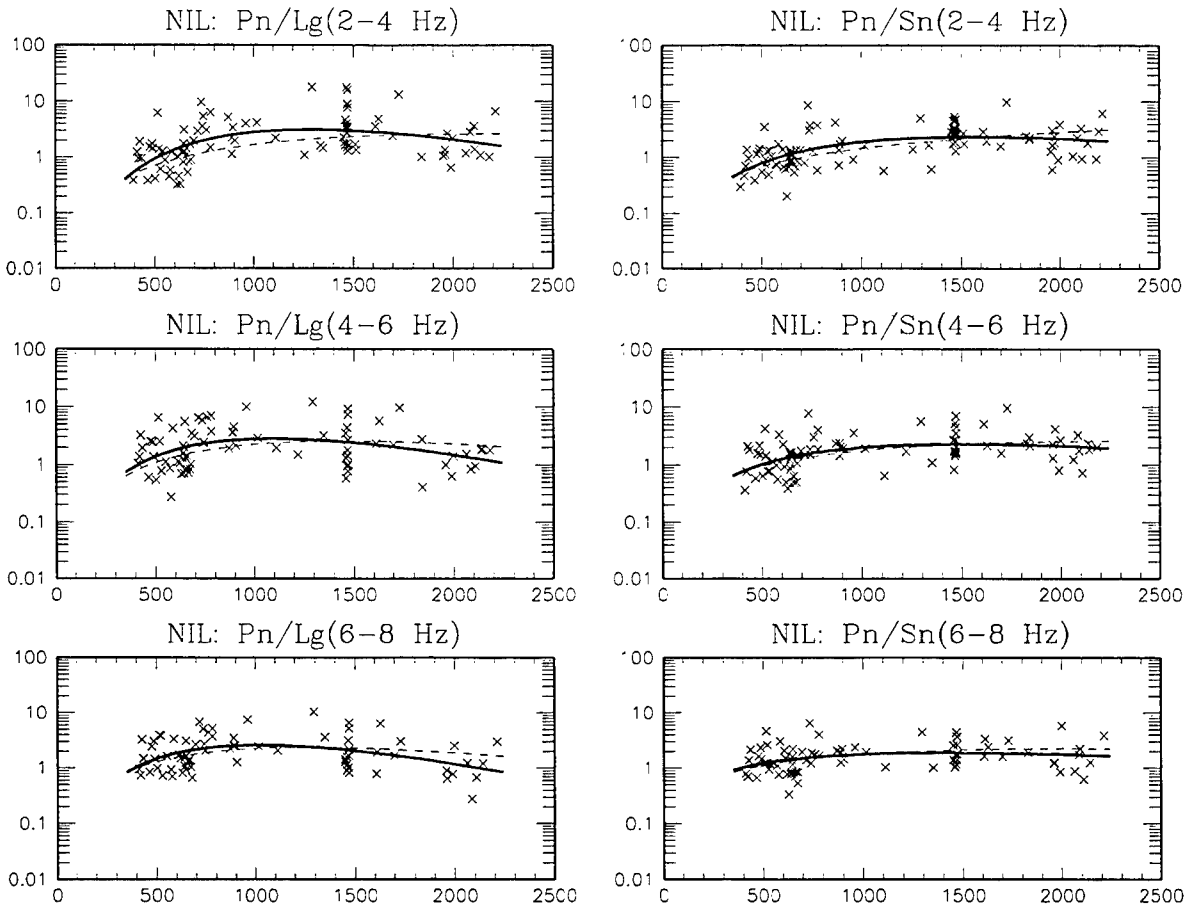

	n	s	s_c	$\hat{\alpha}$	$\hat{\beta}$	$\hat{\gamma}$
Pn/Lg(2-4 Hz)	97	0.382	0.330	2.306	3.617	-1.219E-03
Pn/Lg(4-6 Hz)	80	0.356	0.339	2.119	2.935	-1.159E-03
Pn/Lg(6-8 Hz)	74	0.308	0.288	2.070	2.762	-1.172E-03
Pn/Sn(2-4 Hz)	106	0.321	0.263	1.327	2.319	-6.398E-04
Pn/Sn(4-6 Hz)	87	0.303	0.274	1.145	1.834	-5.251E-04
Pn/Sn(6-8 Hz)	79	0.253	0.245	0.783	1.105	-3.381E-04

Figure A-37. Regional data and best least-square fits (solid curves) of the distance dependence for 112 regional events recorded by NIL.

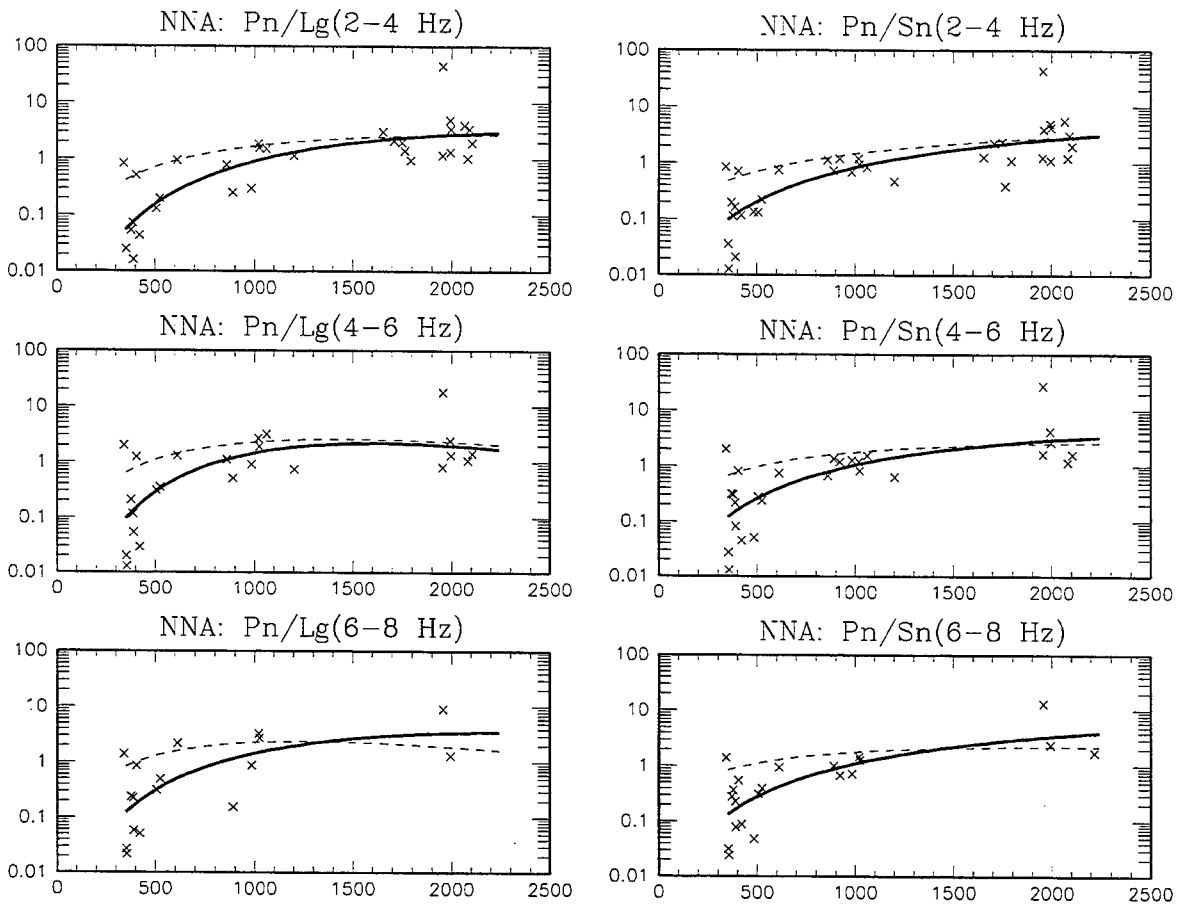

	n	*s*	s_c	$\hat{\alpha}$	$\hat{\beta}$	$\hat{\gamma}$
Pn/Lg(2-4 Hz)	32	0.814	0.479	1.154	3.512	-5.791E-04
Pn/Lg(4-6 Hz)	24	0.760	0.559	2.030	4.213	-1.130E-03
Pn/Lg(6-8 Hz)	17	0.768	0.601	1.311	3.195	-5.906E-04
Pn/Sn(2-4 Hz)	36	0.715	0.443	0.518	2.329	-1.921E-04
Pn/Sn(4-6 Hz)	27	0.722	0.508	0.748	2.485	-2.948E-04
Pn/Sn(6-8 Hz)	21	0.678	0.472	0.673	2.339	-2.141E-04

Figure A-38. Regional data and best least-square fits (solid curves) of the distance dependence for 37 regional events recorded by NNA.

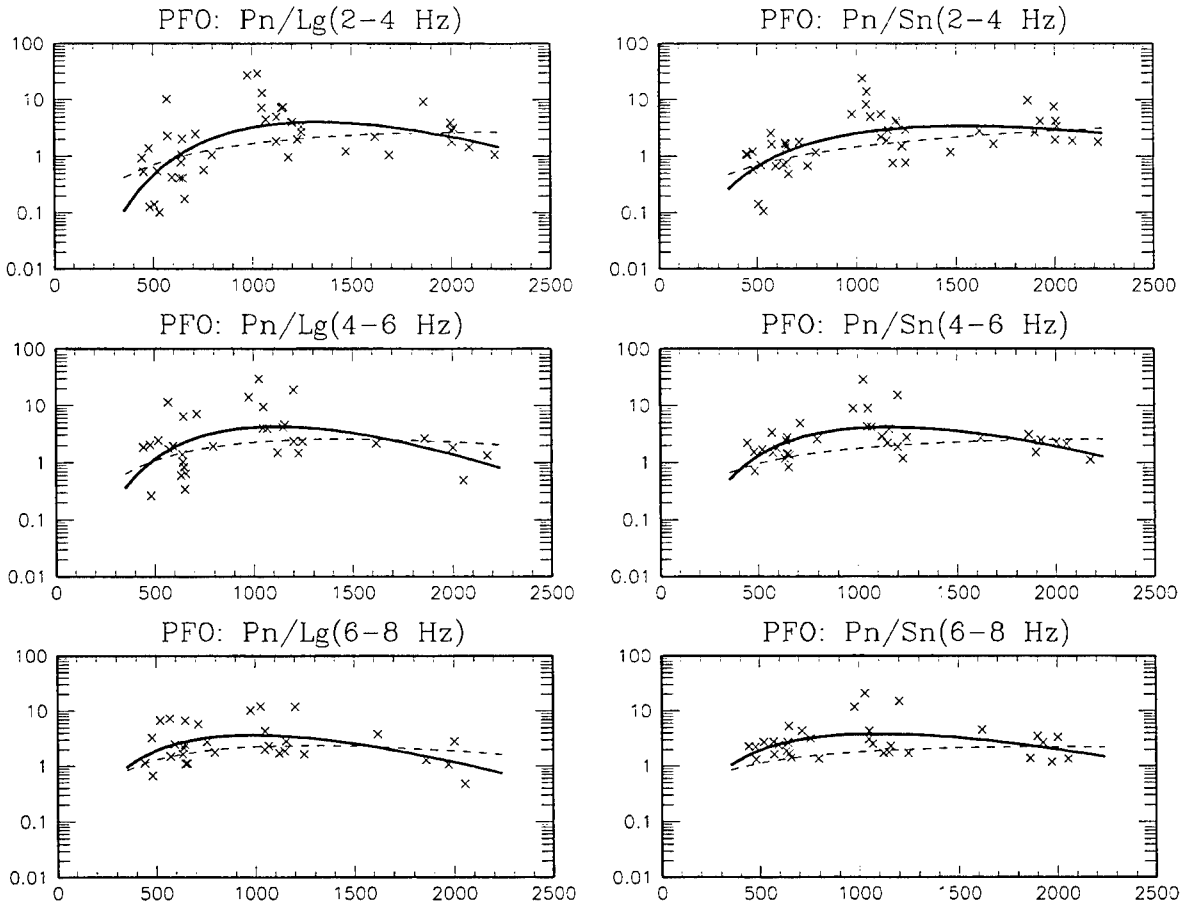

	n	*s*	s_c	$\hat{\alpha}$	$\hat{\beta}$	$\hat{\gamma}$
Pn/Lg(2-4 Hz)	45	0.572	0.460	3.619	6.166	-2.023E-03
Pn/Lg(4-6 Hz)	33	0.483	0.437	3.613	5.295	-2.066E-03
Pn/Lg(6-8 Hz)	31	0.354	0.327	2.720	3.499	-1.543E-03
Pn/Sn(2-4 Hz)	47	0.453	0.372	2.072	3.647	-1.026E-03
Pn/Sn(4-6 Hz)	35	0.338	0.289	2.962	4.284	-1.609E-03
Pn/Sn(6-8 Hz)	33	0.296	0.280	2.224	2.874	-1.141E-03

Figure A-39. Regional data and best least-square fits (solid curves) of the distance dependence for 53 regional events recorded by PFO.

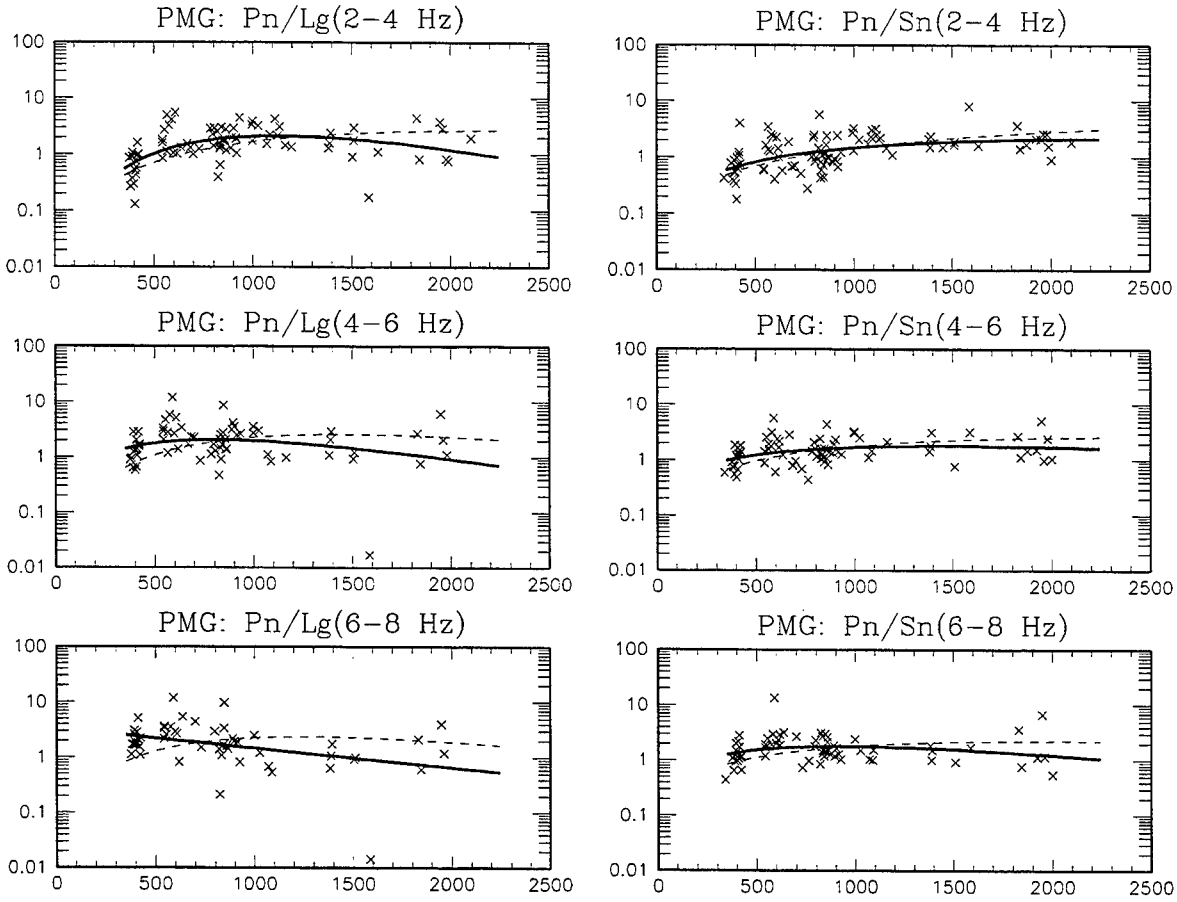

	n	*s*	s_c	$\hat{\alpha}$	$\hat{\beta}$	$\hat{\gamma}$
Pn/Lg(2-4 Hz)	82	0.327	0.281	1.913	2.847	-1.094E-03
Pn/Lg(4-6 Hz)	68	0.372	0.367	1.292	1.397	-7.538E-04
Pn/Lg(6-8 Hz)	57	0.409	0.384	0.481	-0.066	-3.279E-04
Pn/Sn(2-4 Hz)	94	0.303	0.260	0.584	1.188	-2.044E-04
Pn/Sn(4-6 Hz)	77	0.231	0.219	0.652	0.912	-2.663E-04
Pn/Sn(6-8 Hz)	66	0.244	0.242	0.874	0.974	-4.529E-04

Figure A-40. Regional data and best least-square fits (solid curves) of the distance dependence for 96 regional events recorded by PMG.

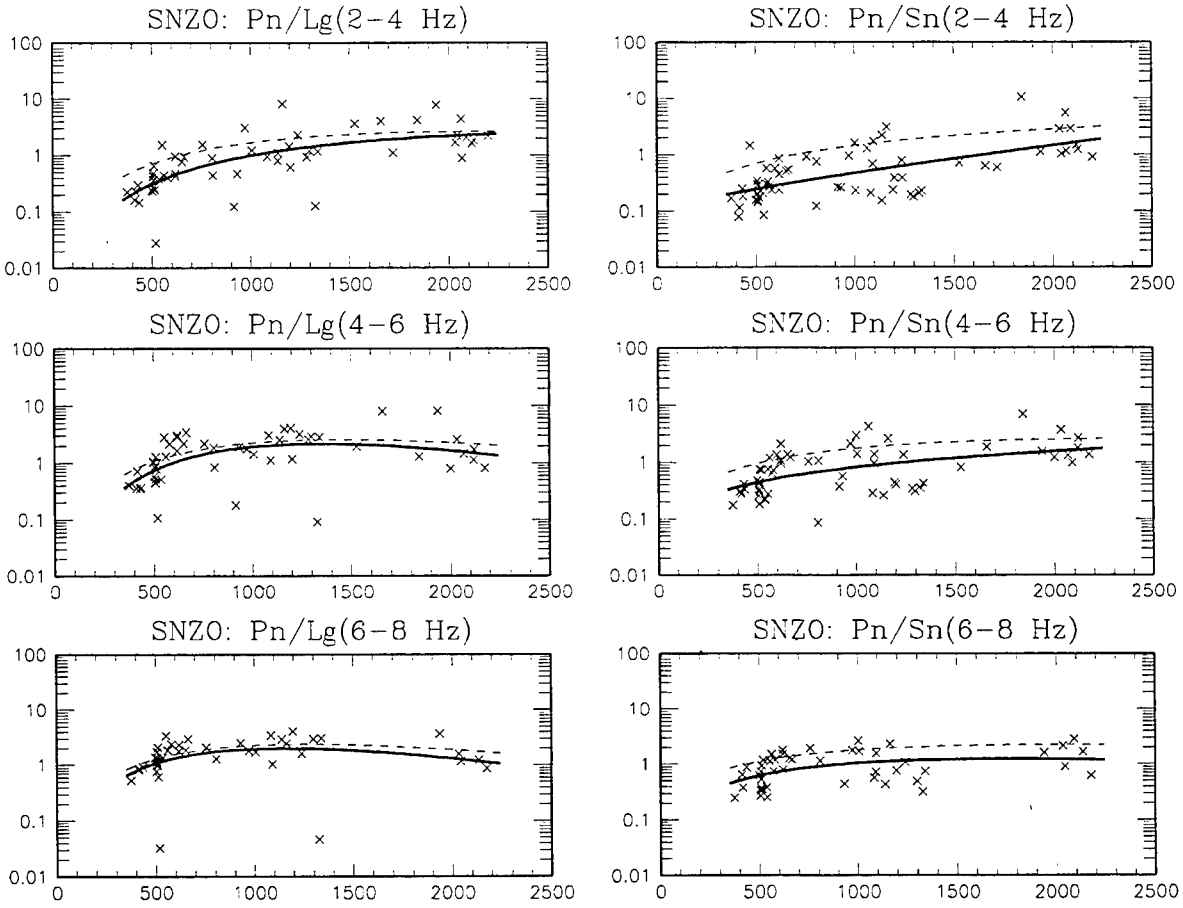

	n	*s*	s_c	$\hat{\alpha}$	$\hat{\beta}$	$\hat{\gamma}$
Pn/Lg(2-4 Hz)	55	0.493	0.350	0.684	2.175	-3.049E-04
Pn/Lg(4-6 Hz)	52	0.419	0.370	1.786	2.996	-9.716E-04
Pn/Lg(6-8 Hz)	42	0.413	0.404	1.550	2.279	-8.597E-04
Pn/Sn(2-4 Hz)	65	0.452	0.354	-0.693	0.256	4.121E-04
Pn/Sn(4-6 Hz)	60	0.394	0.342	0.020	0.818	3.401E-05
Pn/Sn(6-8 Hz)	47	0.289	0.266	0.539	1.237	-3.032E-04

Figure A-41. Regional data and best least-square fits (solid curves) of the distance dependence for 71 regional events recorded by SNZO.

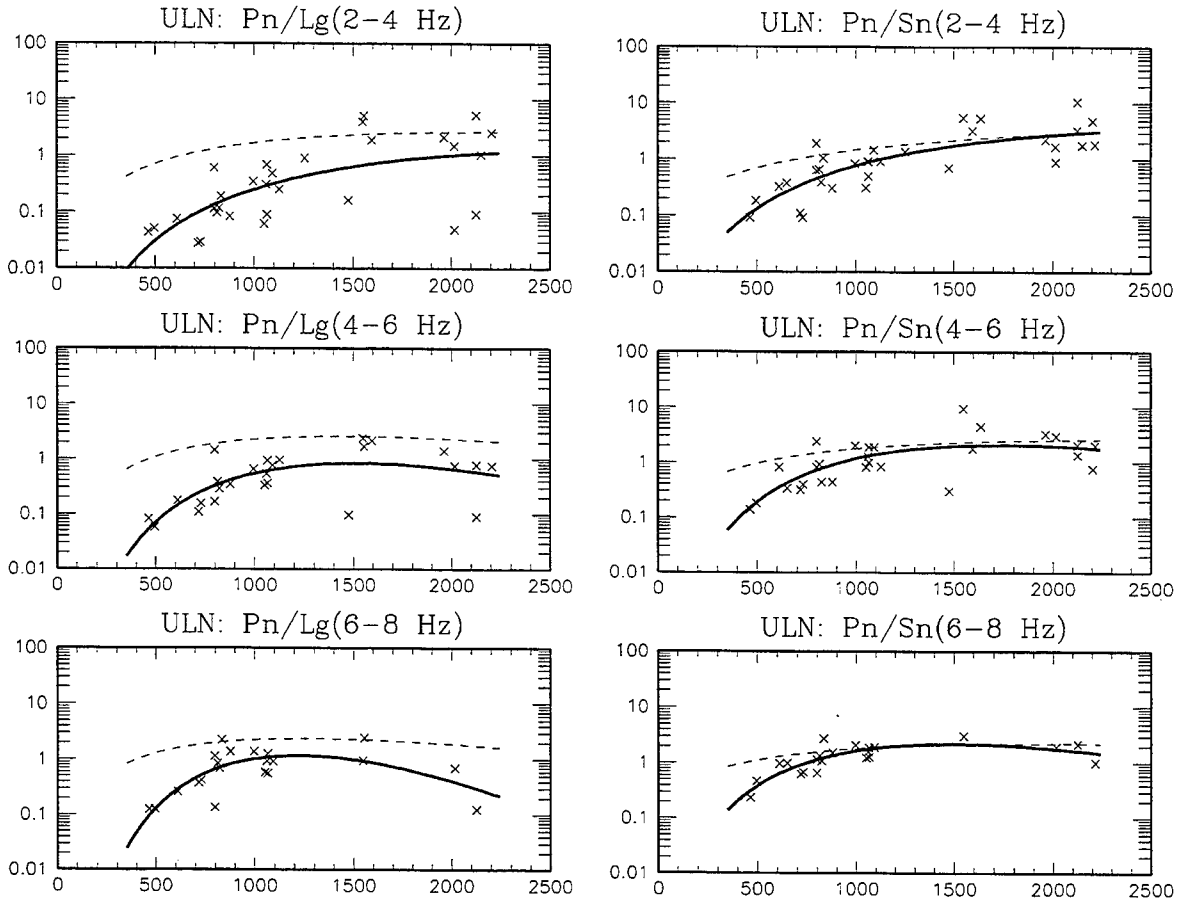

	n	*s*	s_c	$\hat{\alpha}$	$\hat{\beta}$	$\hat{\gamma}$
Pn/Lg(2-4 Hz)	30	0.702	0.539	0.711	4.030	-6.028E-04
Pn/Lg(4-6 Hz)	26	0.469	0.363	2.337	5.628	-1.612E-03
Pn/Lg(6-8 Hz)	21	0.405	0.281	3.885	7.286	-2.592E-03
Pn/Sn(2-4 Hz)	32	0.520	0.316	0.891	3.259	-4.310E-04
Pn/Sn(4-6 Hz)	28	0.431	0.306	1.958	4.445	-1.109E-03
Pn/Sn(6-8 Hz)	22	0.263	0.150	2.117	4.065	-1.184E-03

Figure A-42. Regional data and best least-square fits (solid curves) of the distance dependence for 33 regional events recorded by ULN.

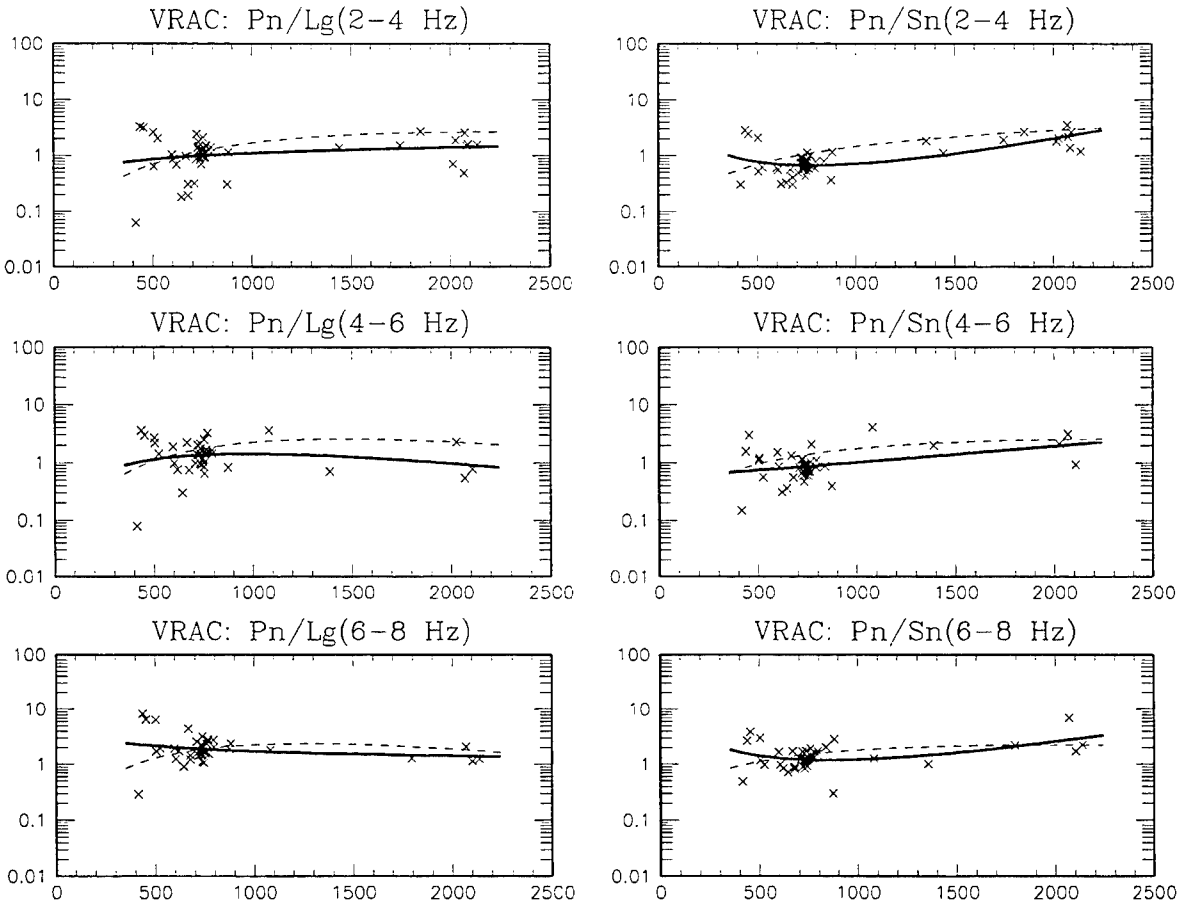

	n	*s*	s_c	$\hat{\alpha}$	$\hat{\beta}$	$\hat{\gamma}$
Pn/Lg(2-4 Hz)	49	0.335	0.334	0.118	0.377	-9.145E-06
Pn/Lg(4-6 Hz)	41	0.304	0.307	0.882	1.183	-5.221E-04
Pn/Lg(6-8 Hz)	41	0.246	0.247	0.152	-0.355	2.177E-05
Pn/Sn(2-4 Hz)	52	0.274	0.206	-1.429	-1.737	9.768E-04
Pn/Sn(4-6 Hz)	43	0.267	0.251	-0.296	-0.041	2.948E-04
Pn/Sn(6-8 Hz)	44	0.230	0.211	-0.969	-1.525	7.862E-04

Figure A-43. Regional data and best least-square fits (solid curves) of the distance dependence for 58 regional events recorded by VRAC.

Appendix B
Selected Bibliography

The following papers and technical reports have been sponsored by this contract:

Bottone, S., M. D. Fisk, G. D. McCartor and R. J. Carlson (1997). Initial Regionalization Efforts for the IMS Seismic Network, PL-TR-97-2090, Phillips Laboratory, Hanscom AFB, MA.

Bottone, S., M. D. Fisk, H. L. Gray and G. D. McCartor (1996). The Dependence of Magnitude Uncertainty on Station Coverage, PL-TR-96-2250, Phillips Laboratory, Hanscom AFB, MA.

Carlson, R. J. and M. D. Fisk (1998). Initial User's Guide for Event Screening Products and Services at the Prototype IDC, MRC-R-1555, Mission Research Corporation, Santa Barbara, CA, to appear as a Phillips Laboratory Technical Report, Hanscom AFB, MA.

Fisk, M. D., S. Bottone, R. J. Carlson, H. L. Gray and G. D. McCartor (1998). Event Characterization Development and Analysis at the Prototype IDC, MRC-R-1548, (this report), Mission Research Corporation, Santa Barbara, CA.

Fisk, M. D., R. J. Carlson, V. Burlacu and G. D. McCartor (1996). Interactive World Wide Web Pages for Custom Event Screening at the Prototype International Data Center, PL-TR-96-2269, Phillips Laboratory, Hanscom AFB, MA.

Israelsson, H., M. D. Fisk, X. Yang, R. G. North (1997). The August 16, 1997 Event in the Kara Sea, CMR-97/38, Center for Monitoring Research, Arlington, VA.

Sain, S. R., H. L. Gray, W. A. Woodward and M. D. Fisk (1997). Outlier detection from a mixture distribution when training data are unlabeled, submitted to *Bull. Seis. Soc. Am.*

DISTRIBUTION LIST

DEPARTMENT OF DEFENSE

DIRECTOR
DEFENSE RESEARCH & ENGINEERING
WASHINGTON, DC 20301-3110
ATTN: DDR&E

DEFENSE TECHNICAL INFORMATION CENTER
8725 JOHN J. KINGMAN ROAD, SUITE 0944
FORT BELVOIR, VA 22060-6218
ATTN: DTIC/OCP

DEFENSE THREAT REDUCTION AGENCY
6801 TELEGRAPH ROAD
ALEXANDRIA, VA 22310-3398
ATTN: CPF, M. SHORE
ATTN: CPFG, R. JIH
ATTN: CPWPT/TECHNICAL RESOURCE CENTER
ATTN: OST, DR A. DAINTY

DEPARTMENT OF DEFENSE CONTRACTORS

ACIS
6T11 NHB
WASHINGTON, DC 20505
ATTN: L. TURNBULL

BATTELLE MEMORIAL INSTITUTE
MUNITIONS & ORDNANCE CENTER
505 KING AVENUE
COLUMBUS, OH 43201-2693
ATTN: TACTEC

BBN CORPORATION
1300 N 17TH STREET, SUITE 1200
ARLINGTON, VA 22209
ATTN: H. FARRELL
ATTN: J. PULLI

BDM FEDERAL INC.
950 EXPLORER BOULEVARD
HUNTSVILLE, AL 35806
ATTN: T. JORDAN

CALIFORNIA, UNIVERSITY AT SAN DIEGO
SCRIPPS INSTITUTION OF OCEANOGRAPHY
P. O. BOX 6049
SAN DIEGO, CA 92166-6049
ATTN: C. D. HEDLIN
ATTN: DR M. A. H. HEDLIN
ATTN: PROF F. VERNON
ATTN: PROF J. A. ORCUTT
ATTN: PROF J. BERGER

CENTER FOR MONITORING RESEARCH
1300 N, 17TH STREET, SUITE 1450
ARLINGTON, VA 22209
ATTN: DR. K. L. MC LAUGHLIN
ATTN: DR R. NORTH
ATTN: LIBRARIAN
ATTN: V. RYABOY

CTB TREATY MANAGER
ROSSLYN GATEWAY
1901 N. MOORE STREET, SUITE 609
ARLINGTON, VA 22209
ATTN: DR R. W. ALEWINE, III

ENSCO, INC
445 PINEDA COURT
MELBOURNE, FL 3940
ATTN: DR D. TAYLOR

ENSCO, INC.
P O BOX 1346
SPRINGFIELD, VA 22151-0346
ATTN: D. BAUMGARDT
ATTN: Z. DER

GEOPHEX, LTD.
WESTON GEOPHYSICAL
325 WEST MAIN STREET
NORTHBOROUGH, MA 01532
ATTN: DR D. REITER
ATTN: J. LEWKOWICZ

ITT INDUSTRIES
ITT SYSTEMS CORPORATION
ATTN: AODTRA/DTRIAC
1680 TEXAS STREET, SE
KIRTLAND AFB, NM 87117-5669
ATTN: DTRIAC
ATTN: DTRIAC/DARE

MAXWELL LABORATORIES, INC.
S-CUBED WASHINGTON RESEARCH OFFICE
11800 SUNRISE VALLEY DRIVE, SUITE 1212
RESTON, VA 22091
ATTN: DR. T. J. BENNETT

MAXWELL TECHNOLOGIES INC.
FEDERAL DIVISION
8888 BALBOA AVENUE
SAN DIEGO, CA 92123-1506
ATTN: DR J. L. STEVENS
ATTN: DR G. E. BAKER

MISSION RESEARCH CORPORATION
8560 CINDERBED ROAD, SUITE 700
NEWINGTON, VA 22122
ATTN: DR M. FISK
ATTN: R. J. CARLSON
ATTN: S. BOTTONE

MULTIMAX, INC
1441 MC CORMICK DRIVE
LANDOVER, MD 20785
ATTN: DR I. N. GUPTA
ATTN: DR W. CHAN
ATTN: L. GRANT

PACIFIC NORTHWEST LABORATORIES
A DIV OF BATTELLE MEMORIAL INSTITUTE
P. O. BOX 999
RICHLAND, MA 99352
ATTN: TECHNICAL STAFF, MS K5-12

S-CUBED
A DIVISION OF MAXWELL LABS, INC.
11800 SUNRISE VALLEY DRIVE, SUITE 1212
RESTON, VA 22091
ATTN: J. MURPHY

SCIENCE APPLICATION INT'L CORPORATION
3309 NW GOLDEN PLACE
SEATTLE, WA 98117
ATTN: A. RATLETON

SCIENCE APPLICATIONS INT'L CORPORATION
10260 CAMPUS POINT DRIVE
SAN DIEGO, CA 92121-1578
ATTN: DR T. C. BACHE, JR
ATTN: DR T. J. SERENO, JR

SOUTHERN METHODIST UNIVERSITY
DEPARTMENT OF GEOLOGICAL SCIENCE
P. O. BOX 395
DALLAS, TX 75275-0395
ATTN: DR B. STUMP
ATTN: E. HERRIN

ST LOUIS UNIVERSITY
P. O. BOX 8148
PIERRE LACLEDE STATION
ST LOUIS, MO 63156-8148
ATTN: PROF B. HERRMANN
ATTN: PROF B. J. MITCHELL

TEXAS, UNIVERSITY AT AUSTIN
P. O. BOX 7726
AUSTIN, TX 78712
ATTN: C. A. FROELICH

WOODWARD-CLYDE CONSULTANTS
566 EL DORADO STREET
PASADENA, CA 91109-3245
ATTN: DR B. B. WOODS
ATTN: DR C. K. SAIKIA

DEPARTMENT OF ENERGY

UNIVERSITY OF CALIFORNIA
LAWRENCE LIVERMORE NATIONAL
LABORATORY
P. O. BOX 808
LIVERMORE, CA 94551-9900
ATTN: K. NAKANISHI
ATTN: W. J. HANNON, JR, L-103
ATTN: M. DENNY, L-205
ATTN: TECHNICAL STAFF, MS L-200
ATTN: TECHNICAL STAFF, MS L-205
ATTN: TECHNICAL STAFF, MS L-208

LOS ALAMOS NATIONAL LABORATORY
P. O. BOX 1663
LOS ALAMOS, NM 87545
ATTN: FRANCESCA CHAVEZ, MS-D460
ATTN: D. STEEDMAN, MS-F607
ATTN: TECHNICAL STAFF, MS-C335
ATTN: TECHNICAL STAFF, MS-D460
ATTN: TECHNICAL STAFF, MS-F665

PACIFIC NORTHWEST NATIONAL LABORATORY
P. O. BOX 999
BATTELLE BOULEVARD
RICHLAND, WA 99352
ATTN: D. N. HAGEDORN, MS K5-12

SANDIA NATIONAL LABORATORIES
ATTN: MAIL SERVICES
P. O. BOX 5800
ALBUQUERQUE, NM 87185-0459
ATTN: TECHNICAL STAFF,
DEPARTMENT 5704, MS 0655
ATTN: TECHNICAL STAFF,
DEPARTMENT 5704, MS 0979
ATTN: TECHNICAL STAFF,
DEPARTMENT 5736, MS 0655
ATTN: TECHNICAL STAFF,
DEPARTMENT 9311, MS 1159

SEISMOLOGICAL LABORATORY 252-21
CALIFORNIA INSTITUTE OF TECHNOLOGY
PASADENA, CA 91125
ATTN: T. AHERNS

UNIVERSITY OF CALIFORNIA
EARTH SCIENCE DIVISION
479 MCCONE HALL, LBNL, 90-2106
BERKELEY, CA 94720
ATTN: L. JOHNSON, MS 90-1116

DEPARTMENT OF THE AIR FORCE

HEADQUARTERS
AFTAC/TTR
1030 SOUTH HIGHWAY A1A
PATRICK AFB, FL 32925-3002
ATTN: V. HSU

AIR FORCE RESEARCH LABATORY
29 RANDOLPH ROAD
HANSCOM AFB, MA 01731-5000
ATTN: DR D. HARKRIDER
ATTN: DR D. REITER
ATTN: GPE, J. LEWKOWICZ

AIR FORCE RESEARCH LABORATORY
5 WRIGHT STREET
HANSCOM AFB, MA 01731-3004
ATTN: RESEARCH LIBRARY, TL

AIR FORCE TECHNICAL APPLICATIONS CENTER
1300 17TH STREET, SUITE 1450
ARLINGTON, VA 22209
ATTN: R. BLANDFORD

AIR FORCE TECHNICAL APPLICATIONS CTR/TTA
1030 SOUTH HIGHWAY AIA
PATRICK AFB, FL 32925-3002
ATTN: CA/STINFO
ATTN: DR B. KEMERAIT
ATTN: DR D. RUSSELL
ATTN: G. ROTHE, TTR
ATTN: M. SIBOL

DIRECTORY OF OTHER (LIBRARIES AND UNIVERSITIES)

ARIZONA, UNIVERSITY OF
DEPT. OF GEOSCIENCES/SASO
TUCSON, AZ 85721
ATTN: PROF T. C. WALLACE

BOISE STATE UNIVERSITY
GEOSCIENCES DEPARTMENT
1910 UNIVERSITY DRIVE
BOISE, ID 83725
ATTN: J. E. ZOLLWEG

BOSTON COLLEGE
INSTITUTE FOR SPACE RESEARCH
140 COMMONWEALTH AVENUE
CHESTNUT HILL, MA 02167
ATTN: PROF L. SYKES

CALIFORNIA INSTITUTE OF TECHNOLOGY
DIVISION OF GEOLOGY & PLANETARY SCIENCES
PASADENA, CA 91125
ATTN: PROF D. V. HELMBERGER

CALIFORNIA-DAVIS, UNIVERSITY OF
DAVIS, CA 95616
ATTN: R. H. SHUMWAY, DIVISION STATISTICS

CALIFORNIA-SANTA CRUZ, UNIVERSITY OF
INSTITUTE OF TECTONICS
SANTA CRUZ, CA 95064
ATTN: DR R. S. WU
ATTN: PROF T. LAY

COLORADO-BOULDER, UNIVERSITY OF
BOULDER, CO 80309
ATTN: M. RITZWOLLER, CAMPUS BOX 390
ATTN: PROF C. ARCHAMBEAU

COLUMBIA UNIVERSITY
LAMONT-DOHERTY EARTH OBSERVATORY
PALISADES, NY 10964
ATTN: DR L. R. SYKES
ATTN: DR J. XIE
ATTN: PROF P. G. RICHARDS

CONNECTICUT, UNIVERSITY OF
DEPT. OF GEOLOGY & GEOPHICS
STOORS, CT 06269-2045
ATTN: PROF V. F. CORMIER, U-45, RM-207

CORNELL UNIVERSITY
DEPARTMENT OF GEOLOGICAL SCIENCES
3126 SNEE HALL
ITHACA, NY 14853
ATTN: PROF M. BARAZANGI

HARVARD UNIVERSITY
HOFFMAN LABORATORY
20 OXFORD STREET
CAMBRIDGE, MA 02138
ATTN: PROF A. DZIEWONSKI
ATTN: PROF G. EKSTROM

IRIS
1200 NEW YORK AVENUE, NW, SUITE 800
WASHINGTON, DC 20005
ATTN: DR D. SIMPSON
ATTN: DR G. E. VAN DER VINK

MASSACHUSETTS INSTITUTE OF TECHNOLOGY
EARTH RESOURCES LABORATORY
42 CARLETON STREET
CAMBRIDGE, MA 02142
ATTN: PROF M. N. TOKSOZ

MICHIGAN STATE UNIVERSITY LIBRARY
450 ADMINISTRATION BUILDING
EAST LANSING, MI 48824
ATTN: K. FUJITA

NEW MEXICO STATE UNIVERSITY
DEPARTMENT OF PHYSICS
LAS CRUCES, NM 88003
ATTN: PROF J. NI
ATTN: PROF T. HEARN

PENNSYLVANIA STATE UNIVERSITY
GEOSCIENCES DEPARTMENT
403 DEIKE BUILDING
UNIVERSITY PARK, PA 16802
ATTN: PROF C. A. LANGSTON
ATTN: PROF S. ALEXANDER

SAN DIEGO STATE UNIVERSITY
DEPT OF GEOLOGICAL SCIENCES
SAN DIEGO, CA 92182
ATTN: PROF S. M. DAY

SOUTHERN METHODIST UNIVERSITY
FONDREN LIBRARY
DALLAS, TX 75275
ATTN: B. STUMP
ATTN: G. MCCARTOR, DEPARTMENT OF PHYSICS
ATTN: H. L. GRAY, DEPARTMENT OF STATISTICS

UNIVERSITY OF COLORADO
CAMPUS 583
BOULDER, CO 80309
ATTN: DR A. L. LEVSHIN

UNIVERSITY OF SOUTHERN CALIFORNIA
520 SEAVER SCIENCE CENTER
UNIVERSITY PARK
LOS ANGELES, CA 90089-0483
ATTN: PROF C. G. SAMMIS

FOREIGN

AUSTRALIAN GEOLOGICAL SURVEY ORGANIZATION
CORNER OF JERRAGOMRRA & NINDMARSH DRIVE
CANBERRA, ACT 2609
AUSTRALIA
ATTN: D. JEPSON

GEOPHYSICAL INSTITUTE OF ISRAEL
HAMASHBIR STREET, 1
HOLON, 58122 ISRAEL
ATTN: DR Y. GITTERMAN

I.R.I.G.M. - B.P. 68
38402 ST. MARTIN D'HERES
CEDEX, FRANCE
ATTN: DR M. BOUCHON

MINISTRY OF DEFENSE/
PROCUREMENT EXECUTIVE
ALACKNESS, BRIMPTON
READING FG7-4RS ENGLAND
ATTN: DR P. MARSHALL

NTNF/NORSAR
P O BOX 51
N-2007 KJELLER, NORWAY
ATTN: DR F. RINGDAL
ATTN: T. KVAERNA

OBSERVATOIRE DE GRENOBLE
I.R.I.G.M. - B. P. 53
38041 GRENOBLE, FRANCE
ATTN: DR M. CAMPILLO

RESEARCH SCHOOL OF EARTH SCIENCES
INSTITUTE OF ADVANCES STUDIES
G. P. O. BOX 4
CANABERRA 2601, AUSTRALIA
ATTN: PROF B. L. N. KENNETT

RUHR UNIVERSTY/BOCHUM
INSTITUTE FOR GEOPHYSIK
P O BOX 102148
463 BOCHUM 1, GERMANY
ATTN: PROF H. P. HARJES

SEISMOLOGICAL DIVISION
IRPG
P.O. BOX 2286
HOLON 58122
ISRAEL
ATTN: A. SHAPIRA

SOCIETE RADIOMANA
27 RU CLAUDE BERNARD
75005 PARIS, FRANCE
ATTN: DR B. MASSINON
ATTN: DR. P. MECHLER

UNIVERSITY OF BERGEN
N-5007 BERGEN, NORWAY
INSTITUTE FOR SOLID EARTH PHYSICS
ALLEGATION 40
ATTN: R. E. HUSEBYE

UNIVERSITY OF CAMBRIDGE
DEPT. OF EARTH SCIENCES
MADINGLEY RISE, MADINGLEY ROAD
CAMBRIDGE CB3 0EZ, ENGLAND
ATTN: PROF K. PRIESTLEY

OTHER GOVERNMENT

US DEPARTMENT OF THE INTERIOR
US GEOLOGICAL SURVEY NATIONAL CENTER
MILITARY GEOLOGY PROJECT
12201 SUNRISE VALLEY DRIVE
RESTON, VA 22029
ATTN: B. LEITH
ATTN: DR J. FILSON
ATTN: W. LEITH, MS 928